UNIVERSITÀ DEGLI STUDI DI NAPOLI FEDERICO II

Dipartimento Ingegneria Civile, Edile e Ambientale

Dottorato di ricerca in Ingegneria dei Sistemi Civili
XXXIV ciclo

Candidato: Ing. Margherita Carmen Ciccaglione

Tesi di dottorato

On the diffusion theory of shoreline evolution

Coordinatore del Dottorato:

Prof. Ing. Andrea Papola

Relatore:

Prof. Ing. Mariano Buccino

Anno Accademico 2021-2022

Alla mia famiglia.

Abstract

As known, coastal erosion phenomenon vastly varies over either the space or the time scale. Short-term coastal erosion (on the time scale of hours and days) due to its inherently reversibility, cannot be considered as a “real coastal erosion”; by contrast, coastal retreatment is intended in a “structural way” and only long-term processes may have permanent effects on coastal evolution in this regard. Without a proper grasp of these processes, shoreline evolution and outcomes of coastal structures may not be anticipated accurately. The ever-growing need to calculate shoreline change over long spatial extents and time frames, has led to a wide use of both analytical and numerical (one-line shoreline response) models, based on the one-line contour theory (Pelnard-Considere, 1956), which reduces, under certain hypotheses, to the diffusion equation. The common thread of present Ph.D. thesis is grasping if, and in what measure, the shoreline diffusion equation could be able to provide theoretical guidance, also useful under the practical point of view, regarding the long-term evolution of sandy coasts. In fact, the analysis of diffusion equation reveals peculiar aspects in coastal evolution also with respect to the long term impact of hard structures. The work is organized to cope with different innovative aspects of the research theme, which have never been deepened by the published research in this field, and namely: (1) the evolution of a stretch of coast of finite length bounded by solid boundary, for which a complete analytical model has been developed. The proposed model provides a clearer view on the limits of the diffusion approach on this problem. (2) The effect of a time-varying diffusivity on long-term shoreline evolution. This aspects regards the theoretical foundations of the “equivalent wave” concept, frequently used in the practical coastal engineering. (3) The organic introduction to the effect of a negative diffusivity on long-term evolution of sandy coasts, and the original interpretation of the effects of a detached breakwater on shoreline change are then studied. In fact, under an intriguing perspective, but not sufficiently deepened, at all, it is assumed that the positioning of a transmissive breakwater is nothing but the introduction of a negative diffusivity into a restricted area of the coast. (4) A more stringent relationship between wave crests and equilibrium shore profile, which demonstrates that the equilibrium position of shoreline does not corresponds to the wave fronts. The theoretical interpretation has been found through the diffusion approach.

The research has been carried out either via theoretical approach, searching for analytical solution of practical interest of the heat equation, or via numerical approach, using the numerical one-contour line model GENESIS (Hanson and Kraus, 1989). Moreover, the analysis regarding the "diffusion aspects" (2) and (3) are supported by shoreline evolution data of Molise coast, relative to a long-term study between 1954 and 2016, which allowed a further comprehension of diffusion problems and peculiar features of coastal evolution. Conversely, the methodology behind (4) has been validated on a small pocket beach within the Bagnoli bay (NA).

Sommario

Come è noto, il fenomeno dell'erosione costiera varia notevolmente sia nella scala spaziale che temporale. L'erosione costiera a breve termine (sulla scala temporale di giorni e ore), caratterizzata da una sua intrinseca reversibilità, non può essere considerata una "vera erosione costiera"; al contrario, il vero e proprio arretramento della costa è inteso in senso "strutturale" e solo i processi a lungo termine possono modificare permanentemente la visione planimetrica delle spiagge. In mancanza di una adeguata comprensione di questi processi, l'ingegnere non è in grado di prevedere con correttezza l'evoluzione del litorale nonché gli impatti delle strutture costiere su di esso. Nel tempo si è sviluppato un utilizzo sempre più massiccio di modelli di previsione, sia analitici che numerici, per la stima del cambiamento della costa nel lungo periodo e su grande scala, entrambi basati sulla teoria "a una linea" (Pelnard-Considére, 1956), che si riduce, sotto certe ipotesi, all'equazione di diffusione.

Il *fil rouge* di questo progetto di ricerca è stato comprendere se e in che misura l'equazione di diffusione delle spiagge fosse in grado di fornirci indicazioni teoriche, ma allo stesso tempo utili dal punto di vista applicativo, riguardo l'evoluzione di medio-lungo termine dei litorali sabbiosi. Infatti, l'analisi dell'equazione di diffusione svela aspetti peculiari nell'evoluzione costiera, anche relative all'effetto a lungo termine delle strutture. A valle di un poderoso lavoro di ricerca bibliografica, lo studio è stato impostato e strutturato per trattare aspetti differenti del tema di ricerca, sinora inesplorati dalla letteratura di settore. E precisamente: (1) lo studio dell'evoluzione di un tratto di costa di lunghezza finita per il quale è stato fornito un modello analitico completo, che consente di avere una visione più chiara riguardo i limiti dell'applicazione dell'equazione di diffusione a questo tipo di problema. (2) L'effetto di una diffusività variabile nel tempo sull'evoluzione *long-term* del litorale. Questo aspetto riguarda i fondamenti teorici del concetto di "onda equivalente", frequentemente utilizzato nella pratica ingegneria costiera, che non sono ma stati approfonditi fino a questo momento. (3) L'introduzione organica all'effetto di una diffusività negativa sull'evoluzione dei litorali sabbiosi, e l'ipotesi che, secondo un prospettiva intrigante, ma non ancora sufficientemente approfondita, il posizionamento di una barriera distaccata dalla linea di riva, con un grande coefficiente di trasmissione, possa riguardarsi come l'introduzione di una diffusività negativa all'interno di una porzione limitata della

costa. (4) Lo studio, poi, di una relazione più accurata e approfondita tra fronti d'onda e profilo di equilibrio delle spiagge, che supera l'opinione diffusa nella pratica ingegneristica di farli coincidere. Questo aspetto è stato affrontato sia mediante un approccio numerico che teorico, basato, quest'ultimo, sull'equazione di diffusione.

In generale le analisi sono state guidate da una metodologia teorica, derivando soluzioni analitiche di interesse pratico dell'equazione del calore, ma anche numericamente, utilizzando il modello numerico a una linea GENESIS (Hanson e Kraus, 1989). Inoltre, l'analisi relativa ai sotto temi (2) e (3) è supportata dai dati di evoluzione del litorale della costa molisana, relativi ad uno studio a lungo termine tra il 1954 e il 2016, che ha consentito un'ulteriore comprensione dei problemi di diffusione e delle peculiarità dell'evoluzione costiera. Al contrario, la metodologia alla base della (4) è stata validata su una piccola *pocket beach* all'interno della baia di Bagnoli (NA).

Contents

List of Figures

List of Tables

Chapter 1: Introduction

1.1. Nature of coastal erosion

The intersection between land and sea, the “coastal area”, has always been appealing to mankind for recreation, residence and transportation purposes. A high majority of the world population lives in very crowded metropolises which are established just near or along the shore for both the ease of shipping and the natural instinct of mankind to live near the coasts. In fact, coasts have always been an attraction for humanity from the beginning of the civilization for the benefits, opportunities and facilities offered as economic potentials. As a result, migration to these areas increased even more in recent years and coastal regions have become the most populated and developed regions of the world.

Moreover, with the inevitable rise of civilizations, starting from the early ‘50s, in many urban agglomerations, the overcrowding and the consequent landscape urbanization along coastal areas have been occurred without any appropriate town-planning scheme. Coastal structures such as ports, quays, etc. were constructed for several needs and uses, without much understanding or caring for the consequences and response of coastal systems to these structures.

The second post-war period represented, in fact, a challenge between man and territory, in which the growing development of civilization was opposed to the natural ecosystems, regarding either river basins, or coasts and seas. Particularly, the management of upstream basins produced heavy consequences on the downstream areas, and so on the coastal zone. Action as building in riverside area and/or within fluvial beds, which have been buried in undersized water piping, hydraulic works as artificial riverbanks, bridles and cementation of waterways, sediment extractions from riverbeds, have produced, year by year, a gradual reduction, until an almost total loss of river solid transport to sea, with a consequent poor nourishment of coastal system. Moreover, the urbanization within 300 m from coastline and destruction of dune areas and implementation of road and railway networks, running parallel and close to coastline, produced the progressive deterioration of the coastal morphological equilibrium and, accordingly, an increase of erosion in sandy beaches as well as flood hazards.

Therefore, this kind of urban approach attained conditions of environmental deterioration in marine and coastal ecosystems and affected the geo-morphological unstable equilibrium, highlighting the risk of erosion on sandy beaches.

For these reasons, the coastal areas have been facing, for more than 70 years by now, a serious and ever-growing problem, namely erosion. Beach berms disappear, shoreline is recessed and the property losses happen resulting from severe erosion, due to either natural or anthropic causes. Currently, this blindness and never-ending interference of mankind with nature, which resulted in brutal impacts of erroneously designed and constructed coastal structures, has created a new understanding towards the conservation and protection.

1.1.1. A focus on Italian peninsula

Basically, previous section represent a general framing of the erosive problem, which is however proper for the Italian coasts: the extreme urbanization beyond the limits of carrying capacities of the environmental system have produced losses in natural ecosystems with heavy consequences on environmental quality. Particularly, on the national coastal areas acts not only the aforementioned human activities that attend on coastal equilibrium, but also natural phenomena (e.g. the rising of sea level and/or the erosional action by hydrodynamic forces), which enormously increase the risk of erosion.

In order to provide some statistics, as regards Italian coastal zone, 30% of national population, as 16.9 million of inhabitants, lives in littoral regions, concentrated in an area restricted to 13% of national territory (ISPRA 2013). An analysis in detail highlights that, along Italian coasts (within 300 m from coastline), have been urbanized 2.056 km^2, as the 34% of the national coastal boundary. Actually, in the time lag 1950–2000, about the 30% of national coastline has suffered withdrawals wider than 25 m. In particular, for sandy beaches (58% of national coastline), spreading out along 4.863 km in overall length, the 46% has suffered large changes producing a total negative sedimentary budget with an overall soil loss of 54 km^2 (ISPRA 2013). This highlights a widespread and marked erosional trend of sandy beaches, at a national level, that in this last decade appears in an exponential and fast growth (Pranzini and Rossi, 2014). Amongst this national assessment, the coastal regions more damaged, owing to larger withdrawals, are Calabrian and Adriatic coasts. In particular, some littoral areas along the Adriatic Sea have different and distinctive morphological characteristics that expose their coastal regions to a high erosional risk.

The coastal risk was identified as a serious national problem as early as the 1970s. Over the years, coastal erosion has become a very important social and economic issue for the country and has often been the theme of assessment studies and impact estimates.

The national situation (1968-1969) of the erosion phenomenon was analysed within the framework of activities carried out by the *Commissione Interministeriale per lo Studio Della Sistemazione Idraulica e della Difesa del Suolo* (Interministerial Commission for the Study of the Hydraulic Arrangement and Land Protection known as the "*De Marchi Commission*"). Results highlighted that since the 1950s erosion processes have involved all of Italy's main river mouths as well as large sections of the coastal strip. Subsequent studies, conducted at national scale in the period 1985-1997, were published on the well-known Atlas of the Italian Beaches (CNR, MURST, 1997). All these studies confirmed that main river mouths are continuing to erode and that coast erosion phenomena are generally worsening. Mitigation cases were found almost exclusively near stretches of coast where local protection interventions had been planned.

As a result, starting from the '80, the first regulations regarding coasts at a national level have been provided (e.g. Law 431/85, "Galasso law", Law 183/89 on land protection, Legislative Decree 112/98, which gives the state the function of defining general approaches and criteria for protecting coasts). However, these were very general, passive, and insufficient and determined different methods of planning at a regional scale. Most notably, they prescribed hard protection structures as the only measure to be adopted to cope with coastal erosion. In fact, the Emilia Romagna region, which first acted against the coastal erosion problem, issued new laws to contrast it (Regional Plane for coastal protection (1981), Project Plane for sea protection and coastal environmental upgrading, (1996)). However, they were regulations based essentially on a "hardening approach", and its principles were taken as example by the other regions, particularly the Adriatic ones. As a result, the planning and execution of protection works mainly occurred without taking into account the dynamics of physiographic units and considering only the administrative limits of the executing body. This approach, as well as the urgency of carrying out the works, has often affected negatively results, worsening the situation or even causing new erosion phenomena on adjacent non-protected shores.

Fundamentally, Italy lacks of clear, integrated and management-aimed regulations for coastal areas. This is the reason why, most of the Italian coasts, particularly the Adriatic ones, are completely covered by hard structures. It is noteworthy that, some of Italian regions (i.e. Liguria, Emilia Romagna and Marche) subsequently adopted integrated coast management programmes to enforce European recommendations. Nevertheless, coastal environment planning and management activities are still weak and extremely fragmented due to the different duties conferred to a considerable number of different players.

1.1.2. Coastal evolution Modelling and Scale of analysis

Importance of understanding the parameters that govern the sediment transport processes is vital in order to establish the evolution trend of a coastal area, or overcome the problems occurring after the construction of structures.

Coastal erosion phenomenon vastly varies over either the space or the time scale. With respect to time scale, variability ranges between hours or even hundreds of years.

Short-term coastal erosion (on the time scale of hours and days) concerns essentially cross-shore phenomena, which are nothing but the dynamics between constructive and destructive forces, leading beach profile to oscillate seasonally about an average “equilibrium” configuration. Cross-shore sediment transport is inherently reversible, and accordingly cannot be considered as a “real coastal erosion” in spite singular storms may have a tremendous impact on coastal properties, even threatening human lives.

By contrast, coastal retreatment is intended in the following in a “structural way” and only long-term processes may have permanent effects on coastal evolution in this regard. For this reason, this PhD thesis will be focusing on them.

Long term processes lead shoreline evolution on time scales between 10 and 100 years, and are mainly related to breaking waves approaching obliquely to the shore. Differently from cross-shore transport, long shore processes are inherently not reversible

Without a proper grasp of these processes, shoreline evolution and outcomes of coastal structures may not be anticipated accurately. Anyhow, it is quasi impossible to fully predict the exact future beach plane form of a site, owing to the complexity of the problem, and the uncertainties of the data. However, there might be a chance to orient all the parameters in a logical manner to predict the future shoreline with basic assumptions. This is possible using mathematical or numerical engineering tools.

The need to calculate long-term shoreline change and compare performance of numerous engineering alternatives over long spatial extents and time frames has led to a wide use of numerical (shoreline response) models, like one shoreline models (Hanson and Kraus 1989), and multi-line shoreline models (Bakker 1969; Perlin and Dean 1983; Reeve and Valsamidis 2014). Among the others, one-line models, based on the original "one-line contour equation" developed by Pelnard-Considére, (1956), have shown practical capability in predicting shoreline change. The most popular models for shoreline change are GENESIS (Hanson, 1989), ONELINE (Dabees, 1998), UNIBEST (Deltares, 2011), LITPACK (DHI, 2005), GSb (Tomasicchio et al., 2020).

Moreover, also more complex process-based models can be adopted for a long-term modelling of beach evolution (coupling stationary mode and surfbeat mode), as demonstrated by Bart, 2017 in his Ph.D thesis.

Despite their simplicity One-line models have proven to be a powerful technique to assist in the understanding of processes involved and, in the case of necessary interventions, selection of the most appropriate project design. They provide a framework for organizing the collection and analysis of data and for evaluating alternative future scenarios of coastal evolution. In situations where engineering activities are involved, models are preferably used in developing problem formulation and solution statements, and, importantly, for efficiently evaluating alternative designs and optimizing the selected design.

As we will better analyse in the following chapters, under certain hypotheses the one-line contour equation, reduces to the diffusion equation, which is one of the cardinal partial differential equation of physics. Originally introduced to describe conduction of heat in solids, it has been subsequently applied to a notable range of physical phenomena, like pollution dispersion in fluids, or diffusive momentum transport in turbulence problems.

The present Ph.D. thesis explores the potentials of the diffusion equation to explain coastal erosion processes and comprehend shoreline evolution issues. The analysis of diffusion equation reveals peculiar aspects in coastal evolution also with respect to the long term impact of hard structures. Seeking and further deepening these aspects is the *leit motiv* of this work.

Therefore, after a massive research on previous literature, some aspects of diffusion theory have been identified, never been explored by the published research in this field so far, and namely: the effect of boundary constraints on the mid-term evolution of a stretch of coast of finite length, for which a complete analytical model has been provided; the effect of a time-varying diffusivity on shoreline evolution; the effect of a negative diffusion, and finally the relationship between wave crests and equilibrium bay shape profile.

Provided the unexplored aspects on diffusion equation, present work has been addressed to investigate the following main aims:

- providing new analytical solutions for the evolution of a coast of finite length, including new sets of boundary conditions. Particularly, the role of the confining constraints has been assessed on the long term response of an artificial nourishment of a given plane shape;
- analysing the impact of detached breakwaters, with a particular concern on the equilibrium of the protected beach, trying to find a physical interpretation of the role played by every structural parameter;
- exploring the engineering impact of the possible instabilities of the diffusion equation, connected to the high angle of waves to the shore.

The study is carried out either via theoretical approach, searching for analytical solution of practical interest of the heat equation, or via numerical approach, using the numerical one-contour line model GENESIS (Hanson and Kraus, 1989). Moreover, the analysis is supported by shoreline evolution data of Molise coast, relative to a long-term study between 1954 and 2016, which allowed a further comprehension of "diffusion problems" and peculiar features of coastal evolution.

1.2. Structure of the thesis

The thesis is structured as follows:

- In Chapter 2, long-shore and cross-shore sediment transport will be introduced conceptually and bulk sediment transport expressions will be discussed with respect to their derivations and capability to cover the related basic parameters. Then a focus on the Littoral Drift Rose (Walton and Dean, 1973; Walton and Dean, 2010) is given.
- One-line theory principles will be introduced in Chapter 3 together with the background, literature review and the basic assumptions and limitations. Moreover,

GENESIS, the most important and used one-contour line model is completely analysed, focusing on its fundamental relationships, empirical parameters, boundary conditions and coastal structures to be modelled.

- In Chapter 4, the switch from one-line equation to diffusion equation is described, considering all the assumptions and limitations. Moreover, an exhaustive review of the whole set of analytical solutions of the diffusion equations proposed in literature is given.
- In Chapter 5 new analytical solutions of the diffusion equation for a limited stretch of coast, including new sets of boundary conditions are provided, with a special focus on the behaviour of artificial nourishments of a given plane shape.
- In Chapter 6, we will assume that the diffusion coefficient to be time dependent, since the wave height and wave direction can vary over a long period with a certain frequency, depending on the wave climate characteristics. Therefore, a time varying diffusivity extra-effect is expected on long-term shoreline evolution. A new analytical solution for a time dependent diffusion is presented; then a discussion on the modelling of ε(t) function is presented. The general solution returns a shoreline evolution tending to a "stationary state", since the diffusion coefficient $\varepsilon(t)$ tends to a constant value ε_0 over a long period, and the mid-term analysis of the Molise coast is then used to validate in such a way this result.
- In Chapter 7 possible instabilities of the diffusion equation are analysed due to high angle of waves to the shore, and the Molise coast case of is then analysed. Moreover, impact of detached breakwaters on the shoreline evolution, as well as for the equilibrium conditions, is studied with the "diffusion approach", and the role of structural parameter is then assessed;
- In Chapter 8 static equilibrium of bays is further deepened with the diffusion approach;
- In Chapter 9, the conclusion and discussion of the results will be presented together with the recommendations for future studies.

Chapter 2: Engineering approach to littoral drift transport

2.1. Nature of the problem

Littoral processes result from the interaction of winds, waves, currents, tides, sediments and other phenomena in the littoral zone. Shores erode, accrete or remain stable depending on the rates at which sediment is supplied to and removed from the shore. Excessive erosion or accretion may endanger the structural integrity or functional usefulness of a beach or of other coastal structures. Therefore, an understanding of littoral processes represents a leading concern to coastal scientists and planners. In fact, study of shoreline change, and prediction of its future development, are essential for integrated coastal management operations, such as development of setback planning, hazard zoning, erosion-accretion studies, regional sediment budgets and conceptual or predictive modelling of coastal morphodynamics.

In this regard, shoreline change can be assessed on different timescales. On the one hand, short-term erosion (hours and days) is accountable for the cumulative damage by a storm, while, on the other hand, the long-term shoreline evolution is rather forced by continuous erosion (or accretion) over months and years.

As well explained by (Hanson and Kraus, 1990), in a long-term shoreline change analysis, the assumption of a clear shoreline trend is needed at the considered timescale. In this way, the "steady part" of the beach change signal is primarily controlled by both waves producing long-shore sediment transport and boundary conditions (such as structures). Cyclical and random events, such as storms or seasonal variations in waves, only produce a "noise component", which overlaps with the steady signal. Consequently, within a long-term analysis of shoreline change, effects due to cyclical phenomena are assumed to cancel over years, while the long-term shoreline trend is led by the spatial variations in the long-shore sediment transport rate.

In light of this, let us consider the scales of analysis involved in shoreline change studies.

The scales of primary concern to coastal planners and managers are time frames of years to decades, long-shore length scales of $10 \div 100$ kilometres, and cross-shore length scales of $1 \div 10$ kilometres. Within coastal zone management, prediction of coastal evolution with numerical models has proven to be a powerful technique to assist in the understanding of processes involved and, in the case of necessary interventions, selection of the most appropriate project design. Models provide a framework for organizing the collection and analysis of data and for evaluating alternative future scenarios of coastal evolution. In situations where engineering activities are involved, models are preferably used in developing problem formulation and solution statements, and, importantly, for efficiently evaluating alternative designs and optimizing the selected design.

Generally speaking, changes in coastal systems are forced by large-scale processes and are realized over relatively long (decadal) time scales. These changes have both natural and anthropogenic causes, e.g., erosion caused by sea level rise or changing supply and transport patterns of sediment caused by large coastal engineering projects. These changes highlight the importance of adequate quantitative tools to analyse and predict changes at these scales. A short-term, process-based approach is not directly suited for the prediction of longer-term coastal evolution, not only because of lack of computer power, but also because it is unclear whether these models include the relevant physics.

Broadly, short-term morphological processes are dominated by time-varying phenomena such as waves, tides, etc. Most of their effects, however, average out in the long run, whence the longer-time evolution is determined by much weaker residual effects, which are often disregarded in short-term models. The time-scales of interest for the present study regarding longer-time coastal evolution are from years to decades. The interesting aspect in this context is the cumulative morphologic effect of events at a decadal scale.

Anyhow, traditionally, and still in most everyday practices, a more aggregated view is taken, which basically implies the adoption of the existence of an explicit morphological equilibrium state under constant external forcing.

These, quite simplified models have proven to be able to reproduce different aspects of beach change successfully (e.i. one-line models). Certainly, when considering even longer, say recent geological, timescales, the modelling efforts are still limited to this type of approach.

Therefore, selecting models for long-term predictions in a specific case is not a trivial task. It requires a thorough analysis of the problem under consideration, and a clear definition of the objectives of the prediction. With that in mind, the appropriate spatial and temporal scales of the problem must be determined and matched with those covered by the available models. Figure 1 gives an overview of scales of applicability for available model types for modelling on yearly to decadal scale.

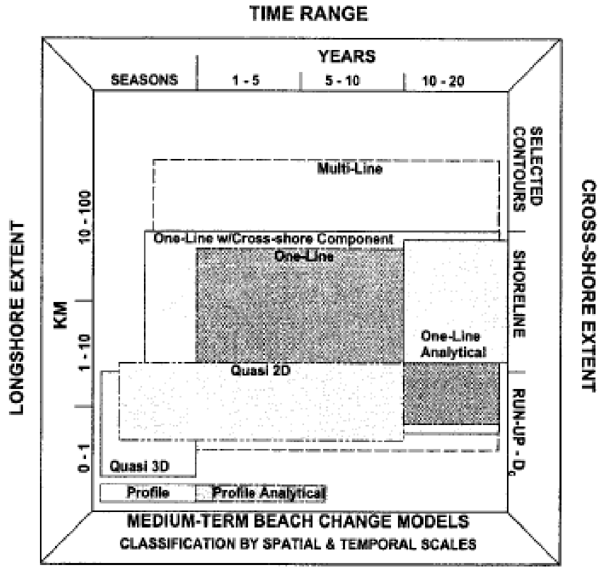

Figure 1 - Classification of beach change models by spatial and temporal scales. (from Hanson et al, 1993)

A definition of the scale of analysis is needed here to make more comprehensive the following paragraphs. Numerous authors presented a definition for the time windows of a shoreline change analysis (e.g. De Vriend, 1993).

In this work, according to Crowell et al (1993), a "Long-Term analysis" refers to a time window >60 years, a "Medium-Term analysis" refers to 10-60 years, and "Short-Term analysis" refers to a time window <10 years.

2.1.1. One-line models for shoreline change analysis

For long-shore shoreline (one- to multi-line) models we assume that both the equilibrium profile shape is known, and that the equilibrium shoreline orientation is known. What we simulate is the adjustment of the profile (in case there's more than one-line) and the shoreline orientation to a change in the forcing and boundary conditions or constraints, where the degree of deviation from equilibrium is proportional to the degree of adjustment. Obviously, adopting the idea of (dynamic) equilibrium is an important issue.

One-line shoreline evolution models have demonstrated their predictive capabilities in numerous projects (Hanson and Kraus, 1989). This class of models calculates shoreline position changes that occur over a period of years to decades. The spatial extent varies from the single project scale of hundreds of meters to the regional scale of tens of kilometres. Changes in shoreline position are assumed to be produced by temporal evolution of spatial differences in the *long-shore* sand transport rate (Hanson and Kraus, 1989). Thus, this type of model is best suited to situations where there is a systematic trend in long-term change in shoreline position, such as recession down-drift of a groin. Cross-shore transport effects, such as storm-induced erosion and cyclical movement of shoreline position associated with seasonal variation in wave climate, are assumed to cancel over a long enough simulation period or are accounted for through external calculation.

Therefore, a good estimation of the primary forcing of evolution of shoreline at longer time scale, the long-shore sediment transport rate is needed.

In the following, an assessment of long-shore and cross-shore sediment transport concept is given; moreover, the processes involved are investigated and finally the main formulae proposed in literature for the estimation of the long-shore transport rate are briefly analysed and reviewed.

2.2. Cross-shore sediment transport concept

The long-shore sediment transport is mostly due to the wave-induced long-shore current, whereas cross-shore transport is a result of the water motions due to the waves and the undertow. However, the coupling between the hydrodynamics and the sediment transport is not all that well understood. Seasonal shoreline changes are usually considered to be in response to the greater incidence of storms during winter and the associated seaward sand transport and storage in nearshore bar features.

2.2.1. The beach profile

The beach profile is the variation of water depth with distance offshore from the shoreline. The equilibrium profile is conceptually the result of the balance of destructive versus constructive forces.

2.2.1.1. *Constructive and destructive forces acting on beach profile*

An equilibrium beach profile represents a balance of destructive and constructive forces acting on the beach. If either of these two competing types of forces is altered as the result of a change in wave- or water-level characteristics, there is an imbalance: the larger force dominates until the evolution of the beach profile brings the forces back into balance.

Many different destructive and constructive forces affect beach profiles. At present, neither the complete identification nor the quantification of these individual forces is well understood; however, it is possible to recognize their presence and, through empirical means, to quantify the role that they play in the establishment of the equilibrium beach profile and also in profiles that are out of equilibrium.

2.2.1.2. *Destructive forces*

Of all the destructive forces, gravity is the most important, as it tries to make the equilibrium profile horizontal. An additional destructive force, which appears to be very significant, is the high turbulence level that exists within the surf zone. Breaking waves transform organized wave energy into highly chaotic turbulent fluctuations. These turbulent fluctuations act to dislodge sediment particles that are marginally stable and, in concert with the gravitational forces acting on these sediment particles, transport them in an offshore direction. The significance of the turbulence is evident to one swimming in the surf zone with different beach profiles. A profile with a mild beach slope will be characterized by relatively low turbulence levels because the breaking process is distributed over a wide surf zone, and, in some cases, it is doubtful whether the turbulence actually penetrates with sufficient strength to the bottom to cause any disturbance of the sediment. In a surf zone with a steep beach profile, a wave will dissipate its energy within a very limited volume, and thus the magnitude of the turbulent fluctuations is necessarily much higher and extends much deeper into the water column. Because of their abilities to remain stable under various levels of turbulent energy, beaches composed of fine and coarse sediments will be associated with mild and steeper slopes, respectively.

Undertow, the seaward return of the wave-induced mass transport, transports suspended sediment offshore and causes seaward-directed shear stresses that contribute to an offshore bedload transport.

2.2.1.3. *Constructive forces*

At least two individual constructive forces can be identified as agents that form beach profiles. The first is due to the net onshore shear stresses at the bottom that result from the nonlinear (asymmetric) form of a shallow-water wave. Both the wave profile and the water particle velocities beneath a periodic nonlinear wave are symmetric about the crest, and the higher velocities occur under the crest but extend over a shorter time period than the negative velocities that occur under the trough.

Even though the theoretical velocity predictions result in a zero mean velocity at the bottom (the velocity is a series of sins or cosine functions that each average to zero over a wave period), the mean shear stress $\overline{\tau_b}$ because of its quadratic relationship to the near-bottom velocity u_{bw}

$$\overline{\tau_b} = \frac{f}{8}\,\rho\,\overline{u_{bw}\cdot|u_{bw}|} \tag{2.1}$$

results in a mean onshore shear stress.

A second constructive force is due to boundary layer drift. At the bottom, motion is rotational, viscous, which implies that the velocity components (u_w and w) are not out of phase of 90°, therefore $\rho\,\overline{u_w w} \neq 0$. This also results in a mean current onshore directed.

2.2.2. Equilibrium beach profile

Consider a beach with a constant slope, by carrying out a balance on the flow rates we obtain, as a net effect:

$$-\frac{\partial q}{\partial x}dx\,dt = -\partial h\,dx \qquad \rightarrow \qquad \frac{\partial q}{\partial x} = \frac{\partial h}{\partial t} \tag{2.2}$$

Eq. (2.2) states that if the flow rate q is increasing, the value of h also increases (intended as a lowering of the seabed).

Assuming that, at the beach profile, the forcings are overall destructive, the "bar profile" or "winter profile" is determined (Figure 2).

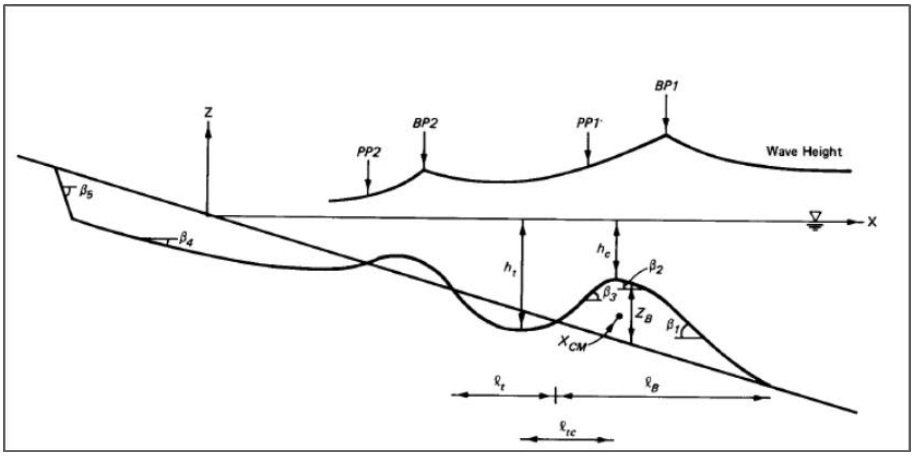

Figure 2 - "Bar profile" or "winter profile"

For a bar profile, the net flow is always positive, throughout the active beach, obviously this flow is none other than the undertow. The trend of the profile is shown in Figure 2: there is a first portion of the profile characterized by a very high slope (shoe), a second part characterized, instead, by a less pronounced slope (terrace) followed by a berm, which provides information on the breaking depth of higher waves. The overall effect is erosive: the shoreline is in fact set back. In constituting the "terrace" the seabed defends itself by becoming more dissipative; at the same time also the formation of the bar represents a defensive mechanism, as it causes the breaking of the highest waves.

On contrary, if the forcings are, on the whole, constructive, the "berm profile" or "summer profile" is determined.

In these conditions, the flow is negative in the whole beach profile considered: in a first section the flow is decreasing, causing an accumulation of material at shore line; subsequently the flow becomes increasing causing a lowering of the seabed (Figure 3).

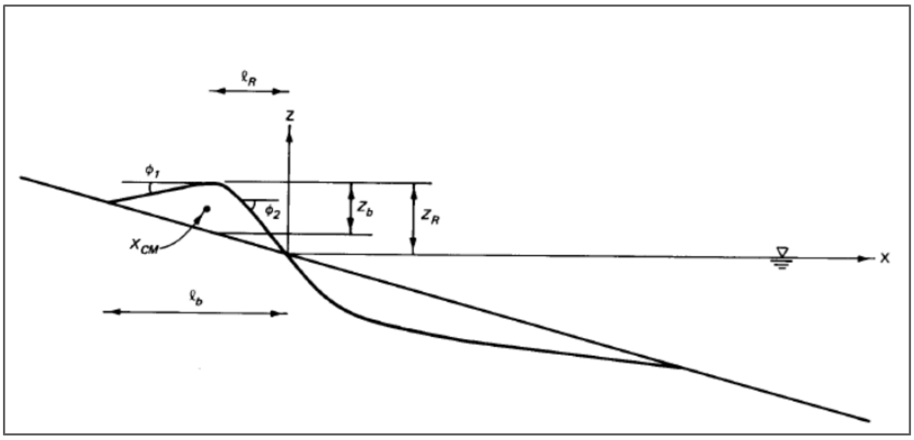

Figure 3 - "Berm profile" or "summer profile"

Note that the slope of the central area is greater than the initial one, for this reason the berm profile is also called the "reflective profile". The berm that forms is mobile over time, unlike the berms of the backshore area, which are fixed at least until the most intense storms arrive.

It is assumed that, in the long term, the nourishing and destructive conditions compensate for each other, causing the profile to oscillate between the bar profile and the berm profile: the average oscillation profile is called the "equilibrium profile".

2.2.3. The Brunn-Dean equilibrium profile

The solid flow through a certain section is proportional to the amount of turbulence injected into the liquid column: the solid flow is, therefore, proportional to the power dissipated by breaking per unit of volume.

The dissipated power per unit area is defined as $\frac{dE_f x}{dx}$, assuming attack: dividing this quantity by the depth h, the dissipated power per unit of volume is obtained. To have equilibrium conditions, the solid discharge must be constant according to the direction of propagation of the wave motion, x; then the power dissipated per volume unit must also be constant. It is expressed as:

$$\frac{1}{h} \cdot \frac{dE_{fx}}{dx} = D_e \tag{2.3}$$

Where D_e indicates the equilibrium dissipation. Developing Eq. (2.3), and considering the values assumed by the wave height and the group speed in the surf zone, $H = \gamma h$ and $C_g = \sqrt{gh}$, we have:

$$h = \left(\frac{24}{5} \frac{D_e}{\rho g^{3/2} \gamma^2}\right)^{2/3} \cdot x^{\frac{2}{3}} \tag{2.4}$$

where the term ($\left(\frac{24}{5} \frac{D_e}{\rho g^{3/2} \gamma^2}\right)^{2/3}$ is defined as a scale parameter A, and dimensionally it is a length to 1/3.

$$A = \left(\frac{24}{5} \frac{D_e}{\rho g^{\frac{3}{2}} \gamma^2}\right)^{\frac{2}{3}} \tag{2.5}$$

Therefore:

$$h = A \cdot x^{\frac{2}{3}} \tag{2.6}$$

Called the "Brunn-Dean equilibrium profile, determined assuming that the flow rate was proportional to the power dissipated per unit of volume.

Form Eq. (2.5) we obtain

$$D_e = \frac{5}{24} \rho g^{\frac{3}{2}} \gamma^2 A^{3/2} \tag{2.7}$$

The A parameter is linked to the particle size, in fact the solid flow rate is greater the finer the material. To derive an explicit dependence of A on the particle size, it can be considered that the dissipated power per volume unit must equal the necessary power to keep the sediments in suspension, concentrated in an elementary volume of fluid. In fact, if the material in the volume settles, the flow rate decreases. Therefore:

$$D_e = \varepsilon\,(\rho_s - \rho_w) g v_F = \varepsilon\,(s-1) \rho g v_F \tag{2.8}$$

Substituting in Eq. (2.5)

$$A = \left(\frac{24}{5} \frac{\varepsilon\,(s-1)\rho g v_F}{\rho g^{\frac{3}{2}} \gamma^2} \right)^{\frac{2}{3}} = \left(\frac{24}{5} \frac{\varepsilon\,(s-1)}{\gamma^2} \right)^{\frac{2}{3}} \cdot \left(\frac{{v_F}^2}{g} \right)^{\frac{1}{3}} \tag{2.9}$$

A depends on the grain size of the sediments through the fall velocity v_F.

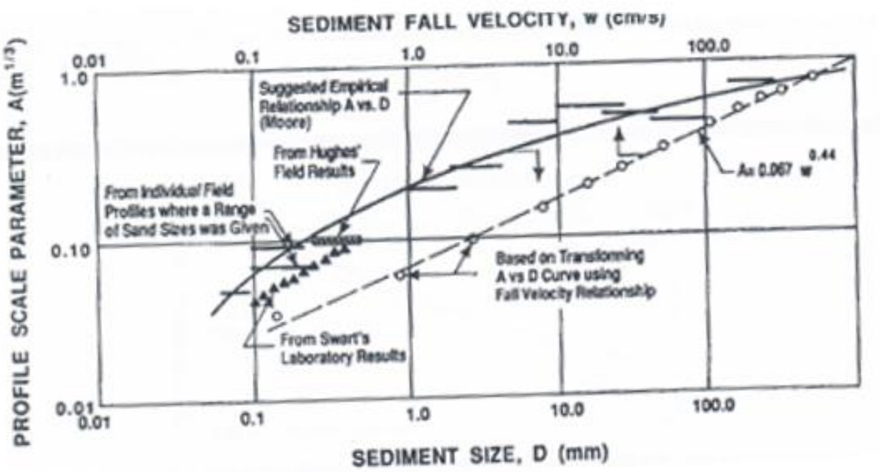

Figure 4 - Scale factor A as a function of the rate of fall (Dean 1987, Moore 1982)

From laboratory data, the following relation has been obtained:

$$A = 2{,}25 \cdot \left(\frac{{v_F}^2}{g} \right)^{\frac{1}{3}} \tag{2.10}$$

valid for a water temperature of about 20 ° C and for ordinary sands, with sedimentation speed between 1 and 10 cm / s.

2.3. Long-shore sediment transport concept

Long-shore sediment transport rate is the governing parameter of long and midterm movement of the shore: it can be defined as shore parallel movement of the sediment caused by nearshore currents driven by oblique waves, wind and tide. In accordance with one-line theory, cross-shore sediment transport rate onshore and offshore balance each other in long term scale yielding an almost unchanged profile viewed in long term scale. Therefore, the spatial variations in the long-shore sediment transport rate are considered to lead to changes in the shoreline.

The prediction of reliable estimates of long-shore sediment transport is of considerable practical importance in coastal engineering since it plays the most significant role whether the shore erodes, accretes or keeps its stability (CEM, 2003). An example is the evaluation of sediment budgets for coastal areas with and without structures (breakwaters, groins). Another example is the long-term stability of beach protections and beach nourishments.

As indicated in literature, most of the beaches are eroding, which is an implication of coastal land loss. The causes of erosion are divided into four main groups by Kamphuis (2000) as follows:

- Decrease in sediment supply
- Comminution (Continuous grinding process of sediment by waves)
- Submergence
- Human interference

Kamphuis (2000) states that the beach material formed thousands of years ago by large amounts of river discharge and ice-age glaciers retreat, however large fluctuations in water levels produce the present environmental conditions which form a base for erosion. A good example of substantial reduction of sediment discharged to deltas by rivers owing to the construction of flow regulation structures is expressed in Buccino et al. (2020) and Rosskopf et al. (2018). Submergence takes place caused by the sea level rises basically due to global warming and melting of glaciers being exposed to higher wave action closer to the shore (Kamphuis, 2000).

2.3.1. Littoral drift and beach drift

Long-shore movement of sediment is a process that consists of the transportation of sediments (clay, silt, pebbles, sand, and shingle) along a coast parallel to the shoreline, which is dependent on the incoming wave direction. Oblique incoming wind squeezes water along the coast, and so generates a water current, which moves parallel to the coast. Long-shore drift is simply the sediment moved by the long-shore current. This current and sediment movement occur within the surf zone. The process is also known as littoral drift.

Beach sand is also moved on such oblique wind days, due to the swash and backwash of water on the beach. Breaking surf sends water up the beach (swash) at an oblique angle and gravity, then drains the water straight downslope (backwash) perpendicular to the shoreline. Thus, beach sand can move down-beach in a saw-tooth fashion many tens of meters per day. This process is called "beach drift" but some workers regard it as simply part of "long-shore drift" because of the overall movement of sand parallel to the coast (Figure 5).

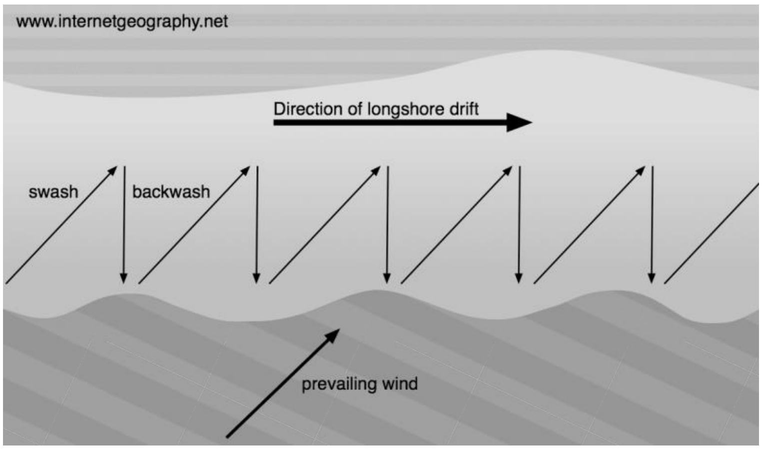

Figure 5 – Beach drifting

Long-shore drift affects numerous sediment sizes as it works in slightly different ways depending on the sediment (e.g. the difference in long-shore drift of sediments from a sandy beach to that of sediments from a shingle beach). Sand is largely affected by the oscillatory force of breaking waves, the motion of sediment due to the impact of breaking waves and bed shear from long-shore current. Because shingle beaches are much steeper than sandy ones, plunging breakers are more likely to form, causing the majority of long shore transport to occur in the swash zone, due to a lack of an extended surf zone.

In the following, we will refer to the key process of sand movement along the shore, the littoral drift, due mainly to the long-shore current from oblique attack.

2.3.2. Gross and net littoral transport

The shoreline may be exposed to waves from a variety of directions in which angles between the shore normal and the wave rays approaching from the left (when looking offshore) are denoted as positive angles (α_L), whereas angles between the shore normal and the wave rays approaching from the right (when looking offshore) are denoted as negative angles (α_R) as shown in Figure 6. The transport rates to the right, occurring due to the waves coming from the left can be summed up to Q_R, and the transport rates to the left resulting from the waves coming from right can be added to form Q_L. Gross sediment transport rate equals to the sum of the absolute magnitudes of these two rates while the net transport is equal to the difference of these two transport rates and larger of Q_R and Q_L dictates the direction of the net sediment transport rate.

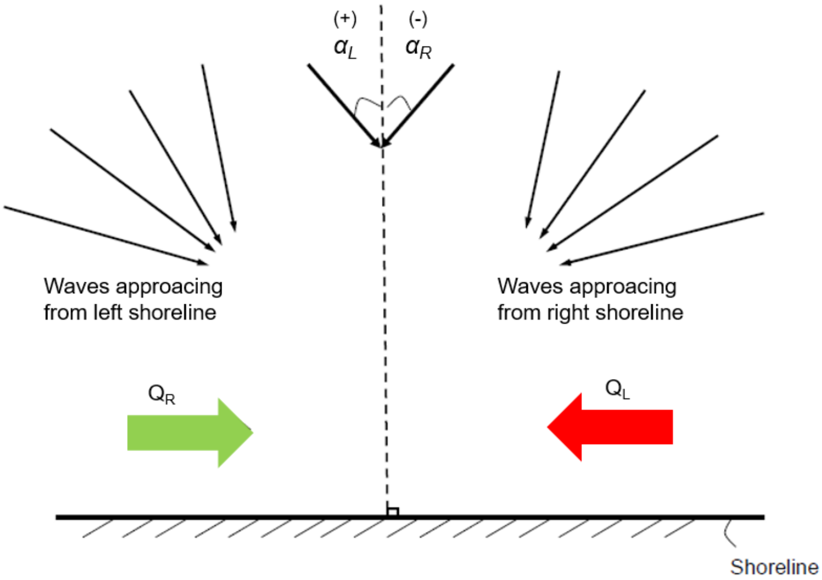

Figure 6 - Long-shore sediment transport directions

In general Q_R is denoted as positive and Q_L is regarded as negative.

$$Q_{GROSS} = Q_R + |Q_L| \tag{2.11}$$

$$Q_{NET} = Q_R + Q_L \tag{2.12}$$

From the points of view of engineering applications, gross transport rate, being irrespective of direction, may be used to estimate the shoaling rates in navigation channels and uncontrolled inlets whereas the net direction transport indicates the accretion and erosion patterns especially in the vicinity of the coastal structures (CEM, 2003).

The ratio between the net and the gross drift provides an estimate of the persistence of the wave climate.

2.4. Littoral drift forcings

The primary forcing of the long-shore sediment transport is the long-shore current from oblique attack.

According to the Near Shore Equations, at the basis of coastal hydrodynamics, Stokes solved it taking into account the variation of the mean sea level, $\bar{\xi}$. The result was a relationship for the so-called edge waves, with amplitude decreasing with the distance from the shoreline.

The momentum equation along the y direction (parallel to the coast), in fact, states that within the surf zone, the Radiation stress gradient S_{xy} is not zero, differently from out of the surf zone, obtaining:

$$\frac{dS_{xy}}{dx} + \overline{\tau_{by}} = 0 \tag{2.13}$$

Therefore, from Eq. (2.13) it is seen that there is a current that moves parallel to the shore, related to the tangential stress at the bottom, $\overline{\tau_{by}}$. The value of the long-shore current speed is equal to (Longuett-Higgings, 1970):

$$U_y = \frac{5}{16}\frac{\gamma m\pi}{C_D}\frac{\sin\alpha_0}{c_0}\, g\, d_b \left(\frac{d_0}{d_b}\right) \tag{2.14}$$

Where

- γ is the breaker index;
- m is the beach slope;
- C_D is the Drag coefficient;
- α_0 is the offshore wave angle;
- c_0 is the offshore wave celerity;
- d_0 is the depth.
- g is the gravity.

The ratio between the depth and the breaking depth, $\frac{d_0}{d_b}$, also represents the ratio $\frac{|x|}{|x_b|}$ due to the flat bottom, and considering that the quantity $\frac{5}{16}\frac{\gamma m\pi}{C_D}\frac{\sin\alpha_0}{c_0}\, g\, d_b$ is the maximum speed value, the following dimensionless relation is obtained:

$$V = \frac{U_y}{U_{max}} = \frac{|x|}{|x_b|} = X \tag{2.15}$$

Which states that the long-shore current speed increases from 0, near the shoreline, to a maximum near the breaking point, where $d_0 = d_b$. Outside surf zone the long-shore current speed tends to zero (Figure 7).

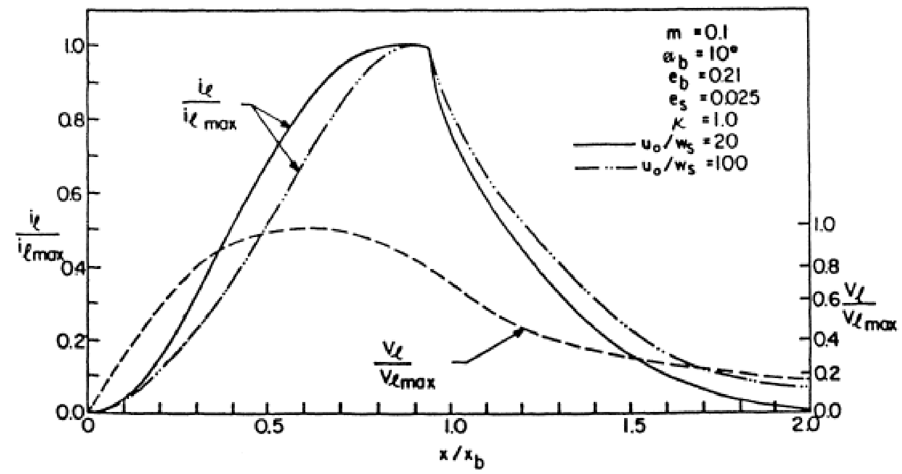

Figure 7 - Normalized long-shore transport distribution across a planar beach (Bodge, 1989)

The long-shore current is the primary causing force of the long-shore sediment transport, its characteristics are completely different compared to the cross-shore mechanism. The cross-shore mechanism is reversible, with accretion during summer and erosion during winter. This rhythmic trend produces, over the year, an equilibrium shape of the beach profile.

On contrary, the long-shore mechanism is irreversible. On the one hand, during summer the surf zone is almost confined, practically vanished, with $U_y = 0$; on the other, during winter, the surf zone is much wider due to the intense storm conditions: turbulence suspends beach sediments which are then captured by the long shore current and moved away. Therefore, the long-shore sediment transport prevails only during winter months, during summer the current does not reverse (as happens in the cross-shore mechanism), consequently an equilibrium condition is not reached.

For these reasons, long-shore transport is of a “structural type”, it depends on the coast exposure, acting in only one direction. Particularly, the presence of a long-shore transport is not worrying in itself, but rather the formation of a transport differential able to cause erosion along a certain stretch of coast.

Another noteworthy long-shore forcing is certainly the long-shore current associated to the nearshore circulations cells, the so-called feeder currents, which are determined by a wave height differential along the shore, caused by a variation of the seabed (Figure 8). Feeder currents feeds the possible rip currents that move offshore. However, in terms of sediment transport, feeders are not as crucial as the rip current.

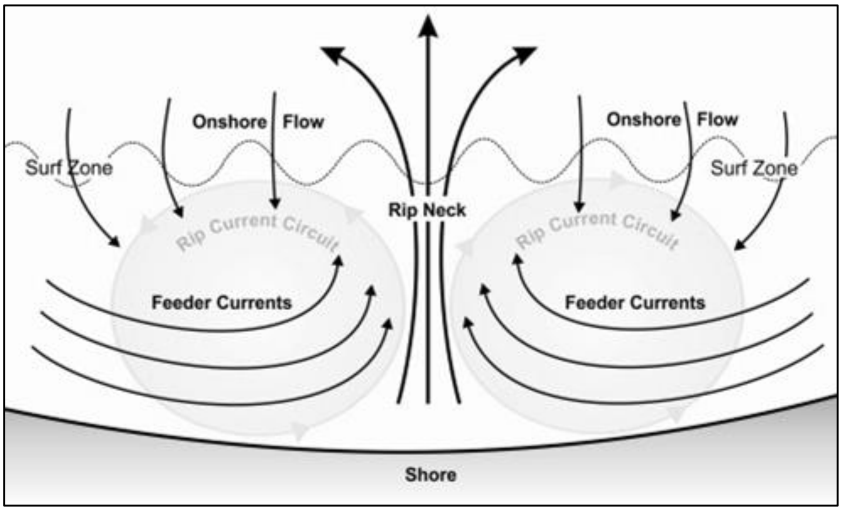

Figure 8 - Schematic of the main features in rip current system.

Moreover, another process of long-shore transport is represented by the diffraction currents, caused by a strong long-shore variability in wave breaking. This variability may be caused by such features as sandbars, by piers and jetties or detached breakwaters.

2.5. Littoral drift formulae

There are many predictive formulas available in the literature for the littoral drift computation. Here we want to give a brief review of the widely referred to long-shore transport formulas to gain an insight into the available methods, commonly used parameters and formula performance. More details can be found for instance, in Mil-Homens et al. (2013), and Samaras and Koutitas (2014), and earlier by Bodge (1989) and Bodge and Kraus (1991).

2.5.1. CERC formula

The most common expression for sediment transport rate is that of the Shore Protection Manual (SPM, 1984). The potential sediment transport rate is commonly related with the long-shore component of wave power.

$$P_l = \left(E\ c_g\right)_b \sin\alpha_b \cos\alpha_b \tag{2.16}$$

where P_l is the long-shore component of wave power in (N/sec). E_b is the wave energy calculated from:

$$E_b = \frac{1}{8}\rho g\, H_b^2 \tag{2.17}$$

And c_{gb} is the group velocity in shallow water given by $\sqrt{gh}$, ρ is the fluid density, g is the gravity H_b is breaking wave height, d_b is breaker depth, α_b is the effective breaking angle with respect to shoreline.

$$I_l = K\, P_l \tag{2.18}$$

where I_l is the immersed weight of sediment transport in (N/sec.), K is an empirical dimensionless coefficient. The expression for the I_l is:

$$I_l = (\rho_s - \rho_w) g (1-n) Q_l \tag{2.19}$$

By equating Eq. (2.18) and Eq. (2.19), yields the well-known CERC formula:

$$Q_l = \frac{K}{16} \cdot \frac{1}{(s-1)(1-n)}\; H_b^{\frac{5}{2}} g^{\frac{1}{2}} \gamma_b{}^{-\frac{1}{2}} sen\,(2\alpha_b) \tag{2.20}$$

The values of the parameters for use are as follows: ρ_s =2650 kg/m^3, ρ_w=1025 kg/m^3 for salt water and 1000 kg/m^3 for fresh water, porosity is most commonly assumed as 40% and the breaker depth index γ_b is taken as 0.78.

The calibration of K coefficient has been a discussion issue for years and many different values have been proposed ranging from 0.2 to 1.6 (van Rijn, 2002). For the coefficient of K a value of 0.39 is presented in SPM (1984) based on computations utilizing the significant wave height, H_s. Komar (1971) indicates that K decreases with both decreasing energy levels and increasing sediment grain sizes.

To relate the CERC formula with the sediment grain size, del Valle et al., (1993) have presented an empirical formula based on transport rates from aerial photographs of 30 year period shoreline change with use of root mean square wave height, H_{rms} and given by $H_{rms} = \frac{H_s}{\sqrt{2}}$ where H_s is the significant wave height.

$$K = 1.4\, e^{(-2.5 D_{50})} \tag{2.21}$$

where D_{50} is the mean grain size in millimetres.

2.5.2. Kamphius' formula

Kamphuis (1991) has also developed a volume bulk expression for long-shore sediment transport based on 3-D hydraulic model tests with regular and irregular waves. By non-dimensionalisation of related sediment transport parameters in addition to simultaneously measured wave heights at deep water and through the surf zone, breaking wave angles, long-shore current velocity distribution, bed load and suspended load distributions in the experiments lead to a more refined sediment transport formula which covers wave steepness, wave breaking angle beach slope and relative grain size. Long-shore sand transport rate (Q_l) according to Kamphius formulation in m^3/hour is given as:

$$Q_l = 6.4 \cdot 10^4 {H_b}^2 T^{1.5} m^{0.75} D_{50}^{-0.25} (\sin 2\alpha_b)^{0.6} \qquad \text{in} \frac{\mathrm{m}^3}{\mathrm{year}} \tag{2.22}$$

$$Q_l = 7.3\ {H_b}^2 T^{1.5} m^{0.75} D_{50}^{-0.25} (\sin 2\alpha_b)^{0.6} \qquad \text{in} \frac{\mathrm{m}^3}{\mathrm{hour}} \tag{2.23}$$

where H_b is the breaker height, T is the significant wave period, *m* is the beach slope at the particular location where breaking occurs. D_{50} is the median grain size diameter of the sediment, α_b is the efficient wave approach angle during breaking. It is seen that Kamphuis's long-shore sediment transport rate expression is proportional to ${H_b}^2$and ((sin $2\alpha_b)^{0.6}$ both of which tend to correct the overestimating trend of CERC expression, which is criticized particularly for major storms (Kamphuis, 2000). Expression of Kamphuis is a recently accepted formula which is used widely since it covers the important parameters such as wave period, grain size and beach slope.

2.5.3. Van Rijn's formula

Van Rijn (2014) tried to develop a more general formula regarding the grain size to be accounted for. To achieve this, the author used laboratory and field data, as well as the results of numerical simulation (to extend the dataset) and proposed a dimensionally homogenous formula for a wide range of particle sizes between 0.1 and 100 mm (i.e. sand, gravel and shingle). The formula considers the effect of swell waves, as the author found a larger long-shore sediment transport rate for regular swell waves compared with irregular wind waves of similar wave height. The formula to calculate the long-shore sediment transport volumetric rate Q_l (in m^3/s) is:

$$Q_l = \frac{0.00018\sqrt{g}}{(1-p)} K_{swell} {H_{sb}}^{3.1} {m_b}^{0.4} D_{50}^{-0.6} \ \sin 2\alpha_b \tag{2.24}$$

The swell factor, K_{swell}, is a coefficient related to p_{swell}, which is the percentage of low-period swell waves of all the wave records (about Q_l10% to 20% for sea coasts and 20% to 30% for ocean coasts). Van Rijn (2014) noticed that 1 < K_{swell} < 1.5 but did not specify any formula for it. Hence, through personal communication, the following approximation has been used in this study:

$$K_{swell} = MAX\left\{1, MIN\left[1.5, 1.5 - 10\left(\frac{H_{sb}}{L_0} - 0.01\right)\right]\right\} \tag{2.25}$$

The main difference between the functional form of Van Rijn's and Kamphuis' formulas is the effect of wave period, which is indirectly considered in K_{swell}.

2.5.4. Tomasicchio *et al.*'s formula

Tomasicchio *et al.* (2013, 2018) revised an equation originally used for designing re-shaped berm breakwaters, by introducing a modified (armour) stability number (N_s^{**}). Their model belongs to the typology based on an energy flux approach combined with an empirical relationship between the wave induced forcing and the number of moving sediment grains/units. Specifically, the GLT model considers an appropriate mobility index and assumes that the units move during up- and down-rush with the same obliquity of breaking and reflected waves at the breaker depth (Tomasicchio et al, 2013). A sediment grain/unit passes through a certain control section if and only if it is removed from an updrift area of extension equal to the longitudinal component of the displacement length $l_d \sin\theta_d$, where l_d is the displacement length and θ_d is its obliquity (Figure 9).

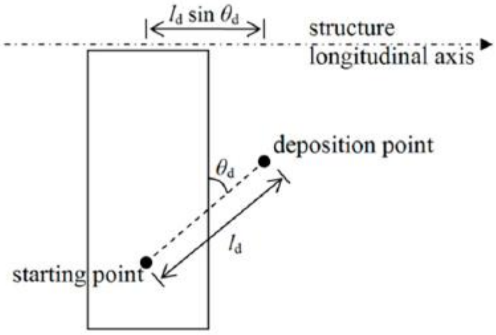

Figure 9 - Definition sketch for the General Long-shore Transport (GLT) model (from Tomasicchio et al. 2020).

This process description is particularly true when considering the wave obliquity, the up-rush and related long-shore transport at the swash zone. By assuming that the displacement obliquity is equal to the characteristic wave obliquity at breaking ($\theta_d = \theta_{k,b}$), and that a number N_{od} of particles removed from a nominal diameter, $D_{n,50}$, wide strip moves under the action of 1000 waves, then the number of units passing a given control section in one wave is:

$$S_N = \frac{l_d}{D_{n,50}} \frac{N_{od}}{1000} \sin(\theta_{k,b}) = f(N_s^{**}) \tag{2.26}$$

Where:

$$N_s^{**} = \frac{H_k}{c_k D_{n,50}} \left(\frac{s_{m,0}}{s_{m,k}}\right)^{-\frac{1}{5}} (\cos\theta_0)^{2/5} \tag{2.27}$$

N_s^{**} is the modified stability number with: H_k = characteristic wave height; $c_k = H_k/H_{s,0}$ where $H_{s,0}$ = significant offshore wave height; θ_0 = offshore wave obliquity; $s_{m,0}$ = mean wave steepness at offshore conditions and $s_{m,k}$ = characteristic mean wave steepness (assumed equal to 0.03). N_s^{**} resembles the traditional stability number, N_s (Van der Meer, 1988), taking into account the effects of a non-Rayleighian wave height distribution at shallow water, wave steepness, wave obliquity and the nominal diameter of the sediment grains/units. The authors in Tomasicchio et al., 2013 reported that H_k has to be considered equal to $H_{1/50}$, but $H_{2\%}$ can also be adopted. In the first case c_k = 1.55, in the second case c_k = 1.40. The second factor in Eq. (2.27) is such that $N_s^{**} \cong N_s$ for $\theta_0 = 0$ if $s_{m,0} = s_{m,k}$.

In the case of a head-on wave attack, under the assumption that, offshore the breaking point, the wave energy dissipation is negligible and that waves break as shallow water waves, the following relation holds:

$$F = \frac{1}{8}\rho g {H_0}^2 {c_{g0}}^2 = \frac{1}{8}\rho g {H_b}^2 {c_{gb}}^2 \tag{2.28}$$

In Eq. (2.28), F = wave energy flux, ρ = water density, g = gravity acceleration, H_0 = offshore wave height, c_{g0} = offshore wave group celerity, H_b = wave height at breaking and c_{gb}= is the wave group celerity at breaking. Eq. (2.28), related to the breaker index $\gamma_b = H_b/h_b$, with h_b = breaking depth, implies:

$$H_b = H_0 \left(\frac{\gamma_b}{4k_0 H_0}\right)^{1/5} = qH_0 {s_0}^{-1/5} \tag{2.29}$$

The authors found the best agreement with field laboratory data assuming $\gamma_b = 1.42$ or the proportionally constant q = 0.56. It follows that, considering the characteristic wave height at breaking $H_{k,b}$, and$s_{m,0} = s_{m,k} = 0.03$, N_s^{**} can be also written as:

$$N_s^{**} = \frac{0.89 H_{k,b}}{c_k D_{n,50}} \tag{2.30}$$

According to the refraction theory for plane and monotonically decreasing profiles, $H_{k,b}$ and $\sin(\theta_{k,b})$, are evaluated as in the following:

$$H_{k,b} = \left({H_k}^2 c_g \cos\theta_0 \sqrt{\gamma_b / g}\right)^{2/5} \tag{2.31}$$

$$\sin(\theta_{k,b}) = \frac{c_{k,b}}{c} \sin\theta_0 \tag{2.32}$$

$$c_{k,b} = \sqrt{g H_{k,b} / \gamma_b} \tag{2.33}$$

where c_g=group celerity and $c_{k,b}$ is the characteristic wave celerity at breaking depth. The displacement length is calculated as:

$$l_d = \frac{(1.4 N_s^{**} - 1.3\,)}{\tanh^2(kh)}\, D_{n,50} \tag{2.34}$$

where k = wave number and h = water depth.

N_{od} has been determined following a calibration procedure based on the least-squares method, taking into account nine high quality data sets of long-shore transport from field and laboratory experiments for a wide mobility range of sediment grains/units: from stones to sand. In total, the nine data sets consist of 245 cases (Tomasicchio et al. 2020). In particular, N_{od} values are partitioned in two intervals: the first interval refers to $N_s^{**} \leq 23$, from reshaping type berm breakwaters to gravel beaches; the second one relates to $N_s^{**} > 23$, for sandy beaches. For$N_s^{**} > 23$, a third order polynomial approximating function provides a satisfactory agreement as shown by the authors. N_{od} is given by:

$$N_{od} = \begin{cases} 20 N_s^{**}\,(N_s^{**} - 2)^2 & N_s^{**} \leq 23 \\ \exp[2.72 \ln(\,N_s^{**}) + 1.12] & N_s^{**} > 23 \end{cases} \tag{2.35}$$

The estimated correlation coefficient is equal to 0.89 for $N_s^{**} \leq 23$ and 0.92 for $N_s^{**} > 23$. The long-shore transport rate, Q_l, can be also expressed in terms of [m^3/s] as in the following

$$Q_l = \frac{S_N {D_{n,50}}^3}{(1-n)T_m} \tag{2.36}$$

where T_m = mean wave period, and n = porosity factor.

2.5.5. Ozasa's formula

In normal situations, along-shore sediment transport on a beach is caused by the oblique breaking of waves, and this mechanism has been extensively studied. In some cases, however, along-shore wave height gradients must also be considered. Such situations often occur when waves diffract around a headland or a breakwater. The Ozaka's formula here reported is that used within the one-line numerical model GENESIS (Hanson and Kraus, 1989), to compute the sediment transport rate.

Bakker (1971) calculated the along-shore current velocity due to oblique wave attack and along-shore variation of wave height. His result was:

$$u = -\frac{5\pi\, \gamma\, \sqrt{8g}\, m}{16\, pk\, \sqrt{f}} \left\{ \frac{h}{\sqrt{h_i}} \frac{dy_0}{dx} + \left(1 + \frac{\gamma^2}{8}\right) \frac{dh_b}{dx} \frac{\sqrt{h}}{\tan\beta} \right\} \tag{2.37}$$

Where:

- u is a long-shore current velocity,
- h is a water depth in the breaker zone,
- h_i is a slightly greater water depth than the maximum breaker depth h_b,
- $y_0$is a position of the line which is an intersection between the still water surface level and the beach prof'de. y_0 is a function of along-shore distance x,
- $\tan\beta$ is a beach slope,
- γ is a ratio between breaking wave heights and water depths in the breaker zone and is usually taken as 0.8,
- k is the yon Karman constant (= 0.4),
- f is the Darcy-Weisbach friction coefficient,
- p is Bijker's 'constant'. According to Bijker (1967) $p \sim 0.45$, but Swart (1974) showed that p is given more accurately by $\sqrt{f_w/2} \cdot 1/k$ where $f_w$is the wave friction factor derived by Jonsson (1966);
- g is the acceleration due to gravity;
- and $m = \frac{\partial h}{\partial y} = \frac{\tan\beta}{\left(1+\frac{3}{8}\gamma^2\right)} = (1-K)\tan\beta$

where $K = \left(1 + \frac{8}{3\gamma^2}\right)^{-1}$ which assuming $\gamma = 0.8, K = 0.194$

Bakker (1971) did not take horizontal mixing into account so Eq. (2.37) is not correct locally. However, the only effect of such mixing is to eliminate the discontinuity of velocity at the breaker line and produce a smoother velocity profile down the beach, see Longuett-Higgins (1970). Thus, by integrating Eq. (2.37) we obtain the total along-shore current:

$$\bar{V} = \left(\frac{2C_2}{3} h_b + \frac{4}{5} C_3 {h_b}^{1/2}\right) C_1 (1 - K) \tan\beta \tag{2.38}$$

Where:

$$C_1 = -\frac{5\pi\, \gamma \sqrt{8g}}{16\, pk \sqrt{f}} = -4.36 \sqrt{\frac{8g}{f}} \tag{2.39}$$

$$C_2 = \frac{1}{\sqrt{h_i}} \frac{dy_0}{dx} \tag{2.40}$$

$$C_3 = \left(1 + \frac{\gamma^2}{8}\right) \frac{dh_b}{dx} \cot\beta = 1.08\, \frac{dh_b}{dx} \cot\beta \tag{2.41}$$

Having obtained an average along-shore current velocity, the authors then found a sediment volume transport rate, according to the work of Komar and Inman (1970) who considered long-crested waves of uniform height incident on an infinitely long, straight and parallel contoured beach. The total immersed weight of sediment transported in unit time past a section of beach, I_l, is given by:

$$I_l = 0.28 \left(EC_g\right)_b \cos\alpha_b \frac{\bar{V}}{U_m} \tag{2.42}$$

where U_m is the maximum orbital velocity under the breaking waves:

$$U_m = \sqrt{g} \frac{H_b}{2\sqrt{h_b}} \tag{2.43}$$

and where α_b is the angle between the breaking wave crests and the shoreline. Assuming that the wave height only varies slowly along the coast so that Eq. (2.19) is still valid and using Eq. (2.37) we find:

$$I_l = \frac{0.56 \left(EC_g\right)_b}{\sqrt{g} H_b} \left(\frac{2C_2}{3} {h_b}^{1/2} + \frac{4}{5} C_3\right) C_1 h_b (1 - K) \tan\beta \ \ \cos\alpha_b \tag{2.44}$$

Now we assume $\tan\beta = A$ (according to Komar (1976), A = constant) and since, $h_i \cong h_b$; $-\frac{dy_0}{dx} \cong \tan\alpha_b \cong \text{sen}\,\alpha_b$ and $\frac{dh_b}{dx} = \frac{1}{0.8}\frac{dH_b}{dx}$.

By using Eq. (2.38)-(2.40) and (2.44) we obtain:

$$I_l = -6.97\left(EC_g\right)_b \cos\alpha_b \sin\alpha_b\, A\sqrt{f}\left(-\frac{2}{3}\sin\alpha_b + 1.08\frac{dH_b}{dx}\cot\beta\right) \qquad (2.45)$$

When $\frac{dH_b}{dx} = 0$ Eq. (2.45) reduces to the Scripps equation, so:

$$4.65\left(EC_g\right)_b \cos\alpha_b \sin\alpha_b\, A\sqrt{f} = 0.77\left(EC_g\right)_b \cos\alpha_b \sin\alpha_b \qquad (2.46)$$

Hence $A\sqrt{f} = 0.166$. since the value of $\sqrt{f}$ varies only slightly, the approximate equality of $A\sqrt{f}$ is thought reasonable, therefore:

$$I_l = 0.385\left(EC_g\right)_b \left(\sin 2\alpha_b - 3.24\frac{dH_b}{dx}\cot\beta\cos\alpha_b\right) \qquad (2.47)$$

which converted to a volume rate of transport is:

$$Q_l = \frac{0.385}{\gamma_s}\left(EC_g\right)_b \left(\sin 2\alpha_b - 3.24\frac{dH_b}{dx}\cot\beta\cos\alpha_b\right) \qquad (2.48)$$

2.6. Littoral Drift Rose

The littoral drift rose (LDR) concept, originally introduced by (Walton, 1973 and Walton and Dean, 2010), represents a powerful help to analyse the long-term shoreline trend. It is a polar representation of littoral transport potential for various shoreline orientations, calculated for a coastal area affected by a uniform deep water wave climate.

Figure 10 provides a definition sketch for calculation of littoral drift at one point on a LDR polar diagram (where the azimuth of the outward normal to the shoreline is defined as b, and a is the azimuth from which the waves originate). The general principle behind the LDR concept is that knowing the azimuth of the seaward facing normal to the shoreline at a given location, and assuming the area of coast represented by the LDR is exposed to the same offshore wave climate, the magnitude and direction of the net (or gross) littoral drift can be found using the LDR for the shoreline area represented.

Considering a wave climate represented by a series of N wave components, $H_{s0,i}$; $T_{p0,i}$; α_{0i}, i = 1, … , N, where H_{s0} denotes significant wave height, T_{p0} is the peak period, and α_0 is the azimuth from which waves originate. Moreover, considering a probability of occurrence, p_i, for each wave component, the net potential littoral drift rate, $Q(\beta)$, for a stretch of coast with normal azimuth β, can be calculated:

$$Q(\beta) = \sum_{\alpha_{0i}=\beta-\pi/2}^{\alpha_{0i}=\beta+\pi/2} p_i \frac{K \cdot \left(H_{s0,i}\right)^{2.4} \cdot \left(T_{p0,i}\right)^{0.2} \cdot g^{0.6}}{16 \cdot (s-1) \cdot (1-n) \cdot \pi^{0.2} \cdot \gamma^{0.4} \cdot 2^{1.4}} \, sin[2(\beta - \alpha_{0i})] \qquad (2.49)$$

where K is a sediment transport coefficient estimated empirically, g is gravity, s =2.6 is the ratio between the specific gravity of sediment and that of water, n=0.4 is the in-place porosity, and γ =0.6 is the breaker index (wave height to depth ratio).

For each possible shoreline orientation, the total positive and negative littoral drifts along the shoreline are calculated for a given time-averaging interval (i.e. 20 years, annual, monthly, etc.). These calculated drift values are plotted in a polar plot, as shown in Figure 10. From the plots, the littoral transport rate for any given shoreline orientation can be determined by entering the plot with the seaward directed normal of the shoreline orientation, and reading off the total positive, total negative, and net littoral drift values.

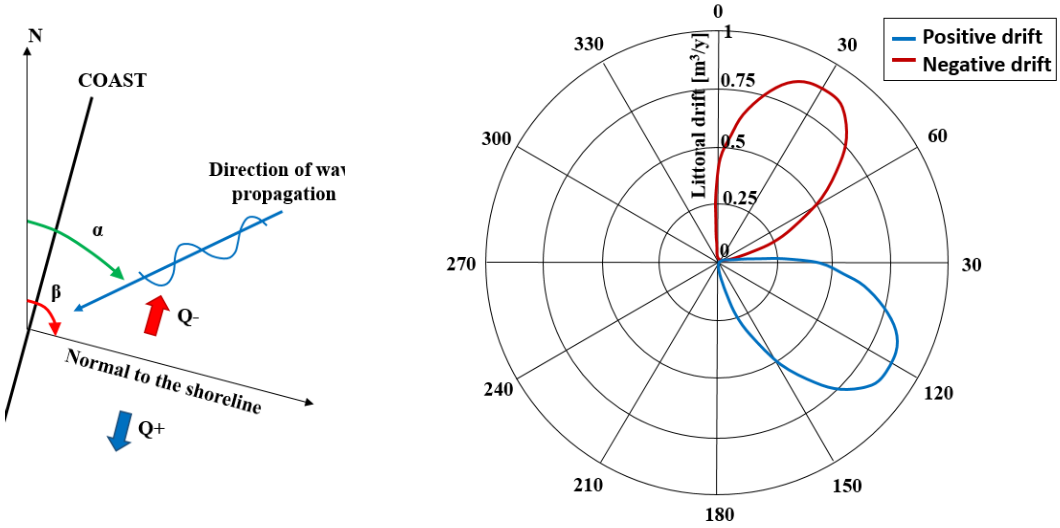

(a) (b)

Figure 10 - a) Definition sketch for a stretch of coast characterized by a shoreline orientation β and affected by a wave propagating from α; b) Example of Net Littoral Drift Rose; blue line stands for positive littoral drift, while redline stands for negative littoral drift

Moreover, it is worth highlighting that since Eq. (2.49) is derived from the well-known CERC formula (SPM, 1984), it is seen the littoral drift, for a given wave angle, to be proportional to $sin[2(\beta - \alpha_{0i})]$. Consequently, the net drift rose average for a real wave climate has lobes that cause the magnitude to vary in a similar manner as $sin[2(\beta - \alpha_{0i})]$.

It is seen from Figure 10, that the graph exhibits a "node". In fact, for a long shoreline with variations of shoreline orientation, it is possible that there is a null point (or a nodal point) in the littoral transport, which occurs at the shoreline angle for which the positive and negative littoral transports have the same magnitude, yielding no net transport.

In the work by Walton and Dean (1973), it was found by examining a number of net LDRs determined as described above that their form was surprisingly similar to that which would occur for a single wave component, equivalent to the whole climate in terms of littoral transport, of parameters $H_{s0,eq.}$, $T_{p0,eq}$, $\alpha_{0,eq}$:

$$Q(\beta) = \sum_{\alpha_{0i}=\beta-\pi/2}^{\alpha_{0i}=\beta+\pi/2} p_i \cdot \frac{K \cdot (H_{s0,i})^{2.4} \cdot (T_{p0,i})^{0.2} \cdot g^{0.6}}{16 \cdot (s-1) \cdot (1-n) \cdot \pi^{0.2} \cdot \gamma^{0.4} \cdot 2^{1.4}} \, sin[2(\beta - \alpha_{0i})] \cong G_{eq} \cdot sin[2(\beta - \alpha_{0,eq})] \tag{2.50}$$

where:

$$G_{eq} = \frac{K \cdot (H_{s0,i})^{2.4} \cdot (T_{p0,i})^{0.2} \cdot g^{0.6}}{16 \cdot (s-1) \cdot (1-n) \cdot \pi^{0.2} \cdot \gamma^{0.4} \cdot 2^{1.4}} \tag{2.51}$$

Thus, the net littoral drift resulting from many deep water waves propagating from arbitrary directions and with arbitrary wave heights ("Total-LDR") can be condensed into a form that is representative of a single wave propagating from a single direction ("Equivalent-LDR"). The equivalent wave direction $\alpha_{0,eq}$ is easily detected from the LDR-graph, as it corresponds to the null-point; while wave height and period can be inferred from Eq. (2.51) by using (for example) common harmonic regression techniques, although a relationship between wave height and period needs to be established.

As discussed in Walton and Dean 2010, the LDR concept has many coastal engineering applications, both in preliminary design and in interpreting shoreline features along natural and modified coastlines where the bottom contours are relatively straight and parallel and where a reasonably uniform wave climate exists over the region designated by an LDR. An additional useful feature of an LDR is that it provides a more complete representation of the long shore sediment transport characteristics at a location than independent calculations of transport for a shoreline at several locations subject to the same wave climate.

As will be shown in the following chapters the LDR concept will be used to explain some peculiar features of the long-term evolution of shoreline.

Particularly, as regarding the equivalent wave approximation, suitable approximation of the Equivalent-LDR to the total one is reached when Total-LDR exhibits nearly symmetrical lobes. This occurs whenever the wave climate is coming from a restricted angle. On the contrary, when in a wider wave sector, with two or more directional modes, a poorer fit is obtained, due to the asymmetrically shaped Total-LDR. Since a direct relationship between the concepts of equivalent wave and “shoreline diffusivity” exists, the poor approximation of the Total-LDR to the equivalent one was found to be interpreted by the shoreline diffusion concept, and the peculiar case of a bimodal wave climate affecting a stretch of coast was investigated. In fact, while for restricted wave sectors the shore diffusivity can be considered constant over time, in a bimodal wave climate, the deviation detected between total and equivalent LDR, due to its asymmetrical shape, would suggest a time-varying diffusivity extra effect on shoreline evolution. This aspect, never investigated in the literature, could represent a limitation in forecast shoreline evolution techniques based on the EW concept, since the LDR equivalent wave is not able to account for a varying diffusivity, but only for a constant one.

Moreover, still regarding the shape of the LDR, an asymmetrical shape would suggest the presence of unstable component affecting the coast, which would cause, in turn, possible instabilities features.

Other aspects concerning the Littoral Drift Rose concept and its applications will be further discussed in the following Chapters.

Chapter 3: One line contour model for beach evolution

3.1. Introduction

A major goal of coastal engineering is to develop models for the reliable prediction of short- and long-term nearshore evolution. Ideally, these models, with appropriate wave and sediment information, would allow prediction of the behaviour of the shoreline and the offshore bathymetry over some given period of time. Further, if coastal structures or beach nourishment were placed along this shoreline, the model would be able to evaluate the effectiveness and impacts of such modifications over any period of time. This coastal model would also be used by coastal planners for shoreline management.

There are two types of coastal models: physical models, which are real models of the region of interest that are physically smaller than the prototype, and equation-based models involving the solution of the equations governing the physical phenomena in the coastal zone. The latter type includes numerical models, solved on a computer, and analytical models which, although simpler, often provide conceptual tools for analysis and understanding.

No fully satisfactory shoreline model presently exists of either type owing to several factors, including our meagre understanding of shoreline sediment transport, the scaling requirements for sediment, the uncertainties of representing the wave environment over short and long periods, and our inability to fully prescribe the hydrodynamics of the surf zone.

However, models of both types have been developed partly to determine how well our present state of knowledge permits us to model the coastal environment, partly to identify topics about which our knowledge is weak, and partly to provide the best possible design tools for coastal projects.

In this chapter, numerical models of shoreline evolution based on one-line theory will be discussed and reviewed, with a special focus on the most famous one-line model GENESIS. A discussion on analytical models is instead presented in Chapter 4.

3.2. Historical background of numerical models

For understanding the consequences of coastal structures and their tracks on shore profile, it is necessary to use either a physical model or a numerical model to simulate shoreline changes depending on the situations. These situations strongly depends on how stable is the shoreline after construction of a structure, assuming that the structure's configuration will not change in the future.

Numerical models possess considerable advantages over physical models when costs, execution times, applicability and scaling problems are concerned. Numerical models have low costs, shorter execution times, may be applicable to various sites and have no scaling problems. Therefore, with the aim of understanding the sophisticated phenomenon defining the shape of shores, models which simulate shoreline changes have been tried to develop for a very long time (Hanson, 1987).

As an outcome of aforementioned reason, dramatic changes and fluctuations in long-shore sediment transportation result in gradual and permanent changes in both bottom and shoreline profiles. Based on these observations, Pelnard-Considére (1956) formulated an equation, which is the first major work that one-line theory is built on, by combining the linearized long-shore sediment transport equation and conservation of mass equation to provide the diffusion equation in terms of shoreline coordinates, y;

Bruun (1954) and Dean (1977) came up with an equilibrium beach profile concept which is the milestone at development of n-line and multi-line models. This concept mentions that a specific beach, depending on sediment properties and regardless of variations in wave climate, has a characteristic profile.

Kraus and Harikai (1983) proved that at beaches where short-term fluctuations are smaller than long-term fluctuations one-line theory based models give accurate shoreline evolutions in the vicinity of structures for a study at Oarai Beach, Japan. Furthermore, Kriebel and Dean

(1985) studied shoreline changes at beaches where short-term changes are more significant than long-term changes, contributing useful information and assistance to one-line models. Hulsbergen et. al. (1976) verified one-line theory by comparing analytical solutions with results of laboratory experiments concerning groins. Besides, several contributors such as Larson, Hanson and Kraus (1987) and Hanson and Larson (1987) compared analytical solutions with numerical solutions.

Even though one-line theory is first introduced in 1956, the first successful implementation of one-line theory is performed by Price, Tomlinson and Willis (1973). Following this study, many new additional studies have been introduced. Some of these important studies include Willis's (1977) work which involved introduction of wave refraction over irregular bottom and representation of a new expression instead of CERC expression, Perlin's (1979) study for detached breakwaters, Le Mehaute and Soldate's (1980) work on presentation of an implicit model and comparison of its results with field data. Despite these studies, none of them offers one-line models as an engineering tool except Kraus, Hanson and Harikai (1985), Kraus et al. (1986) and Hanson and Kraus (1986).

Bakker (1969) extended the one-line theory to include two-lines, one of which represents shoreline and the other represents offshore contour. Inclusion of another contour in y-axis yields understanding of cross-shore motion between two contours because of non-equilibrium beach slope (Bakker et al., 1970). This step together with aforementioned work of Bruun (1954) and Dean (1977) is the introduction of cross-shore motion into one-line motion which would lead to development of n-line models. Bakker (1969) not only extended one-line theory but also conducted several trials along a beach under the existence of single and multiple groin systems and showed that accretion at updrift side of a groin continues up to a beach slope where no more accretion occurs due to steepness of the slope and as a result, sand is bypassed around the top of the groin to its downdrift side.

Hanson (1987) gathered all the previous works and built up a one-line numerical model called GENESIS. GENESIS is an implicit one-line model that evaluates long-term shoreline changes at a beach where several coastal structures exist for various shore and wave climate data using CERC equation. Dabees (2000) developed another one-line numerical model called ONELINE and added new features and improved the coast-structure interaction processes.

Unlike one-line models, n-line models or beach profile models take cross-shore sediment transportation into account as one of the decision makers at the shoreline change processes. As shoreline changes due to cross-shore motion is observed during severe storms, these changes are temporary. However, in several situations, shore profile may not regain its previous shape. In these cases, inclusion of cross-shore sediment transportation parameters is vital for accurate estimations of shoreline changes. Roelvink and Bakker (1993) discussed some of these theories in detail.

Dabees (2000) developed an n-line model called NLINE, which simulates the shore profile changes in 3-D concerning the complicated beach and structure conditions. However, not all of the researches agree with the concept that the more complex the model is, the better result it gives such as Thieler et. al (2000). Cooper and Pilkey (2004) denote that numerical models cannot be specified as only solutions for predicting the behaviour of a certain beach where a structure is constructed. Instead of using these models, they believe that in order to understand the wave-structure interaction, it is better to install several low cost materials that may act like the proposed structure and observe beach behaviour and changes in shoreline. By this method, the procedure time increases, but the possible future errors are omitted and unnecessary waste of investment is prevented.

Within the light of these studies, it is quite easily understood that one-line models remain as a popular tool for engineers to apply at beaches where long-shore transportation dominates the shoreline changes. Moreover, as many discussions are still made over the applicability and effectiveness of these models, it seems like a promising field of coastal engineering and many new studies, theories and improvements may be appended to these models in the way of creating a better model or a more sophisticated n-line model.

3.3. One-line theory

In engineering applications, the two most widely used model types up till now, for coastal evolution analyses, have been the one-line model and the profile change model. In one-line models the changes in shoreline position are assumed to be produced by spatial and temporal differences in the long-shore sand transport rate (Hanson, 1989). This type of model is used to calculate shoreline changes that occur over a period of years to decades. The one-line theory was introduced by Pelnard-Considére (1956), and it has been demonstrated to be adequate in this respect. The theoretical basis of the one-line model is given in the following sections.

3.3.1. Basic Assumptions and one line equation

The foundation of the one-line theory rests on the common observation that some beaches remain steep while others remain gently sloping (Pelnard-Considére, 1956). The theory, thus, assumes that the profile has a specific shape, and as the beach accretes or erodes, the beach profile moves in parallel to itself. Hence, one contour line is enough to describe changes in the beach plane shape and volume. The model presumes that the total long-shore sand transport rate may be parameterized in terms of breaking wave quantities, even though other transport mechanisms may be taken into account (Hanson et al. 2001).

The aim of the one-line theory is to describe long-term variations in shoreline position. Short-term variations (e.g., changes caused by storms or by rip currents) are regarded as negligible perturbations superimposed on the main trend of shoreline evolution. In the one-line theory, the beach profile is assumed to maintain an equilibrium shape, implying that all bottom contours are parallel. Consequently, under this assumption, it is sufficient to consider the movement of one line in studying the shoreline change, and that line is conveniently taken to be the shoreline, which is easily observed.

In the model, long-shore sand transport is assumed to occur uniformly over the whole beach profile down to a certain critical depth D_c called the depth of closure. Therefore, by considering a control volume of sand (Figure 11), balanced during an infinitesimal interval of time and neglecting the cross-shore transport, the conservation of sand volume can be formulated as follows:

$$\frac{\partial y}{\partial t} + \frac{1}{D_c + B} \cdot \frac{\partial Q}{\partial x} = 0 \tag{3.1}$$

where $y(x,t)$ represents the cross-shore coordinate of the shoreline at a given time t (s) and along-shore position x, D_c is the closure depth (m), B is the berm height above the mean water level (m), Q is the littoral drift (m^3/s), and q line sources and/or sinks along the coast ($m^3/s/m$ shoreline).

Eq. (3.1) states that the long-shore variation in the sand transport rate is balanced by changes in the shoreline position. If, in addition to long-shore transport, a line source or sink of sand at the shoreline is considered, Eq. (3.1) takes the following form:

$$\frac{\partial y}{\partial t} + \frac{1}{D_c + B} \cdot \frac{\partial Q}{\partial x} = \pm q \tag{3.2}$$

where q denotes the source or sink of sand per unit length of beach (m /m/sec). The minus sign denotes a sink (loss of sand), and the plus sign denotes a source.

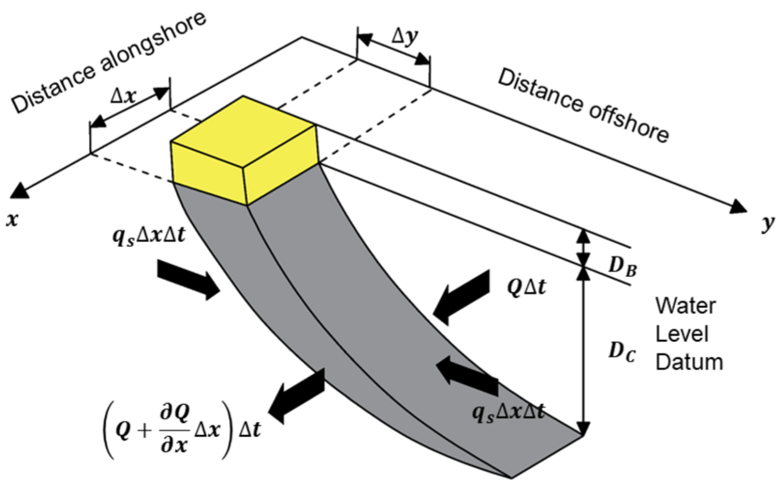

Figure 11 - Schematic Illustration of Hypothetical Equilibrium Beach Profile

In order to solve Eq. (3.1), it is necessary to specify an expression for the long-shore sand transport rate. Long-shore sand transport on an open coast is believed to bear a close relation to the long-shore current which is generated by waves obliquely incident to the shoreline. A general expression for the long-shore transport rate is:

$$Q = Q_0 \sin 2\alpha_b \tag{3.3}$$

where:

Q_0 = amplitude of long-shore sand transport rate (m^3 /sec)

α_b= angle between breaking wave crests and shoreline

In the generally accepted formula for long-shore current, the speed of the current is proportional to $\sin 2\alpha_b$, (Longuett-Higgins, 1970). A wide range of expressions exists for the amplitude of the long-shore sand transport rate, mainly based on empirical results. For example, the Shore Protection Manual (SPM, 1984) gives the following equation:

$$Q_0 = \frac{\rho g}{16} H_{sb}^2 c_{gb} \frac{K}{\left(\frac{\rho_s}{\rho} - 1\right)(1 - n)} \tag{3.4}$$

where:

ρ = density of water (kg/m^3)

g = acceleration of gravity (m/sec^2)

H_{sb} = significant breaking wave height (m)

c_{gb} = wave group velocity at breaking point (m/sec)

K = nondimensional empirical constant

ρ_s = density of sand (kg/ m^3)

n = porosity of sand

The angle between the breaking wave crests and the shoreline, which figures out in Eq. (3.3), (Figure 12) may be expressed as:

$$\alpha_b = \alpha_0 - arctan\left(\frac{\partial y}{\partial x}\right) \tag{3.5}$$

in which:

α_0= angle of breaking wave crests relative to an axis set parallel to the trend of the shoreline

$\frac{\partial y}{\partial x}$ = local shoreline orientation

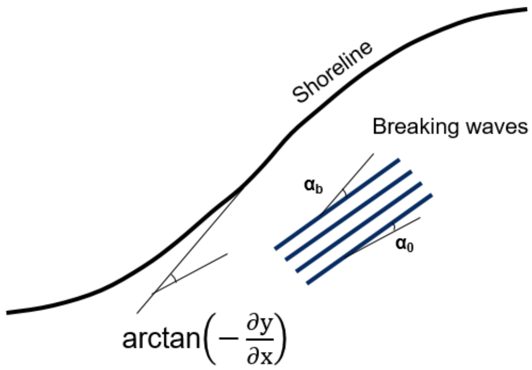

Figure 12 - Definition Sketch for Geometric Properties at Specific Location

3.4. Numerical one-line model: GENESIS (GENEralized model for SImulating Shoreline changes)

By solving Eq. (3.1) numerically, it is possible to calculate the evolution of the shoreline under a wide range of beach, coastal structure, wave, and initial and boundary conditions, which may vary in space and time, as appropriate.

In a numerical model, the shoreline is divided into calculation elements along the x-axis (Figure 13), which runs in parallel to the main trend of the studied beach. Each calculation element has a finite width Δx (Figure 11).

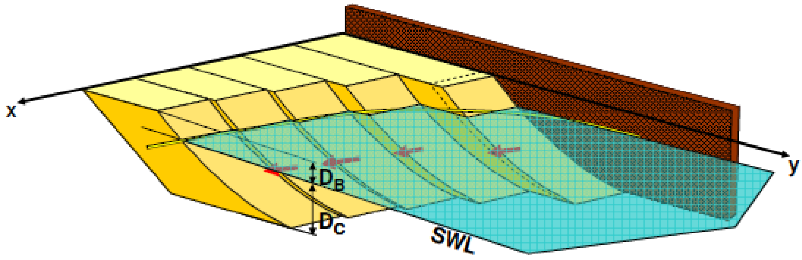

Figure 13 - Perspective view of one-line configuration

GENESIS (GENEralized model for SImulating Shoreline changes), simulates shoreline change produced by spatial and temporal differences in long-shore sand transport. It has been developed by Hanson and Kraus in 1989, in a joint research project between the University of Lund, Sweden, and the Coastal Engineering Research Center (CERC).

GENESIS allows simulation of shoreline change occurring over a period of months to years, as caused primarily by wave action. The horizontal length scale varies from one up to tens of kilometres. The system is generalized in the sense that the model can be used to simulate shoreline change under a wide variety of user specified beach and coastal structure configurations.

3.4.1. Basic assumption of GENESIS model and governing equation

The fundamental assumptions are basically those enounced for the one-line theory. It is also assumed that there is a clear long-term trend in shoreline behaviour, and the horizontal circulation of the nearshore zone, that actually moves sediments, is not considered. To sum up, these assumptions imply that the wave action producing long-shore sand transport (breaking wave height and direction along-shore) and boundary conditions are the major factors controlling long-term beach change.

GENESIS integrates the one-line contour equation (Larson and Kraus, 1987), Eq. (3.1). Following the assumption that the bottom profile moves in parallel to itself, long-shore sand transport is assumed to occur uniformly over the active beach profile. In order to solve Eq. (3.1)**,** the initial shoreline position over the full reach to be modelled, boundary conditions on each end of the beach, and values for Q, q, D_B, and D_c must be given.

First of all, the long-shore sand transport rate is calculated from the wave characteristics at breaking, via the empirical predictive equation:

$$Q_l = \left(H^2 C_g\right)_b \left(a_1 \sin 2\theta_{bs} - a_2 \frac{\partial H}{\partial x} \cos 2\theta_{bs}\right)_b \tag{3.6}$$

Particularly, C_g is the wave group velocity (m/s) and θ_{bs} is the angle of wave crests to the shoreline (the subscript b denotes the breaking condition). The nondimensional coefficients a_1 and a_2 in Eq. (3.6) are given by:

$$a_1 = \frac{K_1}{16\left(\frac{\rho_s}{\rho} - 1\right)(1-n)1.416^{5/2}} \tag{3.7}$$

$$a_2 = \frac{K_2}{8\left(\frac{\rho_s}{\rho} - 1\right)(1-n)\tan\beta\ 1.416^{5/2}} \tag{3.8}$$

where, ρ_s and ρ are the densities of the sediment and water (kg/m^3), n is the sediment porosity, and $\tan\beta$ is the average bottom slope from the shoreline to the depth of long-shore transport, D_{LT}.

The first term of Eq. (3.6) expresses the long-shore transport rate due to obliquely incident waves (commonly known as the CERC-formula). As regarding the K_1 coefficient, its value have been discussed in the previous chapters. However, the order of magnitude for K_1 is well known in the literature, the standard engineering quantity of significant wave height is converted to an rms value by the factor 1.416 to compare values of K_1 determined by calibration of the model. The design value of K_1 suggested by the authors for the GENESIS model, typically lies within the range of 0.58 to 0.77.

The second term in Eq. (3.6) is not part of the CERC formula and is used to describe the effect of another generating mechanism for long-shore sand transport, the long-shore gradient in breaking wave height $\frac{dH_b}{dx}$. This contribution to the long-shore transport rate was introduced into shoreline change modelling by Ozasa and Brampton (1980), as discussed in Chapter 2. The contribution arising from the long-shore gradient in wave height is usually much smaller than that from oblique wave incidence in an open-coast situation. However, in the vicinity of structures, where diffraction produces a substantial change in breaking wave height over a considerable length of beach, inclusion of the second term provides an improved modelling result, accounting for the diffraction current.

Although the values of K_1 and K_2 have been empirically estimated, these coefficients are treated as parameters in calibration of the model and will be called "transport parameters" hereafter. The transport parameter K_1 controls the time scale of the simulated shoreline change, as well as the magnitude of the long-shore sand transport rate. This control of the time scale and magnitude of the long-shore sand transport rate is performed in concert with the factor $\frac{1}{D_c+B}$ appearing in Eq. (3.1). The value of K_2 is typically 0.5 to 1.0 times that of K_1. It is not recommended to vary K_2 much beyond 1.0 K_1, as exaggerated shoreline change may be calculated in the vicinity of structures and numerical instability may occur.

In summary, because of the many assumptions and approximations that have gone into formulation of the shoreline response model, and to account for the actual sand transport along a given coast, the coefficients K_1 and K_2 are treated as calibration parameters in the model. Their values are determined by reproducing measured shoreline change and order of magnitude and direction of the long-shore sand transport rate.

3.4.2. Input data

To run GENESIS, the following input data are required: shoreline position; waves; structure configurations and other engineering activities; beach profiles; boundary conditions. Particularly, as regarding the offshore waves to be inputted into the model, it is rare to have adequate wave gage data for a modelling effort. If gage data are not available, hindcasts can be used.

It is worth highlighting that, when numerical schemes are used for long-term prediction of shoreline evolution, the forecast of wave statistics is required in the form of a time series. Unfortunately, it is seldom possible to know in advance the exact sequence in which the wave parameters will occur. Moreover, in simulations involving long periods and wide spatial extent, it may be impractical to handle a wave data file covering the full simulation period. Instead, a shorter wave data file can be used and repeated, a capability provided by GENESIS.

At the lowest level of effort, statistical summaries of hindcasts can be used. A statistical summary of wave climate, often used in long-term analysis of shoreline change is the Equivalent Wave detected from the Littoral Drift Rose (Walton and Dean, 2010). In this case, wave climate is often inputted as reduced to the Equivalent Wave statistic, characterized by a wave height, wave period and equivalent direction, which repeats itself over and over within the time series.

3.4.3. Empirical parameters

For applications involving bypassing of sand at structures, knowledge of the depth to which sand is actively transported along-shore is required. This depth is called the depth of long-shore transport, D_{LT}, and is assumed to be related to the incident wave conditions which vary with time. GENESIS uses another characteristic depth, termed the "maximum depth of long-shore transport" $D_{LT,o}$, that is nothing but the formulation of Hallermeier (1983), which gives the annual depth of closure as slightly more than twice the extreme annual significant wave height.

As regarding the shape of the shore profile, GENESIS uses the equilibrium profile shape deduced by Bruun (1954) and Dean (1977).

3.4.4. Wave calculation

The modelling system GENESIS is composed of two major sub-models. One sub-model calculates the long-shore sand transport rate and shoreline change. The other sub-model is a wave model that calculates, under simplified conditions, breaking wave height and angle along-shore as determined from wave information given at a reference depth offshore. This sub-model is called the internal wave transformation model, as opposed to another, completely independent, external wave transformation model which can be optionally used to supply nearshore wave information to GENESIS.

In the internal wave transformation model wave propagation from is initially done without accounting for diffraction from structures, then the result is modified by accounting for changes to the wave field by each diffraction source. Consequently, if there are no structures to produce diffraction, the undiffracted wave characteristics are used as input to Eq. (3.1).

On the contrary, if such obstacles are present, breaking wave heights and directions need to be adjusted. Structures such as detached breakwaters, jetties, and groins that extend well seaward of the surf zone intercept the incident waves prior to breaking. Headlands and islands may also intercept waves.

Each tip of a structure will produce a near-circular wave pattern, and this distortion of the wave field is a significant factor controlling the response of the shoreline in the lee of the structure. Sand typically accumulates in the diffraction shadow of a structure, being transported from one or both sides by the oblique wave angles in the circular wave pattern and the decrease in wave height along-shore with penetration into the shadow region.

Accurate and efficient calculation of waves transforming under combined diffraction, refraction, and shoaling to break is required to obtain realistic predictions of shoreline change in such situations.

$$H_b = K_D(\theta_D, D_b)H'_b \tag{3.9}$$

where K_D is the diffraction coefficient, θ_D is the geometric angle for a line from the diffracting tip to the point considered, measured relative to the wave direction at the diffracting tip, H'_b is the breaking wave height at the same cell without diffraction.

GENESIS uses the simplified diffraction calculation procedure for waves with directional spread presented by Goda et al. (1978) to represent diffraction at structures such as detached breakwaters and jetties. The method accounts calculating diffraction of random waves as caused by large land masses based on the concept of directional spreading of waves and penetration of energy to the lee of a land mass or long structure.

Wave transmission at detached breakwaters

Wave transmission is a leading parameter determining the response of the shoreline to detached breakwaters or reefs, and it is defined as the ratio of the height of the incident waves directly shoreward of the breakwater to the height directly seaward of the breakwater. K_T ranges between 0 and 1, for which a value of 0 implies no transmission and 1 implies complete transmission. According to Hanson and Kraus, the diffraction coefficient K_{DT} for transmissive breakwaters is calculated as follows:

The derivation of the phenomenological wave transmission algorithm in GENESIS was developed on the basis of three criteria:

a. As K_T approaches zero, the calculated wave diffraction should equal that given by standard diffraction theory for an impermeable, infinitely high breakwater.
b. If two adjacent energy windows have the same K_T, no diffraction should occur (wave height uniform at the boundary).
c. On the boundary between energy windows with different K_T wave energy should be conveyed from the window with higher waves into the window with smaller waves. The wave energy transferred should be proportional to the ratio between the two transmission coefficients.

The criteria lead to the following expression for the diffraction coefficient K_{DT} for transmissive breakwaters:

$$K_{DT} = \begin{cases} K_D + R_{KT}(1 - K_D) & \theta_D > 0 \\ K_D - R_{KT}(K_D - 0.5) & \theta_D = 0 \\ K_D(1 - R_{KT}) & \theta_D = 0 \end{cases} \quad (3.10)$$

in which R_{KT} is the ratio of the smaller valued transmission coefficient to the larger valued transmission coefficient for two adjacent breakwaters.

3.4.5. Lateral boundary conditions and constrains

GENESIS requires specification of values for Q at both boundaries, cell walls 1 and N+l**,** at each time step. The importance of the lateral boundary conditions cannot be overemphasized, as calculated shoreline positions interior of the grid depend directly upon them. The ideal lateral boundaries are the terminal points of littoral cells, for example, long headlands or long jetties at entrances and inlets. In the following, commonly used boundary conditions are summarized.

3.4.5.1. Pinned-beach boundary condition

It is helpful to plot all available measured shoreline position surveys together to determine locations along a beach that might be used as model boundaries. In doing so it is sometimes possible to find a portion of the beach distant from the project that does not move appreciably in time. By locating the model boundary at such a section, the modelled lateral boundary shoreline coordinate can be "pinned." Expressed in terms of the transport rate, this means: $Q_1 = Q_2$ if implemented on the left boundary, and $Q_{N+1} = Q_N$ if implemented on the right boundary.

If $\Delta Q = 0$ at the boundary, then $\Delta y = 0$ indicating that y does not change. The pinned-beach boundary should be located far away from the project to assure that the conditions in the vicinity of the boundary are unaffected by changes that take place in the project.

3.4.5.2. Gated boundary condition

Groins, jetties, shore-connected breakwaters, and headlands that interrupt, partially or completely, the movement of sand along-shore may be incorporated as a boundary condition if one is located on an end of the calculation grid. If located on the internal domain of the grid, these objects will act to constrain the transport rate and shoreline change, automatically calculated by GENESIS. The representation is the same for both cases, although it occurs in different places in the numerical solution scheme.

The effect of a groin, headland, or similar object located on the boundary is formulated in terms of the amount of sand that can pass the structure. Consideration must be given to sand both entering and leaving the grid. For example, at a jetty located next to an inlet with a deeply dredged navigation channel, sand might leave the grid by bypassing the jetty during times of high waves; in contrast, no sand is expected to cross the navigation channel and jetty to come onto the grid. The jetty/channel thus acts as a selective "gate," allowing sand to move off but not onto the grid. This "gated boundary condition" was termed the "groin boundary condition" in previous descriptions of GENESIS.

3.4.5.3. Moving boundary condition

It is possible to specify a boundary condition in terms of Δy, in other words, how the shoreline moves at the boundary during the simulation period.

3.4.6. Jetties and Groins

Jetties and groins, as shore-normal structures, interrupt the long-shore transport of sand. GENESIS was formulated to represent macro-scale (visible) properties of shore-normal structures. In GENESIS, three non-dimensional parameters exert decisive control on response of the shoreline to shore-normal structures: structure permeability, ratio of net to gross long-shore sand transport rate (which varies between 0 and 1), and bypassing ratio defined as the depth at the groin tip to average deep-water wave height. Some aspects, of interest for the thesis, are summarized next.

3.4.6.1. Sand bypassing

In GENESIS, two types of sand movement past a shore-normal structure are simulated. One type is around the seaward end of the structure, called bypassing, and the other is through and over the structure, called sand transmission. Bypassing is assumed to take place if the water depth at the tip of the structure D_G is less than the depth of active long-shore transport D_{LT}. This depth represents the time-dependent depth out to which sediment is transported along-shore, as opposed to the depth of closure D_c, which may be regarded as an integrated measure over several years. In GENESIS, the calculation of D_{LT} is based on (Hallermeier, 1983). Because the shape of the bottom profile is known from an assumed equilibrium ($y^{2/3}$) profile shape (Dean, 1977), D_G is determined from knowledge of the distance between the tip of the structure and the location of the shoreline.

However, because structures are located at grid cell walls between two calculated shoreline positions in GENESIS, this depth is not unique. In GENESIS the up-drift depth calculated at each time step is used. To represent sand bypassing, a bypassing factor BYP is introduced and defined as,

$$BYP = 1 - \frac{D_G}{D_{LT}}, \qquad (D_G \leq D_{LT}) \tag{3.11}$$

implying a uniform cross-shore distribution of the long-shore sand transport rate. If $D_G \leq D_{LT}$, $BYP = 0$. Values of BYP thus lie in the range $0 \leq BYP \leq 1$, with $BYP = 0$ signifying no bypassing, and $BYP = 1$ signifying that all sand can potentially pass the position of the structure. The value of BYP depends on the wave conditions at the given time step, since D_{LT} is a function of the wave height and period.

3.4.6.2. Sand transmission

A permeability factor $PERM$ is analogously introduced to describe sand transmission over, through, and landward of a shore-connected structure such as a groin. A high (in relation to the mean water level), structurally tight groin that extends far landward so as to prevent landward sand bypassing is assigned $PERM = 0$, whereas a completely "transparent" structure is assigned the value $PERM = 1$. Values of $PERM$ thus lie in the range of $0 \leq PERM \leq 1$ and must be specified through experience and judgment of the modeller based upon, for example, the structural characteristics of the groin (jetty, breakwater), its elevation, and the tidal range at the site. Aerial photographs are often helpful in estimating a structure's amount of void space (hence $PERM$) in relation to other structures on the model grid. The optimal value of $PERM$ for each structure must then be determined in the process of model calibration. With the values of BYP and $PERM$ determined, GENESIS calculates the total fraction of F of sand passing over, around, or through a shore-connected structure as (Hanson and Kraus, 1989).

$$\mathrm{F} = \mathrm{PERM}(1 - \mathrm{BYP}) + \mathrm{BYP} \tag{3.12}$$

This fraction is calculated for each shore-connected (groin-type) structure defined on or at the boundaries of the grid.

Chapter 4: From one-line models to diffusion models

4.1. Introduction

In the simulation of long term morphological changes, computational models are so far very popular. As shown in the previous chapters, various kinds of models based on different approaches have been proposed, such as the one-line shoreline models, multi-line shoreline models, equilibrium type models, and 2D or 3D process based beach profile models. On the one hand, the computational models have proved as powerful and flexible tools for understanding and predicting the long-term evolution of sandy beaches. As known, they can deal with various kinds of initial and boundary conditions.

On the other hand, the analytical or closed form solutions, which are derived from mathematical models, have also several usefulness and advantages. Regarding the advantages of an analytical solution, the following facts have been stated in Larson et al. (1987). The analytical solution can reveal the essential responded features of shoreline with basic physics involved, and they can give the results more readily comprehended rather than the complex numerical and physical modelling, etc. The analytical models also avoid inherent numerical instability and numerical diffusion problems which represent uncertainties in all the mathematical models. Another advantage of the analytical solution is the capacity for obtaining equilibrium conditions from asymptotic behaviour.

This chapter reviews the underlying theory of one-line (diffusion) models and previous work, highlighting the analytical solutions derived from the diffusion mathematical models.

4.2. Background

The analytical solutions of the one-line model of shoreline change, which was first proposed by Pelnard-Considére (1956), were derived for many cases of initial and boundary conditions from various studies, such as (Bakker 1969, Larson et al. 1987; Grijm 1961; Komar 1973; Walton and Chiu 1979; Dean 1983; Larson et al. 1997).

Larson et al. (1987) reviewed the available analytical solutions then and introduced new analytical solutions. The solutions in these two studies describe the shoreline evolution on the semi-infinite or infinite coast (without solid boundaries) or near the coastal structures such as the groin, jetty, detached breakwaters, breakwater, and seawall.

Dean (2003) summarized and presented analytical solutions for the case of finite rectangular beach fill (beach nourishment) on coast bounded by inlets at both ends. By applying the property of linear superposition of the analytical solution for the case of delta formation on an infinite coast, Hoang et al. (2016) presented the erosion of shoreline caused by the reduction of sediment supply from the river and the recovery.

Valsamidis et al. (2017) introduced a modified version of the one-line model, which includes an advection term to reveal the impact of a long-shore current on shoreline evolution. That new equation may describe the morphodynamic evolution of mega-nourishments which have the shape of rectangular or bell-curved.

Furthermore, Hoang et al. (2019) utilized the available solutions introduced by Larson et al. (1987) to investigate the recovery of tsunami-induced concave shoreline after the 2011 Tohoku earthquake and tsunami. They also introduced a new approach to estimate the diffusion coefficient from the erosion propagation distance and elapsed time. The erosion propagation distance is proved to be proportional to the square root of elapsed time.

Larson et al. (2020) developed a semi analytic model to describe the flow through an inlet relating to the simple tide and the inlet morphological response. Regarding confined beaches, Zacharioudaki and Reeve (2008) and Valsamidis and Reeve (2020) presented semi analytical solutions to describe the evolution of shoreline within a groin field.

Walton and Dean (2011) presented an extension of an existing solution for shoreline change at an infinite jetty where waves are time-varying and when the angle of the shoreline is small with respect to the waves breaking at the shoreline. The solution allows the previous constant wave condition solution to be extended to the case where wave properties (i.e., wave direction, wave height, and wave period) are time-varying. Valsamidis and Reeve (2017) present a new analytical solution. It can assess the accretion or erosion caused near the groin due to its proximity to the river which may act either as a source or a sink of sediment material. The solution was presented for various combinations of time-varying wave conditions and sediment supply/removal by the river.

It is worth noticing that the more recent works dealt with the case of bounded coasts, but with some drawbacks. Particularly, Valsamidis & Reeve (2020) described the evolution of shoreline within a groin field, solving the problem only with a semi-analytical approach. Furthermore, Hoang (2020) provided the solution for an “isolated” beach of finite length, which holds, though, only for wave attacks rigorously perpendicular to the coast. Consequently, the analytical solutions describing the shoreline evolution on coast bounded by structures at both ends are still limited, unrealistic or cannot provide quantitatively accurate results of the beach involving complicated initial and boundary conditions, and waves input Main aim of present thesis is providing new analytical solutions for the evolution of a bounded coast, including new sets of boundary conditions. But first, in this Chapter a deep analysis of present analytical solution of the diffusion equation is given.

4.3. The diffusion equation

Larson et al. (1987) presented the process how to simplify and obtain a simplified governing equation of the one-line model, Eq. (3.1). For beaches with mild slopes, it can safely be assumed that the breaking wave angle relative to the shoreline and the shoreline orientation $\frac{\partial y}{\partial x}$ are small. Under these assumptions, the generalized transport relation, as discussed in the previous section, may be linearized to yield:

$$Q = Q_0 \sin\left\{2\left[\alpha_0 - arctan\left(\frac{\partial y}{\partial x}\right)\right]\right\} = Q_0\left(2\alpha_0 - 2\frac{\partial y}{\partial x}\right) \qquad (4.1)$$

If the amplitude of the long-shore sand transport rate and the incident breaking wave angle are constant (independent of x and t) transport relation may be combined with Eq. (3.1) to yield:

$$\frac{\partial y}{\partial t} = \varepsilon\frac{\partial^2 y}{\partial x^2} \qquad (4.2)$$

where:

$$\varepsilon = 2\frac{Q_0}{D_c + B} = \frac{K\rho g\left(H_s^2 c_g\right)_b}{8\left(\frac{\rho_s}{\rho} - 1\right)(1-n)}\frac{1}{D_c + B} \qquad (4.3)$$

Eq. (4.2) is the "shoreline diffusion equation", formally identical to the one-dimensional equation describing conduction of heat in solids. Thus, many analytical solutions can be found by applying the proper analogies between initial and boundary conditions for shoreline evolution and the processes of heat conduction and diffusion.

The coefficient ε, having the dimensions of length squared over time, is interpreted as a diffusion coefficient expressing the time scale of shoreline change following a disturbance (wave action). A high amplitude of the long-shore sand transport rate produces a rapid shoreline response to achieve a new state of equilibrium with the incident waves. Furthermore, a larger depth of closure indicates that a larger part of the beach profile participates in the sand movement, leading to a slower shoreline response. According to Eq. (4.3), the diffusion coefficient is intensely dependent on the breaking wave height, H_b, and the dimensionless empirical coefficient in the long-shore sediment transport rate formula, K. This is a key factor in the long-shore sediment transport rate formula. There have been various studies on this parameter.

As discussed in Chapter 2, the SPM (1984) proposed a formula to quantify the total long-shore sediment transport rate, which is well known as the CERC formula and widely used. It recommended the value of K as 0.39 which was derived from the field study data presented in Komar and Inman (1970). The value of K is associated with whether breaking wave height specifying in terms of the significant wave height or the root mean square wave height. The one presented above was carried out based on the computation utilizing the significant wave height, while the value of K corresponding to the root mean square wave height is 0.92. It is important to note that the CERC formula does not include the influence of grain size. The relationship between the value of K and the grain size was documented by del Valle et al. (1993), (see Chapter 3). The increase in grain size leads to the decreasing value of K.

4.4. The role of diffusion and advection in shoreline evolution

Coastal models available to assess coastline evolution (like GENESIS introduced previously in Chapter 3) are not fundamentally different than the diffusion equation that was used by Pelnard-Considére (1956) to model coastline evolution.

However, due to their simplicity assumptions and limitations, standard coastline models are considered to fail in solving more complex coastline responses (e.g. net along-shore migration), as this requires insight in both the advection and diffusion of the coastline perturbation (Falqués, 2003). Particularly, it is expected that advection can be triggered by specific hydrodynamic conditions, for example, as a result of wind driven currents, asymmetry of the tidal flow and high-angle waves or by feedback between the morphology of the coastline perturbation and hydrodynamics (Ashton & Murray, 2003).

Therefore, in order to overcome these drawback of standard coastal models, advection-diffusion models seemed to represent a reliable tool able to model long-term evolution of unstable shorelines plane forms, like flying spits and along-shore sand waves. In other terms, they have been often invoked to catch more complex phenomena involved in the beach processes. In fact, Larson and Kraus (1991) applied a simple approach towards the modelling of the migration of sediment along the coast by means of adding an advective term to the diffusion equation of Pelnard-Considére.

However, a more recent investigation on advection and diffusion effects at coastline perturbations, provided by Huisman et al. 2013, showed the absolute predominance of diffusion effects on shoreline evolution over advective ones.

The study involved artificial nourishments with varying characteristics, and for each nourishment, the advective and diffusive components, as found in observed coastline evolution in field surveys, have been isolated, and their role have been assessed for coastal processes. The authors hypothesized that the relative importance of advection and diffusion were correlated with the local hydrodynamic forcing conditions as well as the volume and shape of the coastline perturbation.

Measured bathymetrical changes were analysed in order to distinguish advection and diffusion in field situations. The advection has been quantified on the basis of the along-shore migration (i.e. bias) of the nourishments and diffusion on the basis of the spreading of the sediment relative to the centre of gravity (i.e. standard deviation).

A modified version of the Pelnard-Considére equation has been presented:

$$\frac{\partial y}{\partial t} = K\frac{\partial^2 y}{\partial x^2} - V_s\frac{\partial y}{\partial x} \tag{4.4}$$

where y = cross-shore coastline position (m), x = along-shore position (m), t = time (yr), K = diffusion parameter (m^2/yr) V_s = advection parameter (m/yr).

The advection and diffusion coefficients have been fitted such that observed coastline evolution as a result of the considered nourishment was best represented. Particularly, the advection and diffusion coefficients have been calibrated on the available information on the 'coastline impact' of the nourishments. According to the authors, the diffusion coefficient (K) can be considered a proxy for the along-shore spreading and severity of the local wave climate and the advection coefficient (V_s) is a proxy for the along-shore migration rate and net bias of the wave climate.

The bathymetrical data used in the study concerned information for seven nourishment locations along the Dutch coast, very different from each other in terms of nourishment shape, sand volumes and position of the nourishment in the cross-shore profile.

Particularly, at the Delftland coast three nourishments have been selected, called Hoek van Holland nourishments, the Sand Groins (shoreface nourishments) and the Sand Motor (mega nourishment), respectively. Moreover, data of combined shoreface and beach nourishments at the North-Holland and Ameland coast have been also used, and namely the Egmond and Bergen shoreface nourishments, which are considerably small ($\sim 900'000$ m^3), and the Ameland and Julianadorp nourishments which are instead bigger than the others (3 and 6 million m^3). Primary source for the analysis of shoreline change has been the in-situ multibeam data, available before and after the construction of the nourishments. Bathymetric data has been used to compute volumes of sediment in the cross-shore transects (at every 10 to 30 m in along-shore direction).

Results showed that the evolution of coastline perturbations along the Dutch coast is fundamentally dominated by diffusion, even if advection of nourished sediment does contribute to local coastline evolution for some of the smaller nourishments.

Particularly, the diffusion coefficients calibrated for each nourishment investigated has an order of magnitude 10^3 - 10^4 greater than the advection one. Considering the entire diffusion and advective terms of Equation (4.4), the predominance of diffusion processes is confirmed, since the derivative terms, $\frac{\partial^2 y}{\partial x^2}$ and $\frac{\partial y}{\partial x}$, varies of an order of magnitude to each other. This endorses the predominance of diffusion processes on coastal evolution, even involving peculiar beach processes patterns.

According to these results, it seems to be reasonable to account only for the diffusion effects for analysis of shoreline changes, confirming the absolute capability of simple diffusion models (one-line models) to give reliable results in long-term analysis of shoreline evolution.

4.5. Analytical one line models

Analytical solutions to one-line models provide a concise, quantitative means of describing systematic trends in shoreline evolution commonly observed at groins, jetties, and detached breakwaters. Larson et al. (1987) and Larson et al. (1997) gave comprehensive surveys of derived analytical solutions of the shoreline change equation.

The assumptions which comprise the one-line model, in which breaking waves are the dominant sand-moving process, have been deepened in Chapter 3. As regarding the analytical solutions, it is assumed that the angle between the breaking wave crests and the shoreline is small (small-angle approximation), and that the angle of the shoreline with respect to the x-axis is small. In arriving at all solutions, it is tacitly assumed that sand is always available for transport unless explicitly restricted by boundary and/or initial conditions.

4.6. Solutions for shoreline evolution without coastal structures

The basic differential equation to solve is Eq. (3.2), together with the associated initial and boundary conditions. An infinitely long beach is assumed to be exposed to waves of constant height and period with wave crests parallel to the x-axis (parallel to the trend of the shoreline). The shoreline will adjust to reach an equilibrium state in which the long-shore sand transport rate is equal at every point along the shoreline. Since the wave crests are parallel to the x-axis, the equilibrium sand transport rate is zero. An initially straight beach is thus the stable shoreline form in this case. If the shoreline shape at time t = is described by a function $f(x)$, the solution of Eq. (3.2) is given by the following integral:

$$y(x,t) = \frac{1}{2\sqrt{\pi \varepsilon t}} \int_{-\infty}^{+\infty} f(\xi) e^{-(x-\xi)^2/4\varepsilon t} d\xi \qquad (4.5)$$

For $t > 0$ and $-\infty < x < \infty$.

The shoreline position is denoted by y and is a function of x and t. The quantity ξ is a dummy integration variable. Consequently, the change in both natural and manipulated beach forms can be determined if Eq. (4.5) is evaluated. Eq. (4.5) may be interpreted as a superposition of an infinite number of plane sources instantaneously released at $t = 0$. The source located at point ξ contributes an amount $f(\xi)d\xi$ to the system. Infinitely far away from such a single source no effect on the shoreline position is assumed (boundary condition). Eq. (4.5) is used to derive most of the solutions dealing with various shoreline configurations.

4.6.1. Finite rectangular beach fill

At time t =0, the shoreline has a rectangular shape of finite length $2a$ described by Eq. (4.6) (see Figure 14)

$$y(x,0) = f(x) = \begin{cases} y_0 & |x| \le a \\ 0 & |x| \le a \end{cases} \tag{4.6}$$

The solution is:

$$y(x,t) = \frac{1}{2}\, y_0 \left[erf\left(\frac{a-x}{2\sqrt{\varepsilon t}}\right) + erf\left(\frac{a+x}{2\sqrt{\varepsilon t}}\right)\right] \tag{4.7}$$

For $t > 0$ and $-\infty < x < \infty$.

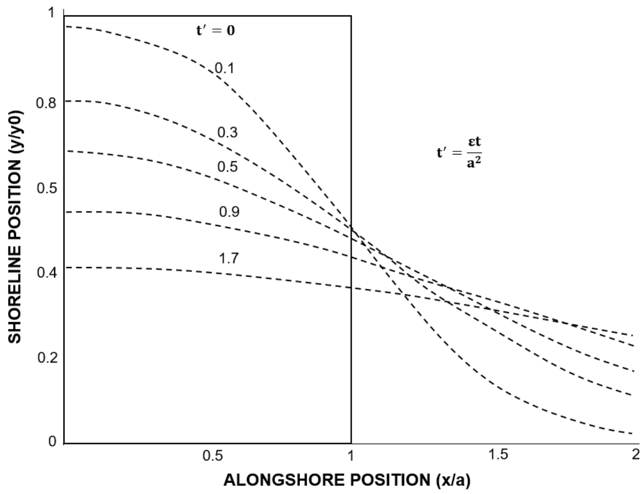

Figure 14- Shoreline evolution of an initially rectangular beach fill exposed to waves arriving normal to shore

The symbol erf denotes the error function which is defined as:

$$\mathrm{erf}\, z = \frac{2}{\sqrt{\pi}} \int_0^z e^{-\xi^2} d\xi \tag{4.8}$$

The error function is tabulated in standard mathematical reference books (e.g., Abramowitz and Stegun 1964). It is convenient to introduce the following dimensionless quantities:

$$y' = \frac{y}{y_0} \tag{4.9}$$

$$x' = \frac{x}{a} \tag{4.10}$$

$$t' = \frac{\varepsilon t}{a^2} \tag{4.11}$$

The quantity used to normalize the time variable expresses half the time elapsed before a square beach fill of length a would completely erode at the constant transport rate Q_0. If the solution is expressed in dimensionless quantities, the resultant shoreline evolution can be displayed in compact form. Figure 14 illustrates how a rectangular fill spreads or diminishes with time according to Eq. (4.7).

Dean (1984) discusses how the sand from two different beach nourishment projects spreads with time. The time t_{P2} for a certain percentage P to be lost from the original rectangular beach fill is compared with the corresponding time t_{P1} for different conditions:

$$t_{P2} = t_{P1} \left(\frac{a_2}{a_1}\right)^2 \frac{\varepsilon_1}{\varepsilon_2} \tag{4.12}$$

This formula is obtained by noting that the same percentage of beach volume is lost during the same dimensionless time. Consequently, a rectangular beach fill which is twice as long maintains its volume four times as long if exposed to the same wave conditions. It is possible to calculate the time it will take for a certain percentage P to be lost from the initial rectangular fill. The following expression is obtained by integrating Eq. (4.7) and comparing the resulting volume at a specific time to the original fill volume:

$$P = \sqrt{t'} \left(\frac{1}{\sqrt{\pi}} - ierfc \ \frac{1}{\sqrt{t'}}\right) \tag{4.13}$$

where $ierfc$ denotes the integral of the complementary error function $erfc$

$$ierfc \ z = \int_0^z erfc \ \xi \ \ d\xi \tag{4.14}$$

$$erfc \ z = 1 - \mathrm{erf} \, z \tag{4.15}$$

Figure 15 shows the percentage of sand volume lost as a function of time.

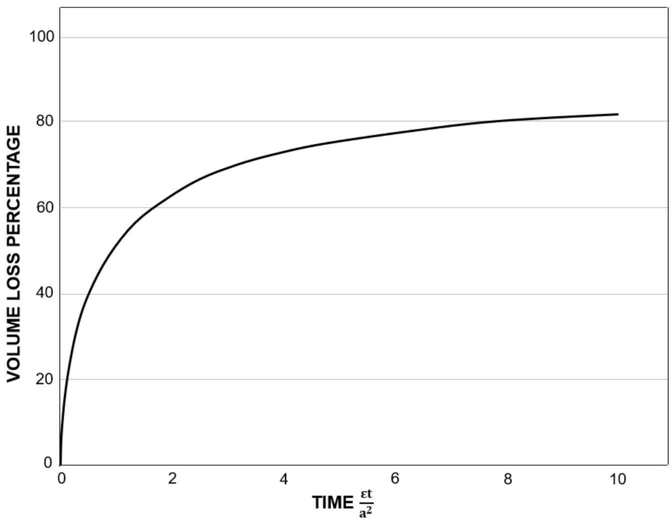

Figure 15 - Percentage of sand volume lost from a rectangular fill as a function of dimensionless time

It is possible to determine the rate of sand to be supplied to the fill in order to maintain the original shape. The boundary condition for this case is that the end of the rectangular fill is kept at the initial position:

$$y(0,t) = y_0 \tag{4.16}$$

Note in this case that the x-axis originates from the corner of the fill instead of from the middle of the fill. The solution describing the resultant shoreline evolution is:

$$y(x,t) = y_0\, erfc\left(\frac{x}{2\sqrt{\varepsilon t}}\right) \tag{4.17}$$

For $t > 0$ and $-\infty < x < \infty$.

Sand has to be added to the corner of the fill at the following rate:

$$Q = \frac{2y_0}{\sqrt{\pi\varepsilon t}}\, Q_0 \tag{4.18}$$

It is advisable to use the analytical expressions describing shoreline evolution for a rectangular fill with great care, even for rough estimations, because the linearization procedure, Eq. (4.1), is based on small shoreline orientation angles, a condition which is violated on the sides of the rectangle. In fact, the linearized transport equation implies an infinitely large initial sand transport rate at the edges of the fill. However, the original transport equation gives a zero transport rate at the corners; thus, a rectangular beach form is stable to parallel incident waves. In reality, sand transport occurs at the corners because of diffraction and refraction, but this realistic situation is not described by the linearized equation. Consequently, the linearization procedure artificially increases the erosion of the fill, implying that the analytical solution overestimates the speed of erosion. The error is, therefore, on the conservative side. This problem is only an apparent one since it is a practical impossibility to create a perfectly rectangular fill in the field.

The solution for a rectangular cut in a beach may be obtained by superimposing Eq. (4.7) with a negative sign on a beach of width y_0.

Dean (2003) further discusses the potentials of Eq. (4.7). First, an important parameter in the solution is $\sqrt{\varepsilon t}/a$ where, again, a is the length of the fill project and ε is the long-shore diffusivity parameter in the diffusion equation.

The larger the value of this time parameter, the more the plane form has changed. If the quantity $\sqrt{\varepsilon t}/a$ is the same for two different situations, then it is clear that the plane form evolutions are also geometrically similar. For example, if two nourishment projects are exposed to the same wave climate but have different lengths, the project with the greater length will last longer. In fact, the longevity of a project varies as the square of the length; thus, if Project A, with a shoreline length of 1 km, "loses" 50 percent of its material in a period of 2 years, Project B, subjected to the same wave climate but with a length of 4 km, would be expected to lose 50 percent of its material from the region where it was placed in a period of 32 years. Thus, the project length is very significant to its performance. The presence of a background erosion rate would reduce the differences between the longevities of these two projects. Consider next the case in which two fill projects are of the same length but are exposed to different wave climates. The coefficient in the one-line model, ε (Eq. (4.3)) varies with the breaking wave height to the 2 power, and thus if Project A is located where the wave height is 1 m and loses 50 percent of its material in a period of 2 years, Project B, with a similarly configured plane form located where the wave height is 0.25 m, would be expected to last a period of 64 years.

It is possible to obtain an analytical expression for the proportion of sand $M(t)$remaining at the placement site, where:

$$M(t) = \frac{1}{\Delta y_0 a}\int_{-a/2}^{a/2} y(x,t)dx \tag{4.19}$$

or

$$M(t) = \frac{\sqrt{4\varepsilon t}}{a\sqrt{\pi}}\left(\exp -(a/\sqrt{4\varepsilon t}\right)^2 + \operatorname{erf} a/\sqrt{4\varepsilon t} \tag{4.20}$$

The greater the dimensionless time $\sqrt{\varepsilon t}/a$ the more $M(t)$ tends to an asymptote of:

$$M(t) \cong 1 - \frac{\sqrt{4\varepsilon t}}{a\sqrt{\pi}} \tag{4.21}$$

which is valid for small *t*; more specifically, for

$$\sqrt{\varepsilon t}/a < \frac{1}{2} \tag{4.22}$$

The quantity $\varepsilon t/a^2$ can be referred to as a dimensionless time. For large values of this parameter,

$$M(t) \cong \frac{1}{2\sqrt{\pi}} \frac{a}{\sqrt{\varepsilon t}} \tag{4.23}$$

A useful meterstick for estimating the half-life of a project is obtained by noting that M =0.5 for $\sqrt{\varepsilon t}/a \cong 0.46$. Therefore, we can define a half-life t_{50} as

$$t_{50} = (0.46)^2 \frac{a^2}{\varepsilon} = 0.21 \frac{a^2}{\varepsilon} \tag{4.24}$$

Note that the half-life does not depend on the volume of fill emplaced.

4.6.2. Semi - infinite rectangular beach fill

The initial conditions for a semi-infinite rectangular beach fill are:

$$y(x,0) = f(x) = \begin{cases} y_0 & x \leq 0 \\ 0 & x > 0 \end{cases} \tag{4.25}$$

Walton and Chiu (1979) give the following solution:

$$y(x,t) = \frac{1}{2} y_0 \, erfc \left(\frac{x}{2\sqrt{\varepsilon t}} \right) \tag{4.26}$$

For $t > 0$ and $-\infty < x < \infty$.

The solution is antisymmetric about the y-axis, taking the constant value $y_0/2$ at x =0. If the shape of the shoreline for x ≥ 0 is approximated by a triangle having height $y_0/2$ so as to conserve mass, the speed of propagation of the triangle's front is inversely proportional to the square root of elapsed time. This relationship is also valid for Eq. (4.19). Figure 16 illustrates the solution of Eq. (4.25). The right side of Eq. (25) for x >0 equals half the solution of Eq. (4.19).

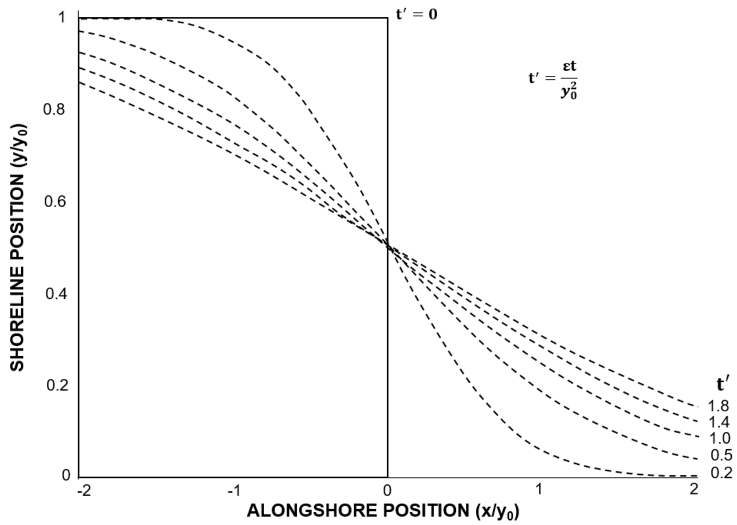

Figure 16 - Shoreline evolution of an initially semi-infinite rectangular beach

4.6.3. Triangular-Shaped Beach

The triangular-shaped solution is also mentioned by Walton and Chiu (1979). The original beach has the shape of a triangle according to the initial conditions as follows:

$$y(x,0) = \begin{cases} y_0\left(\dfrac{a-x}{a}\right) & 0 \leq x \leq a \\ y_0\left(\dfrac{a+x}{a}\right) & -a \leq x \leq 0 \\ 0 & |x| > a \end{cases} \tag{4.27}$$

In this case the solution takes the following form:

$$y(x,t) = \frac{y_0}{2a}\left((a-x)\,\mathrm{erf}\left(\frac{a-x}{2\sqrt{\varepsilon t}}\right) + (a+x)\,\mathrm{erf}\left(\frac{a+x}{2\sqrt{\varepsilon t}}\right) - 2x\,\mathrm{erf}\left(\frac{x}{2\sqrt{\varepsilon t}}\right) + 2\sqrt{\frac{\varepsilon t}{\pi}}\left(e^{\frac{-(x+a)^2}{4\varepsilon t}} + e^{\frac{-(x-a)^2}{4\varepsilon t}} - 2e^{\frac{-x^2}{4\varepsilon t}}\right)\right) \tag{4.28}$$

For $t > 0$ and $-\infty < x < \infty$.

A nondimensional illustration of the shoreline evolution from an initially triangular beach is shown in Figure 17.

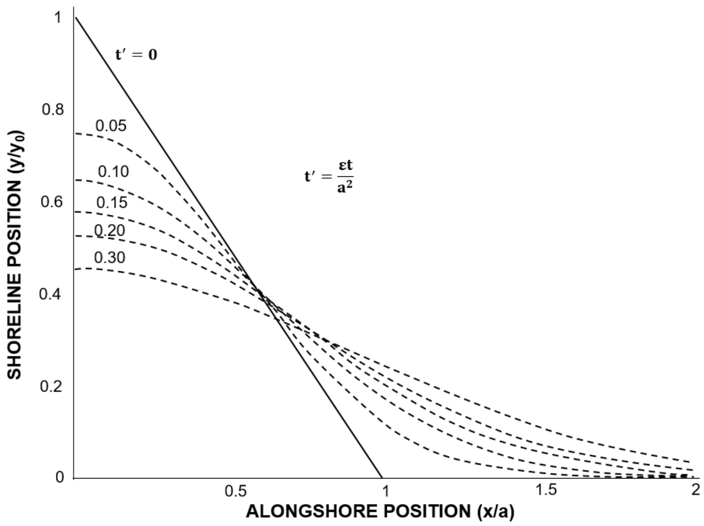

Figure 17 - Shoreline evolution of an initially triangular beach

Depending upon the height-to-width ratio of the triangle, linearization of the transport equation may reduce accuracy of the analytical solution. However, even though the assumptions forming the basis for the linearization procedure appear to be extremely limiting (particularly in requiring small wave angles) , in practice the analytical solution is found to be applicable for angles as large as about 45° between the shoreline and the breaking waves. In order to estimate the effect of the linearization, a comparison was made between the analytical solution and a numerical solution with the original sand transport equation. Figure 18 shows the result as a function of the height-to-width ratio and elapsed time.

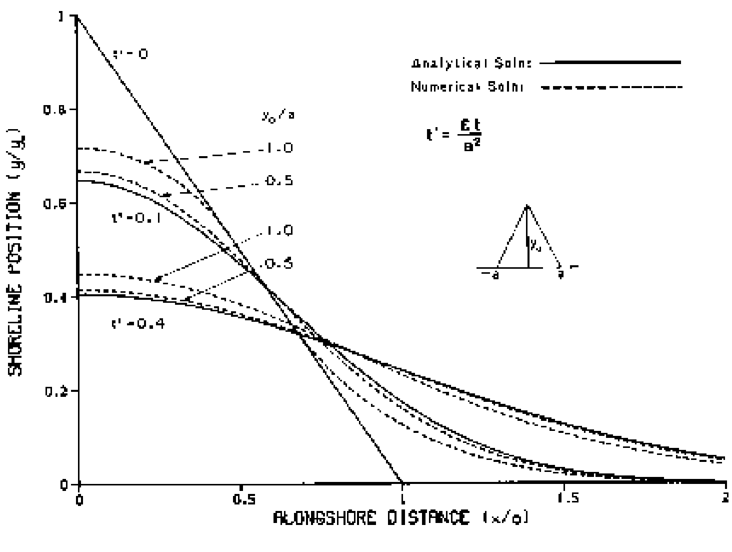

Figure 18 - Comparison between analytical solution with the linearized transport equation and numerical solution with the original transport equation for a triangular beach fill (for height-to-width ratios 1.0 and 0.5). (from Larson and Kraus, 1987)

It is quite clear that the analytical solution produces a higher rate of shoreline change by overestimating the long-shore sand transport rate (since $a > \sin a$). Thus, if the analytical solution is used to estimate the time scale involved in beach nourishment problems, a higher rate of attenuation of the fill will always be obtained than is expected to actually occur.

4.6.4. Trapezoidal-Shaped Beach

A trapezoidal beach form is described by the following initial conditions:

$$y(x,0) = \begin{cases} \frac{y_2 - y_1}{x_2 - x_1}x + \frac{y_1 x_2 - x_1 y_2}{x_2 - x_1} & x_1 \le x \le x_2 \\ 0 & x < x_1,\ \ x > x_2 \end{cases} \tag{4.29}$$

Here y_1 and y_2 denote shoreline positions corresponding to the long-shore locations x_1 and x_2. The solution is:

$$y(x,t) = \frac{1}{2}\left(\frac{y_2 - y_1}{x_2 - x_1}x + \frac{y_1 x_2 - x_1 y_2}{x_2 - x_1}\right)\left(\mathrm{erf}\left(\frac{x_2 - x}{2\sqrt{\varepsilon t}}\right) - \mathrm{erf}\left(\frac{x_1 - x}{2\sqrt{\varepsilon t}}\right)\right)$$
$$+\left(\frac{y_2 - y_1}{x_2 - x_1}\right)\sqrt{\frac{\varepsilon t}{\pi}}\left(e^{\frac{-(x_1 - x)^2}{4\varepsilon t}} - e^{\frac{-(x_2 - x)^2}{4\varepsilon t}}\right) \tag{4.30}$$

For $t > 0$ and $-\infty < x < \infty$.

The solution for the triangular beach form (Eq. 4.30) can be obtained by superimposing two trapezoidal beach shapes which reduce to triangles. In the same way, in principle, the analytical solution for any arbitrary shoreline shape may be obtained by approximating the shoreline with a series of straight lines. Even though the sand transport at each boundary of the trapezoids in such a case is overestimated (because of the large incident wave angle) superimposition of the solutions eliminates these effects. A representative length L has been chosen to normalize the shoreline position and the along-shore distance.

If an arbitrary-shaped shoreline is studied, it is most convenient to approximate it with a series of straight lines and then to superimpose the respective solutions. Consider a shoreline (see Figure 20) divided into N reaches, with each length described by a straight line connecting two neighbouring points denoted by (x,y) and (x, y+i) for a certain reach (the i reach)

$$y(x,t) = \frac{1}{2}\sum_{i=1}^{N}\left(\frac{y_{i+1} - y_i}{x_{i+1} - x_i}x + \frac{y_i x_{i+1} - x_i y_{i+1}}{x_{i+1} - x_i}\right)\left(\mathrm{erf}\left(\frac{x - x_i}{2\sqrt{\varepsilon t}}\right) - \mathrm{erf}\left(\frac{x - x_{i+1}}{2\sqrt{\varepsilon t}}\right)\right)$$
$$+\frac{y_{i+1} - y_i}{x_{i+1} - x_i}2\sqrt{\frac{\varepsilon t}{\pi}}\left(e^{\frac{-(x - x_i)^2}{4\varepsilon t}} - e^{\frac{-(x - x_{i+1})^2}{4\varepsilon t}}\right) \tag{4.31}$$

For $t > 0$ and $-\infty < x < \infty$.

4.6.5. Semi-circular-Shaped Beach

In order to find an analytical solution for a beach formed in a half circle between -a < x < a, the circle is approximated by a polygon with a finite number of corners (Figure 20)

The solution can be obtained using Eq. (4.31) with proper expressions for the line segments. The following quantities are defined:

$$x_i{}^R = a\cos\left(\frac{(i-1)\pi}{N-1}\right) \tag{4.32}$$

$$x_i{}^L = a\cos\left(\frac{i\,\pi}{N-1}\right) \tag{4.33}$$

$$y_i{}^L = a\,sen\,\left(\frac{i\,\pi}{N-1}\right) \tag{4.34}$$

$$k_i = \frac{1}{\tan\left(\frac{i\left(\pi-\frac{1}{2}\right)}{N-1}\right)} \tag{4.35}$$

The integer N is the number of corners in the polygon approximating the semicircle. For example, if N = 3 then a triangular beach form is obtained. The solution can be written with the previously defined quantities:

$$y(x,t) = \frac{1}{2}\sum_{i=1}^{N-1}(k_i x_i{}^L + y_i{}^L - k_i x)\left(\operatorname{erf}\left(\frac{x_i{}^R - x}{2\sqrt{\varepsilon t}}\right) - \operatorname{erf}\left(\frac{x_i{}^L - x}{2\sqrt{\varepsilon t}}\right)\right)$$
$$+ 2k_i\sqrt{\frac{\varepsilon t}{\pi}}\left(e^{\frac{-(x_i{}^R - x)^2}{4\varepsilon t}} - e^{\frac{-(x_i{}^L - x)^2}{4\varepsilon t}}\right) \tag{4.36}$$

For $t > 0$ and $-\infty < x < \infty$.

In the limit $N \to \infty$ the polygon coincides with a semicircle. The solution (N = 101) is illustrated in Figure 19 which shows the shoreline evolution as a function of time for an initially semi-circular-shaped beach.

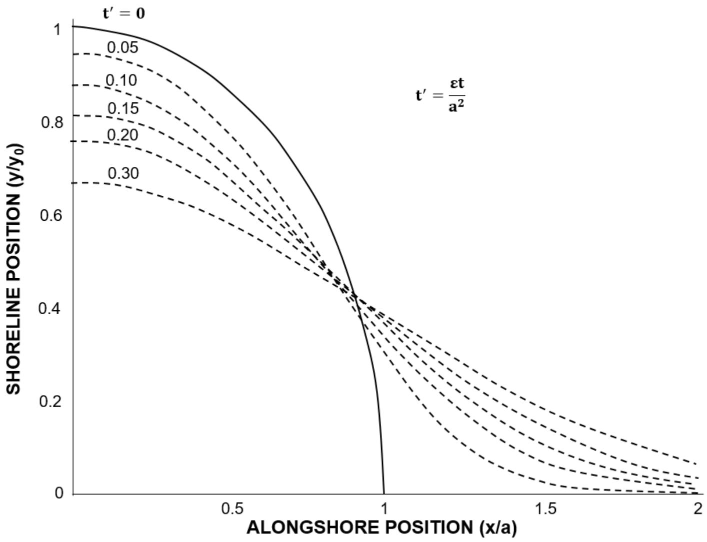

Figure 19 - Shoreline evolution of an initially semi-circular beach

If the beach is formed as a circular segment, the solution may be derived by superimposing Eq. (4.36) with the appropriate summation limits and Eq. (4.7) with reversed sign. In Figure 20 a definition sketch is shown. If the pitch height is denoted by p, then the width of the circle segment becomes $2\sqrt{p(2a-p)}$. Furthermore, the height of the rectangular fill is $a - p$, and the angle a (see Figure 7) is $\arcsin\,(1 - p/a)$. Consequently, the summation of the solutions for the polygon stretches should start at angle α in the semicircle and end at angle $-\alpha$. The solution is:

$$y(x,t) = \frac{1}{2}\sum_{i=m+1}^{N-m-1}\left(y_i{}^L + k_i(x_i{}^L - x)\left(\operatorname{erf}\left(\frac{x_i{}^R - x}{2\sqrt{\varepsilon t}}\right) - \operatorname{erf}\left(\frac{x_i{}^L - x}{2\sqrt{\varepsilon t}}\right)\right)\right.$$
$$\left. + 2k_i\sqrt{\frac{\varepsilon t}{\pi}}\left(e^{\frac{-(x_i{}^R - x)^2}{4\varepsilon t}} - e^{\frac{-(x_i{}^L - x)^2}{4\varepsilon t}}\right)\right)$$
$$-\frac{1}{2}(a-p)\left(\operatorname{erf}\left(\frac{\sqrt{p(2a-p)} - x}{2\sqrt{\varepsilon t}}\right)\right.$$
$$\left. + \operatorname{erf}\left(\frac{\sqrt{p(2a-p)} + x}{2\sqrt{\varepsilon t}}\right)\right) \tag{4.37}$$

For $t > 0$ and $-\infty < x < \infty$.

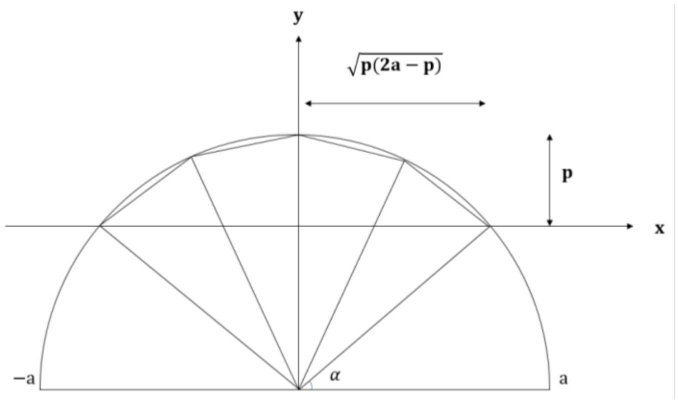

Figure 20 - Definition sketch for a circular segment-shaped beach

The quantity N is, as before, the number of corners in the polygon, and m represents the number of corners minus one contained in the angle α.

Since the tangent of the shoreline orientation is infinite at the corners of the semicircle (x = ±a), the condition of small angles is violated. This condition implies, as previously discussed, that the sand transport is overestimated, leading to a faster dispersion process of the shoreline toward the stable condition (a beach parallel to the wave crests). An analytical solution for a circular segment-shaped beach, however, will show better agreement with the numerical solution of the original sand transport formula if the angle of shoreline orientation is small at the edges.

The situation of a semi-circular cut in a beach is the antisymmetric analogue of the case just described. A solution is obtained by superimposing Eq. (4.36) with opposite sign for a beach of width a.

4.6.6. Rhythmic Beach

For this special case, the beach has a sinusoidal variation in shoreline position, as might occur with *spatially periodic* sand waves.

The initial condition is:

$$y(x,0) = A\cos\sigma x \tag{4.38}$$

where A represents the amplitude of the rhythmic form such as cusps along the beach, and σ denotes the wave number of the shoreline oscillation or cusp. The quantity σ can be expressed also as $2\pi/L$, where L is the beach cusp wave length. The solution to this case is found to be:

$$y(x,t) = A\cos\sigma x\, e^{-\sigma^2\varepsilon t} \tag{4.39}$$

For $t > 0$ and $-\infty < x < \infty$.

Le Mehaute and Brebner (1961) and Bakker (1969) give this solution. The amplitude clearly approaches zero exponentially with time. The smaller the value of σ, or the longer the spacing between the shoreline features, the longer the time for the beach to evolve to a straight beach.

A surprising result occurs when the wave angle of approach α_b is greater than 45° as the sign of ε changes. This results in an *exponential increase* of the periodic shoreline features. This might apply to the situation of cuspate features on long lagoons, as will be discussed in the following Chapters.

4.6.7. Sand Discharge from a River Acting as a Point Source

If a river mouth is small in comparison to the area into which it is discharging sand, the discharge may be approximated by a point source. The sand discharge from the river or the strength of the point source is denoted as q and is a function of time. (The units of q_R are m^3/sec.) A solution may be obtained by considering the continuous sand discharge from the river to be the sum of discretely released quantities of sand at consecutive times. If a certain volume of sand V is instantaneously released at a point x_s at time t_s, the solution can be written

$$y(x,t) = \frac{V}{2D\sqrt{\pi\varepsilon(t-t_s)}}\, e^{\frac{-(x-x_s)^2}{4\varepsilon(t-t_s)}} \tag{4.40}$$

For $t > t_s$ and $-\infty < x < \infty$.

Eq. (4.40) has been discussed by Le Mehaute and Brebner (1961) and by Le Mehaute and Soldate (1977). Accordingly, a superposition of an infinite number of such released quantities can be used to represent the sand discharge from a river. The solution for a point source with a continuous time variable sand discharge q_R may be expressed as:

$$y(x,t) = \frac{1}{2D\sqrt{\pi\varepsilon}} \int_0^t q_R(\xi)\, e^{\frac{-(x-x_s)^2}{4\varepsilon(t-\xi)}} \frac{d\xi}{\sqrt{t-\xi}} \tag{4.41}$$

For $t > 0$ and $-\infty < x < \infty$.

If q_R is constant and equal to q_0, the solution is:

$$y(x,t) = \frac{q_0}{D}\sqrt{\frac{t}{\pi\varepsilon}}\,e^{\frac{-(x_s-x)^2}{4\varepsilon t}} - \frac{q_0}{D}\frac{|x-x_s|}{2\varepsilon}erfc\frac{|x-x_s|}{2\sqrt{\varepsilon t}} \tag{4.42}$$

For $t > 0$ and $-\infty < x < \infty$.

Eq. (4.42) is identical to the solution describing a constant flux $q_0/2$ on the boundary (x = 0) for a beach of semi-infinite extent. Figure 21 illustrates the solution where L is used as a normalizing length, and the point source is located at $x_s = L$. The nondimensional quantity containing the shoreline position is formed as the ratio between the amplitude of the sand transport rate and the sand discharge from the river.

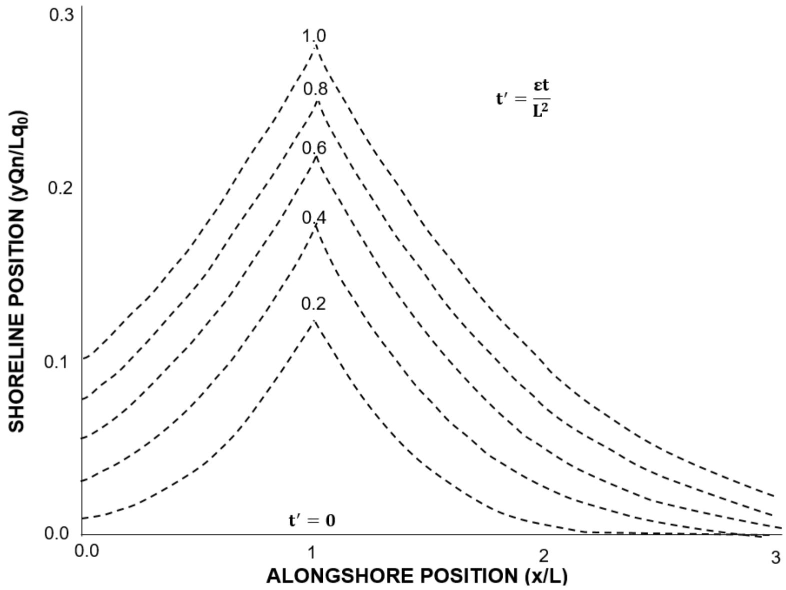

Figure 21 - Shoreline evolution in the vicinity of a river discharging sand and acting as a point source

If the sand discharge has a periodic behaviour, the function q could take the following form:

$$q_R(t) = q_0 + q_s \sin(\omega t + \varphi) \tag{4.43}$$

Where:

q_0 = steady sand discharge from river

q_s= amplitude of periodic sand discharge

ω = angular frequency = $2\pi/T$

T = period of oscillation of sand discharge from river

φ = phase angle of periodic variation

The solution consists of two parts, namely Eq. (4.42) describing the shoreline evolution from a steady point source and the following solution which accounts for the periodic component:

$$y(x,t) = \frac{q_s}{D\sqrt{\varepsilon t}} \int_0^{\sqrt{t}} \sin(\omega(t-\xi^2)+\varphi)\, e^{\frac{-x^2}{4\varepsilon\xi^2}}\, d\xi \tag{4.44}$$

The shoreline behaviour is composed of one contribution that evolves roughly proportional to the square root of elapsed time and another contribution which is a periodic oscillation that damps out along the x-axis with a decay factor $\sqrt{\omega/2\varepsilon}$ (both in the negative and positive directions). Consequently, beyond a certain distance from the discharge the periodic effect of Eq. (4.43) can be neglected, implying that the solution may be approximated by Eq. (4.40) only. Because of the periodic variation in the discharge, sand waves are generated from the river mouth. These sand waves propagate with a speed $\sqrt{2\omega\varepsilon}$ along the x-axis, and the time lag between the oscillation in sand discharge at the river mouth and a specific location is $/4\ +\ x\sqrt{2\omega\varepsilon}$.

4.7. Solutions for shoreline evolution involving coastal structures

In the previous section, the incident wave crests were restricted to be parallel to the x-axis. In such a case, an initially straight beach will always remain straight, unless material is supplied in an irregular way. If the waves arrive at the same angle to the shoreline everywhere, the beach will also be stable if it is initially straight. However, if an obstacle on the beach disturbs the equilibrium transport conditions, a change in shoreline position occurs in order to achieve a new steady-state configuration. Examples of such obstacles are groins, jetties, detached breakwaters, and seawalls. In order to treat such complex cases analytically, the situation has to be idealized to a large degree. Properties which generally vary continuously along the shoreline (breaking wave angle, amplitude of the sand transport rate, etc.) usually must be approximated by means of a series of coupled solutions of simpler problems. Within each solution area the properties are held constant but are allowed to vary from one area to another.

4.7.1. Shoreline change at groins and jetties

The analytical solution for beach change at a groin or any thin shore-normal structure which blocks along-shore sand transport was first obtained by Pelnard-Considére (1956). Initially, the beach is in equilibrium (parallel to the x-axis) with the same breaking wave angle existing everywhere, thus leading to a uniform sand transport rate along the beach. At time t =0 a thin groin is instantaneously placed at x =0, blocking all transport. Mathematically, this boundary condition can be formulated as:

$$\frac{\partial y}{\partial x} = \tan \alpha_0 \qquad\qquad x = 0 \tag{4.45}$$

This equation states that the shoreline at the groin is at every instant parallel to the wave crests. The wave crests make an angle α_0 with the x-axis according to Figure 22, giving rise to long-shore sand transport in the negative x-direction.

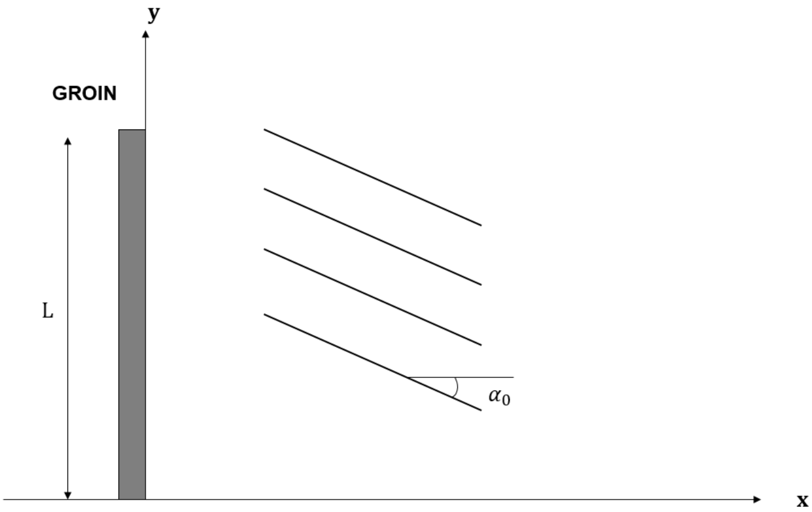

Figure 22 - Definition sketch for the case of a groin

A groin interrupts the transport of sand along-shore, causing an accumulation at the updrift side and erosion at the downdrift side. The solution describing the accumulation part is:

$$y(x,t) = 2\ \tan \alpha_0\ \sqrt{\varepsilon t}\ ierfc\left(\frac{x}{2\sqrt{\varepsilon t}}\right) \tag{4.46}$$

For $t > 0$ and $x \geq 0$.

The solution can also be written as follows:

$$y(x,t) = 2\ \tan \alpha_0 \left(\sqrt{\frac{\varepsilon t}{\pi}}\, e^{\frac{-x^2}{4\varepsilon t}} - \frac{x}{2} erfc\left(\frac{x}{2\sqrt{\varepsilon t}}\right)\right) \tag{4.47}$$

This expression is obtained by integrating the function ierfc by parts. A nondimensional plot of the shoreline evolution updrift of a groin is shown in Figure 23.

The shoreline position has been normalized with a characteristic length (the groin length) and the tangent of the incident breaking wave angle.

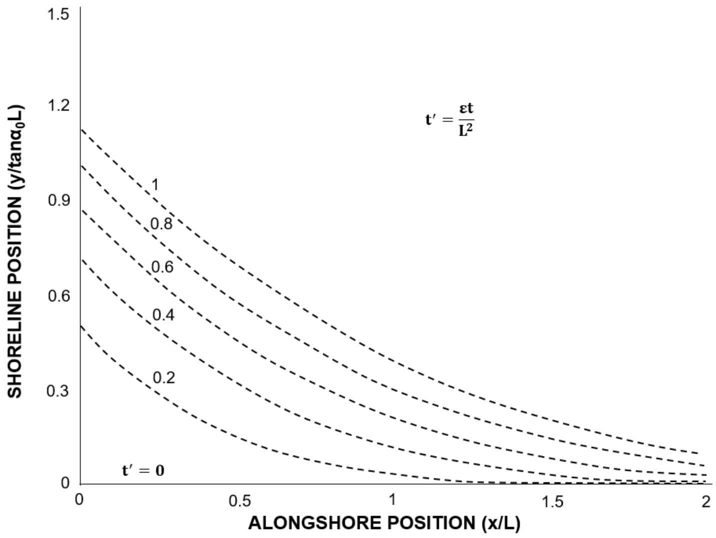

Figure 23 - Shoreline evolution updrift of a groin which is totally blocking the transport of sand along-shore

For a specified amplitude of the sand transport rate and the depth of closure, the ratio of shoreline positions at a given point for two different incident breaking wave angles is proportional to the following ratio of respective tangents of the angles:

$$\frac{y_1}{y_2} = \frac{\tan \alpha_{01}}{\tan \alpha_{02}} \tag{4.48}$$

Eq. (4.47) is valid only until the shoreline has reached the tip of the groin, after which time bypassing of sand is assumed to take place. This bypassing happens when $y = L$ (length of the groin), which occurs at time t_G:

$$t_G = \frac{\pi}{\varepsilon} \frac{L^2}{4 \tan^2 \alpha_0} \tag{4.49}$$

The above relationship for a fixed wave climate reveals that if the groin length is doubled, the time required for the shoreline to reach the end of the groin will increase fourfold.

If bypassing of a groin occurs, the boundary condition at $x = 0$ changes into $x = L$. A correct solution to this situation should fulfil this boundary condition and use as an initial condition the shoreline shape just before bypassing occurred, according to Eq. (4.47). An approximate solution was presented Pelnard-Considére (1956) who used the solution for a shoreline with fixed position y_0 at $x = 0$ and matched it against Eq. (4.47) by equating sand volumes.

With this criterion, the following relationship between the time elapsed before bypassing occurs t_G (in Eq. 4.47) and the actual time in the matching solution t_V, which makes the sand volumes equal, is obtained:

$$\frac{t_V}{t_G} = \frac{\pi^2}{16} \tag{4.50}$$

Thus, in the case of bypassing, it is possible to use Eq. 4.17, if the time t is replaced by $t_* = t - (1 - \pi^2/16)t_G$ for $t > t_G$. The rate of sand bypassing the groin for $t > t_G$ is calculated to produce the following relationship:

$$Q = 2Q_0\alpha_0 \left(1 - \frac{L}{\alpha_0\sqrt{\pi\varepsilon t_*}}\right) \tag{4.51}$$

For $t > t_G$.

Here $2Q_0\alpha_0$ a is the sand transport rate at equilibrium (straight beach) under imposed incident breaking wave angle α_0, and t_* is the modified time in the matching solution using Eq. (4.17).

Formally, the solution downdrift of a groin is the same as that in Eq. (4.47) but with opposite sign. However, if the groin or jetty extends far outside the wave breaker line, diffraction will occur behind the groin altering the breaking wave height and angle; thus the transport capacity does not provide a complete description of the shoreline evolution if diffraction is significant.

Bypassing may occur immediately after construction of a groin and not start just at the time when the groin is completely filled. If the bypassing sand transport rate grows exponentially to a limiting value Q_B the boundary condition at the groin will be:

$$\frac{\partial y}{\partial x} = \alpha_0 - \frac{1}{2}\frac{Q_B}{Q_0}(1 - e^{-\gamma t}) \qquad x = 0 \tag{4.52}$$

The quantity γ is a rate coefficient describing the speed at which the bypassing sand discharge grows toward the limiting value Q_B. The solution downdrift of a groin may be written (for an initially straight beach) as:

$$y(x,t) = -2\left(\alpha_0 - \frac{1}{2}\frac{Q_B}{Q_0}\right)\left(\sqrt{\frac{\varepsilon t}{\pi}}e^{\frac{-x^2}{4\varepsilon t}} - \frac{x}{2}erfc\left(\frac{x}{2\sqrt{\varepsilon t}}\right)\right)$$

$$-\frac{Q_B}{Q_0}\sqrt{\frac{\varepsilon}{\pi}}e^{-\gamma t}\int_0^{\sqrt{t}} e^{\gamma\xi^2 - x^2/4\varepsilon\xi^2}d\xi \tag{4.53}$$

For $t > 0$ and $x \geq 0$.

Larson and Kraus, employing the two dimensionless parameters, Q_B/Q_0 and $\gamma L^2/\varepsilon$, illustrate the solution. The parameter $\gamma L^2/\varepsilon$ describes the rate at which the sand bypassing increases in comparison to the size of the coastal constant (ε). In Eq. (4.53) the second term is a transient which decays with elapsed time.

Accordingly, after sufficient elapsed time, Eq. (4.53) will be identical to the solution given by Eq. (4.47) with a modified incident breaking wave angle at $x = 0$ ($\tan\alpha_0 \approx \alpha_0$). Eq. (4.53) may be used also to describe shoreline change updrift of a groin (with reversed sign) if bypassing occurs immediately after construction of the groin. If, in Eq. (4.53), $Q_B/Q_0 = 2\alpha_0$ the bypassing sand discharge will equal the transport rate along-shore behind the groin at equilibrium conditions. Consequently, the initially eroded area downdrift of the groin will fill when the bypassing sand rate reaches its maximum, and the beach will become straight again.

In order to investigate the effects of the linearization of the governing equation (Eq. (4.2)) on the solution for a groin, numerical simulations were carried out with the original sand transport equation. Selected results are displayed in Figures 24 and 25. From the two figures it is seen that the linearization procedure degrades the solution if the incident breaking wave angle is about 30 deg.

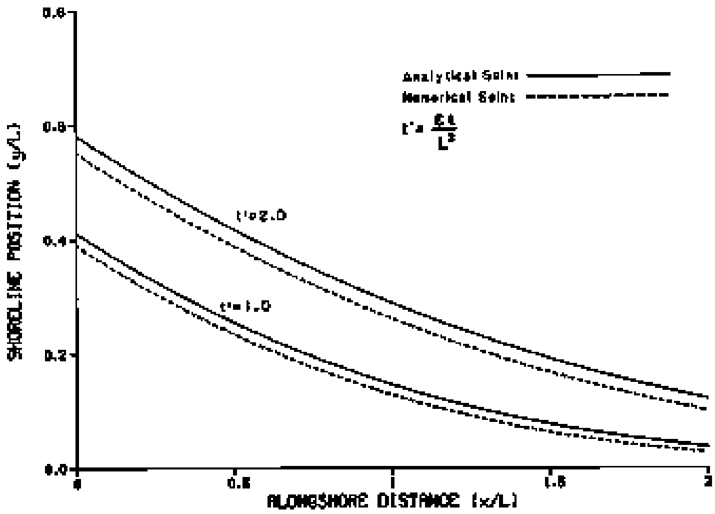

Figure 24 - Comparison between analytical and numerical solutions of shoreline evolution updrift of a groin with incident breaking wave angle 20 deg (original from Larson and Kraus, 1987)

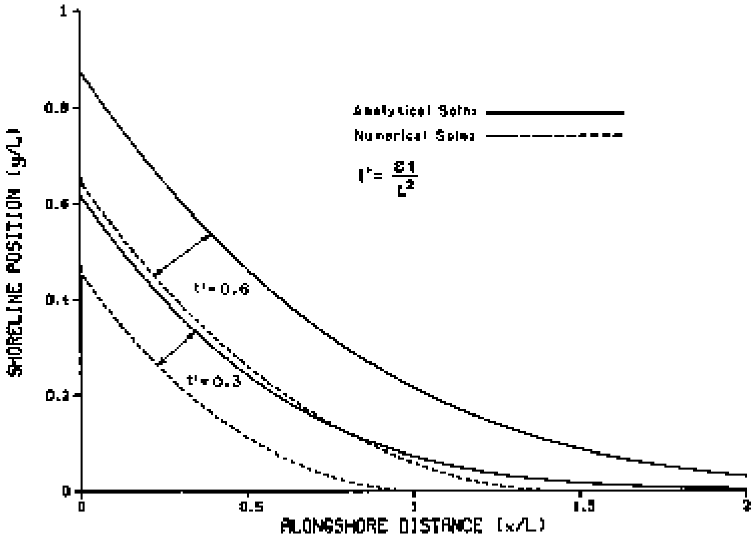

Figure 25 - Comparison between analytical and numerical solutions of shoreline evolution updrift of a groin with incident breaking wave angle 45 deg (original from Larson and Kraus, 1987)

4.7.2. Initially Filled Groin System

Dean (1984) presents an analytical solution for shoreline evolution between two identical groins which define a compartment initially filled with sand. The distance between the groins is denoted by W, and the groin length is L. At time $t = 0$, the shoreline is exposed to the action of waves breaking with angle α_0.

The solution is:

$$y(x,t) = L - W\left(1 - \frac{x}{W}\right)\tan\alpha_0 + \frac{2\tan\alpha_0}{W}$$

$$\sum_{n=0}^{\infty}\left(\left(\frac{2W}{(2n+1)\pi}\right)^2 e^{-\varepsilon(2n+1)^2\pi^2 t/4W^2}\cos\left(\frac{(2n+1)\pi x}{2W}\right)\right) \qquad (4.54)$$

For $t > 0$ and $0 \leq x \leq W$.

The boundary conditions for this configuration are no sand transport at $x = 0$ ($\partial y/\partial x = \tan\alpha_0$) and a constant shoreline position of $y = L$ at $x = W$. Consequently, bypassing occurs at the boundary $x = W$, whereas no sand enters the system at $x = 0$.

This occurrence means that the solution is unsuitable for application to a groin system of more than one compartment. Otherwise, bypassing must be accounted for in the boundary conditions at the updrift groin (left) in each compartment leading to a coupled problem. The last term in Eq. (4.54) approaches zero as $t \to \infty$ and causes a shoreline parallel to the wave crests to be created between the groins.

The final percentage loss of sand from the groin compartment is:

$$\frac{1}{2}\frac{W}{L}\tan\alpha_0 \tag{4.55}$$

From Eq. (4.55), the sand bypassed (discharge rate) at $x = W$ can be obtained. The sand transport rate as a function of time can be written (if it is assumed that $\tan\alpha_0 \approx \alpha_0$):

$$Q(t) = 4Q_0\alpha_0 \sum_{n=0}^{\infty}(-1)^n \frac{2}{(2n+1)\pi} e^{-\varepsilon(2n+1)^2\pi^2 t/4W^2} \tag{4.56}$$

For $t > 0$ and $x = W$.

In Eq. (4.56), the quantity $2Q_0\alpha_0$ is the sand transport rate along a straight beach exposed to the incident breaking wave angle α_0. (This is the transport initially existing when the groin compartment is completely filled.) If Q in Eq. (4.56) is normalized with this quantity, the bypassing sand discharge at the downdrift end groin is conveniently displayed in dimensionless form. Figure 26 shows such a curve.

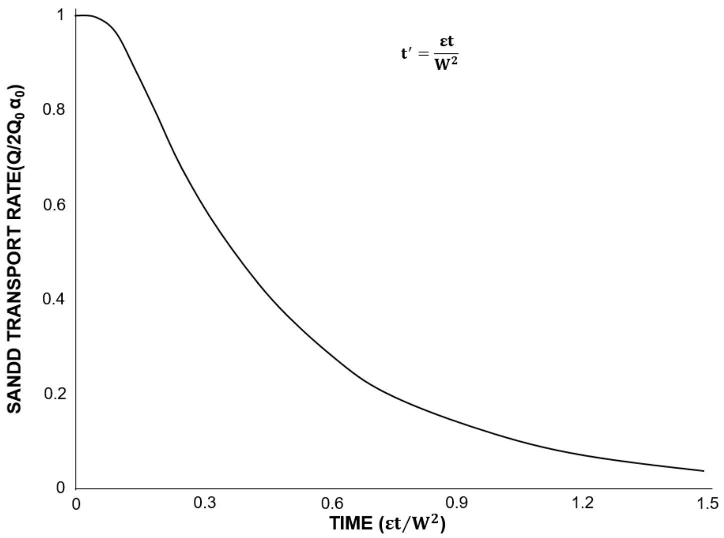

Figure 26 - Bypassing sand transport rate at the downdrift end of a groin $x = W$ as a function of time

4.7.3. Shoreline Change at a Detached Breakwater

A detached breakwater reduces the wave height behind it and produces a circular wave pattern at each tip, thus decreasing the long-shore sand transport rate. The actual effects are quite complex to describe and involve diffraction and the current field resulting from spatial changes in wave height and direction. However, it is possible to find an analytical solution if the situation is idealized. It is assumed that the incident breaking wave crests are parallel to the x-axis and to the detached breakwater. When the waves reach the breakwater, they are assumed to be diffracted at a constant angle behind the breakwater (shadowed region) and remain parallel to the x-axis outside of the breakwater (the illuminated region). The diffraction behind the breakwater is symmetric about the centre of the breakwater and, accordingly, only half of the problem domain needs to be considered. In Figure 27, a definition sketch is shown.

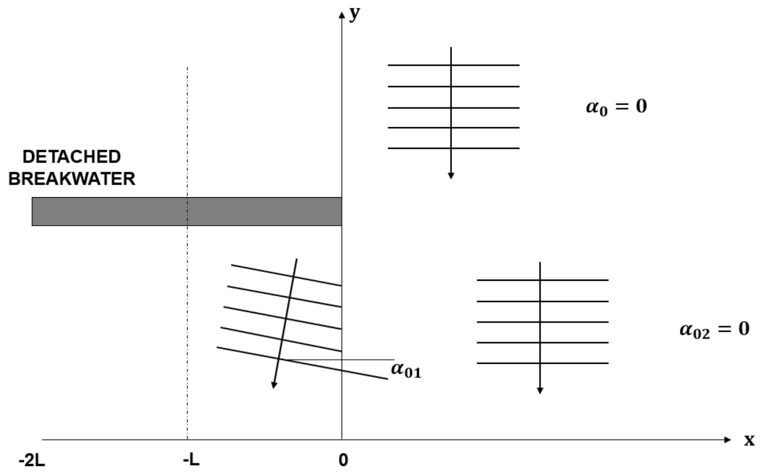

Figure 27 - Definition sketch for the problem of shoreline change in the vicinity of a detached breakwater

Since the incident breaking wave angles and the amplitudes of then sand transport rates respectively, are different in the shadowed and illuminated regions, a coupled problem arises. The boundary conditions for this case are as follows:

a. No sand should be transported across the line of symmetry behind the breakwater.
b. The sand transport rate out of the area on the right side of the breakwater should be equal to that into the area behind the breakwater.
c. The shoreline is continuous over the boundary between the two areas.

Furthermore, the shoreline should be undisturbed $(y = 0)$ far from the structure. With y_1 denoting the shoreline position in solution area number 1 (shadow region) and y_2, denoting the shoreline position in solution area number 2 (the illuminated region), the mathematical formulation of the situation is:

$$\varepsilon_1 \frac{\partial^2 y_1}{\partial x^2} = \frac{\partial y_1}{\partial t} \qquad -L \le x \le 0 \tag{4.57}$$

$$\varepsilon_2 \frac{\partial^2 y_2}{\partial x^2} = \frac{\partial y_2}{\partial t} \qquad x > 0 \tag{4.58}$$

$$y_1(x,0) = y_2(x,0) = 0 \tag{4.59}$$

$$\frac{\partial y_1}{\partial x} = \tan \alpha_{01} \qquad x = -L \tag{4.60}$$

$$\frac{\partial y_1}{\partial x} = \frac{\partial y_2}{\partial x}\frac{Q_{02}}{Q_{01}} + \alpha_{01} \qquad x = 0 \qquad (4.61)$$

$$y_1 = y_2 \qquad x = 0 \qquad (4.62)$$

$$y_2 = 0 \qquad x = +\infty \qquad (4.63)$$

The quantities Q_{01} and Q_{02} are the amplitudes of the long-shore sand transport rate in the respective areas, and α_{01} is the diffracted breaking wave angle behind the breakwater. The angle α_{02} is zero since the wave crests in this area are parallel to the x-axis throughout time. The solution is, with:

$$\delta = \sqrt{\frac{\varepsilon_1}{\varepsilon_2}} = \sqrt{\frac{Q_{01}}{Q_{02}}} \qquad (4.64)$$

$$y_1(x,t)$$

$$= -\frac{\delta\alpha_{01}}{\delta+1} 2\sqrt{\varepsilon_1 t}\, ierfc\left(\frac{-x}{2\sqrt{\varepsilon_1 t}}\right)$$

$$+ \tan\alpha_{01} \sum_{n=0}^{\infty}\left(\left(\frac{\delta-1}{\delta+1}\right)^n 2\sqrt{\varepsilon_1 t}\, ierfc\left(\frac{(2n+1)L+x}{2\sqrt{\varepsilon_1 t}}\right)\right.$$

$$\left.+\left(\frac{\delta-1}{\delta+1}\right)^{n+1} 2\sqrt{\varepsilon_1 t}\, ierfc\left(\frac{(2n+1)L-x}{2\sqrt{\varepsilon_1 t}}\right)\right)$$

$$-\frac{\delta\alpha_{01}}{\delta+1} \sum_{n=0}^{\infty}\left(\left(\frac{\delta-1}{\delta+1}\right)^n 2\sqrt{\varepsilon_1 t}\, ierfc\left(\frac{(2n+1)L+x}{2\sqrt{\varepsilon_1 t}}\right)\right.$$

$$\left.+\left(\frac{\delta-1}{\delta+1}\right)^{n+1} 2\sqrt{\varepsilon_1 t}\, ierfc\left(\frac{(2n+1)L-x}{2\sqrt{\varepsilon_1 t}}\right)\right) \qquad (4.65)$$

For $t > 0$ and $-L \leq x \leq 0$.

$$y_2(x,t)$$

$$= -\frac{\delta\alpha_{01}}{\delta+1} 2\sqrt{\varepsilon_1 t}\, ierfc\left(\frac{\delta x}{2\sqrt{\varepsilon_1 t}}\right)$$

$$-2\frac{\delta^2\alpha_{01}}{(\delta+1)^2} \sum_{n=0}^{\infty}\left(\left(\frac{\delta-1}{\delta+1}\right)^n 2\sqrt{\varepsilon_1 t}\, ierfc\left(\frac{\delta x+(2n+1)L}{2\sqrt{\varepsilon_1 t}}\right)\right)$$

$$+2\frac{\delta\tan\alpha_{01}}{\delta+1} \sum_{n=0}^{\infty}\left(\left(\frac{\delta-1}{\delta+1}\right)^n 2\sqrt{\varepsilon_1 t}\, ierfc\left(\frac{\delta x+(2n+1)L}{2\sqrt{\varepsilon_1 t}}\right)\right) \qquad (4.66)$$

For $t > 0$ and $x > 0$.

The distance L is half the length of the detached breakwater. If Eq. (4.65) and (4.66) are plotted, the following behaviour will be noticed. When the breakwater is placed in front of the initially straight shoreline at time $t = 0$, erosion of the shoreline starts at points in line with the corners of the breakwater. Simultaneously, the shoreline grows to form a salient about the line of symmetry behind the breakwater. Because of the gradient of the shoreline outside the shadow of the breakwater, material is transported toward the breakwater in order to achieve a state of equilibrium with the waves. The shoreline behind the breakwater also approaches an equilibrium configuration which is parallel to the wave crests diffracted at the angle α_{01}. The final shoreline will be inclined at an angle α_{01}, behind the breakwater and be straight outside the breakwater. However, the straight portion of the shoreline will at all times be displaced landward a small distance, controlled by the volume of sand that has accumulated behind the breakwater.

Figure 28 illustrates the solution in dimensionless form for short elapsed times. The length of the salient behind the breakwater increases in time toward a maximum value of:

$$L \tan \alpha_{01} \tag{4.67}$$

The elapsed time is normalized by the quantity $L^{\,2}/\varepsilon$. Although mass is conserved across the boundary between the two solution areas, the gradient of the shoreline is not continuous at this point.

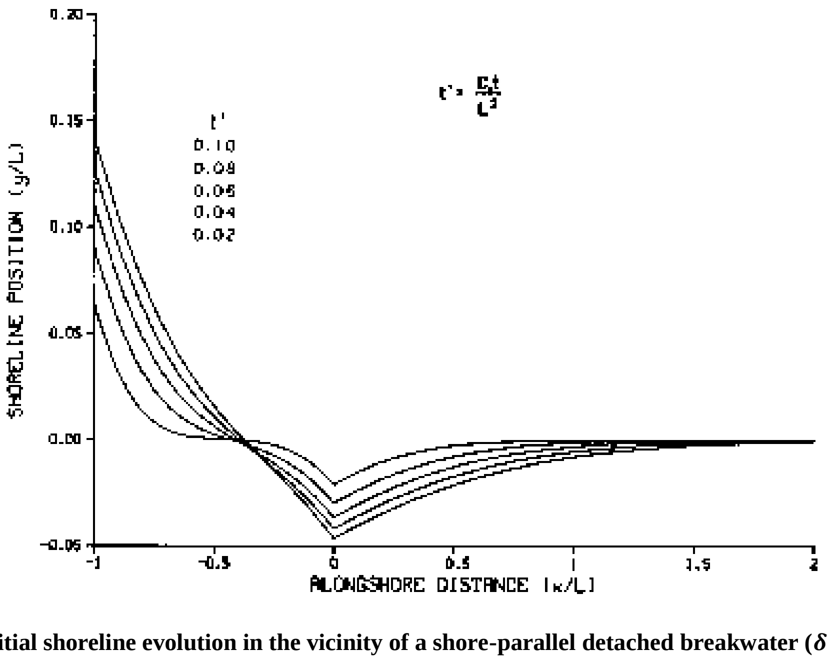

Figure 28 - Initial shoreline evolution in the vicinity of a shore-parallel detached breakwater ($\delta = 0.5$, $\alpha_{01} = 0.4 rad$, $\alpha_{02} = 0$) (original from Larson and Kraus, 1987)

4.7.4. Shoreline Change at a Seawall

The function of a seawall is to prevent the shoreline from retreating along a specific coastal reach. If the shoreline remains well seaward of the seawall, there will be no influence of the seawall on the shoreline evolution. If the shoreline retreats to the seawall, the location of the seawall determines the minimum allowable shoreline position. If erosion takes place beside a seawall (flanking), various changes in the shoreline position might occur depending on the characteristics of the seawall and the incident waves. If flanking of the seawall is not possible the solution for the plane shape of an eroded shoreline will be the same as for erosion downdrift of a groin. In this case, the seawall is functioning as a semi-infinite structure.

The case of erosion at the side and behind a seawall, i.e., flanking of the seawall, must be solved as a coupled problem. The incident breaking wave angle is α_{02} outside the seawall and α_{01} behind it. Wave energy is transported behind the seawall by the process of diffraction.

The ratio between the amplitudes of the long-shore sand transport rate in the two solution areas will be denoted as $\delta^2 (= Q_{01}/Q_{02})$. Mathematically, the situation is formulated as:

$$\varepsilon_1 \frac{\partial^2 y_1}{\partial x^2} = \frac{\partial y_1}{\partial t} \qquad x \le 0 \qquad (4.68)$$

$$\varepsilon_2 \frac{\partial^2 y_2}{\partial x^2} = \frac{\partial y_2}{\partial t} \qquad x > 0 \qquad (4.69)$$

$$y_1(x,0) = y_2(x,0) = 0 \qquad (4.70)$$

$$\frac{\partial y_1}{\partial x} = \alpha_{01} - \frac{1}{\delta^2}\alpha_{02} + \frac{1}{\delta^2}\frac{\partial y_2}{\partial x} \qquad x = 0 \qquad (4.71)$$

$$y_1 = y_2 \qquad x = 0 \qquad (4.72)$$

$$y_1 = 0 \qquad x \to \infty \qquad (4.73)$$

$$y_2 = 0 \qquad x \to \infty \qquad (4.74)$$

It is assumed that the border between the two solution areas at $x = 0$ is stationary in time, although it moves somewhat in the x-direction as time evolves. The solution is:

$$y_1(x,t) = -\frac{\alpha_{01} - \frac{1}{\delta^2}\alpha_{02}}{1 + \frac{1}{\delta}} \left(2\sqrt{\frac{\varepsilon_1 t}{\pi}} e^{\frac{-x^2}{4\varepsilon_1 t}} + x\, erfc\left(\frac{-x}{2\sqrt{\varepsilon_1 t}}\right) \right) \qquad (4.75)$$

For $t > 0$ and $x \leq 0$.

$$y_2(x,t) = -\frac{\alpha_{01} - \frac{1}{\delta^2}\alpha_{02}}{1+\frac{1}{\delta}}\left(2\sqrt{\frac{\varepsilon_1 t}{\pi}}e^{\frac{-x^2}{4\varepsilon_1 t}} - \delta x\, erfc\left(\frac{\delta x}{2\sqrt{\varepsilon_1 t}}\right)\right) \tag{4.76}$$

For $t > 0$ and $x > 0$.

The quantity α_{01} represents a mean diffracted wave angle behind the seawall. A characteristic length L is chosen to normalize the shoreline position.

4.7.5. Shoreline Change at a Jetty, Including Diffraction

In the shadow zone of a long groin or jetty, it may be an oversimplification to neglect the process of wave diffraction. Consequently, although Equation 58 (with reversed sign) may give a satisfactory description of shoreline evolution at some distance downdrift of a jetty, in the vicinity of the jetty this solution does not represent what is commonly observed. Erosion just behind the jetty will be overestimated if diffraction is neglected since the wave height is assumed to be constant along-shore. Accordingly, by allowing a variation in wave height (and thus in the amplitude of the sand transport rate) in the shadow zone, a more realistic description of shoreline change will be obtained.

There are a number of ways to account for a varying amplitude in the long-shore sand transport rate (resulting from varying wave height).

One way is to assume that, outside the shadow zone, the incident breaking wave angle and the amplitude of the sand transport rate are not influenced by the jetty. In the vicinity of the jetty, it is possible to account for a variation in the amplitude of the sand transport rate. An alternative way is to divide the shadow region into distinct solution areas, each having a constant amplitude of the sand transport rate. The incident breaking wave angle may also be varied from one solution area to another. With this procedure, a coupled system of equations is obtained which involves intensive calculations for even a small number of solution areas. If the simple case of two solution areas (one inside the shadow zone and one outside) is considered, the mathematical formulation is the same as for a detached breakwater. However, the incident breaking wave angle outside the shadow region is not zero (in which case no sand transport would occur) but has a finite value. Therefore, the boundary condition on continuity in sand transport across the border between the two solution areas takes the following form:

$$\frac{\partial y_1}{\partial x} = \alpha_{01} - \frac{1}{\delta^2}\alpha_{02} + \frac{1}{\delta^2}\frac{\partial y_2}{\partial x} \tag{4.77}$$

where δ^2 is the ratio between the amplitudes of the sand transport rate inside and outside the shadow region. The analytical solution to this problem is formally identical to Eq.s (4.65) and (4.66), except that certain constants are different. The following substitutions should be made in order to apply to Eq.s (4.65) and (4.66), to the diffracting jetty case:

$$-\frac{\delta\alpha_{01}}{\delta+1} \rightarrow \frac{-\delta^2\alpha_{01} + \alpha_{02}}{\delta(\delta+1)} \tag{4.78}$$

$$-\frac{\delta^2\alpha_{01}}{(\delta+1)^2} \rightarrow \frac{-\delta^2\alpha_{01} + \alpha_{02}}{(\delta+1)^2} \tag{4.79}$$

If α_{02} is zero, the expressions on the right side reduce to those on the left side.

Generalization to an arbitrary number of solution areas is straightforward, in which case the situation is mathematically expressed for the i^{th} area as follows:

$$\varepsilon_1 \frac{\partial^2 y_i}{\partial x^2} = \frac{\partial y_i}{\partial t} \qquad x_i \leq x \leq x_{i+1} \tag{4.80}$$

$$\frac{\partial y_i}{\partial x} = \alpha_{0i} - \frac{1}{{\delta_i}^2}\alpha_{0i+1} + \frac{1}{{\delta_i}^2}\frac{\partial y_{i+1}}{\partial x} \qquad x = x_{i+1} \tag{4.81}$$

$$\frac{\partial y_{i-1}}{\partial x} = \alpha_{0i-1} - \frac{1}{{\delta_{i-1}}^2}\alpha_{0i} + \frac{1}{{\delta_{i-1}}^2}\frac{\partial y_i}{\partial x} \qquad x = x_i \tag{4.82}$$

$$y_{i-1} = y_i \qquad x = x_i \tag{4.83}$$

$$y_i = y_{i+1} \qquad x = x_{i+1} \tag{4.84}$$

Where:

$${\delta_i}^2 = \frac{Q_{0i}}{Q_{0i+1}} \tag{4.85}$$

For the first and last solution areas, other conditions prevail on the outer boundaries, such as no sand transport at the jetty, and $y = 0$ as $x \rightarrow +\infty$.

Extremely complex algebraic manipulations are associated with the analytical solution of coupled systems with several solution areas.

The length of the geometric shadow region is $x = L \tan \alpha_0$, where L is the jetty length and α_0 is the incident breaking wave angle in the illuminated region.

If the amplitude of the long-shore sand transport rate is considered to be a continuous function of x in the shadow zone, Eq. (4.2) is applicable. However, this equation is quite complex, and it is difficult to find analytical solutions even if very simple functions are employed. The related case, in which the incident breaking wave angle is a continuous function of x, is easier to treat analytically and provides interesting solutions, these circumstances, Eq. (4.2) will take the following form:

$$\frac{\partial^2 y}{\partial x^2} = \frac{1}{\varepsilon}\frac{\partial y}{\partial t} + \frac{d\alpha_0}{dx} \tag{4.86}$$

in which $\alpha_0$is a function of x only. This is formally the same equation as that describing heat conduction in a solid containing a finite source. Consequently, if α_0 grows linearly with x ($\alpha_0 = x_m^{\alpha}/B$) the situation will be identical to the one describing a river mouth of finite length which discharges sand at a constant rate (see Larson and Kraus, 1987).

If α_0 is different from zero at the jetty, but still grows linearly along the x-axis in the shadow zone, the variation in breaking wave angle will be:

$$\alpha_0 = \alpha_V + (\alpha_H - \alpha_V)\frac{x}{B} \tag{4.87}$$

in which α_V is the incident breaking wave angle at the jetty, and α_H is the angle in the illuminated region. The mathematical description for this case is almost the same as for a river mouth of finite length which discharges sand but with a modified source term. This is a coupled problem containing two solution areas but with a boundary condition at the jetty given by

$$\frac{\partial y_1}{\partial x} = \tan\alpha_V \tag{4.88}$$

The analytical solution to this problem is:

$$y_1(x,t) = \frac{(\alpha_H - \alpha_V)\varepsilon t}{B}\left(2i^2erfc\left(\frac{B-x}{2\sqrt{\varepsilon t}}\right) + 2i^2erfc\left(\frac{B+x}{2\sqrt{\varepsilon t}}\right) - 1\right)$$

$$- \tan\alpha_V\left(2\sqrt{\frac{\varepsilon t}{\pi}}e^{\frac{-x^2}{4\varepsilon t}} - x\,erfc\left(\frac{x}{2\sqrt{\varepsilon t}}\right)\right) \tag{4.89a}$$

For $t > 0$ and $0 \leq x \leq B$.

$$y_2(x,t) = \frac{(\alpha_H - \alpha_V)\varepsilon t}{B}\left(2i^2erfc\left(\frac{x+B}{2\sqrt{\varepsilon t}}\right) + 2i^2erfc\left(\frac{x-B}{2\sqrt{\varepsilon t}}\right) - 1\right)$$

$$- \tan\alpha_V\left(2\sqrt{\frac{\varepsilon t}{\pi}}e^{\frac{-x^2}{4\varepsilon t}} - x\,erfc\left(\frac{x}{2\sqrt{\varepsilon t}}\right)\right) \qquad (4.89b)$$

For $t > 0$ and $x > B$.

The quantity B is the geometric length of the shadow zone as before.

Another case that allows a fairly easy analytical solution is obtained by assuming that the incident breaking wave angle varies exponentially with distance from the jetty according to: $\alpha_0 = \alpha_m(1 - e^{-\gamma x})$.

Here, the quantity γ is a coefficient describing the rate at which the breaking wave angle approaches the undisturbed value α_m along the x-axis.

The solution is:

$$y(x,t) = \frac{\alpha_m\gamma}{2}\left(-\frac{4}{\gamma}\sqrt{\frac{\varepsilon t}{\pi}}e^{\frac{-x^2}{4\varepsilon t}} + 2\,\frac{x}{\gamma}erfc\left(\frac{x}{2\sqrt{\varepsilon t}}\right) + \frac{1}{\gamma^2}e^{-\gamma x+\varepsilon t\gamma^2}erfc\left(\frac{x}{2\sqrt{\varepsilon t}} - \gamma\sqrt{\varepsilon t}\right)\right.$$

$$\left. - \frac{1}{\gamma^2}e^{-\gamma x+\varepsilon t\gamma^2}erfc\left(\frac{x}{2\sqrt{\varepsilon t}} + \gamma\sqrt{\varepsilon t}\right)\right) + \frac{\alpha_m}{\gamma}e^{-\gamma x}\left(1 - e^{-\gamma^2\varepsilon t}\right) \qquad (4.90)$$

For $t > 0$ and $x \geq 0$.

If a dimensionless quantity γL is introduced, the solution may be displayed efficiently in dimensionless form. For large values of γ Eq. 4.90 approaches Eq. (4.47), which is valid for a jetty and constant oblique breaking wave angle.

The solution obtained for a variable breaking wave angle overestimates the rate of erosion behind the jetty since it is assumed that the amplitude of the long-shore sand transport rate is everywhere the same (and thus that the wave height, in principle, is constant). In reality, diffraction reduces the wave height in the shadow region and, accordingly, the amplitude of the long-shore sand transport rate there. Despite this reduction, Eq.s (4.89a,b) provide a better description of the actual situation than the commonly used solution (Eq.4.47) for which maximum erosion will always appear immediately adjacent to the jetty or long groin.

4.8. Analytical solutions with initially beach fill/cut and bounded by the solid boundaries at both ends

The analytical solutions presented by Hoang et al. (2020) have been derived for the case of bounded coast with initial beach fill or cut.

A bounded coast of length L is considered (Figure 29), whose both ends are fixed by the man-made or natural features, such as breakwaters, jetties, groins, headlands, and rocky cliffs. These features are considered solid boundaries, which are assumed to have enough length to interrupt completely the long-shore sediment at both ends. There is no sediment bypassing at these solid boundaries.

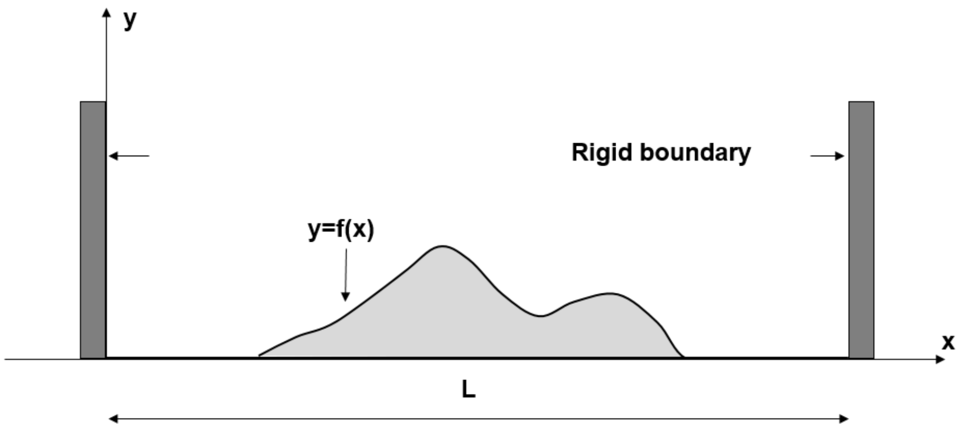

Figure 29 - Schematic diagram of an initially arbitrary shape of beach fill on a bounded coast (with solid boundaries at both ends)

In this study, mathematically, the boundary condition representing the cases of infinite and bounded coasts is that the shoreline gradient ($\partial y/\partial x$) approaches zero at $x = \pm\infty$, and $x = 0$ and L, respectively. It means the incident waves to be assumed perpendicular to the shoreline ($\alpha_b = 0$). This would reduce the applicability of the proposed model.

In fact, in the previous studies by Pelnard-Considére 1956, Larson et al. 1987, Larson et al. 1997, the boundary condition of no bypassing sediment at the solid boundary can be mathematically expressed as $\frac{\partial y}{\partial x} = \tan \alpha_b$. This means that the shoreline at the solid boundary is at every instant parallel to the breaking wave crests. The solid boundary interrupts the transport of sand along-shore, causing an accumulation at the updrift side and erosion at the downdrift side. This drawback of these more recent analytical solution will be discussed in the next Chapter.

4.8.1. General form of the analytical solution

By solving the simplified governing equation of the one-line model, Eq. (2), with appropriated boundary conditions of the bounded coast and initial conditions given in Figure 29, the general form of the analytical solution is obtained:

$$y = \frac{1}{L}\int_0^L f(x')dx' + \frac{2}{L}\sum_{n=1}^{\infty} \exp\left(-\frac{\varepsilon n^2\pi^2 t}{L^2}\right)\cos\frac{n\pi x}{L} \cdot \int_0^L f(x')\ \cos\frac{n\pi x}{L}dx' \qquad (4.91)$$

where L is the total length of sandy coast bounded by the two solid boundaries; n is the number of harmonics.

The analytical solution for the case of the bounded coast, Eq. (4.91), is not purely analytical because it consists of the sum of infinite terms. Different values of the harmonic number n yield different shoreline position results. Theoretically, when the value of the harmonic number is sufficiently large, the fluctuation of shoreline position is relatively small. Depending on the level of accuracy or the purpose of interest, a reasonable value of n can be selected for computation. In this study, an n value of 10000 was employed in all the computations; therefore, the shoreline fluctuation related to the harmonic number is predicted to be very small. According to the theory of the one-line model itself, the simplifications, and the boundary condition taken in this study, the assumptions taken by Hoang, 2020, are those enounced in previous sections.

By processing further Eq. (4.91) with a specific function of initial shoreline, $f(x)$, the corresponding analytical solution can be obtained. In the study, three various-shaped types of initial shorelines such as a trapezoid, rectangle, and triangle have been considered.

4.8.1.1. Analytical solution for the finite trapezoidal-shaped beach fill/cut

Figure 30 shows a schematic diagram of a finite trapezoidal shaped beach fill on the coast bounded by the solid boundaries. The fill portion is located arbitrarily along the coast. This case can be regarded as the beach nourishment on a coast bounded at both ends by solid boundaries such as jetties, breakwaters, and groins, headlands, or a straight pocket beach.

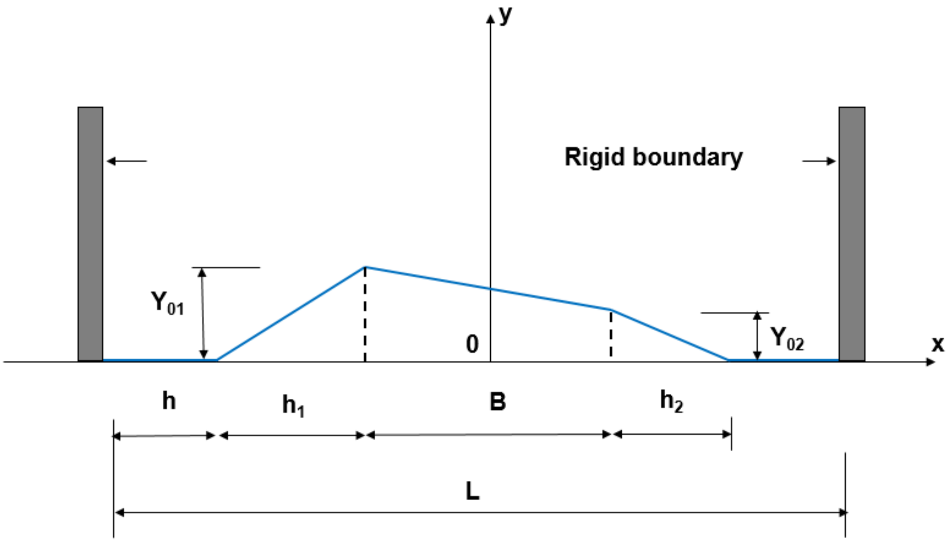

Figure 30 - Schematic diagram of an initially finite trapezoidal-shaped beach fill on coast bounded by the solid boundaries

For the case of the cut portion, it can be regarded as coastal morphology recoveries after being damaged significantly by natural disasters such as storm, or tsunami (e.g., Hoang et al. 2018). Moreover, it can also be the backfill process of the gap remaining in the middle of the coast after other parts being filled.

The initial conditions of this case are as follows,

$y = 0$ for $t = 0$ and $-h - h_1 - B/2 \le x \le -h_1 - B/2$; and $B/2 + h_2 \le x \le L - h - h_1 - B/2$;

$$y = Y_{01}\frac{\left(x + h_1 + \frac{B}{2}\right)}{h_1} \qquad \text{for } t = 0 \text{ and } -h_1 - \frac{B}{2} \le x \le -\frac{B}{2} \tag{4.92}$$

$$y = (Y_{01} - Y_{02})\frac{\left(\frac{B}{2} - x\right)}{B} + Y_{02} \qquad \text{for } t = 0 \text{ and } -\frac{B}{2} \le x \le -\frac{B}{2} \tag{4.93}$$

$$y = Y_{02}\frac{\left(\frac{B}{2} + h_2 - x\right)}{h_2} \qquad \text{for } t = 0 \text{ and } -\frac{B}{2} \le x \le -\frac{B}{2} + h_2 \tag{4.94}$$

while the boundary conditions are given as follows,

$$\frac{\partial y}{\partial x} = 0 \quad at\ x = -h - h_1 - \frac{B}{2} \quad and \quad x = -h - h_1 - \frac{B}{2} \tag{4.95}$$

As can be observed from Figure 30, the beach fill portion can be divided into three sub-portions, two right triangles, and a right trapezoid. The initial shoreline is represented by a series of five functions (straight lines); therefore, the additive property is applied for the integration in Eq. (4.91). The final solution is superimposed on these five solutions. This method is applied to other cases of initial shoreline position which are presented later in this study. The analytical solution for the above conditions is given by:

$$y = \frac{Y_{01}(h_1+B)+Y_{02}(h_2+B)}{2L} + \frac{2L}{\pi^2}\sum_{n=1}^{\infty}\frac{1}{n^2}\left[\frac{Y_{01}}{h_1}\cos\frac{n\pi h}{L}+\left(\frac{Y_{01}}{h_1}+\frac{Y_{01}}{B}-\frac{Y_{02}}{B}\right)\cos\frac{n\pi(h+h_1)}{L}+\left(\frac{Y_{02}}{h_2}-\frac{Y_{01}}{B}+\frac{Y_{02}}{B}\right)\cos\frac{n\pi(h+h_1+B)}{L}-\frac{Y_{02}}{h_2}\cos\frac{n\pi(h+h_1+h_2+B)}{L}\right] \cdot \exp\left(-\frac{\varepsilon n^2\pi^2 t}{L^2}\right)\cos\frac{n\pi\left(x+h+h_1+\frac{B}{2}\right)}{L} \tag{4.96}$$

The solution can be made dimensionless as

$$y^* = \frac{{Y_{01}}^*({h_1}^*+1)+{Y_{02}}^*({h_2}^*+1)}{2L^*} + \frac{2L^*}{\pi^2}\sum_{n=1}^{\infty}\frac{1}{n^2}\left[\frac{{Y_{01}}^*}{{h_1}^*}\cos\frac{n\pi h}{L^*}+\left(\frac{{Y_{01}}^*}{{h_1}^*}+{Y_{01}}^*-{Y_{02}}^*\right)\cos\frac{n\pi(h^*+{h_1}^*)}{L^*}+\left(\frac{{Y_{02}}^*}{{h_2}^*}-{Y_{01}}^*+{Y_{02}}^*\right)\cos\frac{n\pi(h^*+{h_1}^*+1)}{L^*}-\frac{{Y_{02}}^*}{{h_2}^*}\cos\frac{n\pi(h^*+{h_1}^*+{h_2}^*+1)}{L^*}\right] \cdot \exp\left(-\frac{\varepsilon n^2\pi^2 t^*}{{L^*}^2}\right)\cos\frac{n\pi\left(x^*+h^*+{h_1}^*+\frac{1}{2}\right)}{L^*} \tag{4.97}$$

where the dimensionless parameters, in this case, are defined as:

$$x^* = \frac{x}{B};\ y^* = \frac{y}{B};\ t^* = \frac{\varepsilon t}{B^2};\ L^* = \frac{L}{B};\ h^* = \frac{h}{B};\ {h_1}^* = \frac{h_1}{B}\ ;\ \ {h_2}^* = \frac{h_2}{B}$$

The width of the middle beach fill portion (right trapezoid), B, is chosen to normalize the shoreline position, the along-shore distance, and the elapsed time. The solution is now shown in dimensionless quantities; therefore, the resultant shoreline can be seen in a compact form.

So far, there has been only Walton (1994) who presented the analytical solution for the tapered beach fill. There is no other literature revealing the analytical solution for the case of finite trapezoidal-shaped beach fill/cut on the infinite coast.

Figure 31 presents the along-shore shoreline evolution with time according to Eq. (4.97). There is different behaviour of shoreline evolution between the beach fill portion and the adjacent coasts. The shoreline in the beach fill portion is eroded while it is accreted in the adjacent coasts. The waves transport sediment from the beach fill portion to the adjacent coasts on both sides. Since both ends of the coast are fixed by the solid boundaries, thus the sediment amount is conserved.

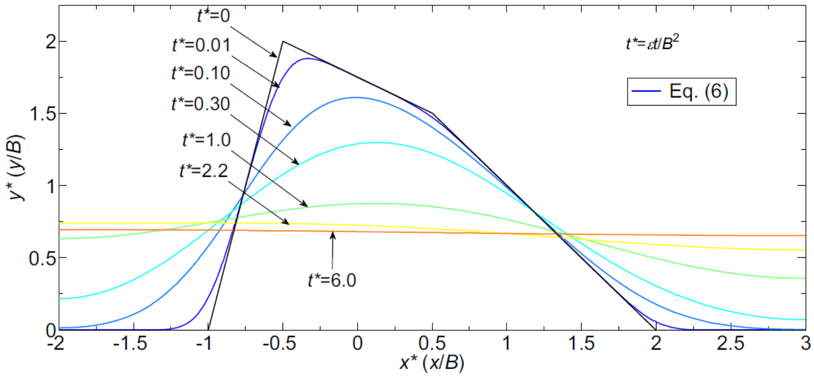

Figure 31 - along-shore shoreline evolution with time according to Eq. (4.96) (from Hoang, 2020)

Consequently, when t* is large, the shoreline approach the equilibrium stage at $\frac{Y_{01}{}^{*}(h_1{}^{*}+1)+Y_{02}{}^{*}(h_2{}^{*}+1)}{2L^{*}}$. At the equilibrium stage, the shoreline tends to an uniform shape between the solid boundaries. This is a consequence of setting boundary conditions $\frac{\partial y}{\partial x}=0$ at both ends.

It is interesting to note that, by changing the sign of Y_{01} and Y_{02} from "+" to "-", the solution for the beach fill case can be applied for the case of beach cut. Anyway, the proposed analytical solution has better applicability to the coast that is initially straight and long enough. The angle between the incident wave crests and the shoreline, α, was previously assumed to be small. In practice, the analytical solution is found to be applicable to an angle as large as 45°. However, depending on the shape of the initial shoreline, the angle cannot be small enough as expected. To clarify that point, Larson et al. (1987) compared the case of isosceles triangular-shaped beach fill and reported that the analytical solution produces a higher rate of shoreline change by overestimating the long-shore sand transport rate because of α > sin α.

4.8.1.2. Analytical solution for the finite right trapezoidal shaped beach fill/cut

Figure 32 shows a schematic diagram of a finite right trapezoidal-shaped beach fill on the bounded coast. This is a specific case of the trapezoidal-shaped beach fill which was just presented in the latter section.

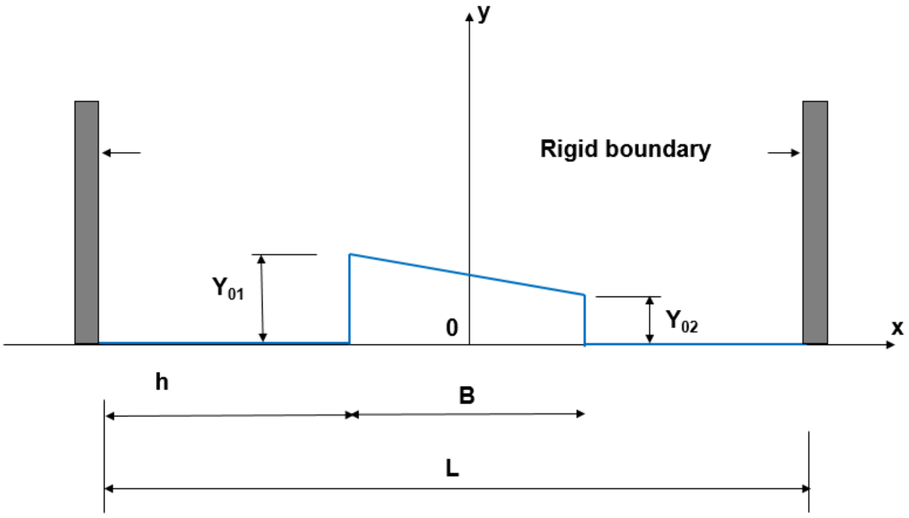

Figure 32 - Schematic diagram of an initially finite right trapezoidal-shaped beach fill on the coast bounded by solid boundaries

The initial conditions of this case are as follows,

$$y = (Y_{01} - Y_{02})\frac{(B+h-x)}{B} + Y_{02} \qquad \text{for } t = 0 \text{ and } -\frac{B}{2} \le x \le -\frac{B}{2} \tag{4.98}$$

$$y = 0 \ \text{ for } t = 0 \text{ and } -h - B/2 \le x \le -B/2; \quad \text{ and } \frac{B}{2} \le x \le L - (h+B) \tag{4.99}$$

while the boundary conditions are given as follows,

$$\frac{\partial y}{\partial x} = 0 \quad at\ x = -h - \frac{B}{2} \quad and \quad x = L - h - \frac{B}{2} \tag{4.100}$$

The analytical solution for the above conditions is given by

$$y = \frac{(Y_{01}+Y_{02})B}{2L} + \frac{2}{\pi B}\sum_{n=1}^{\infty}\frac{1}{n}\left[\begin{array}{c} Y_{02}B\ \sin\frac{n\pi(h+B)}{L} \\ -Y_{01}B\sin\frac{n\pi h}{L} + 2(Y_{01}+Y_{02})\frac{L}{n\pi}\sin\frac{n\pi(2h+B)}{2L}\sin\frac{n\pi B}{2L} \end{array}\right] \cdot \exp\left(-\frac{\varepsilon n^2\pi^2 t}{L^2}\right)\cos\frac{n\pi\left(x+h+\frac{B}{2}\right)}{L} \tag{4.101}$$

The dimensionless form is given by:

$$y = \frac{(Y_{01}{}^{*} + Y_{02}{}^{*})}{2L^{*}} + \frac{2}{\pi}\sum_{n=1}^{\infty}\frac{1}{n}\begin{bmatrix} Y_{02}{}^{*}\ \sin\frac{n\pi(L^{*}+1)}{2L^{*}} \\ -Y_{01}{}^{*}\sin\frac{n\pi(L^{*}+1)}{2L^{*}} + 2(Y_{01}{}^{*} - Y_{02}{}^{*})\frac{L^{*}}{n\pi}\sin\frac{n\pi}{2}\sin\frac{n\pi}{2L^{*}} \end{bmatrix} \cdot \exp\left(-\frac{\varepsilon n^{2}\pi^{2}t^{*}}{L^{2}}\right)\cos\frac{n\pi(2x^{*}+L^{*})}{2L^{*}} \tag{4.102}$$

By changing the value of h, Eq. (4.102) can be applied to the specific cases regarding the position of fill portion such as the fill portion at most left ($h = 0$), in the middle ($h = L/2 - B/2$), at the most right ($h = L - B$). Similar to the previous case, Eq. (4.102) can be applied to the case of finite right trapezoidal-shaped beach cut by changing the sign of Y_{01} and Y_{02}.

A comparison between the analytical solution with solid boundaries and the analytical solution without solid boundary (provided by Larson et al., 1987) is given.

When the value of L^{*} is large, shoreline positions described by both solutions are almost overlapping even with the large value of t*. When the value of L^{*} is getting smaller, they are also overlapping when the value of t* is small; however, the difference of shoreline positions evolution can be observed when the value of t* is getting larger.

Shoreline position in the beach fill portion without solid boundaries, tends to retreat faster than the one described by Eq. (4.102) (with solid boundaries), whereas, on the adjacent coasts, the shoreline position of the case with solid boundaries tends to advance faster than the one without solid boundaries. For the case of the much smaller value of L^{*}, in Figure 31, the distinct deference of shoreline positions described by the two solutions is clear.

Moreover, for solution without solid boundaries and with solid boundaries shoreline positions approach the equilibrium position at 0 and $\frac{(Y_{01}{}^{*}+Y_{02}{}^{*})}{2L^{*}}$ respectively. All of that indicates the effects of solid boundaries on shoreline evolution.

4.8.1.3. Analytical solution for the finite rectangular beach fill/cut

The schematic diagram of the case of a finite rectangular beach fill on the coast bounded by solid boundaries is presented in Figure 33.

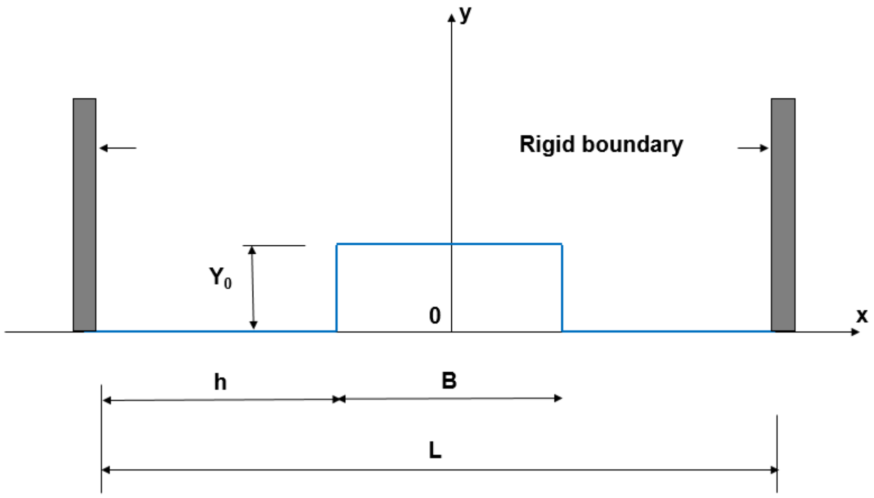

Figure 33 - Schematic diagram of an initially finite rectangular beach fill on the coast bounded by solid boundaries

This is a specific case of the right trapezoidal-beached beach fill presented above when $Y_{01} = Y_{02} = Y_0$.

The initial conditions of this case are as follows,

$$y = Y_0 \qquad \text{for } t = 0 \quad \text{and } -\frac{B}{2} \leq x \leq -\frac{B}{2} \tag{4.103}$$

$$y = 0 \;\; \text{for } t = 0 \quad \text{and } x < -B/2; \quad \text{and} \quad \frac{B}{2} \leq x \tag{4.104}$$

while the boundary conditions are given as follows,

$$\frac{\partial y}{\partial x} = 0 \quad at\ x = -h - \frac{B}{2} \;\; and \;\; x = L - h - \frac{B}{2} \tag{4.105}$$

The analytical solution for the above conditions is given by,

$$y = Y_0 \left[\frac{B}{L} + \frac{2}{\pi}\sum_{n=1}^{\infty}\frac{1}{n}\left(\sin\frac{n\pi(h+B)}{L} - \sin\frac{n\pi h}{L}\right)\right]$$
$$\cdot \exp\left(-\frac{\varepsilon n^2\pi^2 t}{L^2}\right)\cos\frac{n\pi\left(x+h+\frac{B}{2}\right)}{L} \tag{4.106}$$

Similar to the previous cases, Eq. (4.106) can be applied to the case of a finite rectangular-shaped beach cut by changing the sign of Y_0. By substituting the term $h = L/2 - B/2$ into Eq. (4.106), the analytical solution for the case of finite rectangular beach fill in the middle of the bounded coast is obtained.

$$y = Y_0 \left[\frac{B}{L} + \frac{2}{\pi} \sum_{n=1}^{\infty} \frac{1}{n} \left(\sin \frac{n\pi(L+B)}{2L} - \sin \frac{n\pi(L-B)}{2L} \right) \right]$$

$$\cdot \exp\left(-\frac{\varepsilon n^2 \pi^2 t}{L^2}\right) \cos \frac{n\pi(2x+L)}{2L} \quad (4.107)$$

And in dimensionless form:

$$y^* = \frac{1}{L^*} + \frac{2}{\pi} \sum_{n=1}^{\infty} \frac{1}{n} \left(\sin \frac{n\pi(L^*+1)}{2L^*} - \sin \frac{n\pi(L^*-1)}{2L^*} \right)$$

$$\cdot \exp\left(-\frac{\varepsilon n^2 \pi^2 t^*}{L^{*2}}\right) \cos \frac{n\pi(2x^*+L^*)}{2L^*} \quad (4.108)$$

In this case, with respect to the solution without solid boundaries, shoreline positions approach equilibrium position at 0 and $1/L^*$, respectively. Moreover, from results, the evolution of shoreline is practically similar to that given by the case of the right trapezoidal-shaped beach fill.

4.8.1.4. Decaying process of sediment in the rectangular beach fill portion

The decaying process of sediment in the rectangular beach fill portion is considered as the process that sediment is transported out of the beach fill portion by the waves, leading to the erosion of the shoreline. Based on the theories proposed in the previous parts, the decaying process of sediment in the beach fill portion is investigated by the authors concerning the proportional remained of shoreline position at the centreline, y_C, and the proportional area of sediment remained in the beach fill portion, PA. These relationships would help the operator/contractor of the beach nourishment to roughly estimate the amount of sediment remained in the beach fill portion after a certain elapsed time.

Proportional remaining of shoreline position at the centreline of beach fill portion

The decaying process of sediment in the beach fill portion, which subjects to the long-shore sediment transport induced by waves, can be expressed in terms of the remaining shoreline position at the centreline of the beach fill portion.

The evolution of shoreline positions at the centreline of the cases without and with solid boundaries can be described in dimensionless forms as:

$$y_{C1}{}^* = \operatorname{erf}\left(\frac{1}{4\sqrt{t^*}}\right) \quad (4.109)$$

$$y_{C2}{}^{*} = \frac{1}{L^{*}} + \frac{2}{\pi}\sum_{n=1}^{\infty}\frac{1}{n}\left(\sin\frac{n\pi(L^{*}+1)}{2L^{*}} - \sin\frac{n\pi(L^{*}-1)}{2L^{*}}\right)\cdot\exp\left(-\frac{\varepsilon n^{2}\pi^{2}t^{*}}{L^{*2}}\right)\cos\frac{n\pi}{2L^{*}} \quad (4.110)$$

Figure 34 shows the theoretical relationship between t^* and $y_C{}^*$ for the cases without and with solid boundaries.

For the case with solid boundaries, several values of L^* were employed for computation. According to the results, when the value of L^* is small, there is a distinct difference between the relationship obtained from two solutions once the value of t* is large, although they are overlapping in the early stage of the process.

There is another distinct difference between these two cases that needs to be noted. The relationship between t^* and $y_C{}^*$ of the case with solid boundaries approaches the equilibrium position more quickly compared to the case without solid boundaries. This feature would be an advantage and very beneficial for beach nourishment. When the value of L^* gets larger, the relationship between t^* and $y_C{}^*$ from the two solutions is almost the same. For example, they are overlapping each other when the value of L^*equals 15. This indicates that with a large enough value of L^*, and at a certain value of dimensionless elapsed time, t^*, the effect of solid boundaries on the evolution of shoreline becomes a minority.

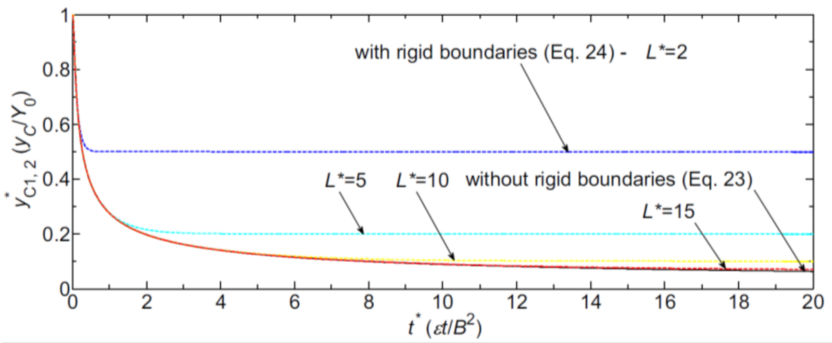

Figure 34 - Relationship between t^* and $y_C{}^*$ (from Hoang, 2020). His Eq. (23) and (24) in the figure are Eq.s (4.109) and (4.110)

Proportional area of sediment remained in the beach fill portion

The proportional area of sediment remained, PA, is defined as the ratio between the area of the sediment left in the beach fill portion to the initial area of the beach fill portion. This parameter represents the total remained amount of sediment in the beach portion over the initial fill amount after being transported to the adjacent coasts by waves.

Dean (2003) revealed the solution to obtain PA for the case without solid boundaries, whereas this study introduces the solution for a case with solid boundaries, Eq. (4.111). The latter equation is obtained when the total amount of sediment transported out the beach fill portion through the boundaries between the beach fill portion and adjacent coasts is integrated from Eq. (4.107) before normalizing to Y_0 and B.

$$PA_1 = 2\sqrt{\frac{t^*}{\pi}}\left\{\exp\left[-\left(\frac{1}{2\sqrt{t^*}}\right)^2\right] - 1\right\} + \operatorname{erf}\left(\frac{1}{2\sqrt{t^*}}\right) \qquad (4.111)$$

$$PA_2 = 1 - \frac{2L^{*2}}{(L^* - 1)\pi^2}\sum_{n=1}^{\infty}\frac{1}{n^2}\left(\sin\frac{n\pi(L^* + 1)}{2L^*} - \sin\frac{n\pi(L^* - 1)}{2L^*}\right)^2$$
$$\cdot\left[1 - \exp\left(-\frac{\varepsilon n^2\pi^2 t^*}{L^{*2}}\right)\right] \qquad (4.112)$$

Eq. (4.112) presents the relationship between t^* and PA for two cases. According to this, when the value of L^* gets larger, the relationship between t^* and PA of the case with solid boundaries is asymptotic with the one obtained from the case without solid boundaries.

In addition, an asymptotic line showing the relationship between t^* and PA of the case without solid boundaries obtained from Eq. (4.113) is also plotted in Figure 34. Eq. (4.113) is obtained when taking the limit of Eq. (4.111). The asymptotic line would be useful for quick estimation of the relationship between t^* and PA_1, especially when the value of t^* is small, for example, $t^* < 0.25$.

$$PA_1 = 1 - 2\sqrt{\frac{t^*}{\pi}} \qquad (4.113)$$

by modifying Eqs. (4.111) and (4.113), the proportion area of sediment backfill in beach cut portion before shoreline position in this area reaching the equilibrium stage, PA_N, for cases without and with solid boundaries, can be obtained as

$$PA_N = 1 - PA \qquad (4.114)$$

4.8.1.5. *Relationship between the total length of adjacent sandy coasts and the decay time*

The authors also provide the relationship between the total lengths of adjacent coasts needs to be filled or nourish, L_s (Eq. 4.115), and the decay time of sediment in the beach fill portion, T_{DC}.

That could help to identify when the shoreline will get a stable condition. Because the position of shoreline in Eq. (4.107) is represented by the exponential function, therefore the decay time is defined to be the time when shoreline position at the central line of the beach fill portion ($x = 0$) becomes a certain percentage, P_D, of the equilibrium shoreline position. Theoretically, the more close to the equilibrium position, B/L, the more stable the shoreline is.

The total length of the adjacent coasts is given by $L_s = L - B$, from which, considering Eq.(4.107), the relationship between the decay time and the total length of adjacent coasts is given by:

$$P_D\left(\frac{1}{{L_s}^* + 1}\right) = \frac{1}{{L_s}^* + 1} + \frac{2}{\pi}\sum_{n=1}^{\infty}\frac{1}{n}\left(\sin\frac{n\pi({L_s}^* + 2)}{2({L_s}^* + 1)} - \sin\frac{n\pi{L_s}^*}{2({L_s}^* + 1)}\right)$$
$$\cdot \exp(-n^2\pi^2{T_{DC}}^*)\cos\frac{n\pi}{2L} \qquad (4.115)$$

where the dimensionless parameters are defined as ${L_s}^* = \frac{L-B}{B}$ ${T_{DC}}^* = \frac{\varepsilon T_{DC}}{L^2}$

Figure 35 (a) shows the relationship between ${L_s}^*$ and ${T_{DC}}^*$given by Hoang, 2020. To provide a more general picture of that relationship with respect to the percentage of shoreline reaching the equilibrium position, there several values of P_D were selected. According to the theoretical results, when the value of ${L_s}^*$ is small, ${T_{DC}}^*$ has a small value, whereas when the value of ${L_s}^*$ is getting larger, the value of ${T_{ER}}^*$ is getting larger too. The dimensionless decay time of morphology is dependent on the ratio between the total length of adjacent sandy coasts to the beach fill width. If that ratio is large, then the dimensionless decay time is long and vice versa. Another important point discussed by the author here that with a certain large value of ${L_s}^*$, the value of ${T_{DC}}^*$for all the percentages becomes almost constant values. If the value of ${L_s}^*$, in Eq. (4.115) is large enough (approaching infinity), the relationship between P_D and ${T_{DC}}^*$ is as follow,

$$P_D = 1 + 2\sum_{n=1}^{\infty}\exp(-n^2\pi^2{T_{DC}}^*)\cdot\cos^2\frac{n\pi}{2L} \qquad (4.116)$$

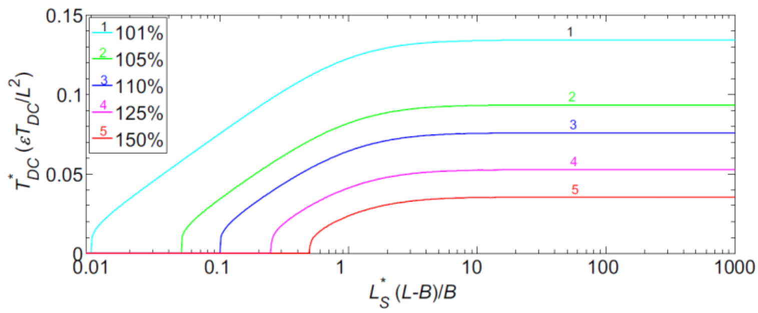

(a)

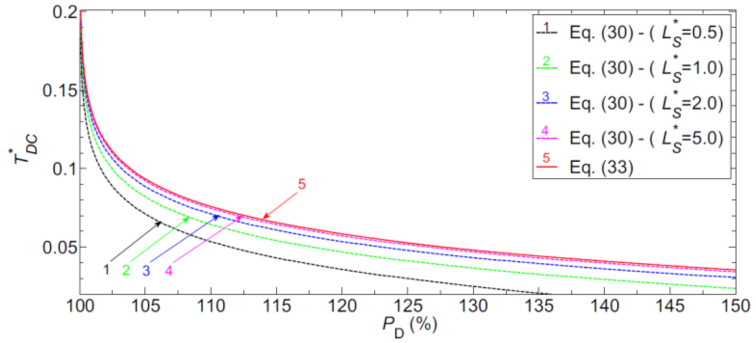

(b)

Figure 35 - The relationships between $L_s{}^*$ and $T_{DC}{}^*$, and between P_D and $T_{DC}{}^*$. (a) The relationship between $L_s{}^*$ and $T_{DC}{}^*$. (b) The relationship between P_D and $T_{DC}{}^*$(original from Hoang 2020), Eq.s 30 and 33 are Eq.s 4.115 and 4.116 of present thesis.

According to the results presented in Figure 35 (b), when the value of P_D is decreasing the value of $T_{DC}{}^*$ is increasing. That increase is accelerated once it approaches closer to the equilibrium position. These results would be very useful for the designing of beach nourishment. That recommends when the shoreline has no further significant decay or when it will be a good time to refill, etc. In addition, the results in that figure also reveal that the relationship between P_D and $T_{DC}{}^*$ of the case the small value of $L_s{}^*$ quickly approaches the relationship for the case of a very large value of $L_s{}^*$ which can represent the case of the infinite coast.

4.8.1.6. Analytical solution for the finite triangular-shaped beach fill/cut

Continuously, another shaped type of initial shoreline, triangle, is considered. The schematic diagram of the case of an initially finite triangular-shaped beach fill on the coast bounded by solid boundaries is presented in Figure 36.

The initial conditions of this case are as follows,

$$y = 0 \qquad \text{for } t = 0 \quad \text{and } -h - h_1 \le x \le h_1; \quad \text{and } \; h_2 \le x \le L - h - h_1 \tag{4.117}$$

$$y = Y_0 \frac{(x + h_1)}{h_1} \qquad \text{for } t = 0 \qquad \text{and} - h_1 \le x \le 0; \tag{4.118}$$

$$y = Y_0 \frac{(h_2 - x)}{h_2} \qquad \text{for } t = 0 \qquad \text{and } 0 \le x \le h_2; \tag{4.119}$$

while the boundary conditions are given as follows,

$$\frac{\partial y}{\partial x} = 0 \quad at\ x = -h - h_1 \;\; and \;\; x = L - h - h_1 \tag{4.120}$$

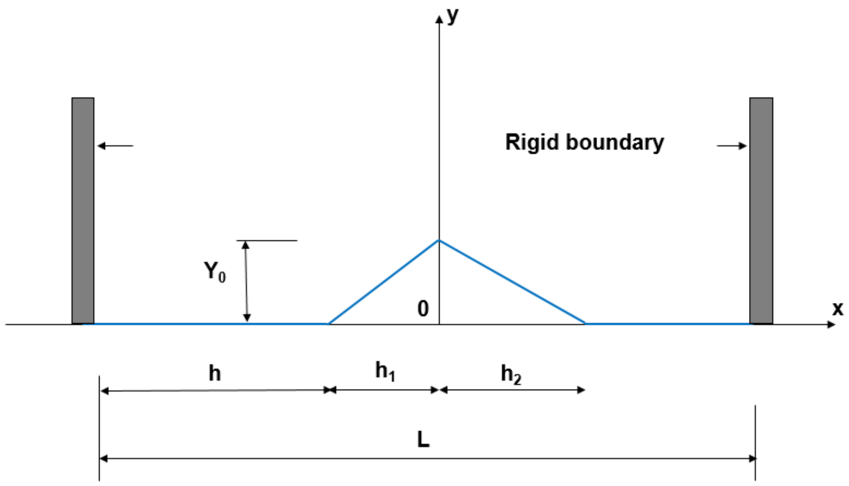

Figure 36 - Schematic diagram of an initial finite triangular-shaped beach fill on the coast bounded by solid boundaries

The analytical solution for the above conditions is given by

$$y = Y_0 \left\{ \frac{h_1 + h_2}{2L} + \frac{2L}{\pi^2} \sum_{n=1}^{\infty} \frac{1}{n^2} \left[-\frac{1}{h_1} \cos\frac{n\pi h}{L} + \left(\frac{1}{h_1} + \frac{1}{h_2}\right) \cos\frac{n\pi(h + h_1)}{L} - \frac{1}{h_2} \cos\frac{n\pi(h + h_1 + h_2)}{L} \right] \cdot \exp\left(-\frac{\varepsilon n^2 \pi^2 t}{L^2}\right) \cos\frac{n\pi(x + h + h_1)}{L} \right\} \quad (4.121)$$

Similar to the previous case, by changing the sign of Y_0, Eq. (4.121) can describe the evolution shoreline of initially triangular-shaped beach cut on the coast bounded by solid boundaries at both ends.

The analytical solutions in dimensionless form for the case of finite isosceles triangular-shaped beach fill on coast bounded by solid boundaries is:

$$y = \frac{1}{2L^*} + \frac{4L^*}{\pi^2} \sum_{n=1}^{\infty} \left[\frac{1}{n^2} - \cos\frac{n\pi(L^* - 1)}{2L^*} + 2\cos\frac{n\pi}{2} - \cos\frac{n\pi(L^* + 1)}{2L^*} \right] \cdot \exp\left(-\frac{n^2 \pi^2 t^*}{L^{*2}}\right) \cos\frac{n\pi(2x^* + L^*)}{2L^*} \quad (4.122)$$

By comparing this solution to that without solid boundaries it is seen that the behaviour of shoreline evolution in these two cases is generally similar to the evolution of shorelines in the case of a rectangular-shaped beach fill in the middle of the coast.

They are also symmetric over the plane e of $x^* = 0$. They are overlapping when the value of t^* is still small. However, the evolution of two shorelines gets a distinct difference when the value of t^* gets larger. Moreover, shoreline positions for shoreline without solid boundaries and with solid boundaries approach equilibrium at 0 and $1/(2L^*)$, respectively.

4.8.1.7. Right triangular-shaped beach fill

The case of finite right triangular-shaped beach fill on the coast bounded by solid boundaries is also analysed. This is a specific case of the finite triangular-shaped beach fill presented in the latter section.

The initial conditions of this case are as follows,

$$y = 0 \qquad \text{for } t = 0 \quad \text{and } 0 \le x \le h; \quad \text{and } B \le x \le L \tag{4.123}$$

$$y = Y_0 \frac{(h + B - x)}{B} \qquad \text{for } t = 0 \quad \text{and } h \le x \le B \tag{4.124}$$

$$y = Y_0 \frac{(h_2 - x)}{h_2} \qquad \text{for } t = 0 \quad \text{and } 0 \le x \le h_2; \tag{4.125}$$

while the boundary conditions are given as follows,

$$\frac{\partial y}{\partial x} = 0 \quad at\; x = 0 \;\; and \quad x = L \tag{4.126}$$

The analytical solution for the above conditions is given by

$$y = \frac{Y_0 B}{2L} + \frac{2Y_0}{\pi B} \sum_{n=1}^{\infty} \frac{1}{n} \left[-B \, \sin \frac{n\pi h}{L} + \frac{2L}{n\pi} \sin \frac{n\pi(2h + B)}{2L} \sin \frac{n\pi B}{2L} \right]$$
$$\cdot \exp\left(-\frac{\varepsilon n^2 \pi^2 t}{L^2} \right) \cos \frac{n\pi x}{L} \tag{4.127}$$

And in dimensionless form is

$$y^* = \frac{1}{2L^*} + \frac{2}{\pi} \sum_{n=1}^{\infty} \frac{1}{n} \left[-B \, \sin \frac{n\pi h^*}{L^*} + \frac{2L^*}{n\pi} \sin \frac{n\pi(2h^* + 1)}{2L^*} \sin \frac{n\pi B}{2L^*} \right]$$
$$\cdot \exp\left(-\frac{n^2 \pi^2 t^*}{L^{*2}} \right) \cos \frac{n\pi x^*}{L^*} \tag{4.128}$$

Chapter 5: Shoreline evolution in a bounded domain

5.1. Introduction

In this Chapter the first original aspect of present research is further examined. As discussed previously, the analytical solutions of the one-line model of shoreline change (Pelnard-Considére, 1956) have been addressed, so far, mainly for the case of open coast ($x=-\infty$ to $x=+\infty$). In fact, Larson et al. (1987) introduced analytical solutions for describing the shoreline evolution on infinite coast (without solid boundaries) or near the coastal structures. Moreover, Dean (2003) summarized and presented analytical solutions for the case of finite rectangular beach fill on infinite coast. It is worth noticing that more recent works dealt with the case of bounded coasts, but with some drawbacks. Particularly, Valsamidis & Reeve (2020) described the evolution of shoreline within a groin field, solving the problem only with a semi-analytical approach. Furthermore, Hoang (2020) provided the solution for an "isolated" beach of finite length, which holds, though, only for wave attacks rigorously perpendicular to the coast. Consequently, the analytical solutions describing the shoreline evolution on coast bounded by structures at both ends are still limited. In this study, the case of a bounded coast of finite length is investigated, and a complete analytical model is assessed. Furthermore, the role of the confining constraints has been assessed on the long-term response of an artificial nourishment of a given plane shape, and simple relationships have been found, useful for the design of nourishments. Nevertheless, the approach proposed below is very general but, although inevitably simplified, allows to take into account different scenarios of engineering interest.

5.2. Approach

The evolution of the shoreline contour $y(x,t)$ is assumed to be ruled by the homogeneous diffusion equation (Eq. (4.2)), with the initial condition:

$$y(x,0) = g(x) \qquad (5.1)$$

Now we assume the x-axis to align to $g(x)$ at the extremes, that is:

$$g(0) = g(L) = 0 \qquad (5.2)$$

which simplifies the maths without generality loss.

A CERC-like equation is selected to represent littoral transport:

$$Q(x,t) = -Q_0 \cdot sen\left[2\left(\frac{\partial y}{\partial x} + \theta_b\right)\right] \qquad (5.3)$$

where the amplitude Q_0 depends on wave parameters at incipient breaking (H_b, T), and θ_b represents the azimuth where waves originate (assumed constant). Thus, under the hypothesis of small angle, we have:

$$Q(x,t) = -Q_0 \cdot sen\left[2\left(\frac{\partial y}{\partial x} + \theta_b\right)\right] \cong -2\,Q_0\left(\frac{\partial y}{\partial x} + \theta_b\right) \equiv -2\,Q_0 \cdot \frac{\partial y'}{\partial x} \qquad (5.4)$$

where the transformed shoreline function:

$$y' = y + \theta_b \cdot x \qquad (5.5)$$

also obeys the diffusion equation (4.2).

Now we set the bypassing relationships at the beach boundaries as follows:

$$Q = -2\,Q_0 \cdot \frac{\partial y'}{\partial x} = -2\,Q_0 \cdot \frac{y \cdot |\theta_b|}{l_{h,1}} \qquad at\ x = 0 \qquad (5.6a)$$

$$Q = -2\,Q_0 \cdot \frac{\partial y'}{\partial x} = 2\,Q_0 \cdot \frac{y \cdot |\theta_b|}{l_{h,2}} \qquad at\ x = L \qquad (5.6b)$$

where l_h indicate the length of the outcrops at the beach's ends.

The Eqs. (5.6a,b) finally read:

$$\frac{\partial y'}{\partial x} l_{h,1} - y \cdot |\theta_b| = 0 \qquad at\ \ x = 0 \qquad (5.7a)$$

$$\frac{\partial y'}{\partial x} l_{h,2} + y \cdot |\theta_b| = 0 \qquad at\ x = L \qquad (5.7b)$$

The essence of the bypassing conditions is that the bounding outcrops (groins or natural headlands) are long enough to prevent littoral transport at t = 0 ($y = 0$). Then, the sand flow increases linearly with y until the structure's head is reached ($y = lh$). This condition corresponds to:

$$\frac{\partial y}{\partial x} = 0 \tag{5.8}$$

that is, the shoreline is parallel to the x-axis.

It is worth noticing the absolute value in the Eqs. (5.6a,b-5.7a,b) is necessary to keep the sign of littoral transport consistent when y turns negative. Figure 37 shows that this corresponds to assuming the shoreline is antisymmetrical beyond the outcrops.

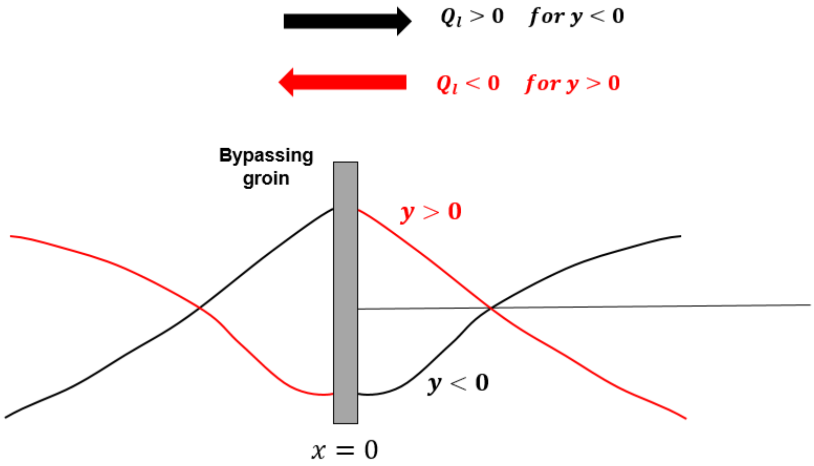

Figure 37 - Definition sketch for the shoreline at the outcrop

5.2.1. The Boundary Problem

The shoreline evolution problem can be readily rearranged as a Boundary Value Problem (BVP) of the transformed variable y'.

One has:

$$\frac{\partial y'}{\partial t} - \varepsilon \frac{\partial^2 y'}{\partial x^2} = 0 \qquad t > 0; 0 \leq x \leq L \tag{5.9a}$$

$$\frac{\partial y'}{\partial x} l_{h,1} - y' \cdot |\theta_b| = 0 \qquad at\ \ x = 0 \tag{5.9b}$$

$$\frac{\partial y'}{\partial x} l_{h,2} + (y' - \theta_b L) \cdot |\theta_b| = 0 \qquad at\ x = L \tag{5.9c}$$

$$y'(x, 0) = g(x) + \theta_b \cdot x = g'(x) \tag{5.9d}$$

which can be split into two further problems, namely:

$$\frac{\partial y_1'}{\partial t} - \varepsilon \frac{\partial^2 y_1'}{\partial x^2} = 0 \qquad t > 0; 0 \le x \le L \qquad (5.10a)$$

$$\frac{\partial y_1'}{\partial x} l_{h,1} - y_1' \cdot |\theta_b| = 0 \qquad at\ \ x = 0 \qquad (5.10b)$$

$$\frac{\partial y_1'}{\partial x} l_{h,2} + y_1' \cdot |\theta_b| = 0 \qquad at\ x = L \qquad (5.10c)$$

$$y_1'(x, 0) = g'(x) \qquad (5.10d)$$

and:

$$\frac{\partial y_2'}{\partial t} - \varepsilon \frac{\partial^2 y_2'}{\partial x^2} = 0 \qquad t > 0; 0 \le x \le L \qquad (5.11a)$$

$$\frac{\partial y_2'}{\partial x} = 0 \qquad at\ \ x = 0 \qquad (5.11b)$$

$$\frac{\partial y_2'}{\partial x} - \frac{\theta_b \cdot |\theta_b| L}{l_{h,2}} = 0 \qquad at\ x = L \qquad (5.11c)$$

$$y_2'\ (x, 0) = 0 \qquad (5.11d)$$

Problem (5.10) describes heat conduction in a bar with Robin boundary conditions, whereas the set (5.11a)-(5.11d) represents an inhomogeneous Neumann problem.

5.2.2. Solution of the Robin BVP

We apply the separation of variable technique and set:

$$y_1'(x, t) = F(x)G(t) \qquad (5.12)$$

Thus, from the Eq. (4.2) we have:

$$F(x)\dot{G}(t) = \varepsilon \ddot{F}(x)G(t) \qquad (5.13)$$

and hence:

$$\frac{1}{\varepsilon}\frac{\dot{G}(t)}{G(t)} = \frac{\ddot{F}(x)}{F(x)} = -{\mu_n}^2 \qquad (5.14)$$

The time dependent component can be solved as:

$$G(t) = Ce^{-\varepsilon \mu_n^2 t} \qquad (5.15)$$

whereas,

$$\ddot{F}(x) + \mu_n^2 F(x) = 0 \qquad (5.16)$$

gives:

$$F(x) = c_n \cos(\mu_n x + \tau_n) \tag{5.17}$$

Hence the general solutions can be written as:

$$y'(x,t) = \sum_{n=0}^{\infty} c_n \cos(\mu_n x + \tau_n)\, e^{-\varepsilon \mu_n{}^2 t} \tag{5.18}$$

Where the constants c_n and τ_n, as well as the modes μ_n are obtained from the boundary conditions.

The condition (5.11a) returns:

$$\frac{\partial y'}{\partial x} = -\sum_{n=0}^{\infty} c_n \cdot \mu_n \ \cdot \sin(\tau_n)\, e^{-\varepsilon \mu_n{}^2 t} = \frac{|\theta_b|}{l_{h,1}} \cdot \ \sum_{n=0}^{\infty} c_n \cdot \cos(\tau_n)\, e^{-\varepsilon \mu_n{}^2 t} \tag{5.19}$$

which gives:

$$\tan(\tau_n) = -\frac{1}{\mu_n} \frac{|\theta_b|}{l_{h,1}} \tag{5.20}$$

whereas from (5.11b), one gets:

$$\tan(\mu_n L + \tau_n) = \frac{|\theta_b|}{l_{h,2}} \tag{5.21}$$

Hence:

$$\tan(\mu_n L + \tau_n) = \frac{\tan(\mu_n L) + \tan(\tau_n)}{1 - \tan(\mu_n L) \cdot \tan(\tau_n)} = \frac{|\theta_b|}{l_{h,2}} \tag{5.22}$$

and finally:

$$\tan(\mu_n L) = \frac{\mu_n \cdot \left(\frac{|\theta_b|}{l_{h,1}} + \frac{|\theta_b|}{l_{h,2}} \right)}{\mu_n^2 - \frac{\theta_b^2}{\left(l_{h,1} \cdot l_{h,2}\right)}} \tag{5.23}$$

The coefficients $c_n$can be obtained from the initial condition:

$$\sum_{n=0}^{\infty} c_n \cos(\mu_n x + \tau_n) = g'(x) \tag{5.24}$$

which gives:

$$c_n = \frac{2}{L} \int_0^L g'(x) \cdot \ \cos(\mu_n x + \tau_n)\, dx \tag{5.25}$$

5.2.3. Solution of the Neumann BVP

The problem (5.11a)-(5.11d) requires a previous homogenization of the boundary conditions. This task is accomplished by introducing a "correction function" $H(x,t)$:

$$H(x,t) = \frac{\theta_b \cdot |\theta_b| L}{2 l_{h,2}}\, x^2 - \varepsilon\, \frac{\theta_b \cdot |\theta_b| L}{l_{h,2}}\, \mathrm{t} \tag{5.26}$$

and a further auxiliary variable:

$$w(x,t) = y'_2 - H(x,t) \tag{5.27}$$

which gives the homogeneous Neumann BVP:

$$\frac{\partial w}{\partial t} - \varepsilon \frac{\partial^2 w}{\partial x^2} = 0 \qquad t > 0;\, 0 \le x \le L \tag{5.28a}$$

$$\frac{\partial w}{\partial x} = 0 \qquad at\ \ x = 0 \tag{5.28b}$$

$$\frac{\partial w}{\partial x} = 0 \qquad at\ x = L \tag{5.28c}$$

$$w\,(x,0) = -H(x,0) = -\frac{\theta_b \cdot |\theta_b| L}{2 l_{h,2}}\, x^2 = W(x) \tag{5.28d}$$

which, according to the solution technique previously described, gives:

$$w(x,t) = \sum_{n=0}^{\infty} w_n \cos\left(\frac{n\pi}{L} x\right) e^{-\varepsilon {\mu_n}^2 t} \tag{5.29}$$

with:

$$w_n = \frac{2}{L} \int_0^L W(x) \cdot \cos\left(\frac{n\pi}{L} x\right) dx \tag{5.30}$$

5.2.4. Three cases of engineering relevance

In the following, three peculiar situations of engineering significance will be examined. First we assume:

$$l_{h,1} = l_{h,2} = 0 \tag{5.31}$$

that is, no structures at the beach's ends.

The problem (5.9) reduces to:

$$\frac{\partial y'}{\partial t} - \varepsilon \frac{\partial^2 y'}{\partial x^2} = 0 \qquad t > 0; 0 \leq x \leq L \qquad (5.32a)$$

$$y' = 0 \qquad at\ \ x = 0 \qquad (5.32b)$$

$$(y' - \theta_b L) = 0 \qquad at\ x = L \qquad (5.32c)$$

$$y'(x, 0) = g(x) + \theta_b \cdot x = g'(x) \qquad (5.32d)$$

and seeing that:

$$y' = y \qquad at\ \ x = 0 \qquad (5.33a)$$

$$y' - \theta_b L = y \qquad at\ \ x = L \qquad (5.33b)$$

the problem reduces to a Dirichlet BVP in the original shoreline variable y(x,t):

$$\frac{\partial y}{\partial t} - \varepsilon \frac{\partial^2 y}{\partial x^2} = 0 \qquad t > 0; 0 \leq x \leq L \qquad (5.34a)$$

$$y = 0 \qquad at\ \ x = 0 \qquad (5.34b)$$

$$y = 0 \qquad at\ x = L \qquad (5.34c)$$

$$y(x, 0) = g(x) \qquad (5.34d)$$

the solution of which is:

$$y(x, t) = \sum_{n=0}^{\infty} y_n \sin\left(\frac{n\pi}{L} x\right) e^{-\varepsilon \mu_n{}^2 t} \qquad (5.35)$$

with:

$$y_n = \frac{2}{L} \int_0^L g(x) \cdot \sin\left(\frac{n\pi}{L} x\right) dx \qquad (5.36)$$

Other situations of engineering significance are:

- Infinitely long outcrops at the ends ($l_{h,1} = l_{h,2} = \infty$);
- Bypassed structure at x=0 and no transport at x=L ($l_{h,2} = \infty$);

In both cases, the problem (5.28) does not possess non-trivial solutions, and accordingly Eqs. (5.11) give the whole beach plane form evolution.

In the case a), for y’ and $|\theta_b|$ to be finite, it must be:

$$\frac{\partial y_1'}{\partial x}(0) = \frac{\partial y_1'}{\partial x}(L) = 0 \tag{5.37}$$

which gives rise to a homogeneous Neumann BVP similar to Eqs. (5.28). Hence we have:

$$y'(x,t) = \sum_{n=0}^{\infty} y'_n \cos\left(\frac{n\pi}{L}x\right) e^{-\varepsilon\mu_n{}^2 t} \tag{5.38}$$

with:

$$y'_n = \frac{2}{L}\int_0^L g'(x) \cdot \cos\left(\frac{n\pi}{L}x\right) dx \tag{5.39}$$

The solution is similar to that proposed by Hoang (2020), but the use of the auxiliary function $y'(x,t)$ allows accounting for the effect of wave angle.

Finally, the case b) turns into a particular Robin problem, the solution of which can be derived from Eqs (5.20-5.23):

$$\tan(\tau_n) = -\frac{1}{\mu_n}\frac{|\theta_b|}{l_{h,1}} \tag{5.20b}$$

$$\tan(\mu_n L + \tau_n) = \frac{\tan(\mu_n L) + \tan(\tau_n)}{1 - \tan(\mu_n L) \cdot \tan(\tau_n)} = \frac{|\theta_b|}{l_{h,2}} = 0 \tag{5.22b}$$

$$\tan(\mu_n L) = \frac{\mu_n \cdot \left(\frac{|\theta_b|}{l_{h,1}} + \frac{|\theta_b|}{l_{h,2}}\right)}{\mu_n^2 - \frac{\theta_b^2}{(l_{h,1} \cdot l_{h,2})}} = \frac{1}{\mu_n}\frac{|\theta_b|}{l_{h,1}} \tag{5.23b}$$

and finally:

$$y'(x,t) = \sum_{n=0}^{\infty} c_n \cos[\mu_n(x-L)]\, e^{-\varepsilon\mu_n{}^2 t} \tag{5.40}$$

with μ_n obeying (5.23b) and:

$$c_n = \frac{2}{L}\int_0^L g'(x) \cdot \cos[\mu_n(x-L)]\, dx \tag{5.41}$$

The analytical solutions derived previously can provide some useful information concerning the placement of a beach fill when in a limited domain. If the fill is placed on a beach in a rectangular plane-form with along-shore length B and an offshore dimension h, then the analytical model can be used to predict the subsequent behaviour of the fill.

From the previous analytical solutions it is possible to determine useful engineering tools which can help engineers and planners in defining the design life of a nourishment through the definition of the decaying process or the “reduction curve”. The decaying process of sediment in the beach fill portion is considered as the process that sediment is transported out of the beach fill portion by the waves, leading to the erosion of the shoreline. Based on the solution proposed, the decaying process of sediment can be investigated concerning percentage of sediment remained in the beach fill area. Dean (2003) revealed the solution, to obtain the remaining percentage for the case of open coast (see Chapter 4), whereas this study introduces the solution for a bounded shoreline of finite length. This tools would help the operator/ contractor of the beach nourishment to roughly estimate the amount of sediment remained in the beach fill portion after a certain elapsed time.

In the following paragraphs, the solutions furnished above are first compared to numerical simulations in GENESIS to test its reliability and assess the role of diffusion at different angles of wave attack.

Then the evolution of a beach fill with an initial rectangular plane form is studied and design curves are proposed and compared to the open coast condition, for easy use in engineering applications.

5.3. Validation

In this section we compare the afore presented analytical solution to numerical outcomes of the one line model GENESIS, which is widely employed for studying the evolution of shorelines in the long-run. Main aim of present section is to test the reliability of the analytical model even when the hypothesis of small angles will lapse.

For the validation of the analytical solution, we considered an initial shoreline position coinciding with a simple (symmetrical) rectangular beach fill, since most of beach nourishment projects, in fact, can be approximated as a rectangular plane form. The domain length is of 1 km, and the rectangular shape of the nourishment is of B=100m and h=10m, with an overall volume of sediment of $1000 m^3$.

Different model scenarios have been created by varying the offshore wave angle α_0 (from 0° to 40°), which denotes a different value of the shoreline diffusivity coefficient ε (Eq. 4.2).

Other model parameters (i.e. offshore wave height, wave period, transport coefficient) have been hold constant.

To measure the model performance, two prediction indices were used:

1. the relative mean square error (RMSE), normalized with respect to the RMS value of the numerical shoreline

$$RMSE/RMS = \sqrt{\frac{\sum_{i=1}^{N}(y_{num} - y_{an})^2}{N}} \Bigg/ \sqrt{\frac{\sum_{i=1}^{N} {y_{num}}^2}{N}} \tag{5.42}$$

2. the relative maximum error, still normalized with respect to the RMS value of the numerical shoreline:

$$ERR_{max}/RMS = \max(y_{num} - y_{an}) \Bigg/ \sqrt{\frac{\sum_{i=1}^{N} {y_{num}}^2}{N}} \tag{5.43}$$

where y_{num} and y_{an} are the numerical and analytical predicted shorelines respectively.

Furthermore, in order to evaluate the reliability of the analytical model to predict the subsequent behaviour of the fill over time, three different reduction times have been selected and compared to that of the numerical model, and namely: t^*_{25}; t^*_{50}; t^*_{75} corresponding to 25%, 50% and 75% respectively of the remaining volume of sediment at the beach fill initial placement.

5.3.1. Evolution with pinned extremes

The validation of the analytical solution with pinned extremes is here reported. The comparison has been made by considering GENESIS model of 1km with pinned extremes and a symmetrical rectangular beach fill of 100m (Figure 38).

Different model scenarios have been created by varying the offshore wave angle from 0° to 40°, and shoreline positions have been compared at selected times of 1, 2, 6, 8, 10, 15 and 20 years. Figure 39 shows normalised RMSE values given by numerical and analytical comparisons.

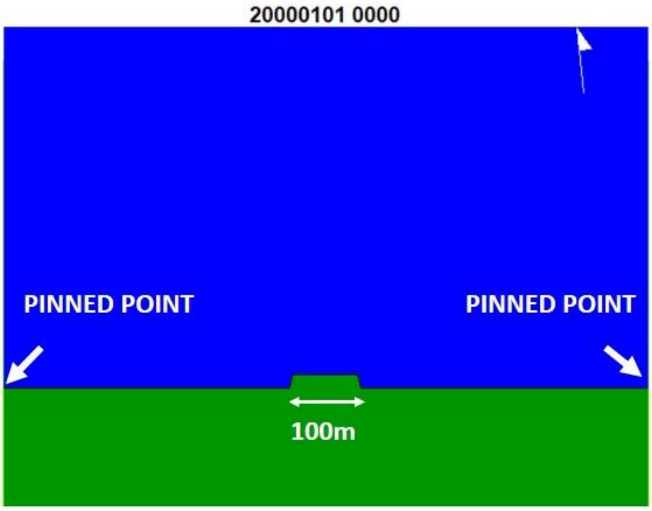

Figure 38 – Pinned domain modelling in GENESIS used for the validation phase

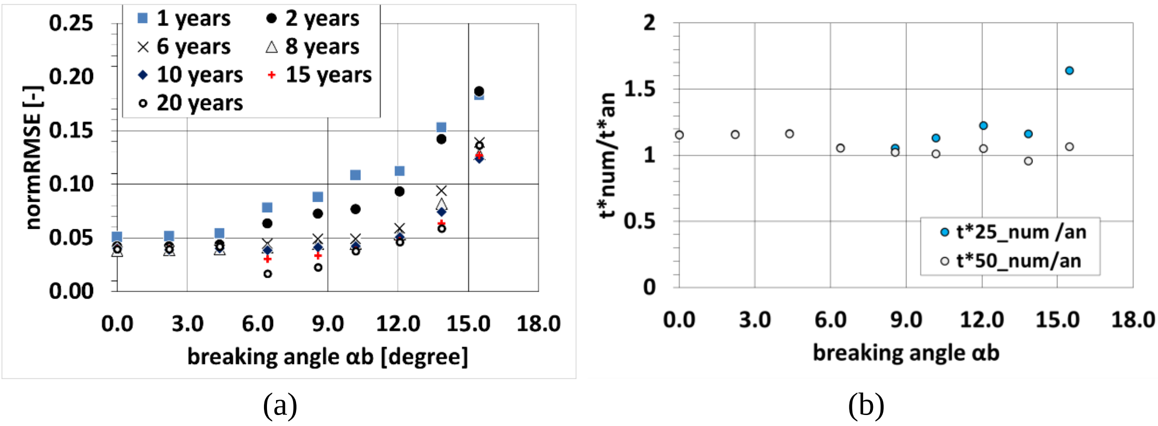

Figure 39 – (a) Normalized RMSE error for the pinned coast condition plotted against the breaking wave angle αb, for the selected times 1, 2, 6, 8 and 10 years. (b) Ratio between the two different reduction times (numerical/analytical), t^*_{25}; t^*_{50} corresponding to 25% and 50% respectively of the remaining volume of sediment at the beach fill initial placement.

Results shown in Figure 39a can be summarised as follows. The error exhibits an increasing trend with breaking angles which starts from about 6% at the 0° angle and reaches about 20% at 16°. The RMSE error is less than 10% up to 10° breaking angle, which corresponds to 25° of offshore wave attack.

Moreover, it is observed that with increasing breaking angles the error tends to grow especially in the short term (1-2 years). This is because, for large offshore angles, say 30° or more, the beach nourishment profile tends to grow at trough. This can be regarded as an incipient negative diffusivity effect (see Chapter 6) which, for very large angles, will lead the profile to increase its height (Figure 40a). These instabilities tend to be reabsorbed in the medium term, leading the error to reduce (Figure 40b).

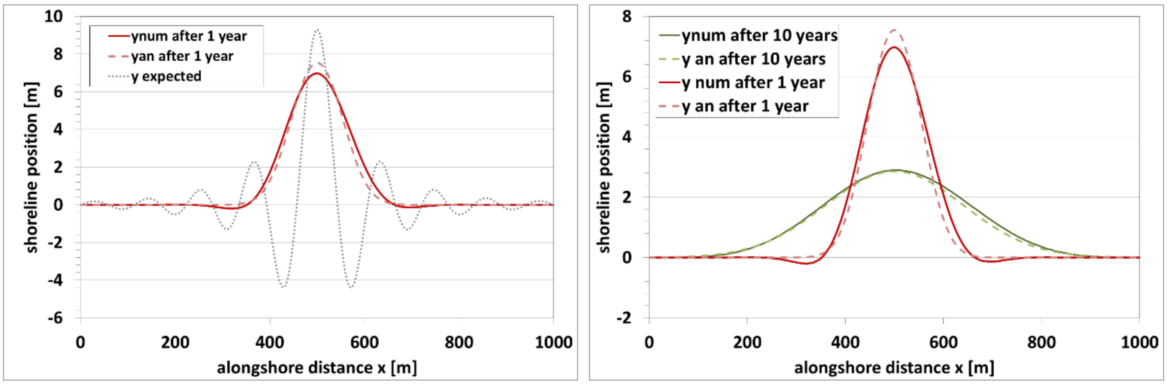

(a) (b)

Figure 40 – (a) Comparison between numerical and analytical shoreline position after 1 year, with an offshore wave angle of 30°. The negative diffusivity effects produce a growing of the shoreline through (red arrows). Little dashed line represents the hypothetical growing of beach bumps caused by a greater wave angle. (b) Comparison between numerical and analytical shoreline position after 1 year and after 10 years, with an offshore wave angle of 30°. It is seen the negative effects to be reabsorbed over time.

Figure 39b displays the three non dimensional different reduction times used to evaluate the subsequent behaviour of the fill over time. The graph shows that t^*_{25} and t^*_{50} are wherever well predicted by the analytical model, except for the case of t^*_{25} with very large angle (α_b=15,5°). A comparison between analytical and numerical reduction curve is reported in Figure 41b: the evolution of the beach fill over time is satisfactorily predicted till 40°.

Briefly, it is possible to say that the analytical solution to produce a good approximation of the effective shoreline evolution over time. Moreover, the agreement is acceptable even when the offshore wave attack becomes greater; shoreline comparisons over years are shown in Figure 41a for offshore wave angle of 40°.

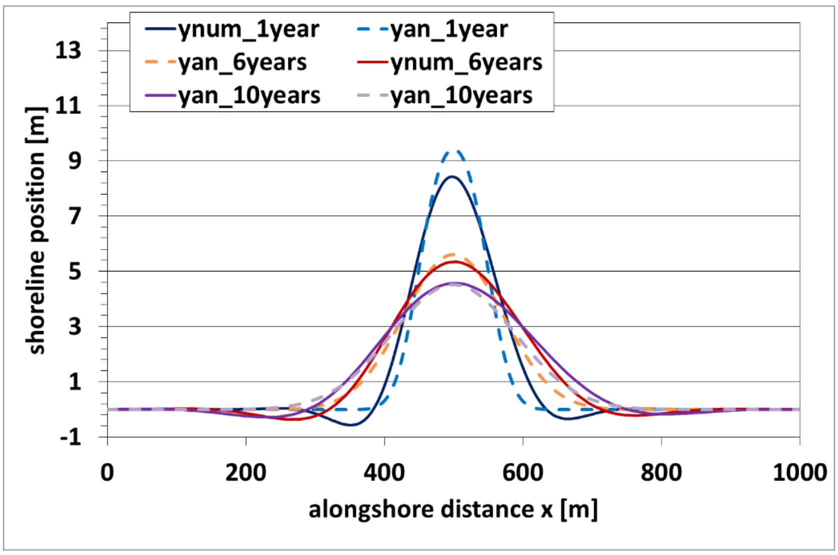

(a)

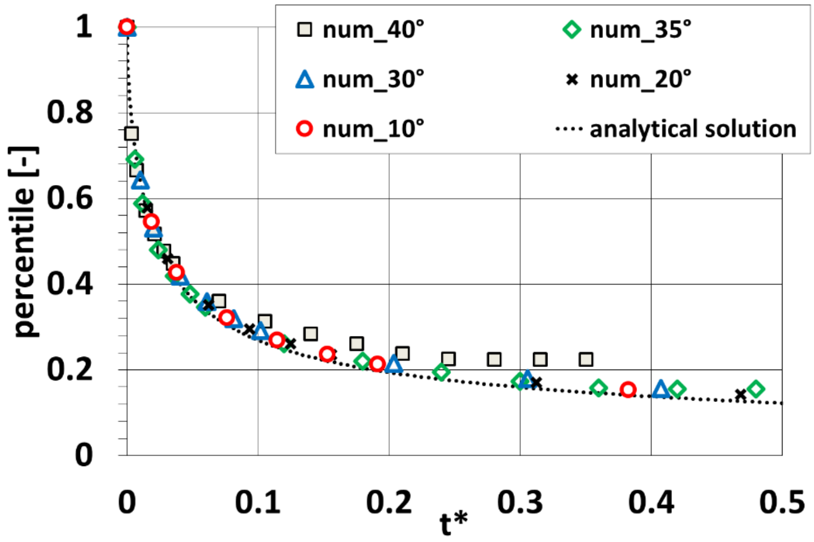

(b)

Figure 41 – (a) Comparison between analytical and numerical shoreline position for 35° of offshore wave angle. (b) Comparison between analytical and numerical reduction curves for different offshore wave angles.

5.3.2. Evolution between infinite outcrops

The validation of the analytical solution with infinite extremes is here reported. As for the “pinned case”, the comparison has been made by considering GENESIS model of 1km, but with two infinite groins at the domain bounds, and a symmetrical rectangular beach fill of 100m (Figure 42).

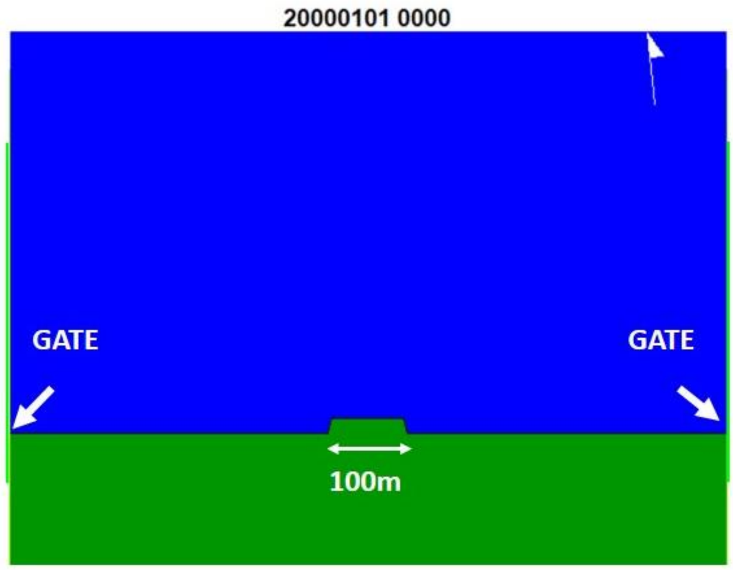

Figure 42 - Gated domain modelling in GENESIS used for the validation phase

Different model scenarios have been created by varying the offshore wave angle from 0° to 40° to take into account the reliability of the analytical model even when the offshore wave angle gets greater, and shoreline positions have been compared at selected times of 1, 2, 6, 8 and 10 years.

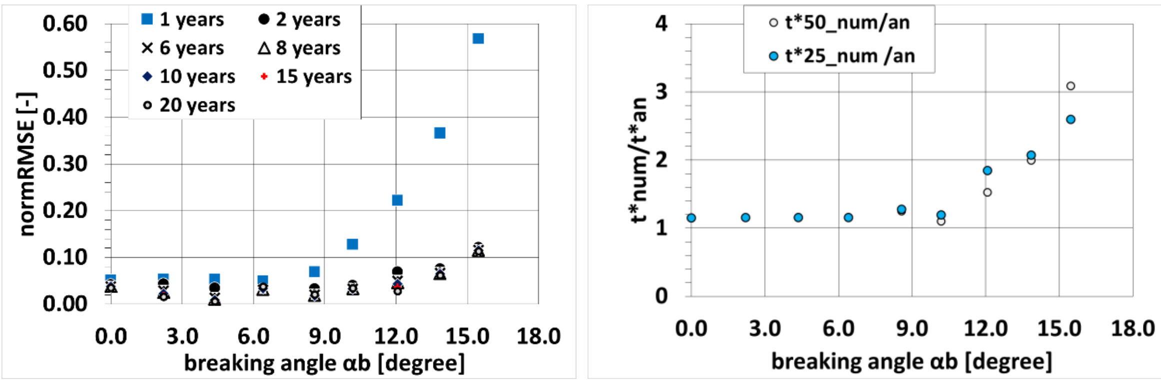

(a) (b)

Figure 43 - (a) Normalized RMSE error for the gated coast condition plotted against the breaking wave angle αb, for the selected times 1, 2, 6, 8 and 10 years. (b) Ratio between the two different reduction times (numerical/analytical), t_{25}^{*}; t_{50}^{*}corresponding to 25% and 50% respectively of the remaining volume of sediment at the beach fill initial placement.

As shown in Figure 43a, in most of cases the RMSE error is similar or less to that of the "pinned case", shown in previous section. The only exception concerns short-term shorelines (i.e. one-year evolution). Differently from what observed for the case of the pinned coast, large errors are here generated by a progressive mismatch at the bounds of the computational domain, where it is seen the numerical solution anticipating the analytical one (Figure 44a,b). Moreover, it is seen the error to grow, as expected, with increasing the breaking wave angle.

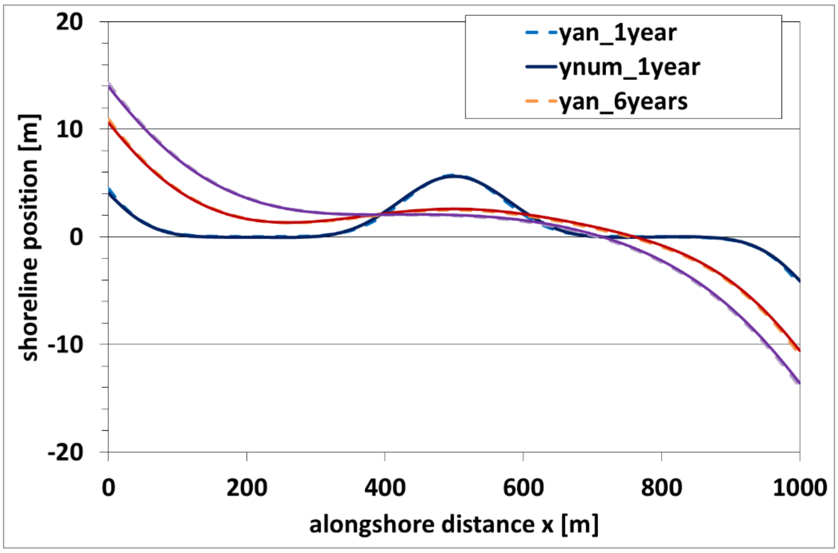

(a)

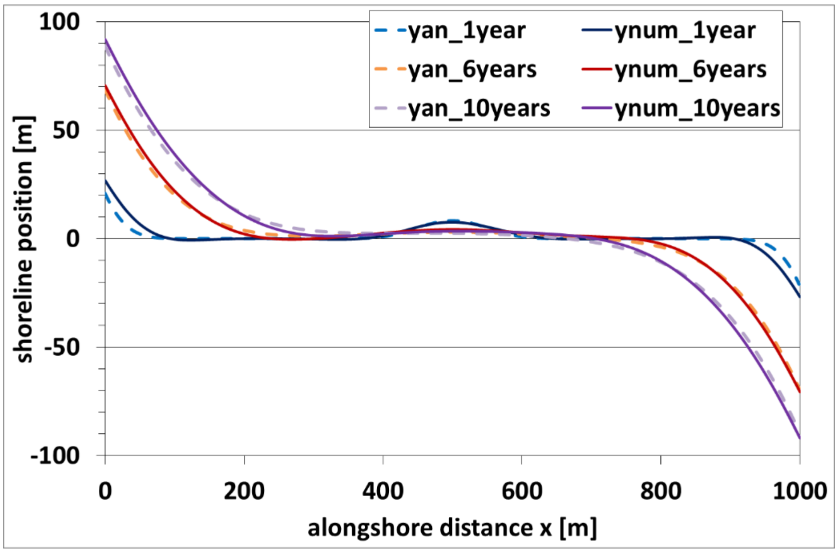

(b)

Figure 44 - (a) Comparison between analytical and numerical shoreline position for 5° of offshore wave angle; (b) Comparison between analytical and numerical shoreline position for 35° of offshore wave angle.

As regarding the beach nourishment characteristics reduction times (Figure 43b), the gated case acts similarly to what observed for the pinned case. The graph shows that t^*_{25} and t^*_{50} are predicted by the analytical model down to 10° breaking (that is 25° offshore), from which an accretive trend is observed. The evolution of the beach fill over time is satisfactorily predicted till 30°, then the numerical curves detached from the analytical one (Figure 45).

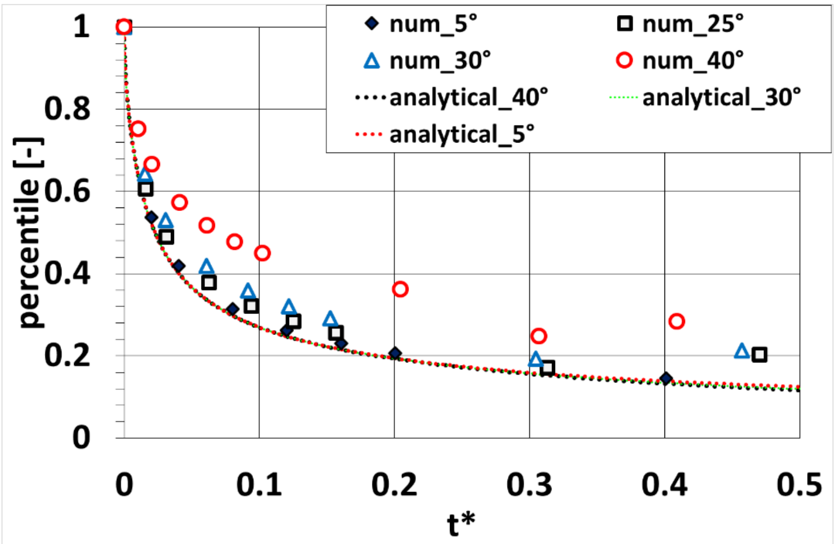

Figure 45 - Comparison between analytical and numerical reduction curves for 5° and 30° offshore wave angles.

5.3.3. Evolution between bypassed and unbypassed outcrops

The validation of the analytical solution with a bypassing groin and unbypassing groin is here reported. As for the previous cases, the comparison has been made by considering GENESIS model of 1km, and a symmetrical rectangular beach fill of 100m. In order to simulate a bypassing condition, on the left side of the numerical domain has been set a bypassing groin, of 50m length. Its length is such that the depth of closure in GENESIS is not reached, and a bypassing transport rate is accounted for (Figure 46).

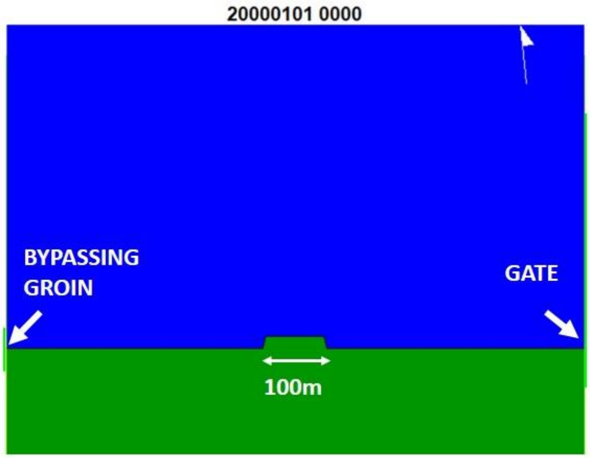

Figure 46 - Bypassed domain modelling in GENESIS used for the validation phase

Also here, different model scenarios have been created by varying the offshore wave angle from 0° to 40° to take into account the reliability of the analytical model even when the offshore wave angle gets greater, and shoreline positions have been compared at selected times of 1, 2, 6, 8 and 10 years. Shoreline comparisons between analytical and numerical solutions are plotted in Figure 47a,b. The match between analytical and numerical solution is surprisingly similar (except for the area just closed to the bypassing groin), validating he accuracy of the analytical one.

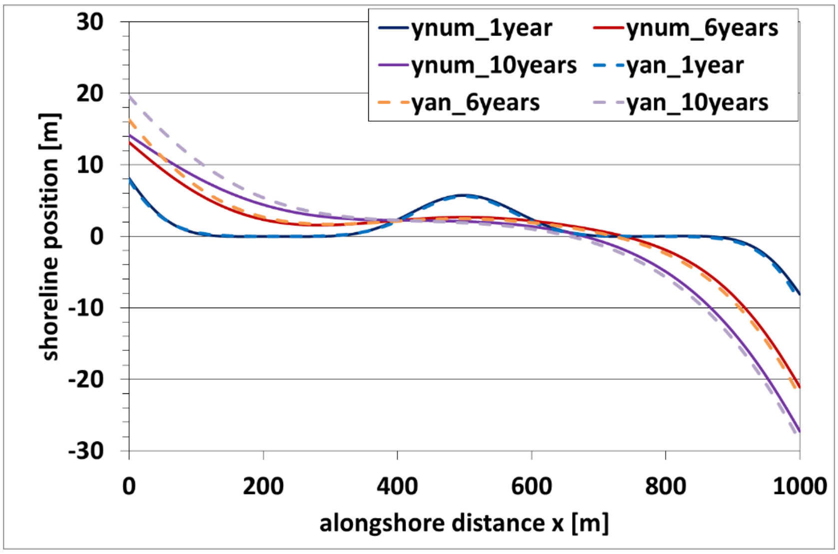

(a)

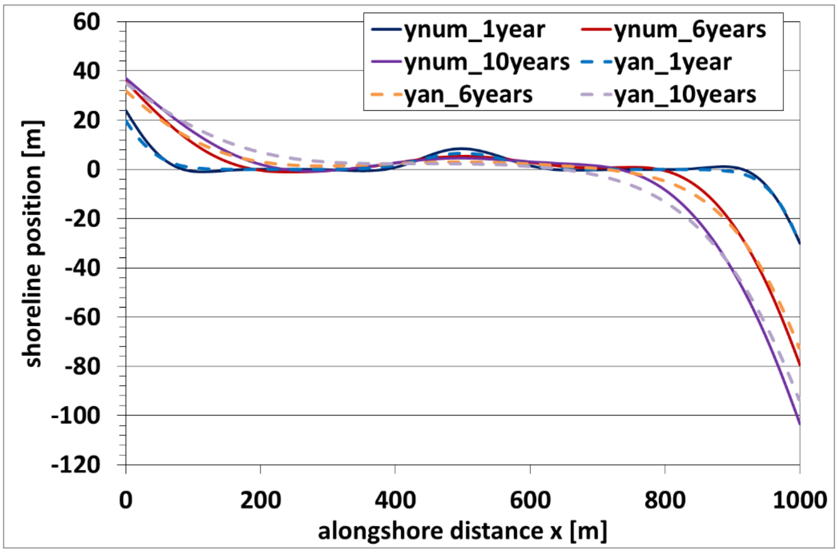

(b)

Figure 47 – Robin boundary condition (a) comparison between analytical and numerical shoreline position for 10° of offshore wave angle; (b) Comparison between analytical and numerical shoreline position for 40° of offshore wave angle.

From Figure 47a,b it is seen surprisingly to increase the match between the solution with increasing the wave angle. Anyhow, even for the Robin boundary condition the fit is surprisingly similar, proving the accuracy and potentials of the analytical solution calculated in previous sections.

5.4. Effect of boundary condition on the evolution of the beach fill: comparison with the open coast case and engineering tools

In this section the effect of boundary conditions are analysed on the subsequent evolution over time of a rectangular beach nourishment with respect to the open coast condition. The evolution of rectangular beach fill for open coast has been provided by Dean, and has been previously discussed in Chapter 4. Three type of dimensionless reduction time, of engineering interest, have been selected to make a comparison between the open coast condition with the pinned coast condition: the half-life reduction time, t_{50}^{*}; the quarter-life reduction time, t_{25}^{*}, and the three-quarter-life reduction time, t_{75}^{*}.

With the considerations given by Dean (2003) regarding the proportion of sand $M(t)$ remaining at the placement site (Eq. 4.20), the reduction time for the open coast are then calculated as:

$$t_{50}^{*} = 0.21\,\pi^2 \left(\frac{B}{L}\right)^2 \tag{5.44}$$

$$t_{25}^{*} = 1.76625\,\pi^2 \left(\frac{B}{L}\right)^2 \tag{5.45}$$

$$t_{75}^{*} = 0.049\,\pi^2 \left(\frac{B}{L}\right)^2 \tag{5.46}$$

5.4.1. Pinned beach

For the pinned beach condition a comparison is depicted in Figure 48-50 for the three reduction time with the two different boundary conditions. Particularly, the dimensionless times are plotted against various ratios B/L o rectangular beach fills, ranging between 0.05 to 0.6. The height of the nourishment is varied in order to conserve the total volume of the nourishment equal to 1000m^3. It is noteworthy that the t* for the case of a pinned beach are calculated independently from the wave angle.

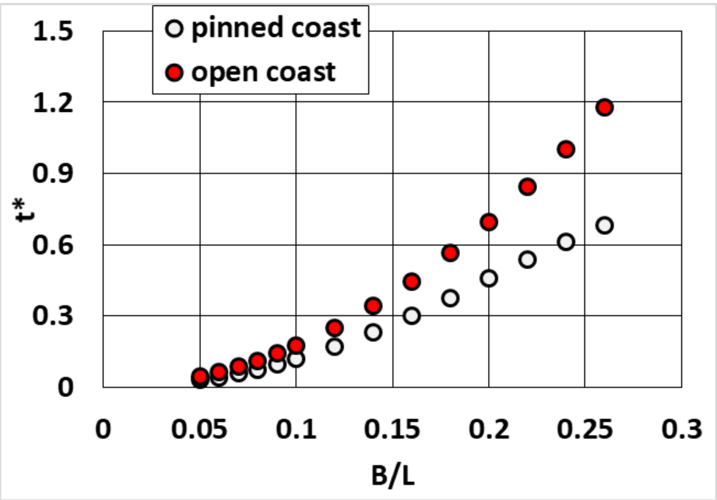

Figure 48 – Dimensionless time value for a 0.25 reduction ratio both for pinned coast and open coast with respect to different B/L rectangular configurations

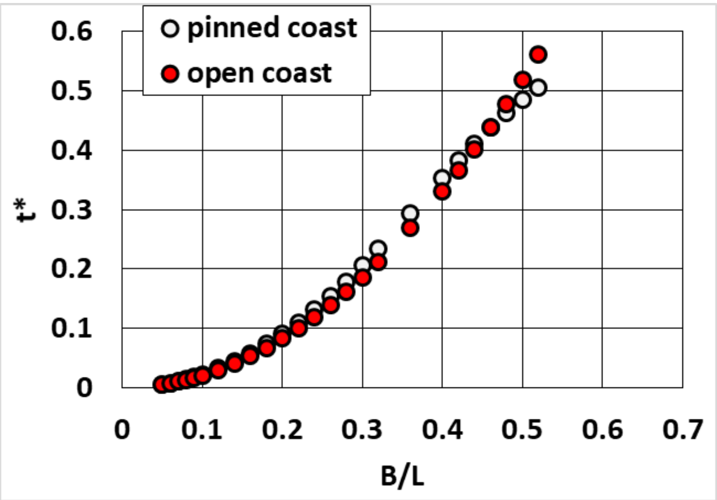

Figure 49 - Dimensionless time value for a 0.5 reduction ratio both for pinned coast and open coast with respect to different B/L rectangular configurations

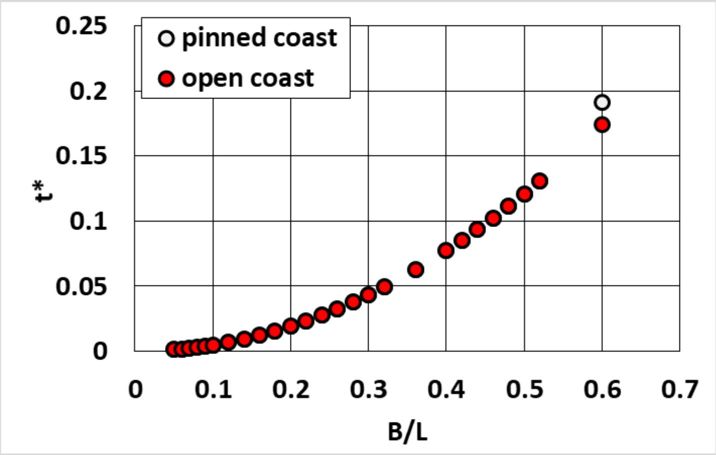

Figure 50 - Dimensionless time value for a 0.75 reduction ratio both for pinned coast and open coast with respect to different B/L rectangular configurations

Note from the graphs that the boundary conditions have a more impact on the lesser reduction ratios, as expected. Moreover, the wider the beach fill the more effective the boundary condition. This can be better appreciated in Figure 51: for narrower beach fills the pinned coast reduction curve practically matches with the open coast one, for wider nourishments the situation is reversed.

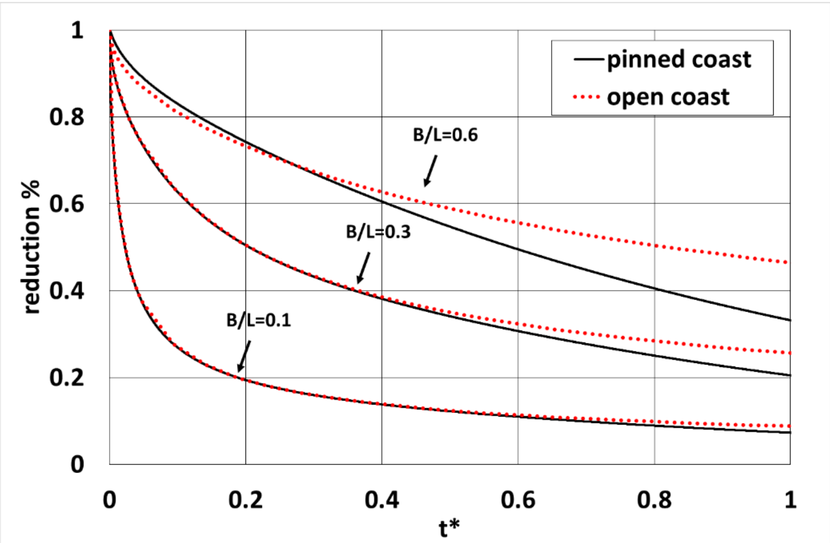

Figure 51 – Comparison between pinned coast reduction curve and open coast reduction curve, for three beach nourishments configurations of B/L=0.1, B/L=0.3; B/L=0.6.

A useful tool provided in this section is a relationship for which the dimensionless time t* can be calculated for a percentile of interest.

For various rectangular beach shape configuration (for varying ratios B/L, and constant volume of 1000m^3), a series of percentiles P has been determined from the reduction curves, from 0.05 to 0.95. For every single percentile the proportion of sand remaining in every B/L configuration has been plotted, and a trend line has been determined. An example is plotted in Figures 52.

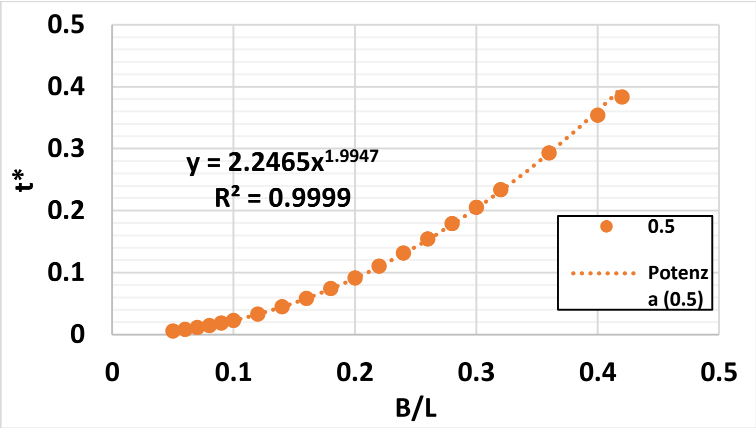

Figure 52 - Trend line for the percentile 0.5 with respect to B/L

Data have been approximated through a power function of the type: $t^* = C\left(\frac{B}{L}\right)^n$. For the case of Figure 52, we have ${t_{50}}^* = 2.2465\left(\frac{B}{L}\right)^{1.9947}$. The same procedure has been carried out for all the percentiles, and the coefficient C and n have been determined. C and n values are reported in Table 1.

Table 1 – C and n coefficients for the pinned coast

P	C	n
0.1	49.206	1.8388
0.15	28.834	1.9376
0.2	17.17	1.9647
0.25	11.054	1.976
0.3	7.5719	1.9832
0.35	5.3909	1.9861
0.4	4.0119	1.9955
0.45	2.9438	1.9883
0.5	2.2465	1.9947
0.55	1.7011	1.9952
0.6	1.2698	1.9896
0.65	0.9641	2.0011
0.7	0.7036	2.0061
0.75	0.4868	2.0079
0.8	0.3141	2.0182
0.85	0.1762	2.0206
0.9	0.08	2.0486

Their values are also plotted against the percentiles values in Figures 53 and 54.

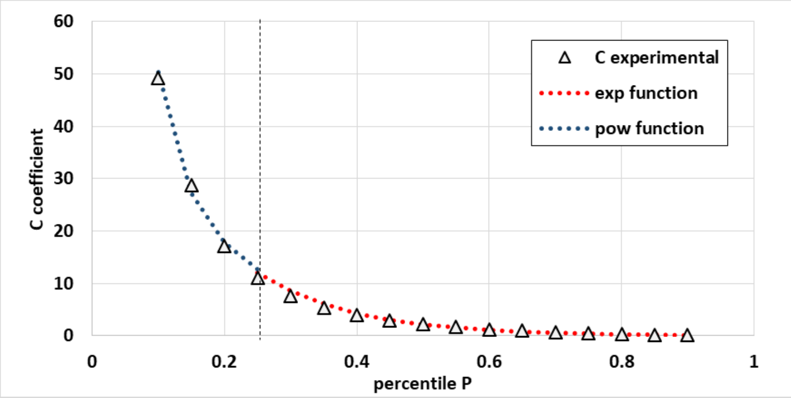

Figure 53 – C coefficient for pinned coast

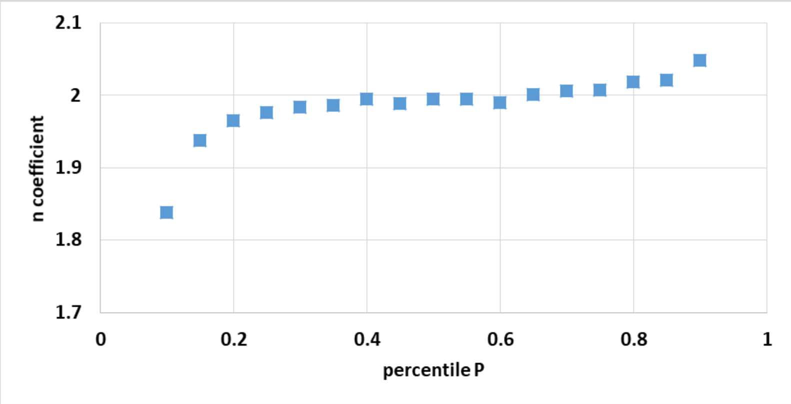

Figure 54 – n coefficient for pinned coast

Particularly, it is seen from Figure 54 that the value of the n coefficient slightly varies around 2, only for small percentiles (0.01 and 0.015) its value moderately deviates from the average value of 2. On the other hand, for the C coefficient a formula can be provided as a function of the percentile. It reads:

$$C(P) = 1.572\ P^{-1.506} \quad for\ P < 0.25 \tag{5.47}$$

$$C(P) = 66.823\exp(-6.855P) \quad for\ P \geq 0.25 \tag{5.48}$$

As a result, for the pinned boundary condition, the dimensionless time t^* can be determined as:

$$t_P{}^* = 1.572\ P^{-1.506}\left(\frac{B}{L}\right)^2 \quad for\ P < 0.25 \tag{5.49}$$

$$t_P{}^* = 66.823\exp(-6.855P)\left(\frac{B}{L}\right)^2 \quad for\ P \geq 0.25 \tag{5.50}$$

5.4.2. Gated beach

We considered the evolution of a stretch of coast of 1 km with pinned extremes. The analytical solution has been provided in the previous section.

5.4.2.1. *Symmetric rectangular beach fill*

Also here a comparison is made considering the open coast boundary conditions, provided by Dean (2003), for the half-life reduction time, t_{50}^*; the quarter-life reduction time, t_{25}^*, and the three-quarter-life reduction time, t_{75}^*.

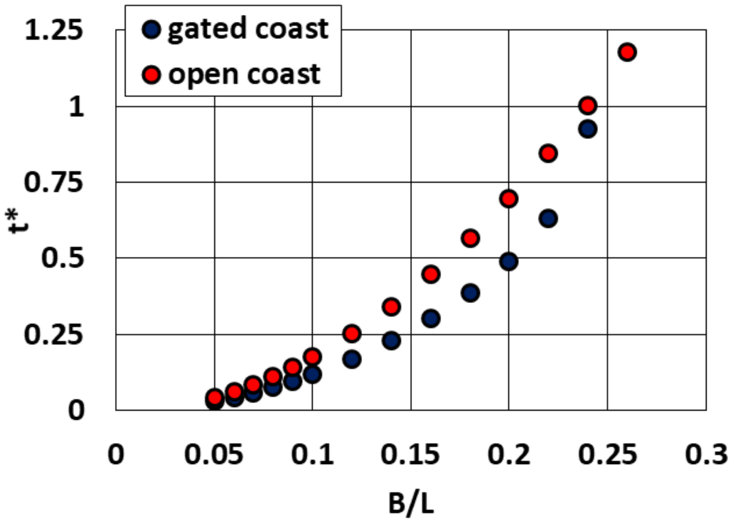

Figure 55 — Dimensionless time value for a 0.25 reduction ratio both for gated coast and open coast with respect to different B/L rectangular configurations

It is noteworthy that the t* for the case of a domain bounded by infinite outcrops are calculated independently from the wave angle. This is because the centre of gravity of the nourishment corresponds to the domain centre. In Figures 55 to 57 are plotted the three dimensionless times against various ratios B/L, ranging between 0.05 to 0.6.

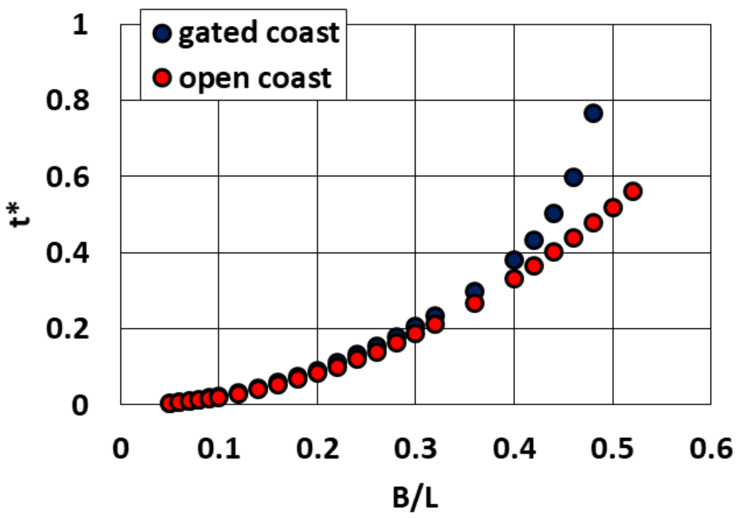

Figure 56 - Dimensionless time value for a 0.5 reduction ratio both for gated coast and open coast with respect to different B/L rectangular configurations

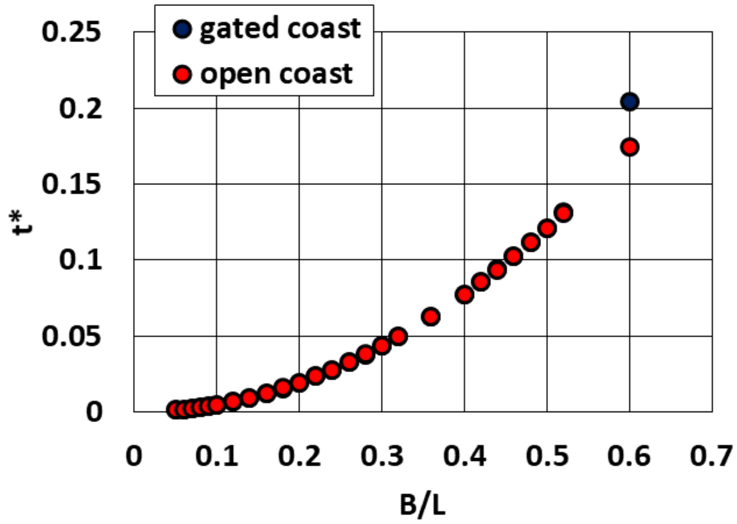

Figure 57 - Dimensionless time value for a 0.75 reduction ratio both for gated coast and open coast with respect to different B/L rectangular configurations

From the graphs, it is noted that the influence of the boundary conditions is effective for smaller values of the ratio B/L: the wider the nourishment, the more influencing the boundary condition. Moreover, for smaller t^*, the reduction percentage is smaller than the case of the open coast, in fact in open boundaries the nourishment should tend to erode faster than in the closed domain. In Figure 58 it is noted the more influencing boundary conditions on wider beach nourishments.

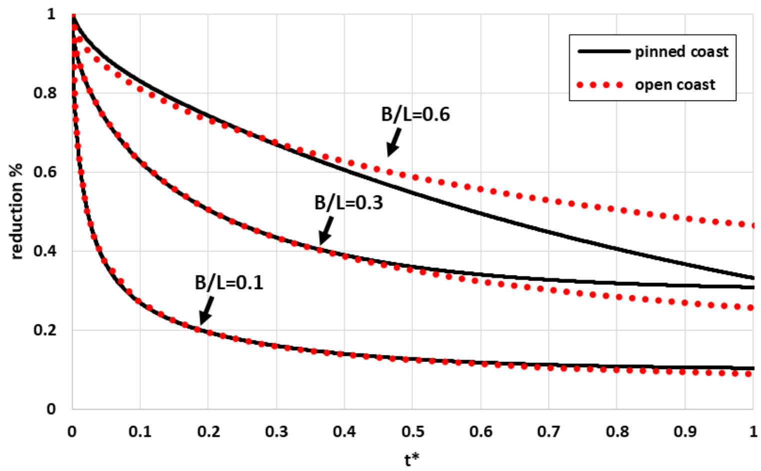

Figure 58 - Comparison between gated coast reduction curve and open coast reduction curve, for three beach nourishments configurations of B/L=0.1, B/L=0.3; B/L=0.6.

Additionally, also here the relationship between the dimensionless time t* and the percentile of interest is given.

Following the same procedure of the pinned case, for various symmetrical rectangular beach shape configuration (for varying ratios B/L, and constant volume of 1000m^3), a series of percentiles $P_{\%}$ has been determined from the reduction curves, from 0.05 to 0.95. For every single percentile, the proportion of sand remaining in every B/L configuration has been plotted, and a trend line has been determined. Data have been approximated through a power function of the type: $t^* = C\left(\frac{B}{L}\right)^n$, the coefficients C and n have been determined for every percentile. C and n values are reported in Table 2.

Table 2 – C and n for the gated coast

P	C	n
0.1	403.53	2.19
0.15	49.688	2.1394
0.2	22.279	2.0643
0.25	12.697	2.0387
0.3	8.4761	2.0287
0.35	5.8821	2.0222
0.4	4.173	2.0116
0.45	3.1999	2.0249
0.5	2.3718	2.0188
0.55	1.7935	2.0191
0.6	1.3625	2.0223
0.65	0.9892	2.0131
0.7	0.7087	2.0094
0.75	0.4874	2.0086
0.8	0.3142	2.0183
0.85	0.1762	2.0206
0.9	0.08	2.0486

Their values are also plotted against the percentiles values in Figure 59 and 60.

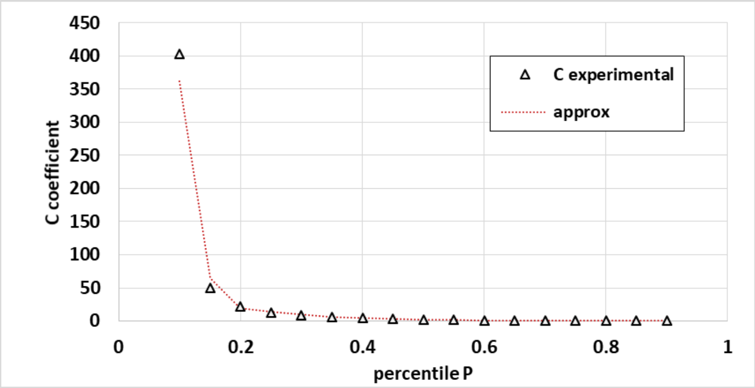

Figure 59 – C coefficient for the gated coast

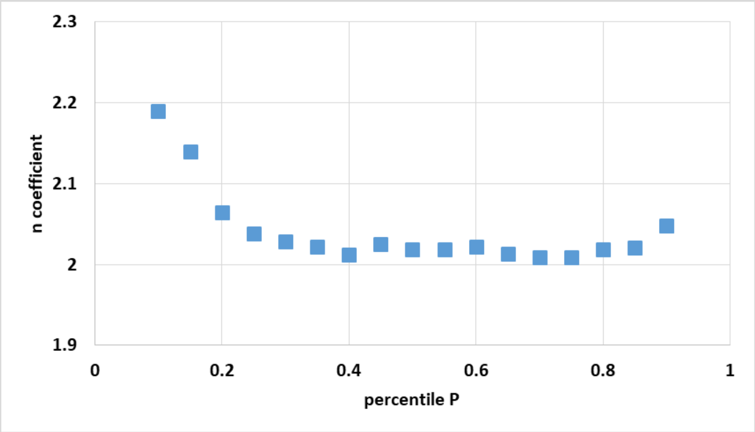

Figure 60 – n coefficient for the gated coast

Particularly, it is seen from Figure 60 that the value of the n coefficient slightly varies around 2: only for small percentiles (0.01 and 0.015) its value moderately deviates from the average value of 2, as occurred for the pinned case of study.

For the C coefficient also a formula can be provided as a function of the percentile in the case of gated boundaries. It reads:

$$C(P) = \max(0.0206\, P^{-4.244}; 78.213\, \exp(-7.047P))$$

As a result, for the pinned boundary condition, the dimensionless time t^* can be determined as:

$$t_P{}^* = \max(0.0206\, P^{-4.244}; 78.213\, \exp(-7.047P)) \left(\frac{B}{L}\right)^2$$

5.4.2.2. Asymmetric rectangular beach fill

In this section we analyse the case of an asymmetric rectangular beach fill, bounded by two infinite outcrops, but with the centre of gravity not matching with the centre of the domain. The scope is to evaluate the reduction time of the nourishment moving toward the downdrift extreme of the domain, where the obliquity of waves causes additional erosion.

Let's first consider a comparison between the analytical solution with the numerical solution has been made, but the results are similar to that of the symmetric beach fill reported in previous section. It is only reported in Figure 62 a comparison between numerical and analytical shorelines. Particularly, the beach nourishment here is not placed at the centre of the domain, its centre of gravity is at x=850m, as shown in Figure 61.

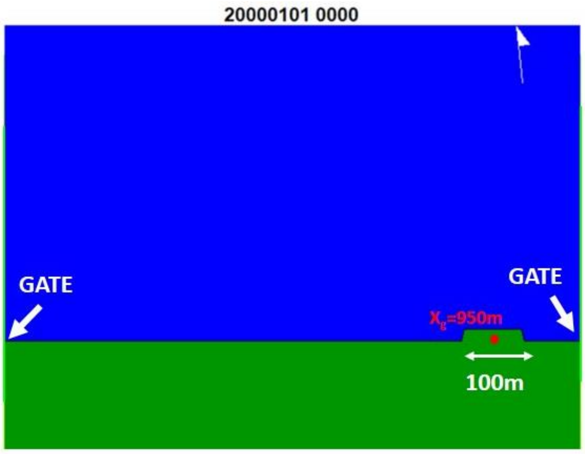

Figure 61 – GENESIS modelling of the asymmetric rectangular nourishment

Analytical and numerical shoreline positions are compared for four different time instants of 1, 2, 6 and 10 years, which have been converted in their corresponding dimensionless values with respect to the diffusivity ε. Matching is again surprisingly similar, validating he accuracy of the analytical solution.

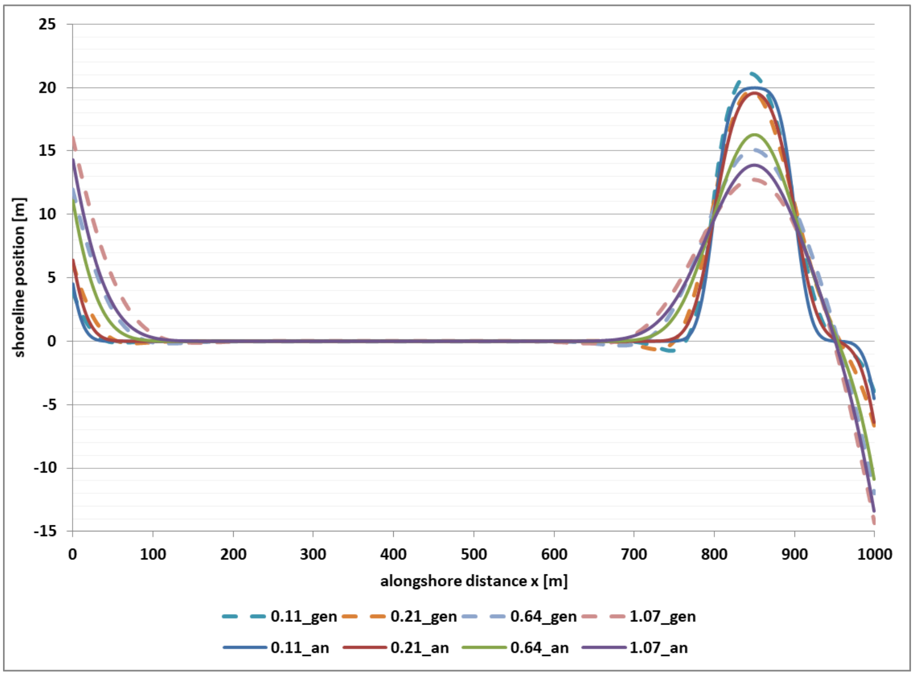

Figure 62 – comparison between the analytical and numerical solution for the asymmetrical beach fill in a bounded domain

We evaluated the reduction ratio for two different B/L values, 0.1 and 0.3 respectively. Moreover, the beach nourishment have been moved toward the downdrift extreme by varying the centre of mass position, from x=550m to x=950m, with a step of 50 m. Moreover, the wave angle has been set to 20° for each configuration.

Reduction curves have been calculated from the analytical solutions and some of the case are plotted in Figures 63 to 65 for three different wave angles of 0° 10° and 20°. The centres of gravity of 950m, 750 m, and 550 m have been selected for the plot.

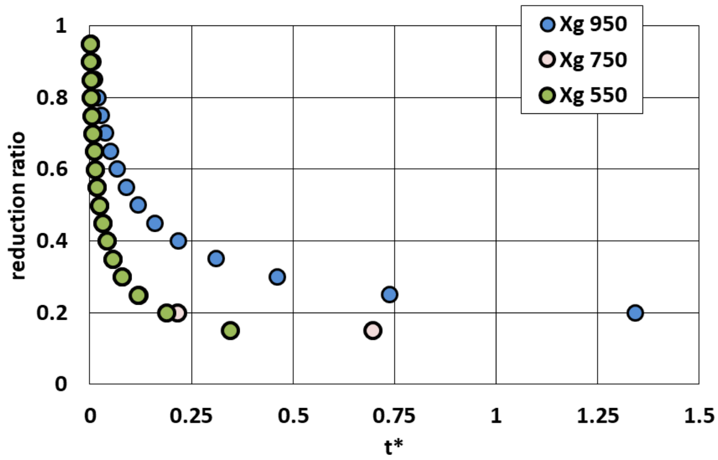

Figure 63 – Reduction curve for an asymmetrical rectangular beach fill with wave angle of 0°

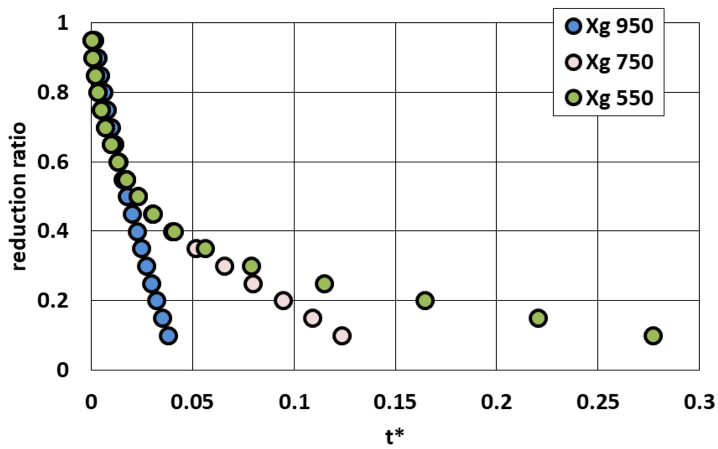

Figure 64 - Reduction curve for an asymmetrical rectangular beach fill with wave angle of 10°

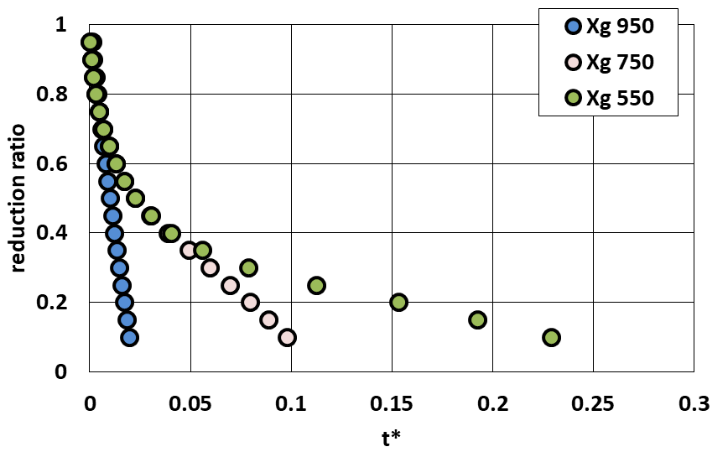

Figure 65 - Reduction curve for an asymmetrical rectangular beach fill with wave angle of 20°

As expected, the beach fill nearer the downdrift groin reduces faster with increasing of the wave angle. The farther the centre of gravity, the lesser the reduction.

Moreover, the dimensionless time at reduction ratios of 0.25, 0.5 and 0.75 are plotted in the following Figures, with respect to the position of the nourishment. It is seen from the figure that, the reduction is faster when the nourishment approaches the right side of the domain. Anyhow, the reduction is much less marked moving towards a 0.75 reduction.

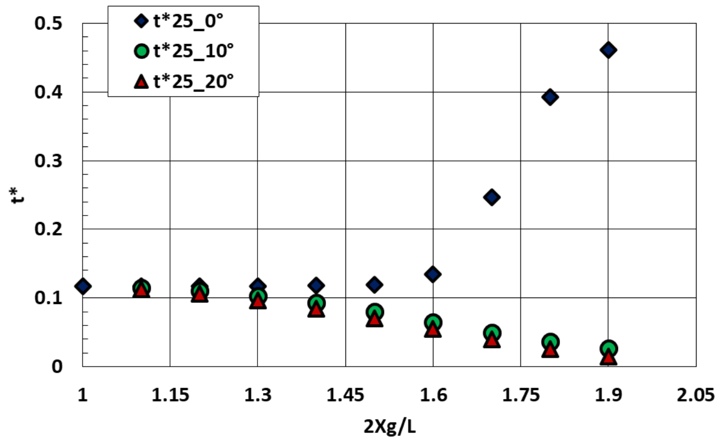

Figure 66 – Reduction ratio 0.25 for a rectangular nourishment of B/L 0.1 with different centre of gravity.

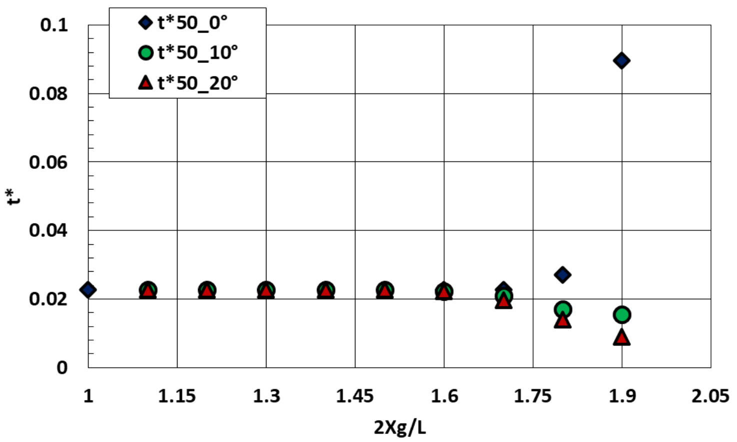

Figure 67 – reduction ratio 0.5 for a rectangular nourishment of B/L 0.1 with different centre of gravity

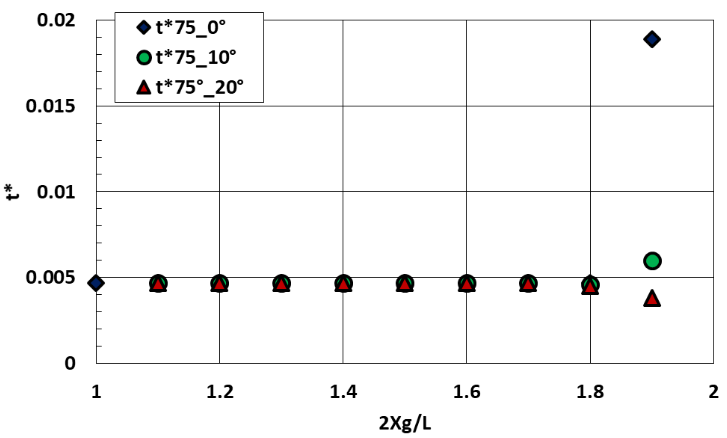

Figure 68 - reduction ratio 0.75 for a rectangular nourishment of B/L 0.1 with different centre of gravity

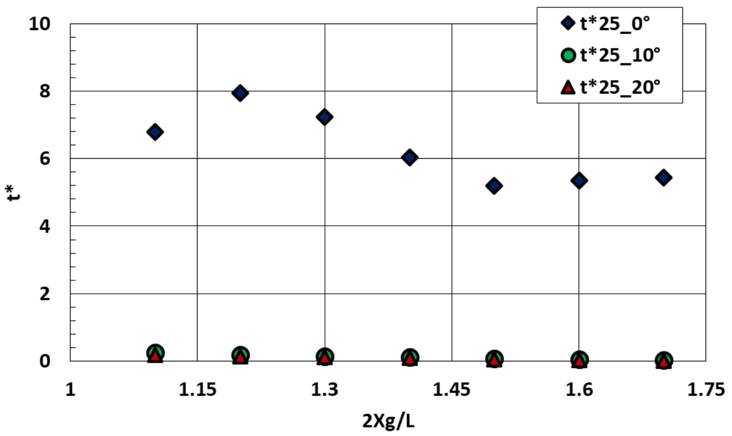

Figure 69 - reduction ratio 0.25 for a rectangular nourishment of B/L 0.3 with different centre of gravity

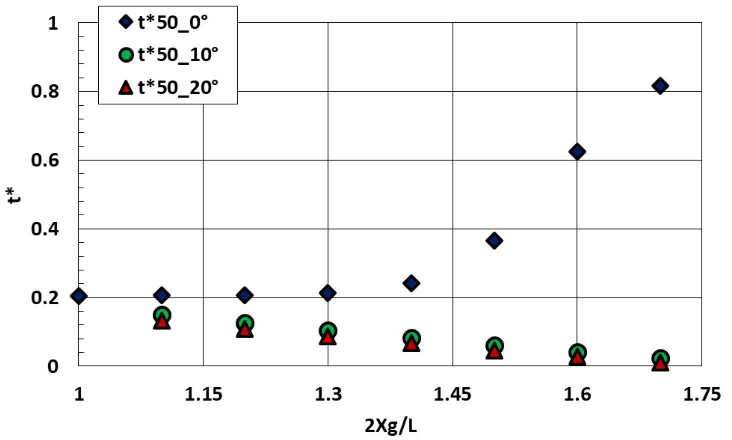

Figure 70 - reduction ratio 0.5 for a rectangular nourishment of B/L 0.3 with different centre of gravity

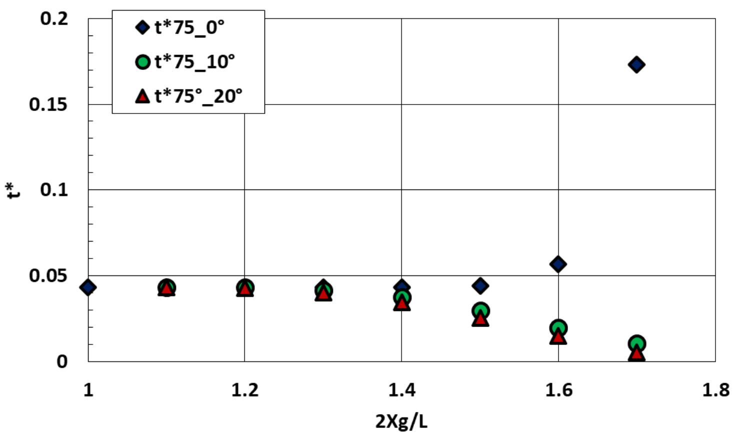

Figure 71 - - reduction ratio 0.75 for a rectangular nourishment of B/L 0.3 with different centre of gravity

5.4.3. Bypassed headlands

For the case of the robin boundary conditions we examined the following configurations:

- Three different values of the ratio B/L, 0.1, 0.3, 0.5 respectively;
- Three different bypassing groin length; 30m; 60m; 120m;
- Three different wave angles: 0°, 10°, 20°

The reduction ratios have been determined for each combined scenarios, results are plotted in Figure 72 panels (a) to (i).

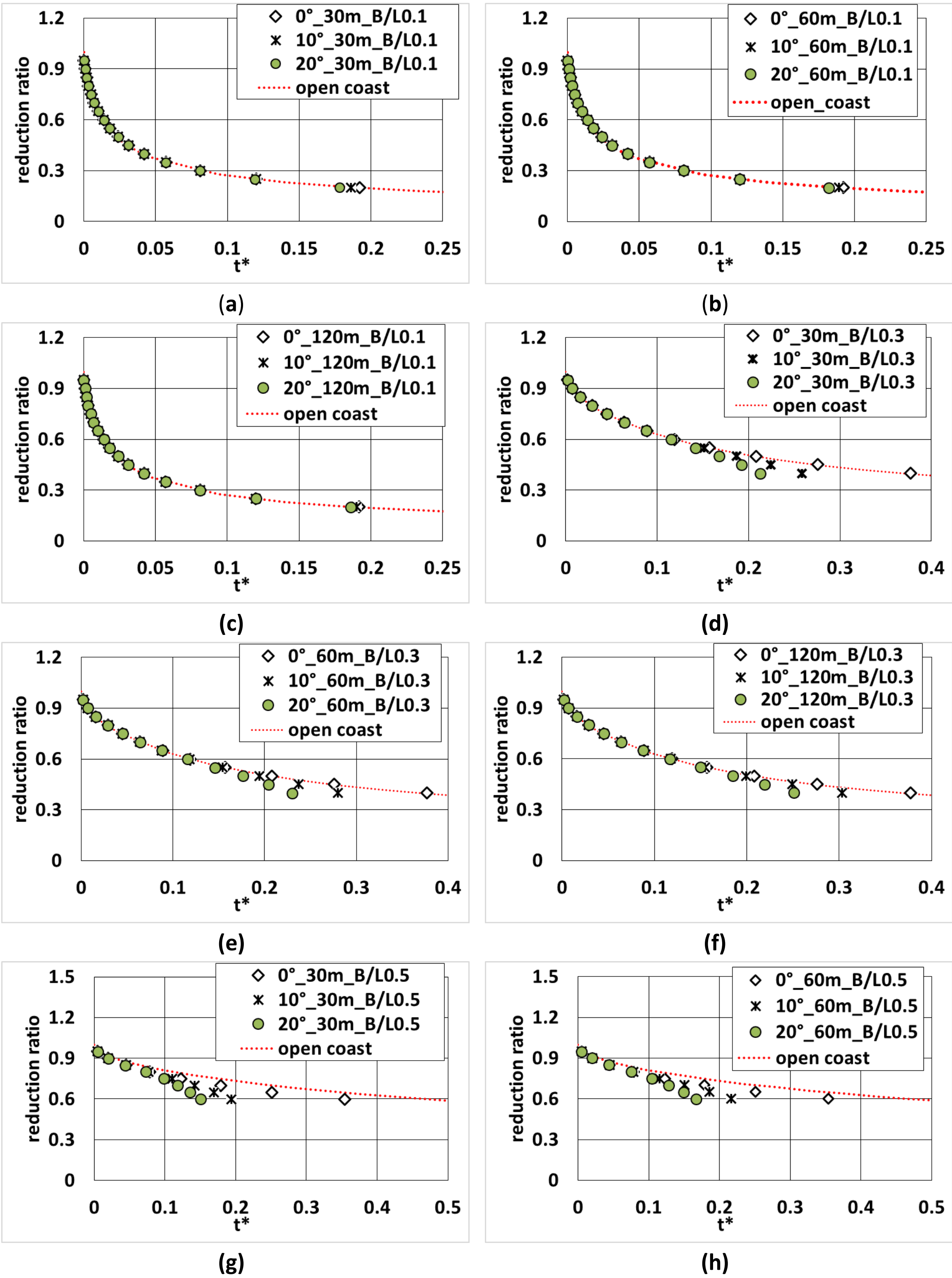

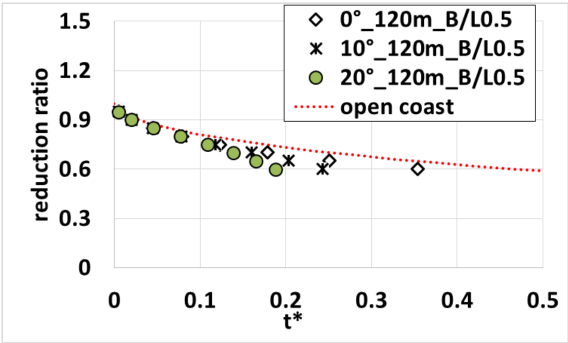

(i)

Figure 72 – reduction curves for the Robin BC coast for the different configurations analysed compared with the open coast case. (a) B/L 0.1; groin 30m (b) B/L 0.1; groin 60m; (c) B/L 0.1; groin 120m; (d) B/L 0.3; groin 30m (e) B/L 0.3; groin 60m; (f) B/L 0.3; groin 120m (g) B/L 0.5; groin 30m (h) B/L 0.5; groin 60m; (i) B/L 0.5; groin 120m

For a rectangular beach fill with a B/L ratio of 0.1, it has been seen the reduction curves to be practically matching for each groin configuration (even for greater obliquity). Particularly, the evolution is not far from the open coast case, the effect of boundary conditions here is practically slight. While, as shown in Figure 72, things change when in wider beach fill. For a B/L ratio of 0.3, the reduction ratio is greater for a more oblique wave and slower for a less oblique one. Moreover, even if values are similar, it is seen that for longer groins (less bypass), the reduction ratio is lower than for smaller groins (more bypass). From Figure 72 it is seen that for a normal wave attack the evolution is similar to that of the open coast, while, with increasing the obliquity, the reduction becomes faster. The same occurs for the ratio B/L equal to 0.5.

It is seen that for the B/L 0.1 case the dimensionless times and practically matching with the open coast case. Things changes when in wider nourishments: dimensionless time becomes slower for the bounded domain.

Chapter 6: Homogeneous diffusion equation with time dependent diffusivity. Solution and engineering outlooks

6.1. Introduction

In this Chapter we come then to one of the key points in the applicative study of coastline evolution, that is the use of the so-called "Equivalent Wave" (EW), which should govern the evolution of the entire coastline in the long run. This is a common concept used in engineering practice, and consists in modeling the evolution of the beach with a single direction among those of the incident wave climate. The theoretical foundations of this engineering practice are shown, which had not been clarified until now.

As shown in previous Chapters, the diffusion coefficient ε is intensely dependent on the wave height and wave direction. Since the wave height and direction, in the traditional oneline theory, are assumed to be constant over x and t, so it is beach diffusion.

In this Chapter, we will assume that the diffusion coefficient to be time dependent, hypothesis not so wrong at all. In fact, the wave height and wave direction can vary over a long period with a certain frequency, which could be, broadly speaking, a wider or smaller frequency (from hours to seasons), depending on the wave climate characteristics. Therefore, the dependence on time of wave height and direction would suggest that the diffusion coefficient is a function of time, and a time varying diffusivity extra-effect is expected on long-term shoreline evolution.

A new analytical solution for a time dependent diffusion is here presented, and is derived for the case of pinned coast with the initial shoreline position modelled as an arbitrary function $f(x)$. First, the boundary conditions representing the pinned coast are discussed. Next, the general analytical solution describing the evolution of shoreline position on the pinned coast is introduced; then a discussion on the modelling of $\varepsilon(t)$ function is presented.

It is observed that the general solution returns a shoreline evolution tending to a "stationary state", since the diffusion coefficient $\varepsilon(t)$ tends to a constant value ε_0 over a long period. This behaviour suggested by the analytical solution is not purely theoretical, but it has been observed for the mid-term evolution of Molise coasts. Since the Molise coast is affected by a bimodal wave climate, wave height and, particularly, wave direction are observed to vary over time with a certain frequency. Consequently, Molisian beaches could be characterized by a time varying diffusion $\varepsilon(t)$, which is expected to affect the shoreline evolution in a different way compared to a constant diffusion beach.

Main result of present Chapter is that even if the beach is expected to ''spread heat'' as a function of time, this time varying diffusivity extra effect on shoreline evolution is negligible, and shoreline evolution is lead by a constant diffusion over a long period.

6.1.1. Boundary conditions and initial condition

The definition sketch for the problem analysed in this chapter is schematically presented in Figure 73, in which $f(x)$ is the function to describe the initial shoreline position. The case presented is a coast with a length of L, bounded by two pinned points, for which shoreline position $y(x,t)$ do not move over time. This implies no interruption on the long-shore sediment transport, and the along-shore littoral gradient constant over time.

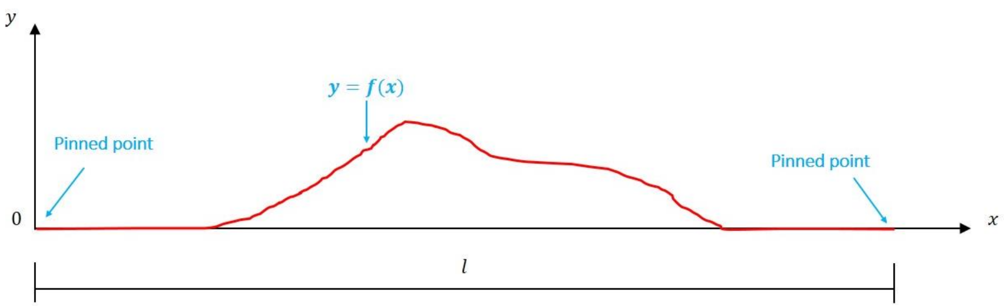

Figure 73 - Schematic diagram of an initially arbitrary shape of shoreline $f(x)$ on a pinned coast.

Mathematically, the pinned boundary conditions for the problem here analysed give rise to a Dirichlet problem, which scope is finding a function that satisfies a certain partial differential equation (PDE), that for us is the diffusion equation, within a region on whose boundary the function assumes certain boundary values.

The mathematical problem of the Dirichlet BVP has been coped in Chapter 5, and the analytical solution is in the form of Eq. 5.35. However, with a time dependent diffusivity, by applying the separation of variable technique, we can solve the problem for $T(t)$ to obtain:

$$T(t) = A\, e^{-\lambda^2 \int \varepsilon(t)dt} = A_0 e^{-\lambda^2 f_\varepsilon} \tag{6.1}$$

Where f_ε is a primitive of $\varepsilon(t)$, such that $\frac{\partial f}{\partial t} = \varepsilon$, and $\varepsilon(t)$ is a known function, which expression will be discussed later.

Therefore, following the same mathematical passages of Chapter 4, we obtain the general solution of the time dependent diffusivity:

$$y(x,t) = \sum_{n=1}^{\infty} A_{0n}\, e^{-\left(\frac{n\pi}{l}\right)^2 f_\varepsilon} \operatorname{sen}\left(\frac{n\pi}{l}x\right) \tag{6.2}$$

Where $A_{0n} = \frac{2}{l}\int_0^l f(x) \operatorname{sen}\left(\frac{n\pi}{l}x\right) dx$.

Now, as the $\varepsilon(t)$ function is concerned, if $\varepsilon(t) = \varepsilon_0 = cost$, the time dependent function $T(t)$ of Eq. (6.1), becomes:

$$T(t) = A_0 e^{-\lambda \varepsilon_0 t} \tag{6.3}$$

And the solution is that of the Dirichlet problem in homogeneous medium (constant diffusivity). On the other hand, if we imagine that $\varepsilon(t) = \varepsilon_0 + f(t)$, such that the $f(t)$ is a bounded above and below function, therefore the primitive of $\varepsilon(t)$ is:

$$f_\varepsilon = \varepsilon_0 t + F_f(t) \tag{6.4}$$

In this case, for a very long period the primitive function f_ε tends to $\varepsilon_0 t$, in other words the diffusivity becomes again a constant, and so that the diffusion process.

6.1.2. Modelling the time dependent diffusion coefficient $\boldsymbol{\varepsilon(t)}$

Now, let's discuss about the $\varepsilon(t)$ function, which is known for us. The sign and magnitude of $\varepsilon(t)$ are determined by the combination between the wave angle, wave height and shore characteristics. Broadly, $\varepsilon(t)$ is a time-dependent coefficient, since the wave angle $\alpha(t)$ and wave height $H(t)$ vary over time for a deep-water wave climate. Considering the "classical approach" of modelling the diffusivity coefficient ε, given by Walton and Dean (2010), the shoreline diffusion can be written as, in terms of deep water waves:

$$\varepsilon = \frac{1}{D_c + B} \frac{K \cdot (H_0)^{2.4} \cdot (T_p)^{0.2} \cdot g^{0.6}}{8 \cdot (s-1) \cdot (1-n) \cdot \pi^{0.2} \cdot \gamma^{0.4} \cdot 2^{1.4}} \cdot \cos\big(2(\beta - \alpha_0)\big) \tag{6.5}$$

In which it is seen that diffusivity intensely depends on wave height H_0 and wave direction α_0, which in general can vary over a long period with a certain frequency. Therefore, wave height and wave direction can be seen as harmonic functions of time, $H_0(t)$ and $\alpha_0(t)$ in the form:

$$\alpha_0(t) = B\cos(\sigma_{\alpha_0} t) \tag{6.6}$$

$$H_0(t) = A\cos(\sigma_{H_0} t) \tag{6.7}$$

Where σ_{α_0} and σ_{H_0} are the two frequencies of variation of wave height and direction respectively, while B and A are the amplitude of the harmonic functions.

Accordingly, diffusion can be modelled as the product of two cosine functions, accounting for two different frequencies, σ_{H_0} and σ_{α_0} .Taking this into account, we obtain a $\varepsilon(t)$ function in the form:

$$\varepsilon(t) = \varepsilon_0 + A_0\cos^m(\sigma_{H_0} t)\cos(\sigma_{\alpha_0} t) \tag{6.8}$$

Particularly, the cosine function simulating the wave height time variation is raised to a coefficient m, which ranges between 2-3 according to the H_0 power of the CERC formula and of Van rijn's (2014) formula. Considering an m-coefficient of 3, the primitive function is:

$$f_\varepsilon = \varepsilon_0 t + \frac{A_0}{\sigma}\frac{1}{8}\left(\frac{3\sin\left(t(\sigma_{H_0}-\sigma_{\alpha_0})\right)}{\sigma_{H_0}-\sigma_{\alpha_0}} + \frac{\sin\left(t(3\sigma_{H_0}-\sigma_{\alpha_0})\right)}{3\sigma_{H_0}-\sigma_{\alpha_0}} + \frac{3\sin\left(t(\sigma_{H_0}+\sigma_{\alpha_0})\right)}{\sigma_{H_0}+\sigma_{\alpha_0}} + \frac{\sin\left(t(3\sigma_{H_0}+\sigma_{\alpha_0})\right)}{3\sigma_{H_0}+\sigma_{\alpha_0}}\right) \tag{6.9}$$

Therefore, the time dependent dampening function $T(t)$ becomes:

$$T(t) = A_0 e^{\left[-\lambda\left(\varepsilon_0 + \frac{A_0}{\sigma t}\frac{1}{8}\left(\frac{3\sin\left(t(\sigma_{H_0}-\sigma_{\alpha_0})\right)}{\sigma_{H_0}-\sigma_{\alpha_0}} + \frac{\sin\left(t(3\sigma_{H_0}-\sigma_{\alpha_0})\right)}{3\sigma_{H_0}-\sigma_{\alpha_0}} + \frac{3\sin\left(t(\sigma_{H_0}+\sigma_{\alpha_0})\right)}{\sigma_{H_0}+\sigma_{\alpha_0}} + \frac{\sin\left(t(3\sigma_{H_0}+\sigma_{\alpha_0})\right)}{3\sigma_{H_0}+\sigma_{\alpha_0}}\right)\right)t\right]} \tag{6.10}$$

It is seen that, as t increases, the term $\frac{A_0}{\sigma t}$ becomes even smaller and the diffusivity tends to a constant value ε_0; in other words, this is to say that the shoreline evolution in the long run is led by a constant diffusion, while the time varying diffusivity extra-effect tends to cancel over time.

As far as the two frequencies are concerned, different situations may be considered within a deep water climate. It is possible to observe the wave height to vary quickly (hours or days), due to the effect of intense storms within a wave climate, but with waves coming from always the same direction. In this case $\sigma_{H_0} \gg \sigma_{\alpha_0}$, and the solution is in the form:

$$y(x,t) = \sum_{n=1}^{\infty} A_{0n}\, e^{-\left(\frac{n\pi}{l}\right)^2\left(\varepsilon_0 + \frac{A_0 1}{\sigma t 8}\left(\frac{6\sin(\sigma_{H_0} t)}{\sigma_{H_0}} + \frac{2\sin(3\sigma_{H_0} t)}{3\sigma_{H_0}}\right)\right)} \operatorname{sen}\left(\frac{n\pi}{l}x\right) \quad \text{for } \sigma_{H_0} \gg \sigma_{\alpha_0} \tag{6.11}$$

In addition, it is possible that the two frequencies have the same order of magnitude, $\sigma_{H_0} \cong \sigma_{\alpha_0}$, so that both the wave height and direction can change on the same time scale, or, even on contrary, wave height does not appreciably vary within the wave climate, $\sigma_{H_0} \cong 0$, while wave direction is observed to change with a certain frequency. These can be interpreted as the cases of bimodal wave climate, where the wave climate characteristics are seen to vary seasonally or monthly. The solutions are:

$$y(x,t) = \sum_{n=1}^{\infty} A_{0n}\, e^{-\left(\frac{n\pi}{l}\right)^2\left(\varepsilon_0 + \frac{A_0 1}{\sigma t 8}\left(\frac{3\sin\left(t(\sigma_{H_0}-\sigma_{\alpha_0})\right)}{\sigma_{H_0}-\sigma_{\alpha_0}} + \frac{\sin\left(t(3\sigma_{H_0}-\sigma_{\alpha_0})\right)}{3\sigma_{H_0}-\sigma_{\alpha_0}} + \frac{3\sin\left(t(\sigma_{H_0}+\sigma_{\alpha_0})\right)}{\sigma_{H_0}+\sigma_{\alpha_0}} + \frac{\sin\left(t(3\sigma_{H_0}+\sigma_{\alpha_0})\right)}{3\sigma_{H_0}+\sigma_{\alpha_0}}\right)\right)t} \cdot \operatorname{sen}\left(\frac{n\pi}{l}x\right) \quad \text{for } \sigma_{H_0} \cong \sigma_{\alpha_0} \tag{6.12}$$

$$y(x,t) = \sum_{n=1}^{\infty} A_{0n}\, e^{-\left(\frac{n\pi}{l}\right)^2\left(\varepsilon_0 + \frac{A_0 1}{\sigma t 8}\left(\frac{8\sin(\sigma_{\alpha_0} t)}{\sigma_{\alpha_0}}\right)\right)t} \cdot \operatorname{sen}\left(\frac{n\pi}{l}x\right) \quad \text{for } \sigma_{H_0} \cong 0 \tag{6.13}$$

For the case of "inhomogeneous medium", the dependence of the diffusivity to the time can be seen as a bounded above and below function, for which as time increases the diffusion process occurs constantly over time. In order to demonstrate it, the case of Molise coast is paradigmatic due to its exposition to the bimodal climate of the Adriatic Sea. The inherent bimodality of wave climate makes wave height and, particularly, wave direction to vary over time with a certain frequency.

Consequently, Molisian beaches could be characterized by a time varying diffusion $\varepsilon(t)$, which is expected to affect the shoreline evolution in a different way compared to a constant diffusion beach.

Actually, results showed that even if the beach is expected to ‘’spread heat’’ as a function of time, this time varying diffusivity extra effect on shoreline evolution is negligible, and shoreline evolution is led by a constant diffusion over a long period.

6.2. The Molise coast case of study

In the frame of a collaboration between the University of Molise and the University of Napoli “Federico II”, a shoreline change study was carried out, in order to analyse the most recent trends of Molise coast evolution, and investigate the possible relationships between wave directions and shoreline response. The reference time window is the period 2004–2016, which updates previous literature studies (Rosskopf et al, 2018); according to the definition originally introduced by Crowell et al. (1993), the analysis can be conventionally referred to as a “Mid-term study”.

In the first part of this section, a qualitative study is presented, where attention is drawn to selected “hot spot” areas of the Molise coast: for each of them, the possibility of generating forcings are discussed. Then, a hypothesis is formulated about the existence of a dominant wave attack for littoral transport, the “Equivalent Wave” (EW), and its degree of correlation with the coastline evolution is examined, in order to assess if EW could be capable of explaining the main trends of the coastal evolution process. Numerical simulations conducted with the one-line model GENESIS have shown that the use of the “equivalent wave” as a stationary forcing, may lead to a reasonable prediction of shoreline response.

It is worth noticing that the EW approach, widely (and trustily) used in the field of practical coastal engineering, is based on the hypothesis that a dominant wave attack for littoral transport exists, strongly correlated with the coastline evolution. In fact, within a long (mid)-term analysis of shoreline change, effects due to cyclical phenomena are assumed to cancel over years, while the long-term shoreline trend is led by the spatial variations in the long-shore sediment transport rate. According to practical coastal engineering, the latter is essentially due to the dominant direction of wave climate, commonly well represented by a single wave component, equivalent to the whole climate in terms of littoral transport (see Chapter 2, LDR).

In this regard, the second part of present chapter is presented. Here, on contrary, the degree of correlation between the equivalent wave parameters and long-term trend of shorelines is quantitatively assessed, accounting for a time-dependent diffusion process, which is expected within a bimodal climate. Particularly, this second quantitative analysis is based on the assumption that the shoreline diffusivity is correlated to the Littoral Drift Rose concept.

In fact, among several techniques developed to evaluate the long-shore sediment transport rate, the Littoral Drift Rose (LDR) concept (Walton and Dean, 1973; Walton and Dean, 2010) represents a potentially useful tool in order to examine shoreline evolution. Particularly, major finding concerning the LDR concept is that the net littoral drift due to a deep water climate, coming from different directions (Total-LDR), can be reduced into a form (Equivalent-LDR) that is representative of a single Equivalent Wave component (EW) propagating from a single direction. It is worth highlighting that, a suitable approximation of the Equivalent-LDR to the total one is reached when Total-LDR exhibits nearly symmetrical lobes. This occurs whenever the wave climate is coming from a restricted angle. On contrary, when in wider wave sector, with two or more directional modes, a poorer fit is obtained, due to the asymmetrical shape of the Total-LDR. Since a direct relationship between the concepts of Equivalent Wave and "shoreline diffusivity" exists, the poor approximation of the Total-LDR to the Equivalent one is found to be interpreted by the time-dependent shoreline diffusion process, which deals with the peculiar case a stretch of coast affected by of a bimodal wave climate.

In fact, while for restricted wave sectors the shore diffusivity can be considered constant over time (no appreciable variations in $H(t)$ and $\alpha(t)$, $\sigma_{H_0} \cong 0, \sigma_{\alpha_0} \cong 0)$, in bimodal wave climate the deviation detected between total and equivalent LDR would suggest a time varying diffusivity extra-effect on shoreline evolution mainly related to the inversion in wave direction ($\sigma_{H_0} \cong 0, \sigma_{\alpha_0} \neq 0$).

The results presented in this quantitative analysis apply to the Trigno river mouth ''hot spot'' area (5.2 Km), located in the northern part of the Molise coast region. After reconstructing the Molise LDR graph, a numerical study has been carried out using the one-contour line model GENESIS, in order to: (1) assess the explanatory power of the LDR equivalent wave and its significance within a bimodal climate; (2) check the role of a time-varying diffusivity upon the shoreline response. First feature has been examined inputting within the GENESIS model an "annual scanned" time series built from the EW of Molise coast, while the second has been achieved implementing two different time-resoluted wave climate: the ''Monthly LDR-equivalent wave climate'' and the ''Frequency-equivalent wave climate''.

6.2.1. Molise coast study area and Early Literature

The Molise coast extends for 36 km and is prevalently exposed to waves coming from the northern quadrants. The rocky cliff of Termoli promontory splits the coastline into two reaches. One stretches from the harbour of Marina Sveva to the promontory of Termoli; the second reach extends between the Termoli harbour and the Saccione stream mouth and includes the harbour of Marina di Santa Cristina (Figure 74).

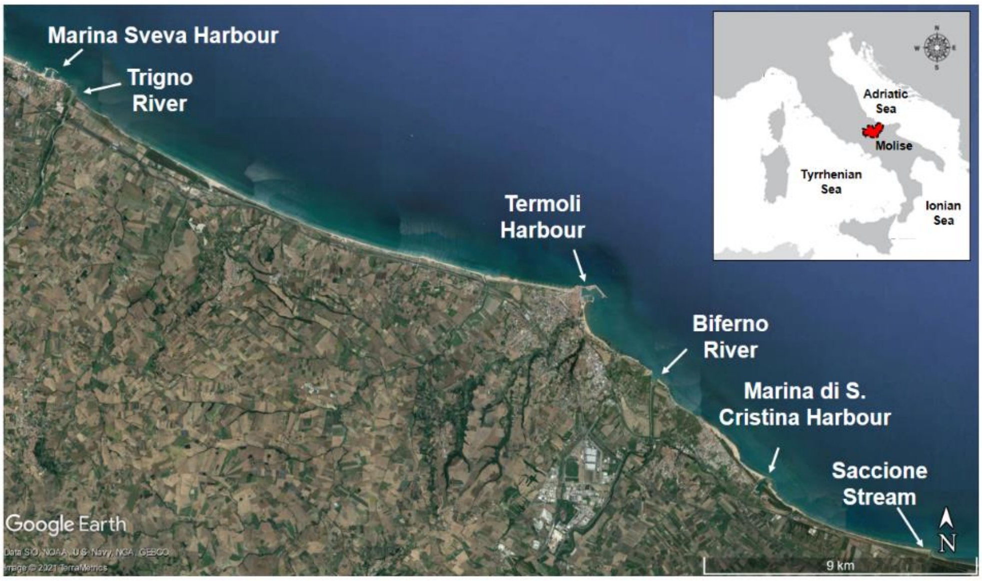

Figure 74 - Detail of Molise coast

Molise beaches are composed of medium sand (average diameter 0.26 mm) and are characterized by a very gentle foreshore (slope less than 1% between 0 and 10 m below the Mean Water Level, MWL). The average berm height is 2.0 m above the MWL (Rosskopf et al, 2018; Aucelli et al., 2009). Starting from the mid-20th century, a significant erosion has been taking place, which has been recognized to be caused to a large extent by the restrictions imposed to the river flows and the consequent decrease in sediment delivery to the coast (Rosskopf et al, 2018; Aucelli et al., 2009; Aucelli et al., 2018).

In particular, the S. Salvo check-dam, built across the Trigno River during the period 1954–1977, and the Ponteliscione dam, built across the Biferno River between 1965 and 1977, have strongly contributed to channel incision and narrowing (De Vincenzo et al., 2017) and deprived the coastal sedimentary budget of significant volumes; De Vincenzo et al. (2017, 2019) estimated that from 1965 to 2007, nearly $4.4 \times 10^6\, m^3$ of sediments have accumulated within the Ponteliscione dam reservoir.

The response to progressive shoreline erosion was of a fully "structural" nature and nowadays nearly 62% of the coast is covered by hard protection measures; structures include mainly segmented systems of detached breakwaters, either submerged or emerged, and groins.

The evolution of the Molise coast has been intensively investigated in recent decades. Among the most relevant research, Aucelli et al. (2007) analysed the 1954–2000 shoreline changes of a 10 km long reach astride the Termoli promontory. The authors performed an accurate analysis of both wind and wave climates and concluded the main wave forcings to come from either the NW or NE. The maximum erosion risk was localized in the "densely structured" area neighbouring the Biferno River mouth. Finally, based on the shoreline orientation of the examined coastal segment, a net NW to SE littoral drift was postulated. Recently, Rosskopf et al. (2018) extended the analysis to the whole Molise coastline and widened the reference time interval to 1954–2014. The coast was partitioned into nine physiographically homogeneous sub-reaches, the length of which ranged between 2 and 7 km; then, the average rate of shoreline change was calculated for the different time windows. The authors warned that in spite of the substantial stability observed during the period 2004–2014, a new erosion process might be arising either at the northern or the southern part of the coast.

Although a prevailing NW to SE littoral drift was inferred, a number of possible inversion areas were indicated, such as at the Trigno river mouth or right at the south of the Termoli harbour. Finally, a more in-depth knowledge of wave forcing was auspicated for future research work.

6.2.2. Wave Climate analysis

Data acquired by a directional wave buoy located in the offshore waters fronting the town of Ortona, 56 km north the mouth of Trigno River, have been used to infer the wave climate at Molise coast (Figure 75). The device is anchored at a depth of 70m below the low tide level, at a latitude of 42°24’54.0’’ N and a longitude of 14°30’20.99’’ E.

Significant wave height, H_s, peak period, T_p, and azimuth of the mean wave direction, α, have been recorded in the period 1989-2012, at an average interval of 3hrs. Wave heights and periods have been adjusted to the sea offshore the Molise coast ("virtual buoy" in Fig. 68), according to the relationships originally introduced by Hasselmann (1973) in the frame of the JONSWAP project. Assuming the same wind to blow at both the "real" and "virtual" buoy location, it is readily obtained that (Contini and De Girolamo, 1998):

$$\frac{H_{s,VIRT}}{H_{s,REAL}} = \left(\frac{F_{VIRT}}{F_{REAL}}\right)^{\frac{1}{2}}; \qquad \frac{T_{p,VIRT}}{T_{p,REAL}} = \left(\frac{F_{VIRT}}{F_{REAL}}\right)^{\frac{1}{3}} \tag{6.14}$$

where F indicates the "effective fetch" (Saville, 1952). Note that, consistently with Hasselmann (1973), the mean direction of waves has been assumed to coincide with that of wind.

Figure 75 - Ortona wave buoy and "virtual" wave buoy at the Molise coast.

The histogram of wave direction for angular sectors of 22.5° is displayed in Figure 76, where the offshore directed waves have been removed for sake of clearness. The graph exhibits two well defined modes; one is around 350°N and coincides with the NNW dominant direction indicated by Aucelli et al. 2007; the other is close to 80°N, whereas the authors indicated 23°N.

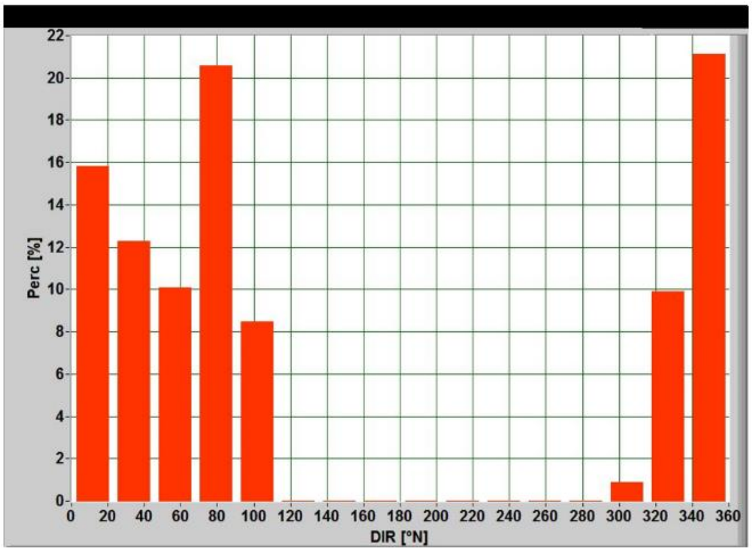

Figure 76 - Histogram of wave directions. Onshore directed angles have been removed.

The reason of this apparent inconsistency is because waves from ENE-E have a lower height; hence they bring forth less energy. This is shown in Figure 77, where along with the mean wave height, also the 90th percentile of the directional wave height distribution is reported. The graph indicates that highest waves tend to come from 0-45°N, in accordance with Aucelli et al. 2007, with a maximum in the sector 0-22.5°N. The bimodality of wave climate is observed to occur almost seasonally and monthly (Figures 78 and 79), so indicating an inherent bimodal climate that affect the Molise coast, where frequent inversion of littoral transport direction can be expected. This second aspect is further supported by the graph shown in Figure 80, where it is noted that a predominance of waves coming from 340°N is observed during warmer months, while waves originating from 80°N prevail during winter months.

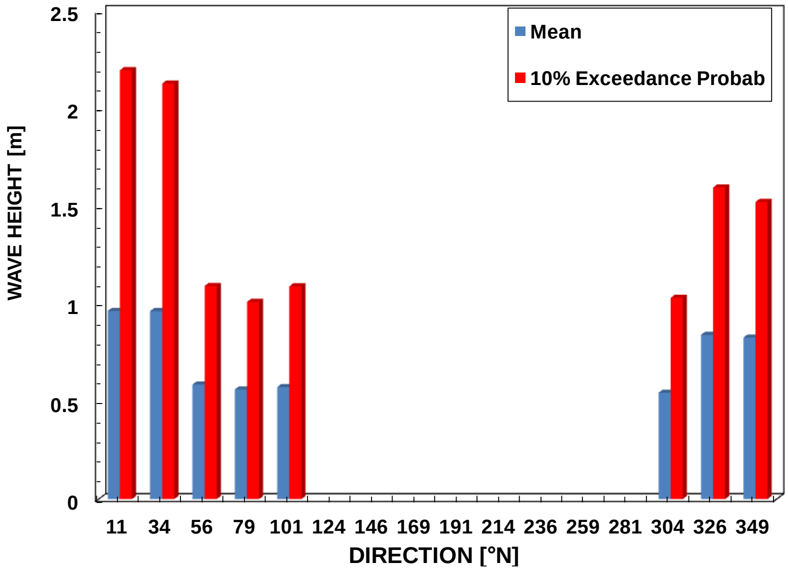

Figure 77 - Directional distribution of mean and 90th percentile wave height.

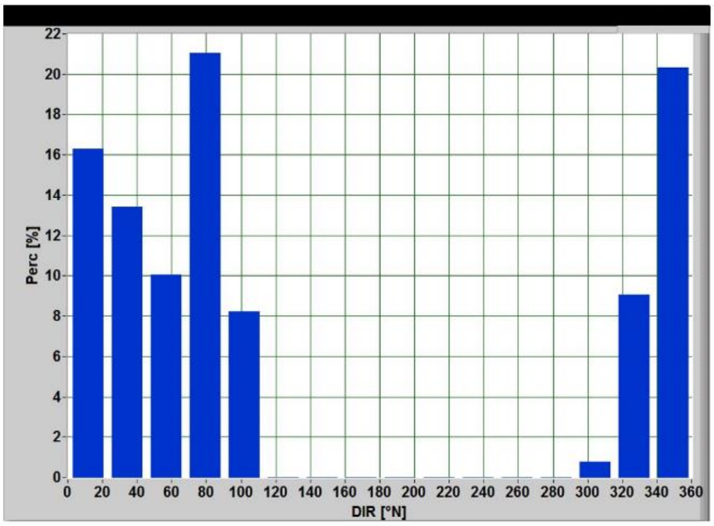

Figure 78 - April to October Histogram of wave directions for angular sector of 22.5° for the Molise coast.

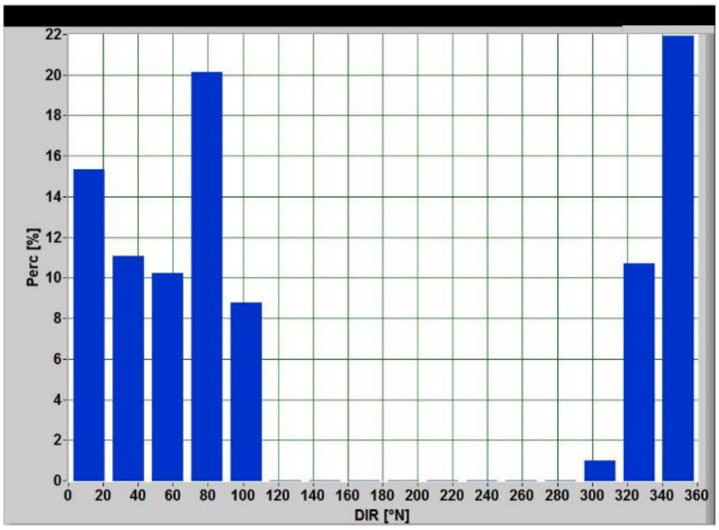

Figure 79 - October to April Histogram of wave directions for angular sector of 22.5° for the Molise coast. Onshore directed angles have been removed.

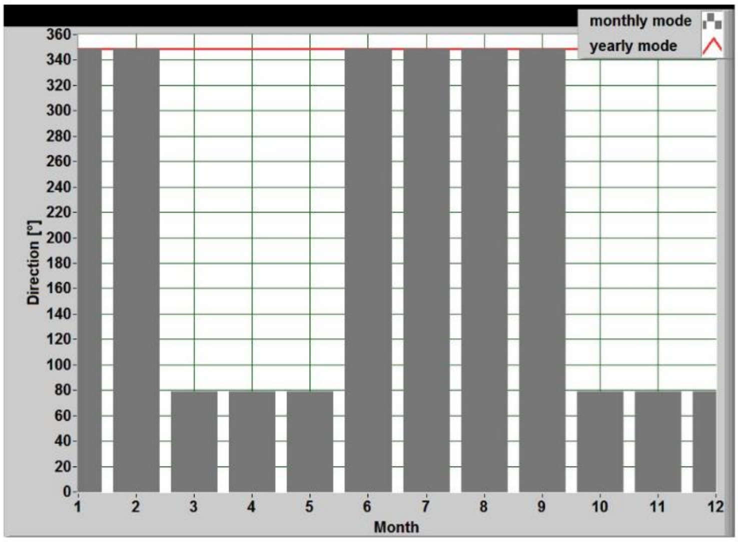

Figure 80 - Monthly variation of the Molise wave climate directional mode.

From Figure 80 it is seen that the waves in January and February, which may be included in the winter season, are dominant from 350°N. This anomaly in the winter dominant direction could be explained by reasoning on the prevailing wave energy field and wind conditions. As reported by Buccino et al. 2020, although two modes (80°N and 350°N) predominates within Molise climate, waves from ENE-E have a lower height; consequently, also their wave energy is lower. By contrast, higher energy values are found for a wave sector ranging between 316°N and 45°N. Since, in general, a greater amount of energy is associated to storm weather conditions (Nov-Feb), it is reasonable to expect the dominant direction to reverse and turn towards the greater energy.

The significant wave height exceeded by 12 hrs a year (H_E), has been estimated for each angular sector after fitting a 2 parameters Weibull distribution to the wave data. An average value of 4.08m has been obtained keeping only the onshore directed angles; this value has been used for depth of closure calculation (Dc ≈2 HE) according to Hallermeier (1983).

The joint Hs-Tp distribution (e.g. Figure 81) revealed small wave height (less than 1 m) to have a modal peak period included between 3 and 6 s, whereas for waves between 1.5 and 4.5 m, the modal Tp progressively moves to the interval 6-9 s. Finally, the period of largest waves (larger than 4.5 m) is invariably included between 9-12 s. The overall mean peak period (direction independent) equals 5.08 s.

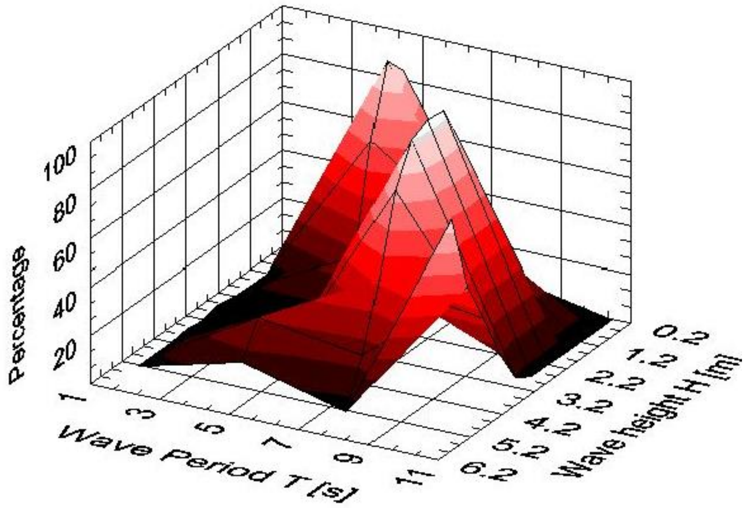

Figure 81 - Joint distribution (H_s- T_p) for the angular sector 0-22.5°N.

6.2.3. Analysis of shoreline changes

A shoreline change analysis has been carried out by comparing the Molise coastline positions in 2004, 2011, 2014 and 2016. According to Crowell et al. (1993), this study can be considered as a medium-term investigation.

6.2.3.1. Approach

As shown in Table 3, data come from the digitalization, in ArcGis environment, of photograph reliefs from different sources.

Table 3 - Summary of shoreline data.

DATE	SOURCE	REFERENCE	SCALE	RMS Error (m)
2004	Ortophoto map	Rosskopf et al. [1]	1:2500	2
2011	Ortophoto map	Rosskopf et al. [1]	1:2500	2
2014	Google Earth	Rosskopf et al. [1]	1:500	1
2016	Google Earth	New data	1:500	1

The shoreline location has been assumed to coincide with the instantaneous waterline; as discussed in Rosskopf et al. (2018), this “dry-wet” approach can be considered reasonable in virtue of the low tidal environment.

Table 3 also reports the uncertainties related to the digitalization procedure (last column, RMS), being other possible sources of inaccuracy, such as georeferencing, airphoto, etc., virtually absent; RMS values are consistent with those indicated by Crowell et al. 1993 and Hapke et al. (2010). Rough data have been linearly interpolated, and finally re-sampled at a 10 m interval.

The Linear Regression Rate (LRR) has been used as indicator of the rate of shoreline change; as widely known, it represents the slope of a least-square straight-line fitted through the shoreline positions at the various available times. However, unlike previous literature works, the following procedure was adopted here:

a. the LRR at a given along-shore horizontal axis, x, is calculated after gathering all data falling within a centred window of 40m width. The window, is then progressively moved forward;
b. the obtained slope, say sx, is tested for significance at a 95% probability level, according to the well-established linear regression theory;
c. whenever the test is not satisfied, LRR is finally set to zero.

Note the point c. implies: $LRR \neq 0\ only\ if: Prob\ [LRR = 0] \leq 0.05$

The use of a sliding window allows collecting a larger number of points, making the statistical test less unstable. Moreover, the procedure keeps holding its meaning (at least up to certain extent), even when comparing two shorelines only.

Finally, it is worth highlighting that the 95% probability level at the previous point b, has been chosen with the purpose of including also the uncertainties related to the interpolation/resampling procedure. From the LRR(x) function, accretion and erosion areas have been identified as those segments of coast where the shoreline change rate exceeds a certain limit value, say v_{LIM}, and remains above it for a minimum length, l_{LIM}. For the scopes of the regional analysis here presented, l_{LIM} has been subjectively set to 500 m, whereas the RMS values of Table 3 have been used to define v_{LIM}. The approach employed is similar to that suggested, among the others, by Hapke et al. (2010).

Let's assume the shoreline measures, y(t$_i$), to be uncorrelated, unbiased, Gaussian random variables of variance (RMSi)^2. Then: $VAR[y(t_2) - y(t_1)] = (RMS_2)^2 + (RMS_1)^2$

Hence, we have, at a 95% probability level:

$$v_{LIM} \cong \mp 1.96 \cdot \frac{\sqrt{(RMS_2)^2 + (RMS_1)^2}}{t_2 - t_1} \tag{6.15}$$

Values of v_{LIM} for the intervals 2004-2016, 2004-2011, 2011-2016 and 2014-2016 are reported in Table 4.

Table 4- Values of vLIM for different time windows.

PERIOD	v_{LIM} (m/year)
2004-2016	0.37
2004-2011	0.80
2011-2016	0.90
2014-2016	1.41

6.2.3.2. Results

Figure 82 shows the 2004-2016 LRR function, whereas Figure 83 displays the corresponding erosion/accretion areas. In both the graphs, the along-shore coordinate, x, is oriented NW to SE; horizontal dashes indicate detached breakwaters, whereas vertical dashes represent groin fields.

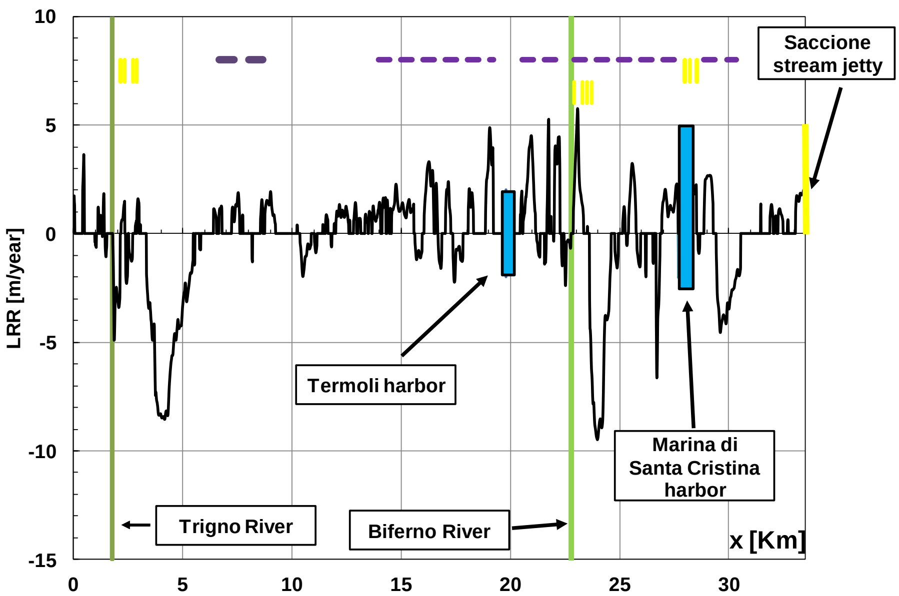

Figure 82 - 2004-2016 LRR function. Horizontal dashes indicate detached breakwaters; vertical dashes indicate groin fields.

From the inspection of Figure 83, it is easily observed that:

- The foremost erosion areas (E1 and E3) are located south of the Trigno and Biferno Rivers, with a maximum LRR of -8 m/y and -9 m/y respectively. In both cases the retreat has an area located just south of a groin field, which in the case of the Biferno River is further protected by detached breakwaters;

- The area neighbouring the Marina of Santa Cristina harbour has accreted northwards (A4, max LRR +2.2 m/y) , and eroded southwards (E4, max LRR -4 m/y); similarly to what observed above, the erosion zone is located south of a groin/breakwater system, which protects the coast for 1.5 km.
- The area located just north of the Saccione Stream jetty has accreted by nearly 700 m, at a maximum rate of 1.8 m/y.

All the previous outcomes support the idea of a net NW to SE littoral drift.

As indicated in literature (Rosskopf et al., 2018) the erosion process at the main rivers mouths (E1 and E3) has been triggered by a reduction in the sediment delivering caused by dam construction.

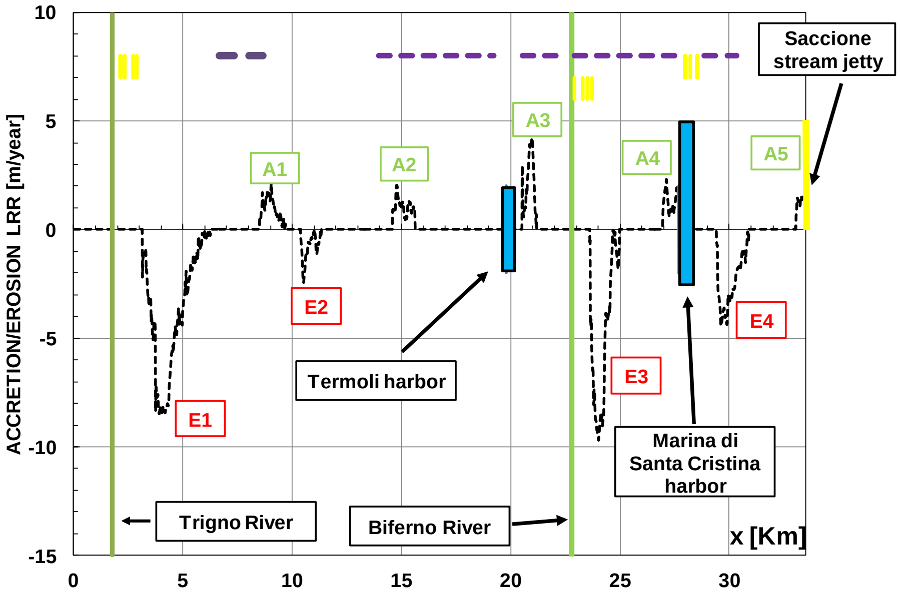

Figure 83 - 2004-2016 Erosion/Accretion areas LRR function. Horizontal dashes indicate detached breakwaters; vertical dashes indicate groin fields.

However, it is noteworthy that despite closing the whole waterfront, shore-parallel barriers at the Biferno River mouth did not stop the erosive trend, although mitigating it appreciably. Table 5 indicates in this area (segment S7 of Rosskopf et al. 2018) that the average erosion rate has reduced by 50% compared to the period 1986-1998; oppositely in the neighbourhood of the Trigno River mouth (S1, not defended by breakwaters) the rate of retreat has increased by 46%. A dominant NW-SE sediment transport would also explain the origin of the accretion zone A3 (+3 m/y). The latter is located within a "densely structured area", where a series of detached breakwaters extend for 2 km north-side the Biferno River mouth; moreover, a good deal of coast is supplementary defended by rock revetments.

Table 5 - average LRRs at the Trigno and Biferno River mouths.

Stretch	Av. LRR 1986-1998 (m/year)	Av. LRR 2004-2016 (m/year)
Trigno (S1)	-1.39	-2.04
Biferno (S7)	-2.31	-1.11

As shown in Figure 84 (lower panel), the accumulation has occurred simultaneously to the construction of a new basin of the Termoli harbour; the sediments, made available by dredging operations, have been likely conveyed southwards by littoral currents and finally trapped within the structure system. Figure 84 also displays the shoreline north the detached breakwaters that has remained substantially stable through the years, with a small accretion area right south of the harbour.

Figure 84 - View of the area A3. Yellow dotted straight-line represents sheltering by 10°N waves. (Section 5).

The dynamics for which the areas A2 (+2 m/y), A1 (+1.5 m/y) and E2 (-1.5 m/y) have originated by, is not readily explained. The accretion areas are located behind long systems of detached breakwaters, which distance each other about 5.5 km; however, while A2 is situated at the northern edge of the barriers, A1 is formed at the southern one. Finally, the erosion zone E2 is located nearly 1.5 km southwards the structures end.

To have a deeper insight on these areas, the dominant direction of waves (if any) has to be considered, as well as the variability of shoreline orientation. The effects of both these variables are analysed in the next sections.

6.3. The equivalent wave concept and its applications: qualitative analysis for the Molise coast

According to Rosskopf et al. 2018, a primary need for the comprehension of Molise coast evolution is establishing more stringent relationships between wave climate and shoreline response; at this first stage of research, this task is accomplished via the so-called "Equivalent Wave" (EW) concept, i.e. assuming that shoreline changes may be significantly correlated to a single component of the wave climate.

Although well accepted in applied coastal engineering, it is noteworthy that scientists do not agree on the EW existence. Silvester (1984) reasoned that "it is normal to correlate volumes of accretion taken over a year with some average swell condition for the same period", but concluded that "the selection of some meaningful average, including direction, is in the realms of fantasy". On the other hand, Walton and Dean (1973), in examining the directional distribution of littoral drift at many coastal areas observed "it was surprisingly similar to that which would occur for a single wave component".

In the qualitative analysis presented in the following, the EW direction is inferred empirically from the observation of the shoreline trend, and its height and period are estimated via simple averaging operations. Then, several applications are discussed, which confirms the presence of a single wave component dominating the whole shoreline evolution.

6.3.1. EW direction and parameters

According to Pelnard-Considére (1956), shoreline orientation at any "un-bypassed" groin is expected to be in every instant nearly normal to the dominant wave attack; hence, it may be taken as an indicator of the EW direction.

For the case under study, of particular interest are the accretion areas A4 and A5 of Figure 83. However, only little information can be drawn from the first, since the beach is protected by detached breakwaters that diffract the incoming waves.

Conversely, A5 can freely adjust to the sea and, consequently, may represent a more reliable indicator. Panels b), c) and d) of Figure 84 show that this segment of coast has kept a nearly constant orientation in time, which is close to 10°N. Hence, under the hypothesis of straight-parallel bottom contours, the latter can be assumed as the offshore EW direction.

It is noted that 10°N is somehow halfway between the prevailing wave directions indicated by Aucelli et al. 2007, i.e. 350°N and 23°N, and corresponds to the angular sector associated with the highest waves (Figure 76). This is consistent with the hypothesis formulated by Silvester (1984) that shoreline may be sculptured by waves correlated to the most intense storms.

Once the EW direction has been established, its height, H_{m0E}, has been estimated as the average wave height in the directional sector 0-22.5°N (H_{m0E} = 0.96m, Figure 77); on the other hand the peak period, T_{pE}, has been simply equalled to the mean measured value, 5.08s. It is worth noticing that in the applications presented below, the EW characteristics will be assumed constant throughout the coastal area.

6.3.2. Shoreline response to structure systems

The EW concept has been tentatively used to analyse the shoreline response behind some structure systems. As anticipated, the approach here followed is mainly of qualitative nature and relies on rather crude assumptions; accordingly, the obtained results have to be considered as preliminary.

As a first point, it could be argued that under a 10°N wave attack, the head of the Termoli harbour breakwater completely shelters the shoreline south of it (upper-right panel of Figure 85), and this would explain the aforementioned stability of that reach of coast; then, the resulting diffraction currents, directed northwards, might be responsible of the accretion observed just below the harbour basin. The effect of diffraction is clearly recognizable from the curvature of the shoreline and is consistent with the inversion in the littoral drift direction observed by Rosskopf et al. (2018).

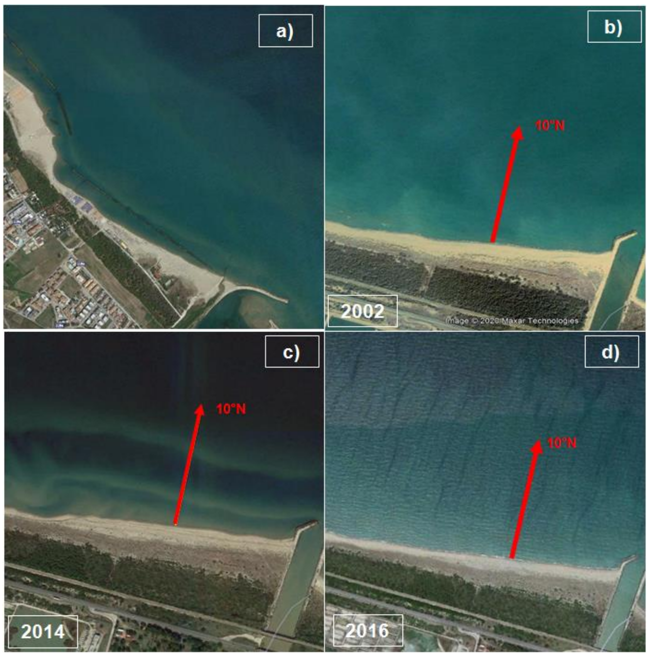

Figure 85 - Panel a) shoreline neighbouring the area A4; panels b) to d), shoreline orientation at the Saccione Stream jetty.

Simplified models implemented in GENESIS have been employed for the arrays of detached breakwaters neighbouring the accretion area A2 and the erosion area E4 in Figure 83. Hereafter, these structure systems will be referred to as SA2 and SE4 respectively. SA2 is located nearly 20 km north of the Saccione Stream jetty and extends for 2.1 km with an average azimuth of 13°N; the latter, is in fact very close to the EW direction. As shown in Figure 86, the shape of coast behind the system has remained relatively constant through the years.

The breakwaters have variable length and are either emerged or submerged or "partially underwater", that is alternating submerged and emerged parts; the typical gap width is 30 m. Additionally, two groins are located behind the barriers, the length of which equals 50 m and 100 m respectively.

The GENESIS model, pictured in Figure 87a, is made up on a 30 m wide grid, with the initial shoreline parallel to the barrier system; the distance between the structures and the initial shoreline (180-230 m) has been estimated north of the breakwaters, from the first null-point of the LRR(x) function. "Pin points" have been used as lateral conditions at the model boundaries, which are located 2 km far from the breakwater ends. The transmission coefficients K_t, i.e. the ratio between the wave height right behind the barrier and that just in front of it have been preliminarily set at 0.4 for emerged barriers and 0.7 for submerged and partially underwater structures. The Equivalent Wave has been run for 50 years, to let the beach plane form attain a stable shape.

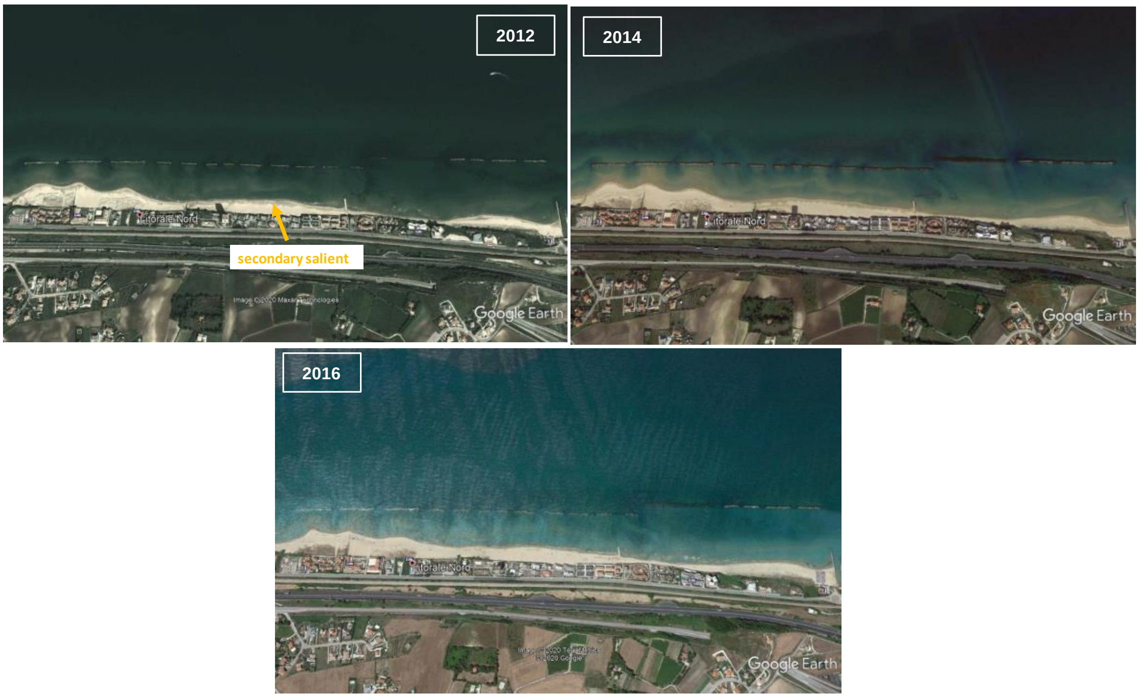

Figure 86 - Shoreline plane -form at S_{A2}

In general, simulation results correlate quite well to the observed shoreline trend (Figure 87b); the triple humped salient is reasonably reproduced, although slightly tapered, and so is the coast between the groins.

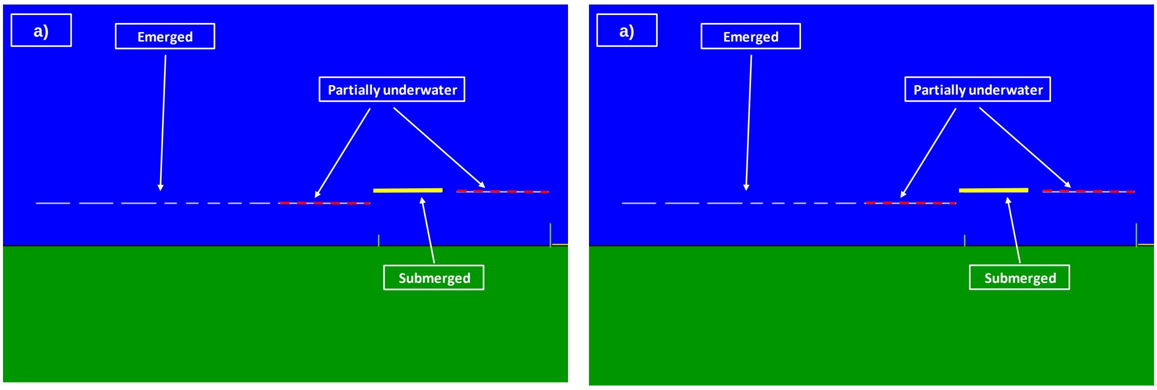

Figure 87 - a) S_{A2} as modelled in GENESIS. b) Shoreline response under EW (K_1 =0.1, K_2 = 0.15).

The shoreline trend behind the first group of barriers is instead some flattened; this is either due to the simplified initial shoreline condition or because GENESIS cannot simulate in detail the multiple diffraction emanating from the short breakwater segments. Moreover, since the partially underwater barrier at the right-end side of the first breakwater group is simulated as a continuous structure, the secondary salient (Figures 87a,b) is moved nearly 0.4 km southwards compared to the observed position.

Interestingly, the simulated average rate of shoreline change around A2 is reasonably like the measured one (Figure 88).

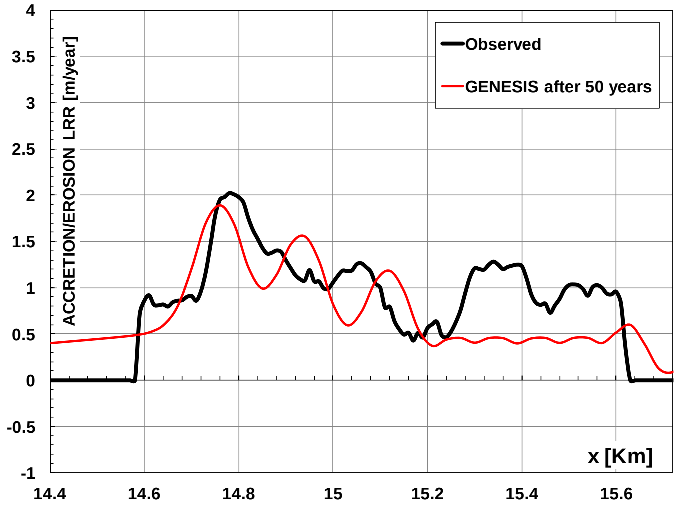

Figure 88 - Observed vs numerical shoreline change rate at A2.

To check the sensitivity of solution to wave direction, the EW angle has been shifted by 10° either to the North or to the South. As shown in Figure 89, waves from 0°N lead to a significant skewness of the main salient, whereas waves from 20°N do not capture the shoreline trend. Obviously, this result is not to be understood as those waves were ineffective to the shoreline evolution, but their "explanatory power" appears less notable compared to 10°N.

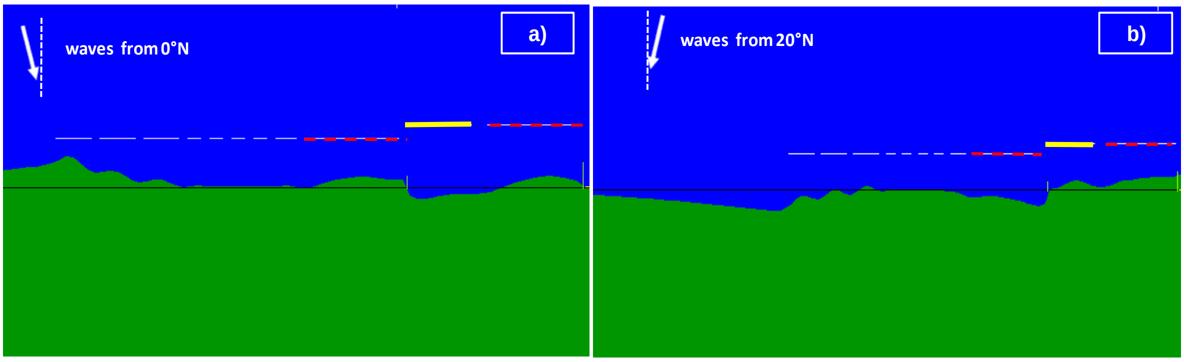

Figure 89 - Shoreline response of SA2 to waves from 0°N (a) and 20°N (b). K1 =0.1, K2 = 0.15

As already mentioned, SE4 follows a field of groins located just south of the Marina of Santa Cristina harbour. The system, 3 km north the Saccione Stream jetty, is made up of two parts. The first includes 9 short barrier segments (6 emerged and 3 submerged), whereas the second, 450 m southwards, encompasses four submerged breakwaters (Figure 90). The structures are oriented at 25°N and extend for 1.5 km.

The GENESIS model used to study this area has the same characteristics as those described for SA2; however, a 15 m wide grid has been used to better represent either the breakwater segments (30-75 m length) or the gaps (45 m wide). As far as the lateral boundary conditions are concerned, a “gate” has been imposed northwards to simulate the groin system; on the other hand a “pin” point has been set nearly 0.7 km south the breakwaters, at the centre of a large area where LRR(x) is uniformly zero.

Figure 90 - Shoreline plane -form at S_{E4}.

Also in this case, EW seems to lead to a shoreline trend reasonably consistent with the observations; as shown in Figure 90, a wide salient is produced behind the first group of structures, followed by a nearly 1 km long deficit area corresponding to E4. Furthermore, the latter is again realistically simulated in GENESIS (Figure 91a,b).

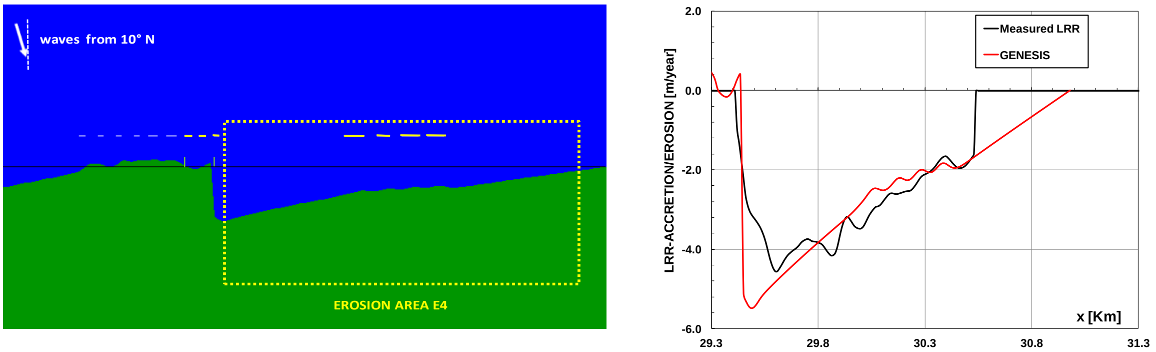

Figure 91 – (a) GENESIS model outputs at S_{E4} (K1 =K2 =0.1). (b) Measured vs. simulated shoreline change rate at E4.

Figure 92 suggests that a more southern wave attack does not reproduce the shoreline trend properly. However, it stresses that the areas located between the structure groups (breakwater segments or groins) tend to undergo erosion irrespectively of wave direction. For example, the area F1 may erode as “downdrift” effect of either of the breakwater series, depending on whether waves come from the North or the South. The same is valid for the area F2, which is located downdrift the groin system under wave attacks coming from the North and downdrift the first group of breakwaters when the wave climate reverses.

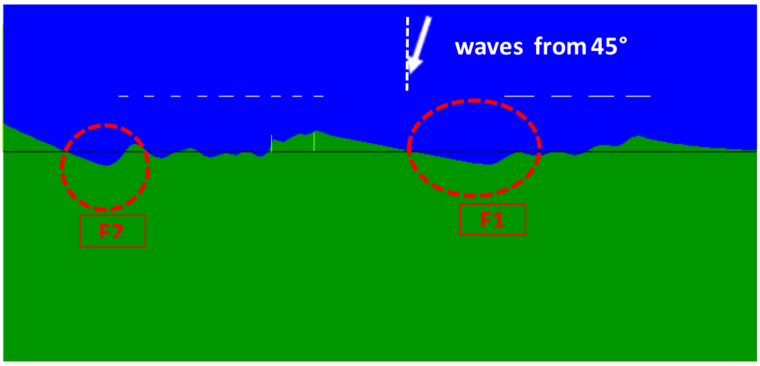

Figure 92 - Shoreline response of SE4 to a 45°N wave attack.

This concept closely resembles the idea of "negative shoreline diffusivity" introduced by Walton and Dean (2010) which lead to the instability of coastlines.

This features will be deepened in Chapter 7.

6.4. Quantitative analysis on equivalent wave: the Trigno river mouth area

The focus of quantitative analysis here presented is on a stretch of coast extending from the groin armouring the Trigno river south-side mouth, up to 5.2 Km southwards (Figure 93), and encompasses the sandy beaches of *Costa Verde* and *Marinelle.* In the first 2 km, the reach is defended by a system of 11 groins, with an average length of 68m and a mean spacing of 170m.

Figure 93 - The study area (from A to B, 5.2 Km) located just south the mouth of the Trigno river. The northern part is covered by a 11 groin field.

The analyses of the most recent evolution trends of the Molise coast all indicate this area as subject to intense erosion, with local rates of retreat as large as -8m/year. However, the Trigno river mouth, and the nearby shoreline, have been experiencing significant evolution for nearly 150 years, as well documented in literature (Aucelli et al. 2004).

Halfway through the XX century, the deltaic mouth system had been completely scrapped, consequently moving towards a wave-dominated morphology. In this period, while the delta eroding, sediment redistribution was nourishing adjacent beaches, which accreted accordingly. This trend continued until human interventions modified the natural feeding to the shore, so triggering an erosive process starting from the mid-1950s.

Particularly, the S. Salvo check-dam, built about 10 km far from the coast (1954-1977), produced over time channel tightening, leading to a significant sediment volume reduction of the coastal budget (Scorpio et al. 2015). In fact, upstream of the San Salvo check-dam, the channel lowered by ca. 1.5 m during the period 1954-2007 (Aucelli et al., 2011); conversely, downstream of the check-dam, channel lowering was much greater: from 1954 to 1986, it reached ca. 6.0 m and from 1986 to 2007, further very intense channel lowering of ca. 4.5 m occurred (Aucelli et al., 2011). The significant differences in channel lowering rates between the two stream portions show that the check-dam structure significantly limited river incision upstream. However, since the collapse of the bridge during the flood event in January 2003 (Aucelli et al., 2004), the upstream portion started to experience progressive channel incision, now directly affecting the clayey bedrock. The ongoing erosion has been faced over years with the use of hard structures transverse to the shore; the Trigno mouth has been armoured around 1980, while the eleven groins southwards have been built in 1998.

Table 7 reports the shoreline change rate, averaged along the entire reference reach, for either 30 years or 12 years' time windows; according to Crowell et al., 1993, both the timeframes can be categorized as "mid-term" intervals. Inspection of data reveals an increase of the erosive trend in the last 30 years; after the placement of the groin system (1998), the average rate of retreat is of the order of -2 m/year and seems to further accelerate in the most recent times (1998-2011 vs. 2004-2016).

Table 6 - Shoreline change rate, averaged along the Trigno river mouth stretch of coast, for either 30 years or 12 years time windows.

Time window	Average shoreline change (m/year)
1954-1986	-1.52
1986-2016	-2.02
1986-1998	-0.61
1998-2011	-1.94
2004-2016	-2.33

The Linear Regression Rate function (LRR) for the period 2004-2016 is shown in Fig. 88. In the groin protected area, the average erosion speed equals -0.94 m/year, while it exceeds -8m/year southwards. This of course confirms the existence of a prevailing NE to SW littoral drift component, as widely discussed in previous research (Rosskopf et al., 2018; di Paola et al., 2020; Buccino et al., 2020).

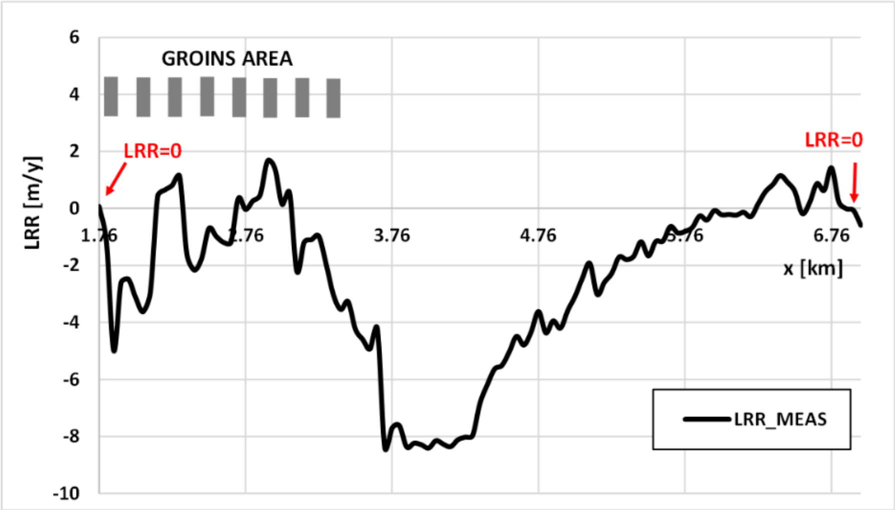

Figure 94 - Linear regression rate (LRR) function of the Trigno river mouth area during the period 2004–2016 . The vertical dashes indicate groins, red arrows indicate the LRR=0 boundary condition.

Importantly, referencing the x-along-shore axis with respect to the 36 km of Molise coast, LRR is seen to vanish at both x = 1760m (corresponding to the hydraulic right side of Trigno mouth) and x = 6960m, (red arrows in Figure 94), indicating a negligible rate of evolution, on average, over the period 2004-2016.

6.4.1. Littoral Drift Rose concept and shore diffusivity

The Littoral Drift Rose (LDR) represent a powerful help to analyse the long-run shoreline trend, its features have been discussed deeply in Chapter 2. The LDR concept, is based on the well-known CERC formula for littoral drift (SPM, 1984), from which, for each possible shoreline orientation, the annual (or monthly) littoral drifts (positive and negative) are calculated. Particularly, for a certain shoreline orientation β, the LDR graph shows a ‘’node’’. One of the major finding concerning the LDR concept is that, in terms of littoral drift, the effects of a deep-water wave climate could be equated to a single equivalent wave component, of parameters $H_{s0,eq}$., $T_{p0,eq}$, $\alpha_{0,eq}$., of which $\alpha_{0,eq}$ is easily detected from the LDR-graph, as it corresponds to the null-point. Most notably, the equivalent direction parameter (equal to the LDR null-point) is that of significant importance in shoreline evolution forecast, as it is nothing but the dominant direction of wave climate that persistently affect and sculpt the shoreline over years. In practical coastal engineering, the total wave climate is in fact seldom reduced to the equivalent wave component in mid-long term analysis of shoreline evolution, a procedure that has been widely applied in literature, particularly in the field of static equilibrium crenulated bays, as will be discusses in Chapter 8.

Anyhow, main point of present study regards the fact that, the "Total-LDR", in most cases, is approximable to a single wave component coming from a constant direction ("Equivalent-LDR"). This feature can be discussed in terms of shore-diffusivity as follows.

According to Walton and Dean (2010) and Ashton and Murray (2006a,b), stable/unstable behaviour of the coast can be interpreted via the shoreline ''diffusion'' equation. In the most general case the $\varepsilon(t)$ is a time-dependent coefficient, since the wave angle $\theta(t)$ varies over time for a deep-water wave climate. Therefore, considering the common practice, within a mid-term shoreline analysis, of reducing the wave climate into the LDR equivalent wave component, only a constant time-averaged diffusivity, $\hat{\varepsilon}$ is accounted for, as, all we do is mediate over time the diffusivity equation. Therefore, since both first and second term of the diffusivity equation are time-dependent, it stands to reason to expand in Taylor series the $\varepsilon(t)$ coefficient, so as:

$$\varepsilon(t) = \hat{\varepsilon} + \frac{\partial \varepsilon}{\partial t} dt + \cdots \tag{6.16}$$

In light of this, if the wave sector is relatively small, it is possible to neglect the higher order terms, and consequently the shoreline diffusivity would be constant over time. The latter consideration, in the context of LDR concept, shows that the degree of approximation of the Total-LDR to a single wave component is nothing but the degree of approximation of the total shore diffusivity $\varepsilon(t)$ to a constant one. In other words, the difference between Total and Equivalent LDR almost represents the difference $\hat{\varepsilon} - \left[\frac{\partial \varepsilon}{\partial t} dt + \cdots\right]$.

Accordingly, as long as the Total-LDR is well approximable to the Equivalent-LDR (symmetrical lobes), a negligible effect of the time variation of wave climate on the diffusivity is observed. Obviously, this occurs when in narrower wave sectors, where wave climate exhibits a single directional mode and a limited directional variance, like in many areas of the Tyrrhenian Sea (e.g. see Chapter 7 and 8).

Conversely, any deviation of the total LDR to the equivalent one (asymmetrical lobes) would denote an influence of the directional climate variability on the general diffusivity of the coast. This is exactly what happens for the Molise coast case of study, as will be shown in next paragraph.

6.4.2. Molise LDR

LDR for the Molise climate is shown in Figure 95a. It is seen the “positive lobe” (littoral drift rightwards) to be located right to the negative one (littoral drift leftwards). Moreover, the Equivalent Wave parameters have been estimated from the Molise LDR graph: the equivalent wave direction is equal to 9°N, corresponding the null-point of the real LDR, while the equivalent wave height and period have been fitted to have the same littoral transport magnitude , yielding to $H_{s0,eq}$ = 0.83 m and $T_{p0,eq}$ = 5.08s. It is surprising to observe how the equivalent wave direction of 9°N corresponds to that of 10°N empirically detected in previous section simply observing shoreline trend of the undefended stretch of coast near the Saccione stream mouth.

In Figure 95b Total-LDR and Equivalent-LDR are compared. It is seen that due to the inherent bimodality of the local wave climate, the Total-LDR of Molise coast shows asymmetrical lobes, with the negative lobe greater that the positive one. For a wave climate to be satisfactorily approximated by a single wave component, it is necessary the Total-LDR to have nearly symmetrical lobes. This normally occurs in mono-modal climates with a limited directional variance. Conversely, with widely varying wave directions, as the case of the Adriatic Sea here presented, a weaky fit is achieved. As a matter of fact, the Molise “Equivalent Wave” is not able to wholly approximate the littoral rose and fits properly only the part of the rose included between 340 and 70°N.

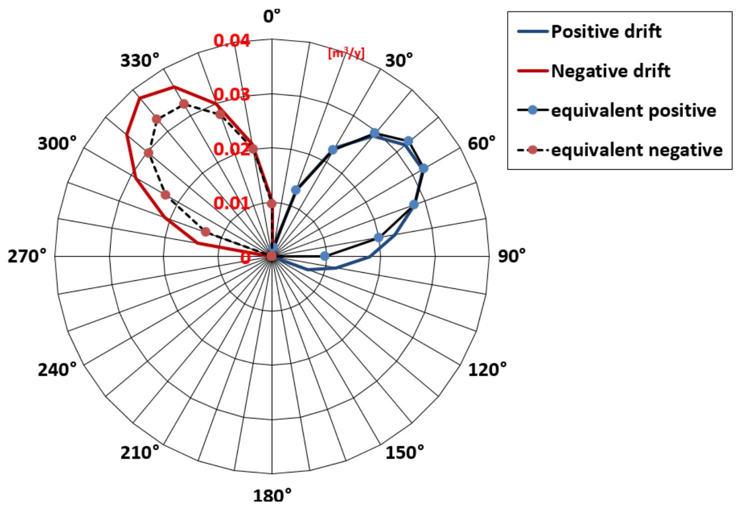

Figure 95- Comparison between Total and Equivalent LDRs of Molise coast. Littoral drift in cubic meters per year. Blue line represents drift to right when looking offshore, while red line represents drift to left when looking offshore.

In summary, to resume what stated in the previous paragraphs, on the one hand a proper fit of the Total-LDR by a single component indicates a constant shore diffusivity in the mid run.

This is obvious whenever the wave climate is coming from a restricted angle. For the case of study here presented, the observed poor approximation of the Total-LDR to the Equivalent one would indicate that the Molise coast diffusivity is not constant over time, thus denoting that the higher order terms of the Eq. (6.16) are not negligible, since the directional variability of wave climate is significantly large. This aspect could represent a limit within a mid-term analysis of coastal evolution based on the equivalent wave concept. The latter could result not significant in forecasting shoreline evolution, since its inability of account for the time-varying diffusivity extra-effect.

Therefore, in the following sections we first try to quantify the explanatory power of the LDR equivalent wave and its significance within a bimodal climate and secondly, we try to assess the role of an inconstant diffusivity upon the shoreline response.

Particularly, second feature has been achieved by considering the $\frac{\partial \varepsilon}{\partial t}$ terms of Eq. (6.16) as based on two different time-resoluted equivalent climate, and namely, an equivalent climate with a monthly time scan, and an equivalent frequency-based climate, with a 6hr time scan.

6.4.2.1. Monthly-equivalent LDR wave climate

Where a strong directional variability is observed, there might be the chance of a monthly (or seasonal) inversion of the equivalent direction of waves.

As discussed in Walton and Dean (2010), in fact, LDR null-point can change its position over the year. In such situations the annual equivalent wave representation could be ‘’splitted’’ into monthly varying LDRs, so obtaining monthly equivalent wave parameters (wave height, wave period and wave direction). To this aim, monthly LDRs have been reconstructed from Molise wave climate, and, from them, equivalent wave components have been obtained.

A wave time series can be built using monthly varying equivalent sea state parameters, which repeat theirselves year per year. For the Molise climate, equivalent direction reversers every month, as depicted in Figure 96, therefore the time-varying diffusivity effect changes over time with a resolution of one month.

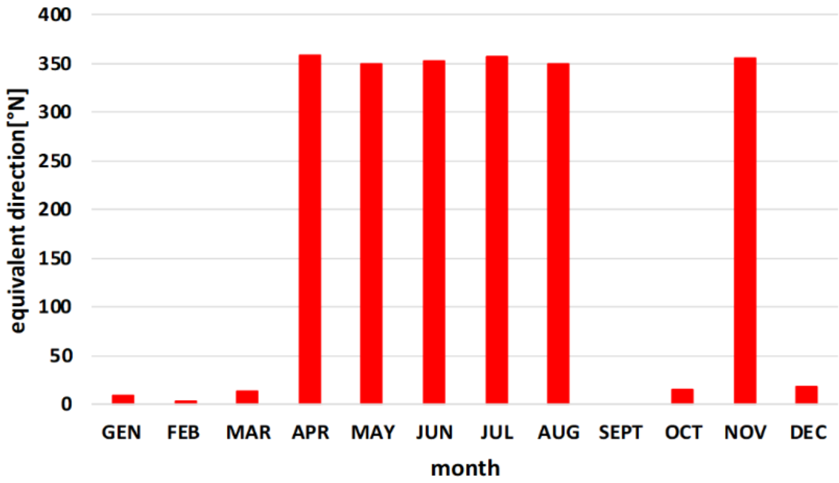

Figure 96 - Monthly variation of the LDR equivalent direction of Molise climate.

6.4.2.2. Frequency-equivalent wave climate

According to the Initial Distribution Approach (Holthuijsen, 2007) wave information is firstly used to build up a sea-climate matrix. Wave data were grouped into angular sectors 10°N wide (0 to 350) and, for each sector, 20 wave height classes have been considered, between 0 and 10m; each wave height class is provided with its frequency of occurrence and the corresponding average of peak periods, $\overline{T_p}$.

A statistically equivalent series of wave attacks has been then achieved from the sea-climate matrix, assuming wave directions to be random variables uniformly distributed between 0°N and 350°N. For each wave direction, 20 wave attacks have been used, with significant wave height corresponding to the centre of the wave height classes and peak period equalling $\overline{T_p}$. Each event is supposed to have a yearly duration equal to the frequency of occurrence of the corresponding wave class. Notably, the procedure has been repeated year by year, which implies the sequence of wave directions changes from one year to another. In the application discussed below, durations less than six hours have been discarded since their effect on the mid-term shoreline evolution is assumed negligible.

6.4.3. Numerical study

6.4.3.1. Software, Boundary Conditions and model parameters

The numerical analysis carried out herein employs the popular software GENESIS, the properties of which have been discussed in Chapter 3. GENESIS integrates the One-Line Equation, Eq. (3.1), and allows accounting the presence of coastal structures, which may transmit waves in the sheltered area by either wave breaking or overtopping. In GENESIS, the littoral drift is computed empirically, as a function of the breaking wave parameters (height, period and angle) and two transport coefficients, K_1 and K_2. It is important to point out that, despite the empirical genesis of K_1 and K_2, they are treated as calibration parameters of the numerical model, in order to overcome the many assumptions of the model and to account for the actual littoral transport.

As such, the solution of the one line equation is determined upon the knowledge of the following quantities:

- Initial Shoreline, y_0 (x);
- Lateral boundary conditions;
- Structure characteristics;
- Transport coefficients;
- Values of D_c and D_B
- Wave climate

The shoreline position at 2004 has been used as the initial condition; original data has been passed through a Godin filter with a 1000 m window width, to smooth out any abrupt changes in the shore orientation (Figure 97). The Godin filter has been selected as it is rather steep and induces no oscillations at the reach bounds.

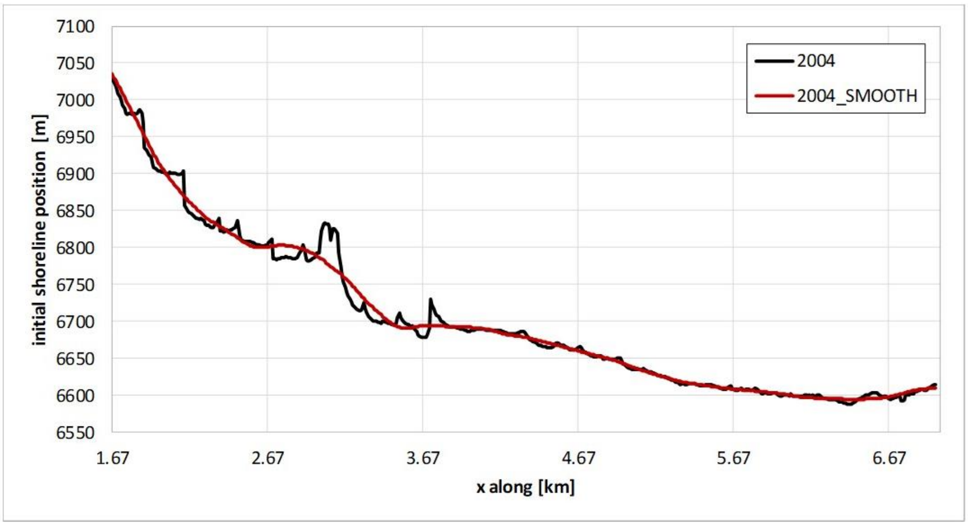

Figure 97 - Shoreline position at 2004: black line represents unsmoothed coastline position; red line represents smoothed coastline position.

Lateral boundary conditions are assigned by tentatively assuming that the "zero LRR sections" that bound the study area are "pinned", i.e. undergo no variations in the shoreline position at any instant in time. Both the jetty, which armours the Trigno estuary and the groins located southwards, have been reproduced in GENESIS with the same length and mutual distance as in the real life. To reduce the degrees of freedom in the numerical simulations, all the structures are assumed non-diffractive ($K_2 = 0$), so that the solution of one line equation depends upon the transport coefficient K_1 (which is referred hereafter as K) and the permeability of structures P.

Both the above quantities are treated as calibration parameters, under the only constrain that their value is physically consistent. As per K, a previous application of one line equation to the Molise coast suggested an order of magnitude value of 0.1, so that the range 0.04-0.3 has been (some subjectively) chosen. Otherwise, P is varied in the reasonable interval 0-0.3 and is supposed to attain the same value for all the structures. According to the early literature (De Vincenzo et al, 2017), the depth of closure has been equated to 9.4m, while the active berm height is set at 1.5m.

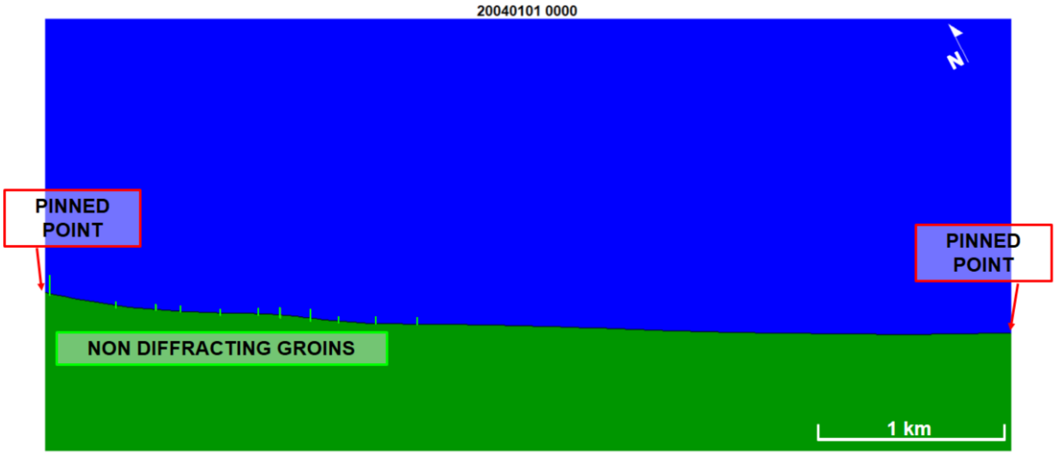

Figure 98 - GENESIS configuration of the modelled area. All the structures defending the area since 2004 have been reproduced with the same length and mutual distance.

The dependence of the shoreline response on wave climate (particularly wave direction) is the core of this section, and is broadly discussed in the Results Section.

6.4.4. Results

6.4.4.1. Annual LDR Equivalent wave climate

First of all, in order to test the degree of correlation of the dominant wave attack for littoral transport with the coastline evolution, the LDR equivalent wave has been inputted into the model GENESIS (Figure 98) in the form of a 12 years (2004-2016) time series. Different model scenarios have been created by varying the transport coefficient K and the groins permeability P. The shorelines outputting from the GENESIS model has been used to calculate the ‘’LRR predicted function’’ which has been then compared with the ‘’LRR measured function’’ of the Trigno mouth area.

To measure the model performances, two prediction indexes have been used and namely:

- the R^2 statistics, indicating correlation between measured and predicted LRR;
- the Relative Mean Square Error (RMSE), given by:

$$RMSE = \sqrt{\frac{\sum_{i=1}^{N}\left(LRR_{meas_i} - LRR_{pred_i}\right)^2}{N}} \tag{6.17}$$

where N is the total number of the shoreline position, while LRR_{meas} and LRR_{perd} are the accretion/erosion indexes measured and predicted, respectively.

Figure 99 shows the superimposition between the RMSE surface and the R^2 contour lines obtained by the comparison between the measured and predicted LRR functions of each model scenarios. The best performances (maximum R^2 and minimum RMSE) are found at groins permeability P of 0.2 and a K value of 0.2. The graph shows a good prediction power of the equivalent wave, as it is able to account for about 90% of the total Trigno LRR variance.

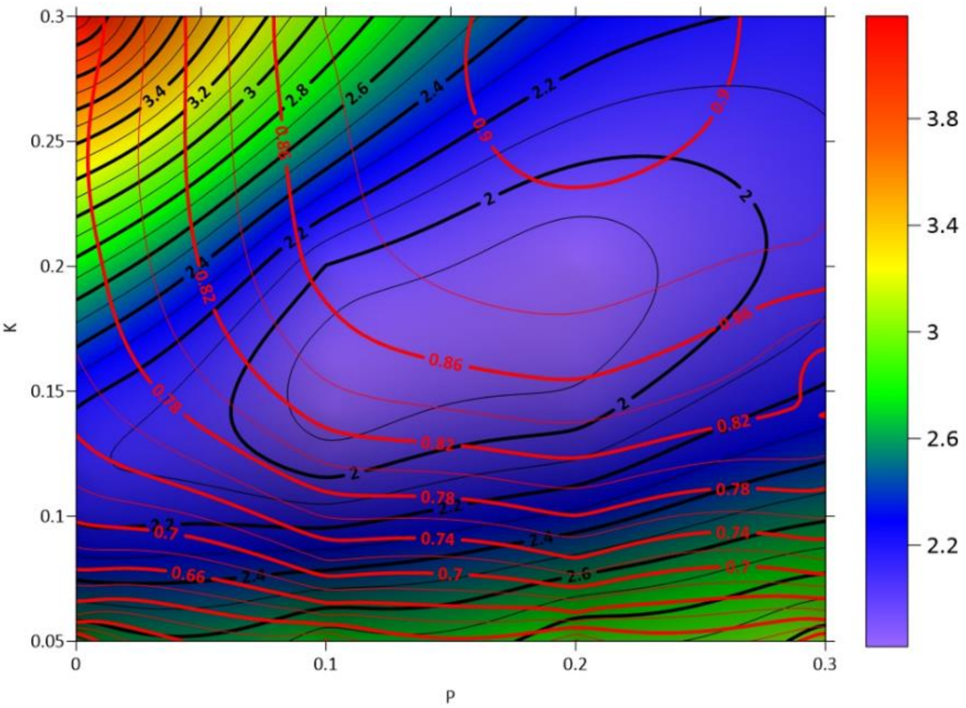

Figure 99 - Superimposition between the RMSE surface (black contour lines) and the R2 surface (red contour lines) for the annual LDR equivalent climate (9°N). x-axis is the groins permeability P, while y axis is the GENESIS transport coefficient K. Surfaces have been obtained by comparing the ''measured'' and ''predicted'' LRR functions of each K-P scenarios.

Anyhow, the RMSE and the R^2 surfaces are not ''in phase'': in fact, contours have an initial sub-parallel pattern, but with the RMSE decreasing faster than the R^2 increasing with the K parameter. Therefore, the surfaces attain the absolute maximum of R^2 and the absolute minimum of RMSE in separate areas of the K-P space.

Moreover, it is noted that, in the best scenario, the RMSE value is relatively large, anyway, as the absolute minimum ranges between 1.5-2 m/y, which is considerably higher than the expected error given by the shoreline surveys (see previous sections). Therefore, in order to test if the equivalent wave parameters returns the best prediction of the Trigno shoreline evolution, we first carried out a significance analysis of the equivalent direction by varying the angle of ±30° with respect to 9°N. The best performances for the seven equivalent directions analysed are summarised in Figure 100, highlighting that the maximum R^2 and minimum RMSE lie between ± 10° around the equivalent LDR direction of 9°N. Particularly, it is noted that for the three best equivalent directions of 0°N 9°N and 20°N the values attained by the performance indexes are very close to each other: the observed invariance confirms that the LDR equivalent direction of 9°N is well-correlated to the real shoreline trend, and it can be trustily used in the medium-long term shoreline analysis.

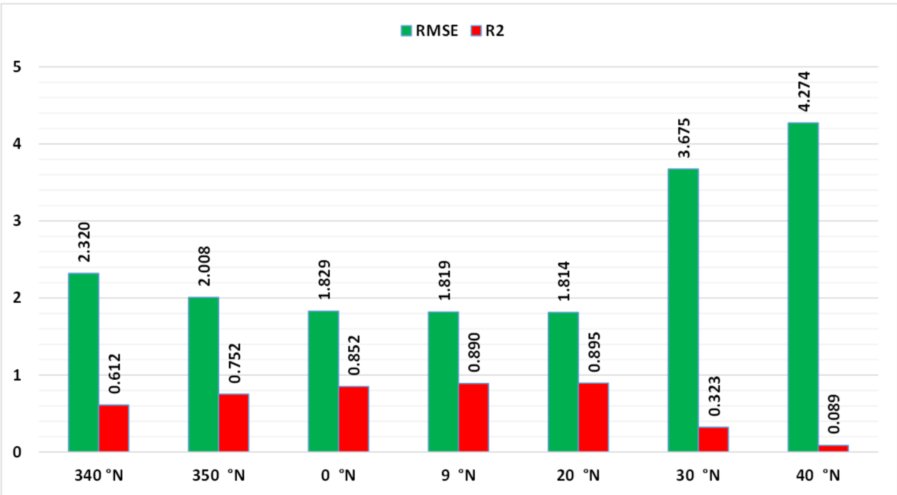

Figure 100 - Best performances indexes (R^2 and RMSE) for the 7 equivalent directions analysed within the LDR equivalent direction significance study. Values have been obtained by comparing the ''measured'' and ''predicted'' LRR functions.

Anyhow, the numerical model systematically overestimates the real average trend of the coast. In Figure 101 (panel a. 0°N; panel b. 9°N; panel c. 20°N) is shown the surface representing the difference between the arithmetic mean of measured and calculated LRR: the null values of this difference are not found for the best K-P scenarios (as expected) but rather there is an average systematic overestimation around 1-1.5m.

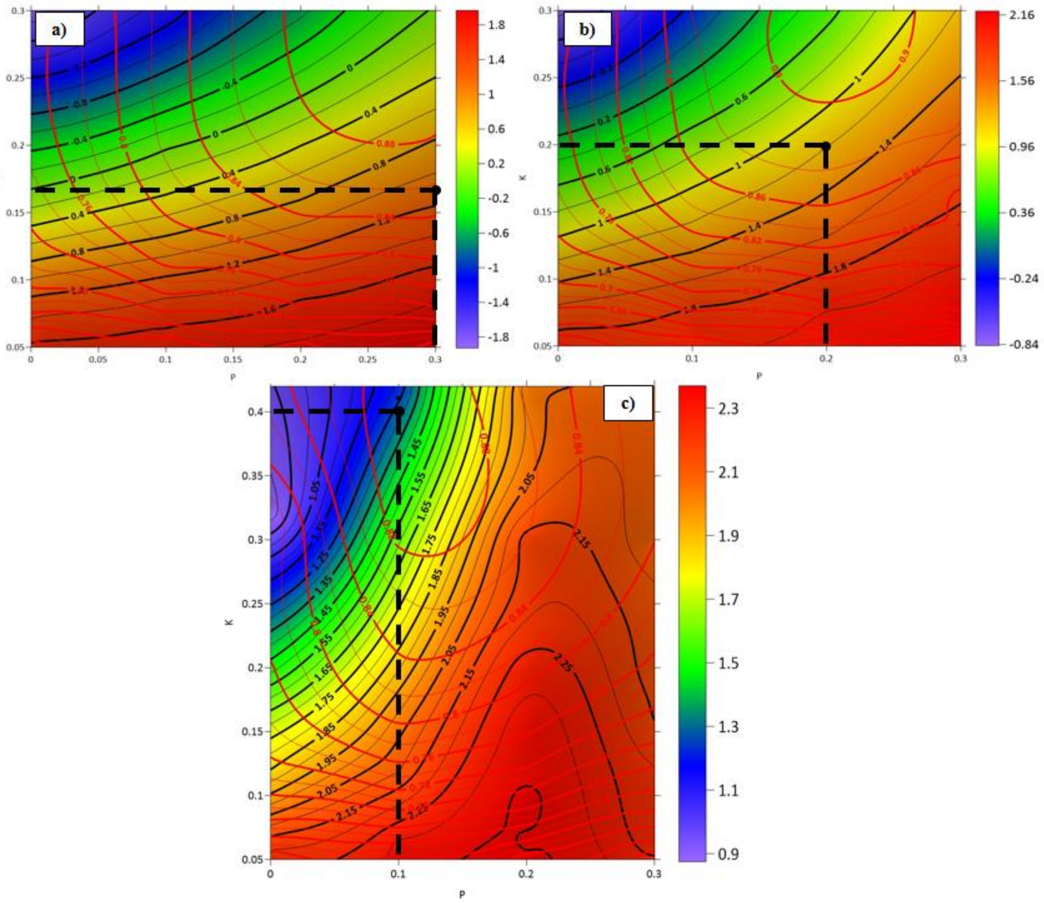

Figure 101 - Comparison of difference between the arithmetic mean of measured and calculated LRR surface (black contour lines) and R^2 surface (red contour lines). Panel a) 0°N; Panel b) 9°N; Panel c) 20°N. x-axis is the groins permeability P, while y axis is the GENESIS transport coefficient K. black dashed lines indicates the K-P scenarios with the best performances (minimum R^2 maximum RMSE).

The reasons of this underlying bias produced by the annual equivalent wave component can be likely found, at first sight, in the influence of the more angled climate components. This can be outlined by observing separately the area covered by groins (first 2 km) and the remaining un-protected 3 km reach of coast. Figure 102, shows the LRR functions for the three best equivalent directions (0°N; 9°N; and 20°N), in the protected area the overestimation reduces moving towards 0°N; on contrary, in the unprotected area it reduces moving towards 20°N. This seems to confirm that the equivalent direction varies and reverses over time, a predictable behaviour when in bimodal wave climate conditions.

Anyhow, by strictly focusing on the groins area, (Table 7), it is noted that the more angled directions produce a bias reduction: in fact, the RMSE and the mean are the lowest, so confirming that the reversal of the equivalent direction would influence the predicted shoreline trend. However, the correlation index remains relatively low for the 340°N and 350°N, and tends to increase moving towards the LDR equivalent direction, attaining the 70% of the explained variance.

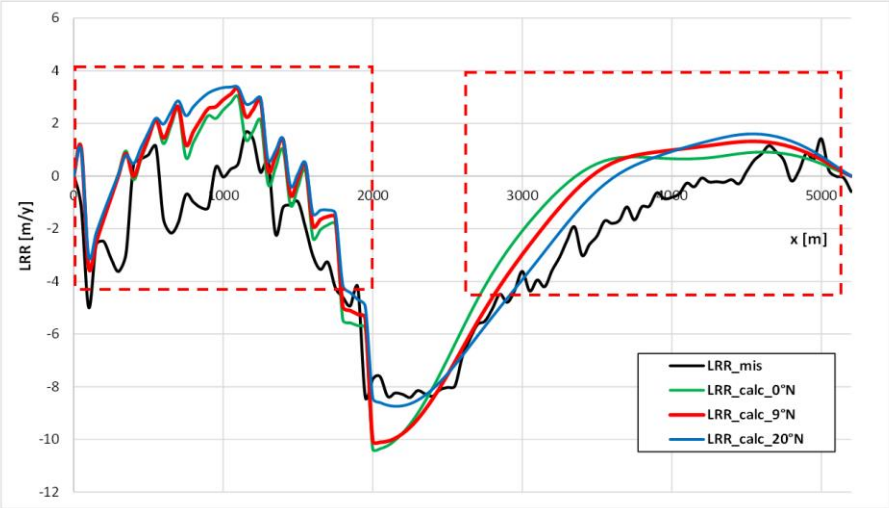

Figure 102 - LRR functions for the three best equivalent directions (0°N; 9°N; and 20°N) compared with the LRR measured function of the Trigno area. Red dashed boxes indicate the two sub-areas where an overestimation is observed: left one (first 2km) is located within the groins area, while the second one is located within the unprotected zone (last 3 km).

To sum up, the significance analysis of the equivalent direction confirms that, by reducing the total wave climate to a single equivalent wave component, and consequently accounting for a constant value of the shore diffusivity, the LDR equivalent wave is significantly better correlated to the real shoreline trend, although a biased result is produced.

Table 7 - Groin area performance indexes (RMSE, R2 and mean μ) for the best scenario for the shifted direction

DD [°N]	P [-]	K [-]	RMSE [m/y]	R2 [-]	μ [m/y]
340	0.3	0.1	2.091	0.503	1.122
350	0.3	0.12	2.034	0.601	1.169
0	0.3	0.16	2.138	0.689	1.418
9	0.2	0.2	2.301	0.709	1.699
20	0.1	0.4	2.546	0.714	1.528
30	0	0.16	2.839	0.114	1.772
40	0.3	0.05	3.900	0.302	1.062

However, the fact that the more angled components are found to act on the bias, as shown in Table 7, suggests that it is not possible to neglect the directional variability of wave climate (this will be then deepened in Chapter 6, by analysing a possible effect of negative diffusion). Therefore, in order to go in deep with climate reversal, a time-varying diffusivity extra-effect on shoreline response has been considered within the analysis. Two different wave climate resolution has been inputted into GENESIS model, the monthly equivalent climate and the frequency-equivalent time series.

6.4.4.2. Monthly LDR Equivalent wave climate

The role of the monthly representation of LDR is analysed, this mainly because of the likely annual inversion of the equivalent direction in bimodal wave climate. In this case, GENESIS scenarios have been set inputting a 12 years wave time series with a monthly variation of the equivalent parameters: direction, wave height and wave period.

Figure 103 shows the superimposition between the RMSE surface and the R^2 contour lines obtained by the comparison between the measured and predicted LRR functions of each model scenarios. With respect to the results obtained with the annual equivalent component (Figure 99), the monthly scan of wave climate shows a good prediction power as well, and the best performances (maximum R^2 and minimum RMSE) are found at groins permeability P of 0.2 and a K value of 0.2 (Table 8).

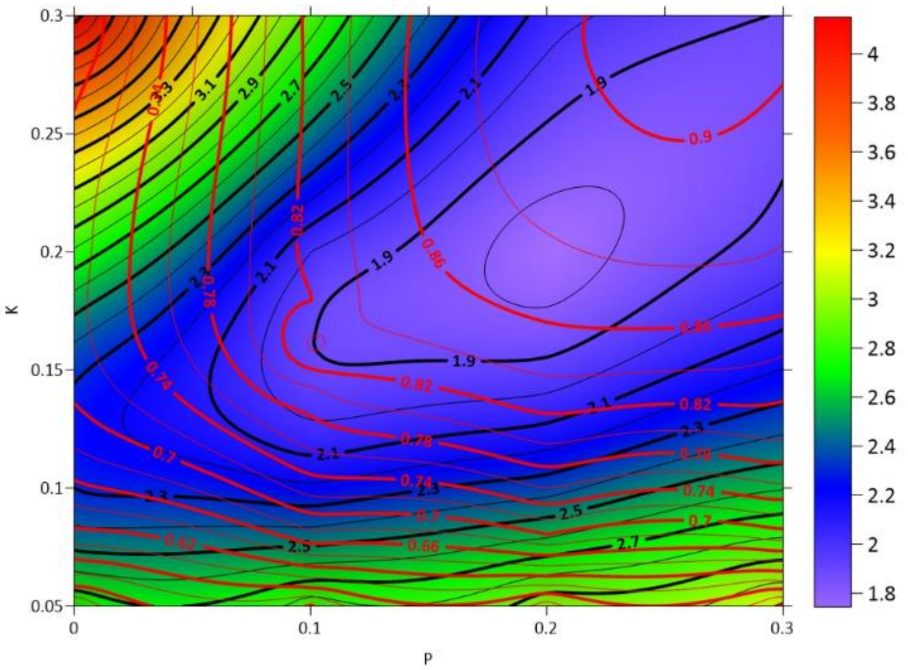

Figure 103 - Superimposition between the RMSE surface (black contour lines) and the R^2 surface (red contour lines) for the monthly LDR equivalent climate. x-axis is the groins permeability P, while y axis is the GENESIS transport coefficient K. Surfaces have been obtained by comparing the ''measured'' and ''predicted'' LRR functions of each K-P scenarios.

As noted, by comparing the performance indexes, the monthly equivalent climate produces a little reduction of the RMSE (from 1.819 m/y to 1.743 m/y), while the R^2 is still high but slightly lower (from 0.89 to 0.876). In a nutshell, there is not an appreciable improvement on the predicted shoreline trend. Not only that, but also the overestimation is still found at the initial and final part of the study area, and the arithmetic residual mean is still 1,20 m/y. In addition, focusing on the groins area for the best monthly scenario (P=0.2 and K=0.2), the prediction remains quite the same, with no tangible improvement: particularly, as will be shown in Table 8, the correlation is the same, while a little bias reduction by 0.2 m/year is detected.

Table 8 - Performance indexes (RMSE, R2 and mean μ) for the monthly LDR equivalent climate.

P [-]	K [-]	R^2 [-]	RMSE [m/y]	μ [m/y]
0	0.12	0.6841	2.248	1.23
0.1	0.16	0.8449	1.902	1.13
0.2	0.2	0.8766	1.743	1.20
0.3	0.2	0.9041	1.896	1.17

6.4.4.3. Frequency-equivalent time series

A 12 years frequency equivalent time series has been inputted in GENESIS model, where wave height, wave period and wave direction variation have been forecasted according to the frequency of appearance of the real Molise wave climate, therefore obtaining a more accurate climate representation able to account for both climate reversal and, to some extent, extreme events produced by storms .

Results are shown in Figure 104 and Table 10.

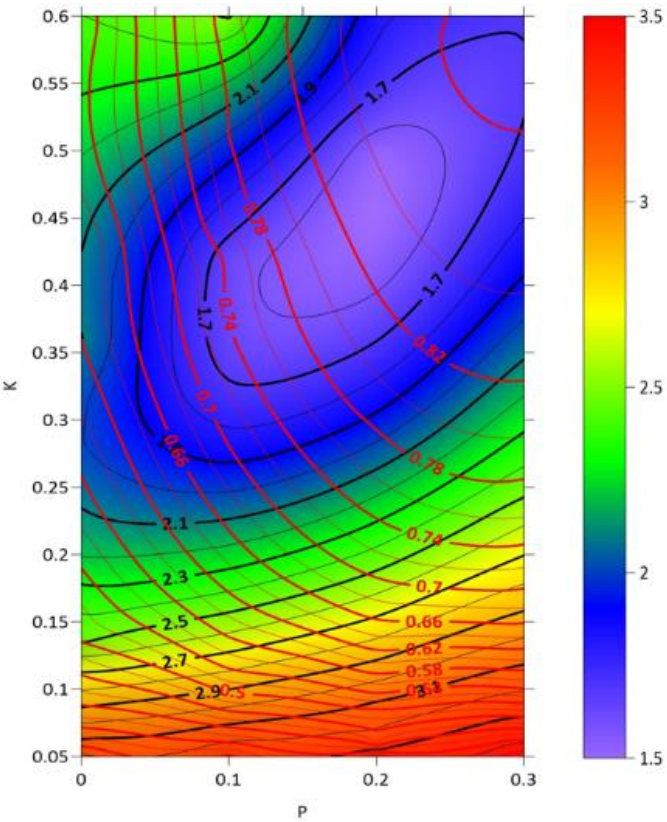

Figure 104 - Superimposition between the RMSE surface (black contour lines) and the R2 surface (red contour lines) for the frequency- equivalent climate. x-axis is the groins permeability P, while y axis is the GENESIS transport coefficient K. Surfaces have been obtained by comparing the ''measured'' and ''predicted'' LRR functions of each K-P scenarios.

The best prediction is obtained with a groins permeability of 0.2 and a transport coefficient of 0.46. It is noted that, similarly to the monthly climate, an increased scan of wave climate produces a bias reduction and, at the same time, a little reduction of the degree of correlation, which is still really high, anyway (R^2= 0.835). By comparing these results to the other two climate resolution (annual and monthly equivalent climate), the frequency equivalent time series seems to be the best prediction model, due, in particular, to the greatest bias reduction (RMSE=1.5 m/y and μ=0.7 m/y).

Table 9 - Performance indexes (RMSE, R^2 and mean) for the frequency- equivalent climate

P [-]	K [-]	RMSE [m/y]	R2 [-]	μ [m/y]
0	0.36	2.105	0.620	0.081
0.1	0.38	1.643	0.744	0.519
0.2	0.46	1.519	0.835	0.721
0.3	0.55	1.693	0.864	1.054

Nevertheless, a more accurate analysis shows that the effect of the equivalent time series on the model is a simple translation of the calculated trend toward the measured, likely determined by the effect of the extreme waves, which produces, by contrast, a reduction of the correlation. The paradigmatic example can be shown restricting the attention to the area defended by groins. As shown in Fig 105 and in Table 10, the narrower the climate resolution the more unbiased the numerical model, but the lower the correlation R^2. In fact, although LDR results appear very biased, a correlation around 70% is observed, by contrast the very opposite occurs for the frequency equivalent climate. In this case, the bias reduces but the correlation coefficient dramatically decreases by 20 points (Table 10).

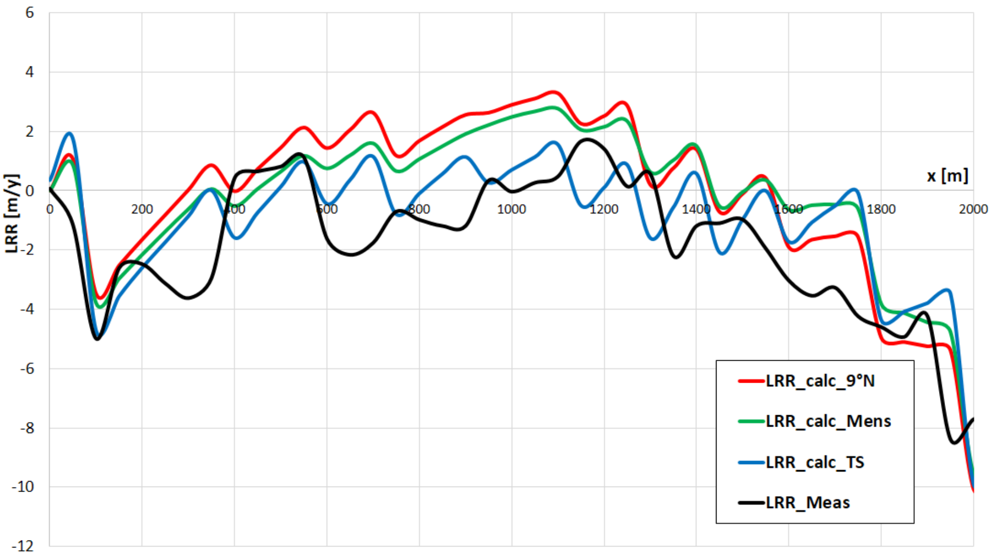

Figure 105 - Focus of the LRR functions within the groins area (2 km) for the three different time-resoluted climate analysed.

Table 10 - Comparison between annual LDR equivalent climate, Monthly LDR equivalent climate and frequency-equivalent climate.

CLIMATE	P [-]	K [-]	RMSE [m/y]	R^2 [-]	μ [m/y]
ANNUAL LDR (9°N)	0.2	0.2	2.301	0.709	1.699
MONTHLY LDR	0.2	0.2	2.112	0.688	1.574
FREQUENCY EQ.	0.2	0.46	1.897	0.505	0.830

To sum up, the explanatory power of the reduced climate scans, which accounts for the time-varying shore diffusivity $\frac{\partial \varepsilon}{\partial t}$, is surprisingly lower than the LDR component one. It is noted that the time-varying shore diffusivity seems to not affect the shoreline trend, in fact, the correlation is drastically lower within the groins area, but it is able to have an influence on the bias.

Such results indicate a doubtful role of the time-varying diffusivity. Anyhow, since the frequency-equivalent climate, to some extent, accounts for of extreme waves, it is clear that their effect is a local translation of the coastline, which tends to deviate from the long-term trend. It is worth highlighting that, the bias could be related to physics phenomena (storms events), but it could be due to different factors, like the boundary conditions of the GENESIS model, or the non-uniform shoreline trend over years.

However, as will be discussed in Chapter 6, these aspects seems to be correlated to the effect of negative diffusivity components which acts over the coast producing an accretion on the erosion/accretion trend by the formation of shoreline sand waves.

In conclusion, results confirmed the reliability of the Equivalent Wave approach, even within a bimodal climate. The study attain to a relevant result: over a long- period the shoreline evolution is practically governed by a constant diffusion, better represented by the equivalent LDR wave. Moreover, the possible effect of a time-varying diffusion, which is expected with a large directional variability, produced insignificant results with respect to the Equivalent Wave concept.

Anyhow, the possible effect of diffusion will be accurately deepened in Chapter 7.

Chapter 7: Negative diffusion, instability of the diffusion equation and potential impact on shoreline evolution

7.1. Introduction

Recent research has revealed that the plane view evolution of a coast due to gradients in along-shore sediment transport is highly dependent upon the angles at which waves approach the shore, giving rise to an instability in shoreline shape that can generate different types of naturally occurring coastal landforms.

Traditional finding showed that on an open, long, sandy coast, the wave-driven, along-shore sediment transport tends to smooth the coastline if the angle between wave crests and the shoreline is relatively small (Komar, 1998). However, for waves approaching at a large angle with respect to the shoreline, the gradients in along-shore drift, which originate from shoreline irregularities, may reinforce those irregularities, rendering the rectilinear coast unstable. This had been suggested in the past by a number of authors (Bakker, 1968; Grijm, 1961; Walton and Dean, 1973; Wang and LeMehaute, 1980; Zenkovich, 1959), who recognized the potential of this instability mechanism to generate shoreline features at large spatial scales (1–10 km), such as cuspate shorelines, sand waves, and sand spits.

However, a systematic exploration, using a mathematical modeling approach, was first presented by Ashton and Murray (2001) and later pursued by Falqués (2003), Falqués and Calvete (2005), and Ashton and Murray (2006a). Furthermore, it was shown that a number of shoreline morphologies around the world, were related to this instability (Ashton and Murray, 2006b).

In particular, Ashton, Murray, and Ruessink (2003) and Falqués (2006) examined the stability properties of the Dutch coast under its wave climate and concluded that the long-term shoreline sand waves observed there might have originated from this instability.

All those studies have shown that the coupling of waves and coastline features via the along-shore drift may lead to a positive feedback and that the so-called high-angle wave instability may be relevant for coastal morphology. Although this positive feedback is a robust output of the models, the physics behind the instability has not been deeply discussed in the literature.

Thus, the aim of the present Chapter is to provide further insight into processes behind high-angle wave instability. No new modelling is presented, but, instead, the physics is discussed with the use of very simple concepts based on the LDR approach. For the first time it is organically introduced the effect of high angles waves on shoreline evolution, which can cause sudden retreats of shoreline, and the conditions for which the "diffusion process" transforms into a "fusion process" are shown.

Moreover, the last sections of this Chapter regards the interpretation of a detached breakwater on shoreline change. In fact, under an intriguing perspective, but not sufficiently deepened, at all, it is assumed that the positioning of a transmissive breakwater is nothing but the introduction of a negative diffusivity into a restricted area of the coast.

7.2. Unstable shorelines and background

Everyone knows that sand very rarely forms a flat surface. In the desert there are sand dunes, in rivers there are sand bars, but sand features are probably most abundant at the boundary between the land and the sea: the near shore area. Well-known rhythmic features made of sand in the near shore area include dunes, ripples and long-shore bars. Many more are described in the literature; these include beach cusps, mega cusps, oblique bars, bar rips, long-shore shoreline undulations, barrier islands, evolving spits and capes. Sand features in the near shore area are present on a wide range of scales, from centimetres (e.g. wave ripples) to hundreds of kilometres, (e.g. the Carolina Capes). Many of the features are mobile, some migrate in a specific direction, one example being the pro-grading spit, and some migrate back and fourth depending the hydrodynamic forcing, sediment supply or other factors; an example is the movement of a long-shore breaker bar which moves onshore in fair weather and offshore during stormy weather. Most of the sand features exhibit rhythmic or quasi rhythmic behaviour, either as a rhythmic shape, e.g. the dunes in the dessert, or as a rhythmic migration pattern, e.g. the off-shore migration of a breaker bar and the subsequent formation of a new breaker bar closer to the shore which then migrates offshore.

Long-shore shoreline undulations are found on many coasts around the world, some examples are shown in Figures 106 to 108. Figure 106 shows one shoreline undulation on Long Point in Lake Erie. A spit is seen on the downstream end of the shoreline undulation, the spit is seen to migrate parallel to the shoreline. The length is seen to be around 2 km.

Figure 107 shows the long-shore undulations on the shoreline at Srd. Holmslands Tange on the West Coast of Denmark. The shoreline undulation are seen to be much less pronounced and no spits are formed on the downstream end. The length of the undulation is seen to be around 5 km.
On the West Coast of Namibia some very large shoreline undulation are seen in Figure 108. The length of the undulations is 60 km (there are three undulation on the stretch of shoreline which is ≈ 180 km long), and the width are between 8 and 12 km. As in Lake Erie spits are forming on the down drift side of some of the undulations, the direction in which the spits migrate is more or less parallel to the overall shoreline orientation (Kærgaard, 2011).

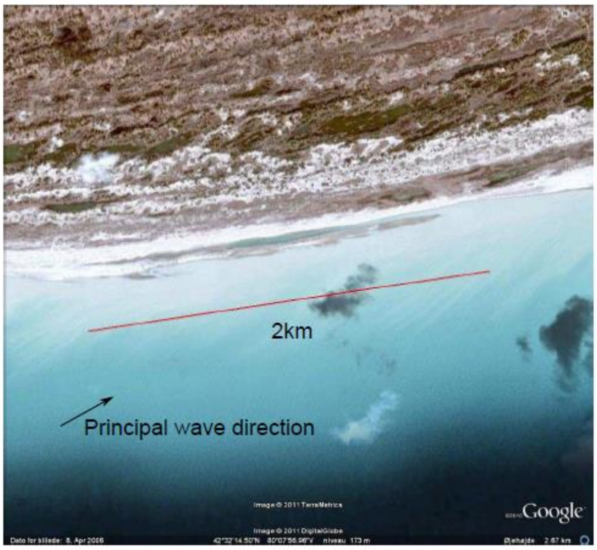

Figure 106 - Example of a long-shore shoreline undulation in Lake Erie, Canada.

Figure 107 - Example of a long-shore shoreline undulation on Danish West Coast, Denmark.

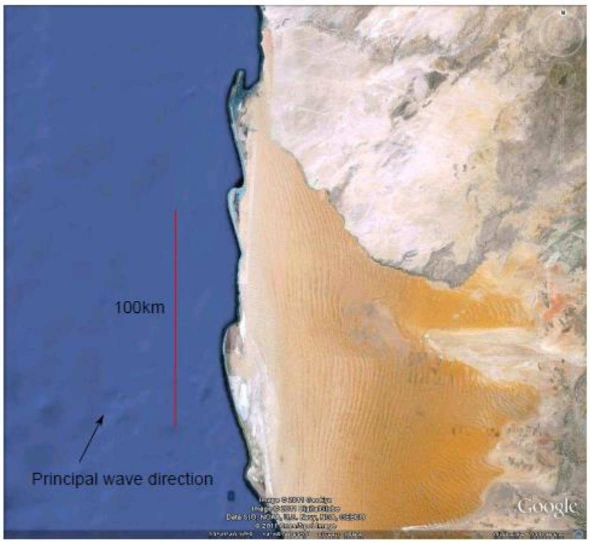

Figure 108 - Example of long-shore shoreline undulations on the west coast of Namibia

Bakker (1964) highlighted possible instabilities of the diffusion equation with respect to a river mouth. Field observations of long-shore shoreline undulations were reported by Bruun (1954a). He looked for periodic long-shore features on the shoreline of the Danish North Sea Coast. He found evidence of large shoreline features with lengths from 0.5-2 km and widths of 60-80 m, traveling up to about one length per year. He speculated that there might be a connection between breaches in the long-shore bar (rips) and the undulations, since the trough of the undulation was often found behind a breach and the crest just ahead. Bruun also found evidence of sand waves traveling in the direction of the littoral drift at the 6-m depth contour and the 9-meter depth contour. He called these sand waves sand humps, and they had lengths from 1.5-3 km and amplitudes of 1-2 m. The connection, if any, between the sand waves and the shoreline undulations was not established. Bruun further speculated whether sudden increases in bottom shoaling of navigation channels without a marked change in the weather or wave climate could be due to the arrival of either sand humps or shoreline undulations to the place in question. In this way the first economic interest in long-shore shoreline undulations was established.

Shoreline undulations along the Dutch coast has been studied by Verhagen (1989). Although he calls the features sand waves it is clear the paper is concerned with long-shore shoreline undulations. He finds long-shore shoreline undulations with migration velocities around 50-200 m/yr, periods of 50-150 years and amplitudes of 30-500 meters. On one part of the Dutch shoreline groins were constructed; the long-shore shoreline undulation were not affected by the groins, i.e. the celerity and amplitude of the long-shore undulation were the same before and after the construction of the groin field. This is related to the large scale of the undulations compared with the scale of the groins.

The long-shore shoreline undulations on Long Point in Lake Erie, Canada have been described in Davidson- Arnott and Heyningen (2003). The lengths of the long-shore undulations at Long Point are found to be 750 to 2050 m and the widths are found to be 40 to 100 m. The incidence angle of the waves at Long Point is very oblique due to the geometry of Lake Erie and the prevailing wind climate. The migration rates are between 100 and 300 m/year, however the maximum migration rates were much larger. The initial formation of the long-shore undulations is related to the onshore migration of and subsequent welding to the beach of a near shore bar. After the initial formation the undulations grow in both length and amplitude as they migrate in the down drift direction. A maximum length of 1.5-2 km is observed, beach waves longer than this tend to break up into two shorter undulations.

7.2.1. Formation mechanism of the shoreline undulation: the instability condition

The mechanism behind the formation of the shoreline undulations is not well understood. In the papers mentioned above, the formation of the undulations is at best only tentatively explained. A possible explanation for the existence of the long-shore undulations is an instability mechanism of an otherwise straight and uniform coastline under very oblique wave incidence. The instability is explained in the following way.

When waves approach a shore at an oblique angle, nearshore wave-breaking produces a shore-parallel current. On a sandy shoreline, this current transports sediment. This along-shore sediment flux, Qs, is a nonlinear function of the local shoreline angle relative to the wave crests, exhibiting a maximum (Figure 109). A maximum for q exists around α = 45°, as stated by energetic approach by Komar and Inman (1970) (the CERC formulation). The instability in shoreline shape occurs when waves approach at a relative angle greater than that which maximizes sediment transport (which we call `high-angle' waves). In this case, moving along-shore in the transport direction (`downdrift'), Q_s will decrease along the crest of a perturbation as the angle between the shoreline and the waves becomes progressively farther from the transport-maximizing angle (Figure 109). This convergence of sediment flux causes accretion; the perturbation will grow. (This conclusion involves the common assumption that the rate of any cross-shore sediment exchange between the nearshore region and deeper water is negligible compared to the along-shore flux).

Finite-amplitude effects will eventually dictate the evolution of a growing feature. For the case of high-angle waves approaching from a constant direction, as the amplitude of the feature increases, sediment flux at the inflection point downdrift of the crest will approach zero. This will lead to the extension of a spit-like protuberance. In addition, the angle between the shoreline and the wave crests at the inflection point on the updrift side of a feature will approach, but not increase beyond, the angle that maximizes sediment transport. However, the inevitably continued erosion updrift of this point will cause the inflection point to migrate continually towards the crest. This erosion of the updrift flank and accumulation at the crest and downdrift of it will cause the feature to translate downdrift while growing. (If the relative angle between the waves and the regional shoreline trend is only slightly greater than the transport-maximizing angle, subtle, low-amplitude shoreline features will result).

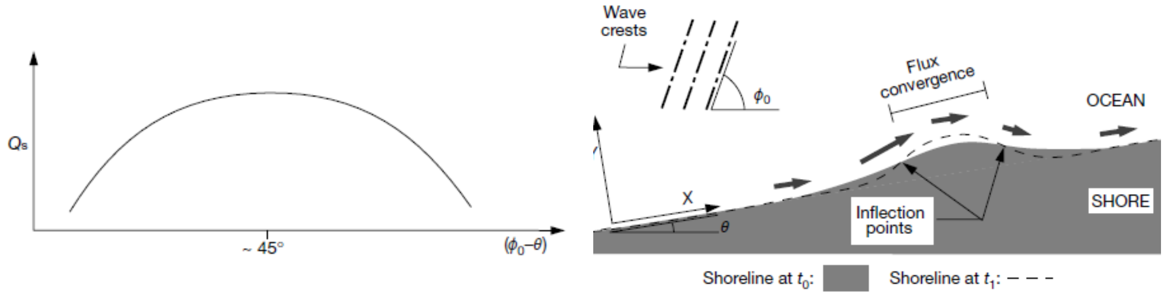

(a) (b)

Figure 109 - As a result of the basic instability, shoreline perturbations grow in the presence of high-angle waves. a, Schematic relationship between along-shore sediment flux, Qs, and the relative angle between wave crests in deep water (before nearshore refraction), φ0, and the local shoreline orientation, v, showing a maximum for φ0 2v < 458. b, The relative magnitude of the along-shore sediment flux, shown by the length of the arrows, and the consequent zones of erosion and accretion on a perturbation to a straight shoreline when the angle between the wave crests and the shoreline trend is greater than that which maximizes the sediment flux.

From the figure it is further seen than if the incoming wave direction is below the critical angle, undulations formed by any of the processes named above (welding of shoals, welding of near shore bars or variations in sediment supply from rivers) will disperse since the long-shore sediment transport on the down drift side will then be larger than the long-shore sediment transport on the up drift side.

Ashton and Murray (2001) were the first to try to model the evolution of shorelines subject to the instability. In this work the long-shore littoral drift was determined using a CERC formulation approach for the description of the long-shore transport. Waves were transformed from off-shore to breaking using linear theory for refraction and shoaling and assuming parallel depth contours (again applying Snell's law). Their model simulates the non-linear evolution of small perturbations resulting in a variety of large scale shoreline morphologies. They speculate that the instability is responsible for the formation of the capes seen on the shoreline of North Carolina, on the east coast of the United States, as some of their model results resemble these features. The effect of non-parallel depth contours on wave refraction in conjunction with the instability was first included in an analysis by Falqués and Calvete (2005). They looked at the diffusivity and instability of sandy coastlines. Their work is a linear stability analysis of a uniform shoreline subject to very oblique wave incidence described using a one-line model approach. The long-shore sediment transport is determined using a CERC formulation approach, which means that inertia effects in the long-shore current are ignored. The main new contribution was the determination of the most unstable undulation length. This length scales with breaker zone width (with a scaling factor of 50-100) but also scales with other parameters. Furthermore, they determined that for a shoreline undulation to be unstable, the shoreline undulation must be felt a certain distance offshore.

7.2.2. Comparing Different Sediment Transport Formulations

Ashton and Murray (2006b) further investigate the relevance of the high wave angle instability along natural shorelines, showing that many different formulations for along-shore sediment transport all predict the high wave angle instability. In fact, the authors demonstrate that a basic instability in shoreline shape follows from the presence of a maximum in the relationship between along-shore sediment flux and deep-water approach angle. For example, the common ''CERC'' formula predicts that a coastline is unstable whenever deep-water waves approach at angles greater than approximately 42° (Ashton et al., 2001). Many other formulae, both theoretical and empirical, exist that relate wave-driven along-shore sediment flux to wave characteristics such as height, angle, and period. They looked briefly at some of these relationships to determine whether the maximum in sediment transport, or its occurrence around a deep-water angle of 45°, is unique to the CERC formula, or if other relationships also exhibit an easily exceeded deep-water maximum.

Amongst the large number of formulations for breaking- wave-driven along-shore sediment transport that have been presented in the literature, the authors selected several that are frequently referred to, have different derivations, and offer significantly different functional predictions. Besides the semi empirical CERC formula, they also investigate the (semi) empirical Kamphuis (1991) formula with laboratory fit parameters, the analytically derived Bailard (1984) formula, and the Deigaard et al. (1988) formula developed using detailed numerical modelling. For illustration purposes only, they analysed a hypothetical formula that is similar to the CERC relationship, but lacking a breaking wave maximum in sediment flux.

Table 11 - Investigated Sediment Transport Formulations and Corresponding Maximizing Angles for Breaking and Deepwater Waves (from Ashton and Murray, 2006b)

Name	Formula	Maximizing Angle $(\phi_b - \theta)$	Maximizing Angle $(\phi_0 - \theta)$
CERC	$Q_s = \left[\frac{K\rho g^{\frac{1}{2}}}{(\rho_s-\rho)(1-p)}\right] H_b^{\frac{5}{2}} \cos(\phi_b - \theta)\sin(\phi_b - \theta)_b$	45°	42°
Kamphuis	$Q_s = (2.27m^{0.75}\ d_{50}{}^{-0.25}\ T^{1.5})H_b{}^2 \cos^{0.6}(\phi_b - \theta)\sin^{0.6}(\phi_b - \theta)$	45°	34°
Bailard	$Q_s = [0.05 + 2.6 \sin^2 2(\phi_b - \theta) + \frac{0.007u_{mb}}{W}]H^{5/2} \cos(\phi_b - \theta)\sin(\phi_b - \theta)$	45°	52°
Deigaard	$\frac{Q_s}{Q_{s,\max}} = (\sin\{2(\phi_0 - \theta)[1 - 0.4\frac{(\phi_0-\theta)}{90°}(1 - \frac{(\phi_0-\theta)}{90°})]\})^{5/2}$	N/A	50°
Hypothetical	$Q_s = C_{Hyp}H_b{}^{5/2}(\phi_b - \theta)$	90	46°

With the exception of the ‘‘hypothetical’’ formula and the Deigaard formula (which is defined for deep-water wave angles), all of these relations show a maximum in Q_l for waves with breaking angles $(\beta - \alpha_b)$ of 45° if breaking wave height (H_b) is held constant (Figure 2a). Because of refraction, such large breaking wave angles are unlikely for typical wave conditions. However, this does not mean that the high wave angle instability is unlikely to occur. Both H_b and the breaking wave angle (α_b) respond to changes in the shoreline orientation (β), and neither H_b nor α_b can be assumed constant along an undulating shoreline. Plotting Q_l versus deepwater angles $(\beta - \alpha_0)$ shows that, depending on the formula, Q_l is maximized for some angle between 35° and 50° for 2 m, 10 s waves (Figure 110).

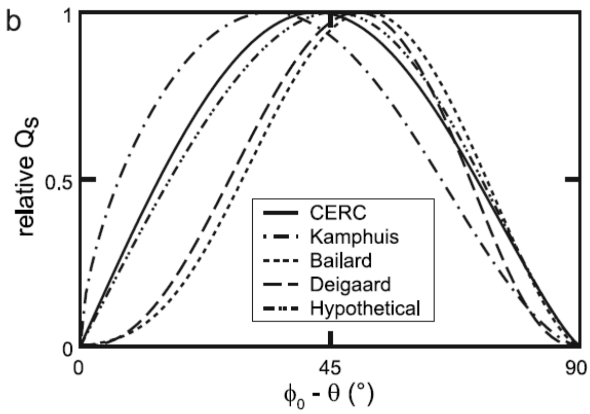

Figure 110 - Relative along-shore sediment transport versus deep-water wave angle (original from Asthon and Murray, 2006 a),

Effectively, contrary to traditional findings, the deep-water angle of wave approach strongly affects plane view coastal evolution, giving rise to an antidiffusional ‘‘high wave angle’’ instability for sufficiently oblique deep-water waves. When along-shore sediment flux reaches the maximum value that occurs for a deep water angle between 35° and 50° (as detected for several common along-shore sediment transport formulae) the coast becomes unstable.

7.2.3. Recent research in numerical modelling of shoreline perturbations

To investigate the long-term effect of this instability, Ashton and Murray (2001) developed a numerical model. This model is similar to others that discretize the semi-empirical CERC relationship for along-shore sediment flux versus breaking-wave height and angle relative to the shore. The model, however, is designed to address morphological evolution on large temporal and spatial scales, and can accommodate arbitrary shoreline shapes. It is not designed to simulate the details of any particular geographical location, but to investigate more generally how shorelines might respond to high-angle waves.

The model simulations presented involve approach angles selected from a probability distribution function (PDF) controlled by two variables. The fraction of waves approaching from high versus low angles, or the proportion of unstable waves, is controlled by U. The other variable, the wave climate ‘‘asymmetry’’, A, determines the fraction of waves approaching from the left relative to the regional shoreline trend (i.e., the fraction of waves that will result in along-shore sediment transport to the right facing offshore) (Figure 111). After a specified duration (typically a simulated day), a new wave approach angle is selected according to the PDF.

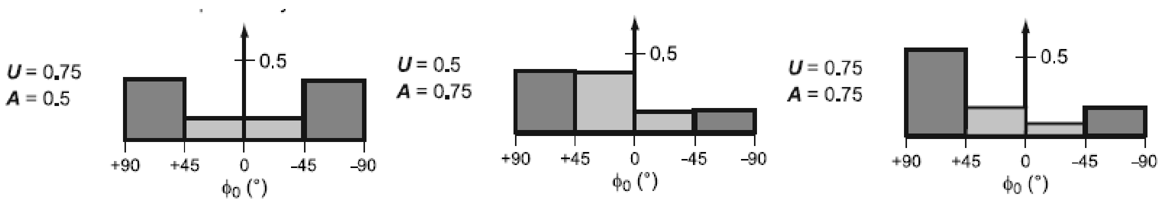

Figure 111 - Sample wave climate probability distribution functions, where U represents the fraction of unstable, high angle waves and A represents the fraction of waves approaching from the left, looking offshore (φ0 > 0).

These two variables, U and A, represent the ‘‘parameter space’’ explored here. Other wave variables, such as height and period, are held constant in and across all simulations shown here (H0 = 2m, T = 8 s, representing a passive margin, open ocean coast such as the U.S. east coast). These wave variables held constant do not affect the instability or subsequent model behaviours; rather, they affect the time scaling of the simulations.

7.2.3.1. Shoreline plane -shape predictions

In all simulations with wave climates predominated by high-angle waves (U > 0.5), undulations arise from the initially straight, slightly perturbed shoreline. At first, these bumps have small wavelengths, on the scale of the model grid resolution. Finite amplitude interactions soon dominate shoreline evolution, and these undulations continue to grow and interact, increasing in wavelength and aspect ratio. Whenever the input wave climate is asymmetric, with more waves approaching from one along-shore direction than another (A >< 0), the growing features translate in the direction of net sediment transport. Simulations suggest five basic types of shoreline response as the wave climate variables U and A are varied (Figure 112).

The first mode is the simplest: whenever more low-angle than high-angle waves approach the shore (U < 0.5), the shoreline flattens (not shown). They have classified the other, more interesting behaviours for high-angle wave climates into four general categories: migrating along-shore sand waves, cuspate bumps, flying spits, and reconnecting spits (Figure 107). Although Figure 112 displays the end-members of this classification scheme, there exists a continuum between these responses.

Along-shore sand waves

For climates with a slight predomination of high-angle waves and a moderate amount of directional asymmetry, simulated bumps translate in the direction of net transport, increasing in size over time (Figure 107b). High-angle waves from the dominant transport direction cause erosion on a bump’s updrift flank. Beyond this inflection point, high-angle waves deposit sediment, driving the updrift inflection point toward the bump’s crest. Much of this deposition occurs downdrift of the crest, with low-angle waves in the distribution spreading it farther downdrift. These along-shore sand waves grow over time by merging; when one migrating feature overtakes another, the two features join, creating a larger sand wave. If the cross-shore/along-shore aspect ratio of the features is significant, ‘‘shadow zones’’ extend from each bump, trapping all the sediment transported past its crest. Gross along-shore sediment transport therefore imposes an upper limit on downdrift migration rates. Both small and large features can trap sediment in their shadow zones at the same rate. However, for the same amount of trapped sediment, a smaller sand wave will translate further downdrift than a larger sand wave; migration rates scale inversely with the plane view area of the feature. Therefore smaller sand waves translate downdrift faster than larger ones, eventually overtaking the larger features and merging with them. This behaviour is similar to that of simulated Aeolian ripples, which is not entirely surprising as a fundamentally similar angle-based instability initiates the evolution of both systems.

Cuspate bumps

When there is little to no asymmetry in the wave climate, features still interact and grow, but do so through an entirely different mechanism. Without a strong asymmetry to the wave climate, features extend in the cross-shore direction faster than they translate along-shore, and do not merge by overtaking one another. Instead, as these ‘‘cuspate bumps’’, extend offshore, they interact by influencing each other’s local wave climates through wave shadowing. As cuspate bumps emerge, slightly larger shapes grow faster than, and at the expense of, their smaller neighbours by outcompeting them for high-angle waves. As a larger bump extends offshore, its tip will experience a relatively large proportion of high-angle waves while shadowing smaller neighbouring bumps from many of the highest-angle waves. Eventually, as a larger bump grows, robbing a smaller neighbour of more and more high-angle waves, it does not just outcompete its neighbour for high angle waves, the smaller bump’s wave climate eventually becomes predominated by low-angles waves and it diffuses away. As these smaller bumps disappear, their mass is added to the neighbouring larger bumps, further reinforcing the positive feedback feeding the larger bumps. Simulations show the development of a series of cuspate bumps of roughly similar spacing and height whenever wave climates are relatively symmetric (Figure 112a). As U is increased, these features increase their cross-shore extent and become more cuspate, changing from sinusoidal undulations (Figure 112c) to more pointed features (Figure 112d).

This increased aspect ratio for higher-angle wave climates arises due to the eventual development of a quasi-steady state in which the transport of sediment toward the cape tips by high-angle waves is approximately counterbalanced by low-angle waves sweeping sediment back toward the embayments. For wave climates with larger proportions of high-angle waves, steeper flanks are required to increase the effectiveness of the low-angle waves transporting sediment toward the embayments. With slight wave climate asymmetries, these features migrate in the direction of net along-shore transport, but do so slowly, and do not ‘‘overtake’’ one another as the along-shore sand waves do. Slight wave climate asymmetries can also increase the ‘‘pointiness’’ of the cape tips.

As bumps grow, the local wave climates along their flanks change because of both wave shadowing and the change in the shoreline orientation itself. A rotated shoreline feels a different proportion of high- and low-angle waves than one with the global average orientation. Ultimately, the local wave climates along the flanks become predominantly low-angle. These locally low-angle waves explain why new, small bumps do not continue to form along the flanks of larger bumps: A little bump superimposed upon a larger one will feel a different wave climate than the large bump itself.

Spits

For more asymmetrical wave climates, spits begin to extend off of the ends of growing cuspate bumps (Figure 112e). These seaward extending ‘‘flying spits’’ evolve in a manner similar to that predicted for a single shape influenced by waves from a single high angle (Figure 112). Once formed, spits continue to extend seaward due to sediment deposition in shadow zones behind the spit tip. This shadow zone traps all of the sediment that enters, which tends to be a significant quantity as flying spits only occur in strongly asymmetrical wave climates (Figure 112a). Because the spits themselves represent relatively small quantities of sand, and they extend at rates determined by gross along-shore sediment transport, spits extend offshore at rates much faster than the migration rate for cuspate bumps. r toward, and eventually reconnect with, the mainland.

Spits also interact and eliminate one another, increasing in cross-shore extent and wavelength over time. Rapid spit extension tends to block downdrift neighbours from the dominant waves. Within the protected lee of the flying spits, waves are effectively blocked from both the dominant high-angle direction and from all low angles. Consequently, wave climates in the lee are typically dominated by high-angle waves approaching from a direction opposite to that of the net along-shore drift. This leads to the formation of ‘‘reverse’’ flying spits off of both the mainland coasts and on the landward face of the main spit. Sometimes, the reverse spits off of the mainland can fuse with the main spit, enclosing a lagoon (Figure 112e). Between the parameter space where cuspate bumps and full-fledged flying spits form, slightly different evolution occurs, generating features we have termed ''reconnecting spits'' (Figure 112f). As with flying spits, spit heads form off of the end of the initial cuspate bumps.

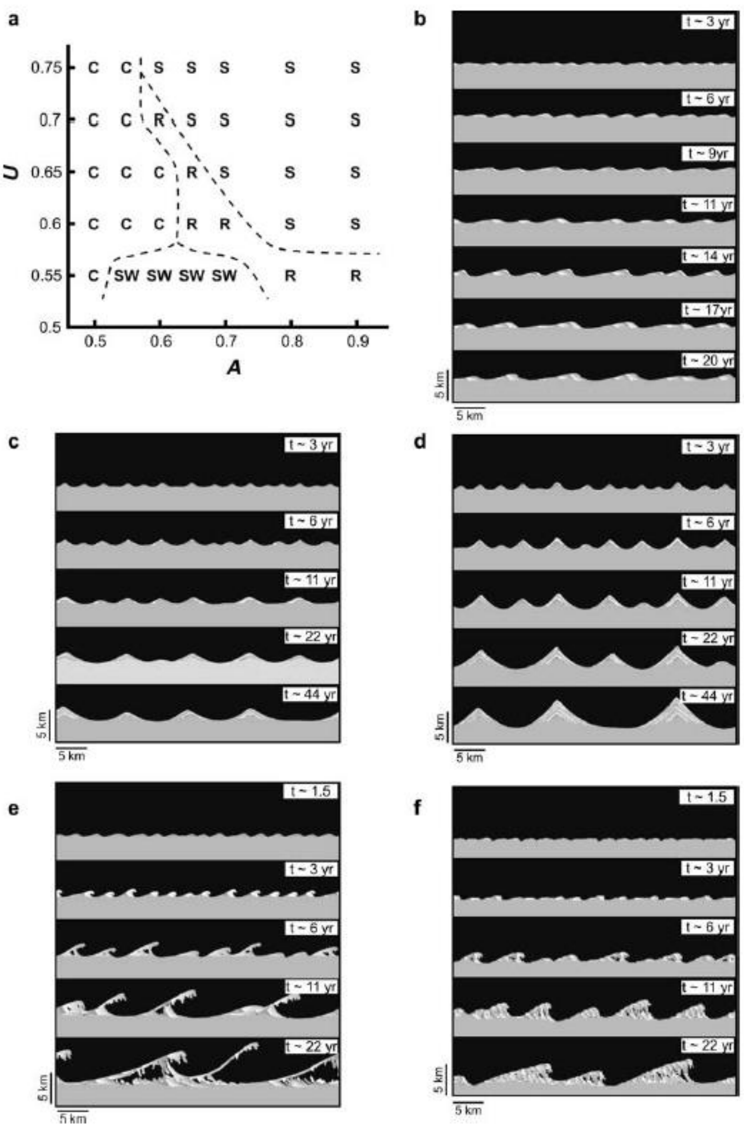

Figure 112 - (a) Different modes of simulated shoreline response as U and A are varied. C represents cuspate bumps, SW represents along-shore sand waves, R represents reconnecting spits, and S indicates flying spits. Also shown are progressive stacks of the plane view model domain demonstrating typical simulation responses: (b) migrating along-shore sand waves (SW, A = 0.65, U = 0.55), (c) subtle cuspate bumps (C, A = 0.5, U = 0.6), (d) more pronounced cuspate bumps (C, A = 0.5, U = 0.7), (e) flying spits (S, A = 0.7, U = 0.65), and (f) reconnecting spits (R, A = 0.7, U = 0.6). Cells along the shoreline are plotted with a shading brightness proportional to the fractional amount of sediment within the cell. Sediment deposited contemporaneously is plotted with the same colour. Animations of these simulations can are in the auxiliary material. (from Ashton and Murray, 2006a)

7.2.4. Net sediment flux and shoreline instability and diffusivity

Ashton and Murray (2006a) presented an interesting approach to gain into stability and instability, by considering the effect of the total wave climate on shoreline diffusivity.

As known, for a nearly straight coastline, coastline evolution can be described by a linear diffusion equation, where the diffusivity is either positive (stable) or negative (unstable) (Ashton and Murray, 2006a, their Eq. 8). Every approaching wave condition contributes to sediment transport and the consequent evolution of the coastline. The overall effect of a wave climate on a coastline can be determined from the net diffusivity, μ_{net} (ms^{-2}), calculated from the sum of the individual diffusivities induced by each wave condition (analogous to the LDR approach of Walton and Dean, 2010), and from a dimensionless "stability index", Γ, that measures the competition between stability and instability (Ashton and Murray, 2006b). They use these indices to quantify the behaviour and state of a coastline under the influence of a particular wave climate.

For each wave at each location along a coastline, individual along-shore sediment flux values are calculated using their formulation of the long-shore sediment transport rate (obtained from the CERC formula), and individual diffusivity values are calculated with respect to the local coastline orientation using the shoreline diffusivity equation obtained by Ashton and Murray (2006a, their Eq. 8; 2006b). Summing over individual fluxes and diffusivities at each coastline location over n wave events gives the net flux and diffusivity, respectively:

$$Q_{net} = \frac{\sum_{i=1}^{n} Q_i \Delta t_i}{\sum_{i=1}^{n} \Delta t_i} \tag{7.1}$$

$$\mu_{net} = \frac{\sum_{i=1}^{n} \mu_i \Delta t_i}{\sum_{i=1}^{n} \Delta t_i} \tag{7.2}$$

The "stability index", Γ, is given by:

$$\Gamma = \frac{\sum_{i=1}^{n} \mu_i \Delta t_i}{\sum_{i=1}^{n} |\mu_i| \Delta t_i} \tag{7.3}$$

where Δt_i (s) is the time step.

Γ ranges between 1 for a fully low-angle wave climate and -1 for a fully high-angle climate. Mapping Γ along a coastline for different wave climates elucidates the nature of the response of a coastline to those wave climates (Ashton and Murray, 2006b). The authors have used calculations of Γ to quantify the behaviour of coastlines characterized by capes and spits that have grown under an anti-diffusive wave climate in contrast to those formed under a different, more diffusive wave climate. They subsequently investigated how μ and Γ changed during the transition from anti-diffusive to diffusive wave climates in order to reveal how domains of erosion and deposition would change along a coast with changing wave climate.

7.3. Modelling unstable shoreline: analytical and numerical approach

As exhaustively seen in previous chapters, one-line contour models are largely used to predict large-scale shoreline evolution. Traditional one-line investigations assume that α_b and H_b are constant along an undulating shoreline. Assuming small breaking wave angles, and considering the littoral drift as given by the CERC formula, yields the diffusion equation, which traditionally predicts that all perturbations to a straight coast will flatten over time at a rate independent of wave angle.

Wang and LeMehaute (1980) warned that if the small breaking angle assumption did not hold, the diffusion equation could lead to an unstable shoreline for breaking wave angles greater than 45°.

In this regard, according to various expressions proposed in literature, the diffusion coefficient is intensely dependent on the breaking wave characteristics, wave height, H_b, wave direction, α_b, and the dimensionless empirical coefficient in the long-shore sediment transport rate formula, K (for which deep discussions have been made in previous chapters).

Walton and Dean (2010), proposed a modelling of the diffusion coefficient of the following form (called the "classical approach"), considering the long-shore transport rate given by the CERC formulation:

$$\varepsilon = \frac{K g^{0.6} H_0^{12/5} T^{1/5}}{8(s-1)(1-n)2^{1.4}\pi^{0.2}\gamma^{0.4}} \frac{1}{(D_c + D_B)} \cos\big(2(\beta - \alpha_0)\big) \tag{7.4}$$

In which it is seen the ε coefficient depending on the off-shore wave characteristics. Particularly, the classical approach does not account for the dependence of H_0 and α_0 on β.

Ashton and Murray (2001, 2006a,b) proposed their formulation for the diffusion coefficient, still modelling the littoral transport as the CERC formulation. In this new approach the wave height at breaking is not constant, i.e., depends on the orientation of the coastline, and additionally, the small incidence angle hypothesis is not more valid. Under these assumptions the diffusion coefficient reads:

$$\varepsilon=\left(\frac{\sqrt{g\gamma}}{2\pi}\right)^{1/5}KH_0^{12/5}T^{1/5}\frac{1}{(D_c+D_B)}\left\{\cos^{1/5}(\beta-\alpha_0)\left[\cos^2(\beta-\alpha_0)\right.\right.$$
$$\left.\left.-\frac{6}{5}\operatorname{sen}^2(\beta-\alpha_0)\right]\right\} \qquad (7.5)$$

Shoreline diffusivity decreases from a maximum for waves approaching directly onshore, passes through zero at the angle maximizing Q_l, and becomes negative for even more oblique wave angles. According to Ashton and Murray (2006 a,b), this new shoreline evolution equation, as opposed to the Pelnard-Considére formulation, accounts for all of the changes to wave properties due to simple wave refraction over shore-parallel contours. The authors states that the classical modelling overpredicts shoreline diffusivity. Overprediction will be particularly pronounced for long-period swell waves that significantly increase their heights as they shoal. This could explain the apparent strong period dependence of the diffusivity suggested by Falqués (2003). As shown by Eq. (7.4), the actual diffusivity only weakly depends upon wave period; the period dependence described by Falqués strictly pertains to the overprediction of shoreline diffusivity by previous methods.

Anyhow, regardless the less or more correct assumption in describing the shore diffusion, it is seen the coefficient to be extremely dependent on the deep water wave angle $\beta-\alpha_0$. This dependence can lead the diffusion coefficient to become negative for wave angles >45°.

7.3.1. Analytical modelling of negative shoreline diffusion

Lets' consider the homogenous Dirichlet BVP problem, introduced in Chapter 5, of which the general solution was in the form of Eq. (5.35). In the general solution it is seen the time function to be an exponential function, in which compares the diffusion coefficient ε. The shoreline response strictly obeys to the sign of the coefficient. If the diffusion coefficient is considered positive, the response of the shoreline to an external perturbation of the system is to damp out any protuberance of the initial shoreline position. The positive sign of diffusion occurs when in stable conditions, in other words when the wave angle is less than 45°.

In this Chapter, we want to focus on the case of negative diffusivity coefficient, which occurs when in unstable conditions ($\alpha_0>45°$).

What does it means, in a mathematical point of view, to have a negative diffusion?

By representing the initial condition $f(x)$in terms of a sine Fourier series, we see the initial shoreline made up on a series of n components characterized by a certain frequency, particularly, small bumps or holes will be characterized by the lower frequencies. When we enter in Eq. (3.35) with a negative diffusion, the response is to enhance the lower frequencies of the shore, therefore, bumps will accrete and holes erode. This effectively resembles what happens in an unstable shoreline condition. However, the negative diffusion tends to a lack in a stationary condition: mathematically, in fact, the shoreline is not able to attain an equilibrium condition, and the result is of a continuous enhancing of initial frequencies.

Although in physics the mathematical modelling here proposed means nothing, it is able to provide, in a simplified manner, an interpretation of evolution of shoreline instabilities in the long-run, that have been recognized in various studies in literature since the ‘50s.

7.3.1.1. Modelling a beach bump under unstable condition

Let’s consider a straight coastline of 1 km length, initially perturbed by a small bump of 20 cm (Figure 113). The coastline has fixed limits at x=0 and x=1000m.

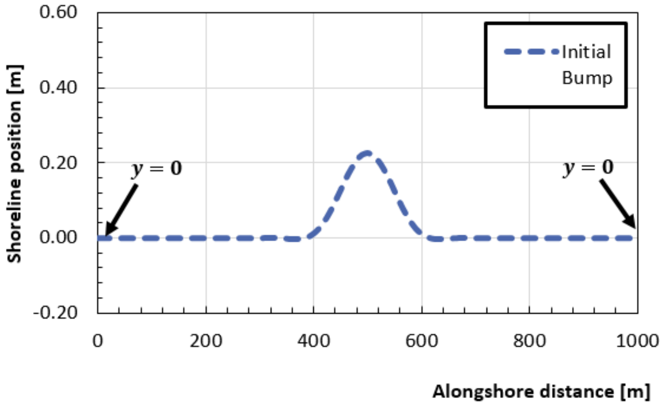

Figure 113 – definition sketch of a straight coastline of 1 km length, initially perturbed by a small bump of 20 cm, with fixed bounds.

The analytical solution is determined and the shoreline response is analysed by varying the sign and magnitude of the diffusion coefficient. Moreover, the analytical solution is compared with the corresponding numerical modelling carried out with GENESIS (Figure 114), in with the changing in sign and magnitude of the shoreline diffusivity is obtained by varying the off-shore wave angle.

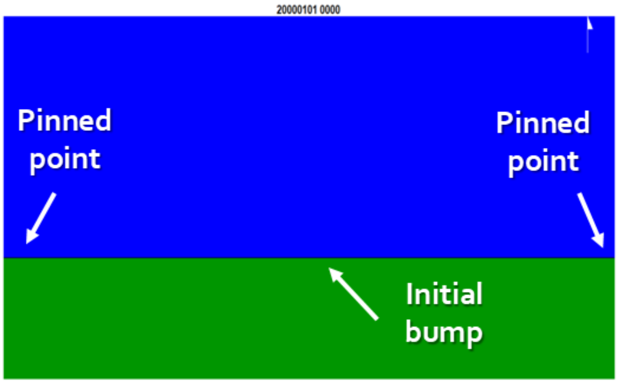

Figure 114 – modelling of the coastline in GENESIS.

In Figure 115 are displayed results. It is seen that with the increasing of the off-shore wave angle, which ranges from 0 to 80°, the initial bump tends to grow when arriving at high wave angle (>45°). Particularly, it is seen the numerical solution to fit properly the analytical one, confirming the absolute power of the simple one-line theory to predict shoreline evolution.

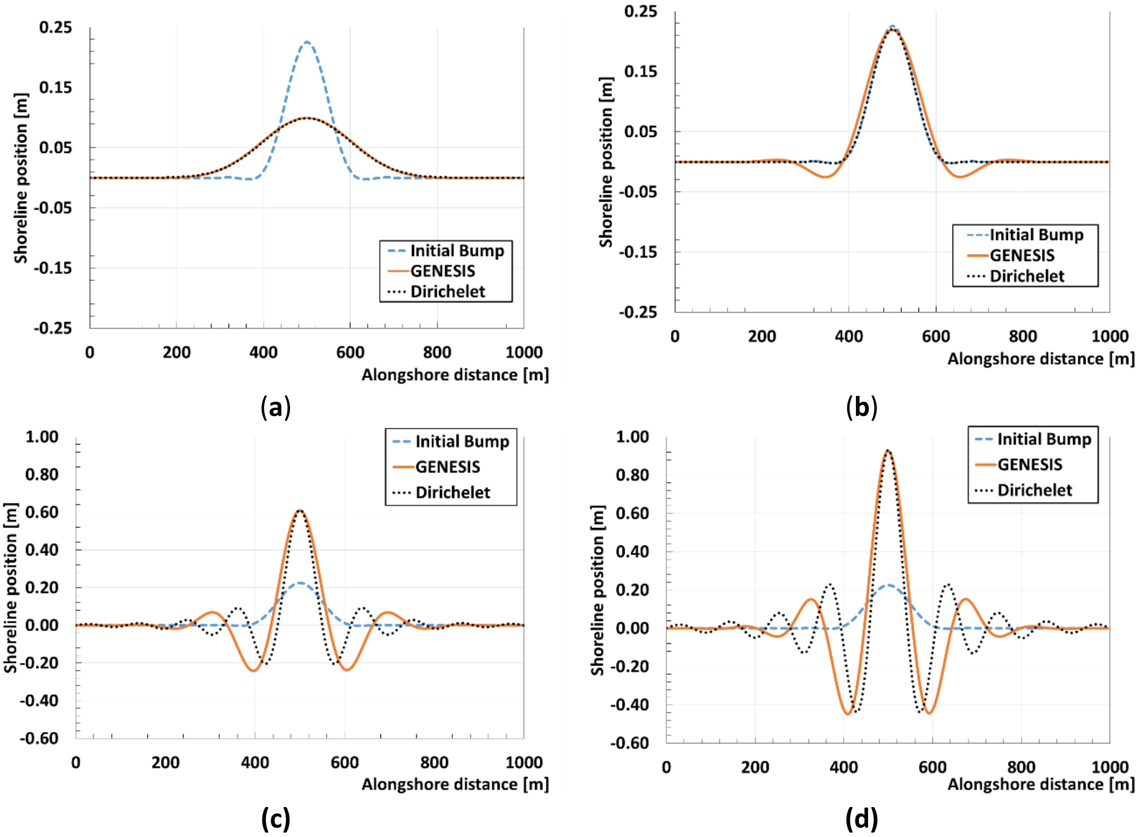

Figure 115 – evolution of an initial bump under different wave conditions. (a) 10° (b) 50° (c) 70° (d) 80°.

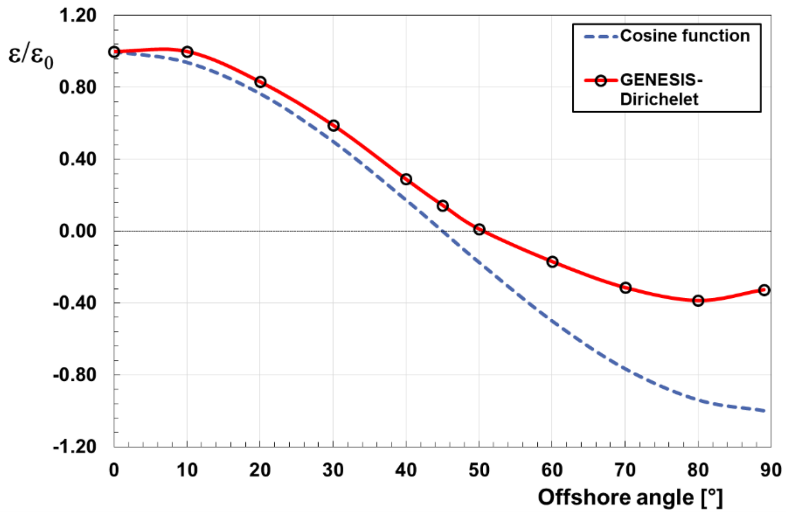

Figure 116 – diffusivity values with varying off-shore angle and comparison with the classical modelling of the diffusion coefficient given by a cosine function

Figure 116 depicts the diffusion inversion predicted by the numerical and analytical modelling. It is seen that diffusivity attains to negative values for wave angles around 50°-51°, slightly larger than the values predicted by the classical long-shore transport formulations.

7.3.1.2. Modelling a sinusoidal shoreline under unstable condition

The simple case to model is an initial slightly sine-undulating shoreline. For this special case, the beach has a sinusoidal variation in shoreline position, so a single initial frequency is given. The initial condition is $y(x,0) = A\cos\sigma x$ where A represents the amplitude of the rhythmic form such as cusps along the beach, and σ denotes the wave number of the shoreline oscillation or cusp. The quantity σ can be expressed also as $2\pi/L$, where L is the beach cusp wave length.

We considered a numerical modelling carried out with GENESIS, for a domain length of 12 km, fixed limits. The initial amplitude of the shoreline is equal to 10m while the undulation wave length is of 2000m. The simulation period is fixed at 100 years.

In Figure 117 is depicted the stable case, in which, with an off-shore wave angle of 10° (positive diffusivity), the initial frequencies of the shoreline are damped out.

On contrary, Figure 118 shows the unstable case of a high off-shore wave angle of 80°, which causes a negative shoreline diffusion. As shown, the initial frequencies are accreted.

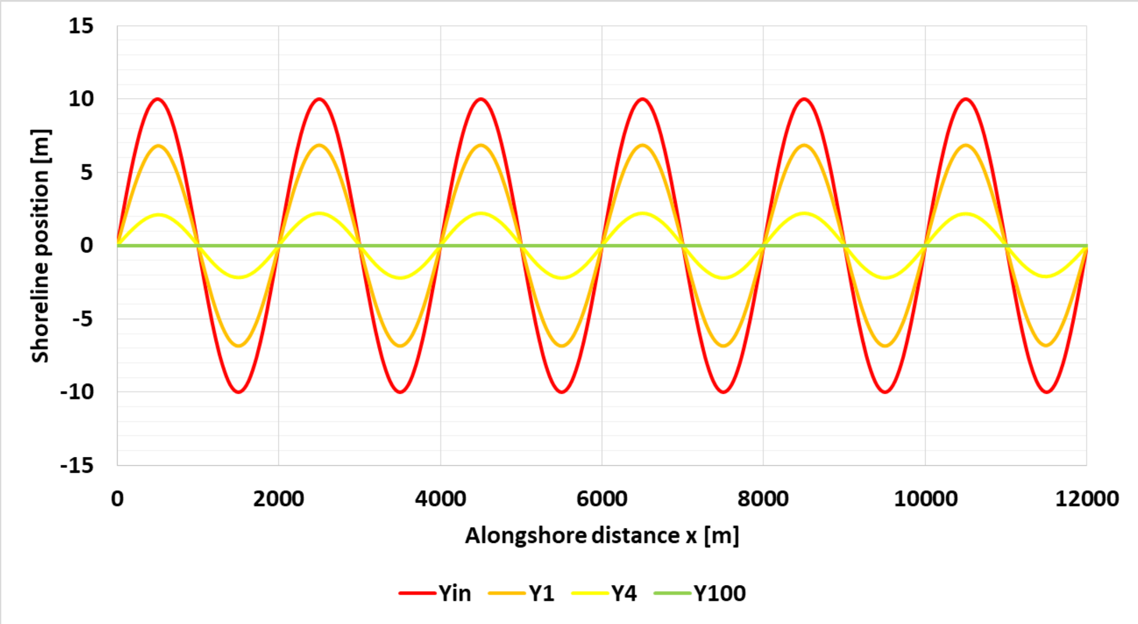

Figure 117 – evolution of an initial sine shoreline with positive diffusivity

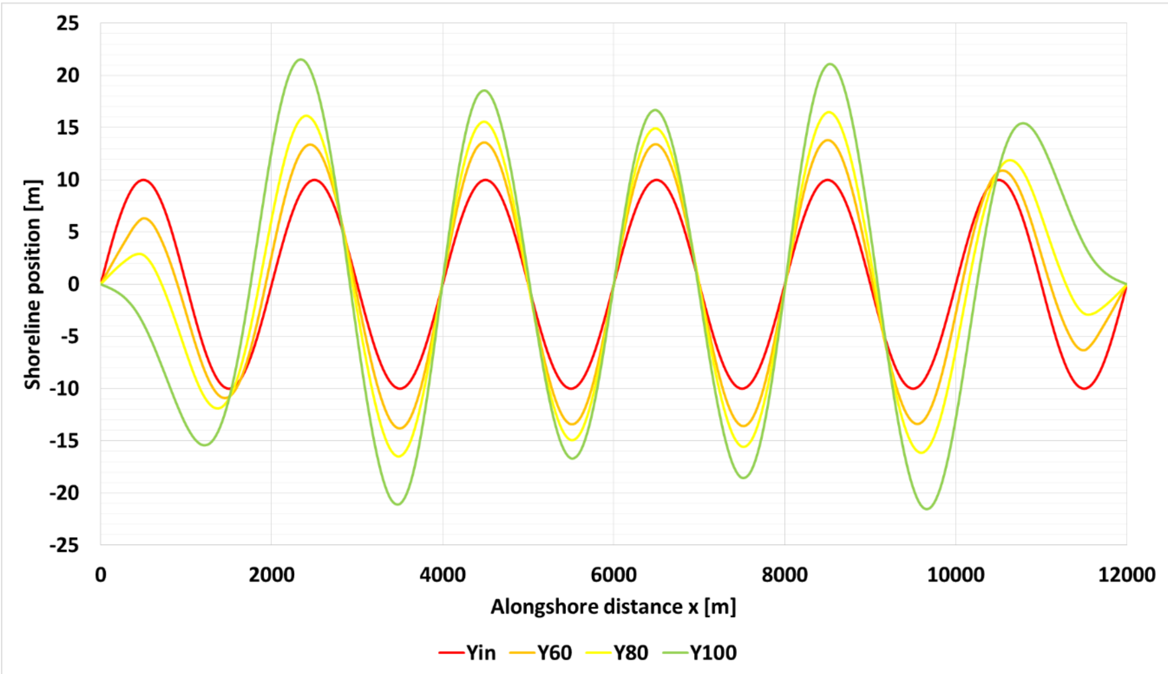

Figure 118 – evolution of an initial sine shoreline with negative diffusivity

7.4. Negative diffusion in littoral transport: shape and asymmetry of the Littoral Drift Rose

The general principle behind the LDR concept is that knowing the azimuth of the seaward facing normal to the shoreline at a given location, and assuming the area of coast represented by the LDR is exposed to the same offshore wave climate, the magnitude and direction of the net (or gross) littoral drift can be found using the LDR for the shoreline area represented.

As discussed in previous Chapters, from the LDR graph, the littoral transport rate for any given shoreline orientation can be determined by entering the plot with the seaward directed normal of the shoreline orientation, and reading off the total positive, total negative, and net littoral drift values. Moreover, it is worth highlighting that since Eq. 4.49 is derived from the well-known CERC formula (SPM, 1984), it is seen the littoral drift, for a given wave angle, to be proportional to sin $(2(\beta\text{-}\alpha_0))$. Consequently, the net drift rose average for a real wave climate has lobes that cause the magnitude to vary in a similar manner as sin $(2(\beta\text{-}\alpha_0))$.

Moreover, to highlight LDR properties, as shown in previous chapters, it is seen from that the graph exhibits a “node”, which represents no net transport. Moreover, the Total LDR can be summarized into a single wave component, equivalent to the whole climate in terms of littoral transport. Thus, the net littoral drift resulting from many deep water waves propagating from arbitrary directions and with arbitrary wave heights can be condensed into a form that is representative of a single wave propagating from a single direction.

7.4.1. LDR use for gain insight into stable and unstable shorelines

One key property of the littoral drift rose is to gain insight into the stability or instability of the coastal segment investigated. As discussed in and Walton and Dean (1973), the littoral drift rose can lend itself to a geomorphic characterization of the shoreline and to the predicted damping (or growth) of natural or man-made perturbations that occur at the shoreline. In the scenario where one predominant component of wave action occurs orthogonal or near orthogonal to the general shoreline orientation, a LDR of the type shown in Figure 119a results where the positive drift lobe of the net LDR is to the right of the negative lobe. This is the most common type of LDR on the open coast, where longer fetches lie normal to the shoreline, leading to damping of natural or man-made perturbations to the shoreline.

In the less common case where long fetch lengths for wave growth and/or predominant wave energy directions exist more parallel to the shore and short fetch lengths (and/or non-dominant wave energy directions) exist perpendicular to the shore, an unstable littoral drift rose results in which the negative (net) drift lobe of the rose lies to the right of the positive (net) drift lobe. Figure 119b shows an extreme example of an unstable shoreline scenario where the wave climate consists of two equal but opposite wave components parallel to the general shoreline orientation. For this scenario, a perturbation in the shoreline (however initiated) is unstable and grows (i.e. see Walton and Dean,1973).

Walton and Dean (2010) show a ubiquitous example of this physical situation for an elongated bay/lagoon where numerous cuspate features dominate the shoreline. The authors have postulated these features to originate from an initial perturbation of the shoreline (say a stream delta or barrier overwash) that continues to grow (under the ‘‘unstable’’ LDR type scenario) rather than damp out.

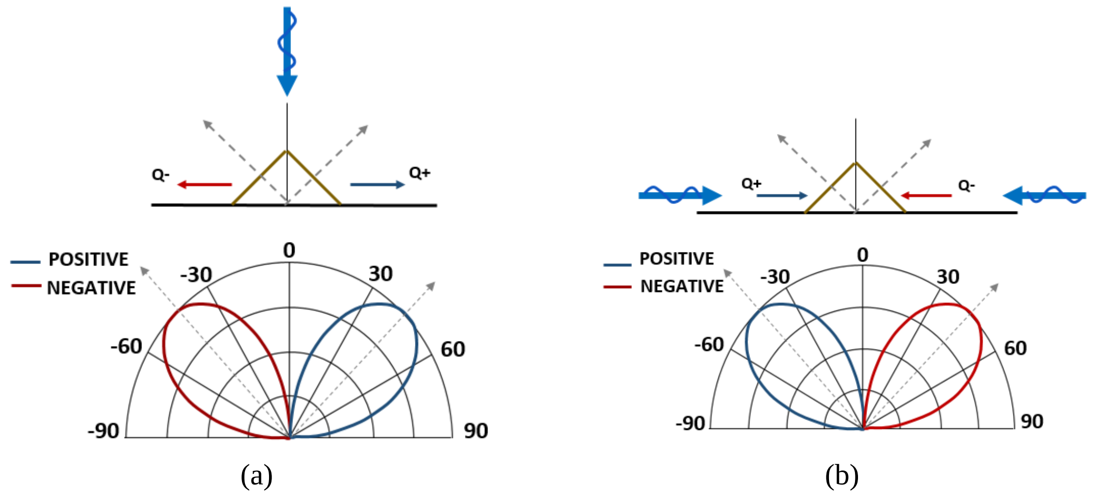

Figure 119 – (a) Stable littoral drift rose. Note blue line (positive drift) lobe of LDR is on the right side of diagram. (b) Unstable littoral drift rose. Note blue line (positive drift) lobe of LDR is on the left side of diagram.

As wave angles were assumed ‘‘small’’ by Pelnard-Considére (1956) in his diffusion formulation, only the former ‘‘damped’’ (positive sign) case was considered where (for wave angles <45°) it can be shown using the LDR approach that stable shoreline conditions result. As stated by the authors, a positive sign for the diffusion coefficient is utilized for the typically encountered ‘‘stable’’ or ‘‘damped’’ behaviour, while the minus sign represents the more rarely encountered ‘‘unstable’’ behaviour which was shown to occur for large wave angles by Walton (1973) and Walton and Dean (1973).

Within the work presented by Ashton and Murray (2006 b), they compile wave metrics of coastal stability while rotating through different shoreline orientations, an analysis that resembles that of ‘‘littoral drift roses’’ presented by Walton and Dean (1973; 2010), where deep-water wave values are used to compute net and gross sediment transport for a range of hypothetical shoreline orientations.

According to Ashton and Murray, although Walton and Dean do not comment on the root distinction between stable and unstable climates, they provide examples of both. Looking at these examples in terms of the change in net Qs, for the sample stable climate $\partial Q/\partial \theta > 0$, and for the unstable climate $\partial Q/\partial\theta < 0$. At some extent, they are alluding to the high-angle wave instability. Anyhow, Ashton and Murray stated that the LDR concept obscures two important aspects of the shoreline instability: first, they suggest that the magnitude of the fluxes, and not the magnitude of the flux gradients, determines shoreline stability. Moreover, although null (or ‘‘nodal’’) points excellently illustrate negative sediment budgets, ‘‘null’’ points are not necessary for shoreline instability. The unstable climates presented by Walton and Dean will cause instability not just at the point of zero flux, but along a larger section of the coast where $\partial Q/\partial\theta < 0$. Ashton and Murray concluded that the LDR concept and its unstable "null point" remains a special case of the more general high wave angle instability.

Nevertheless, according to the present study approach, the LDR concept represent a powerful help in understanding the possible occurrence of instabilities at a certain stretch of coast. No one in literature have further presented its potentials, clarifying to what extent the simple approach of the LDR concept could help engineers in understanding peculiar unstable features of wave climates, and so of long-term coastal evolution.

7.4.2. Comparing different LDRs of the Italian Seas

It is clear that the unstable condition is common for elongated water bodies, where long fetch lengths for wave growth and/or predominant wave energy directions exist more parallel to the shore and short fetch lengths (and/or non-dominant wave energy directions) exist perpendicular to the shore. An example has been provided by Walton and Dean (2010) in examining wave climates of the Florida coasts (Figure 120 and 121).

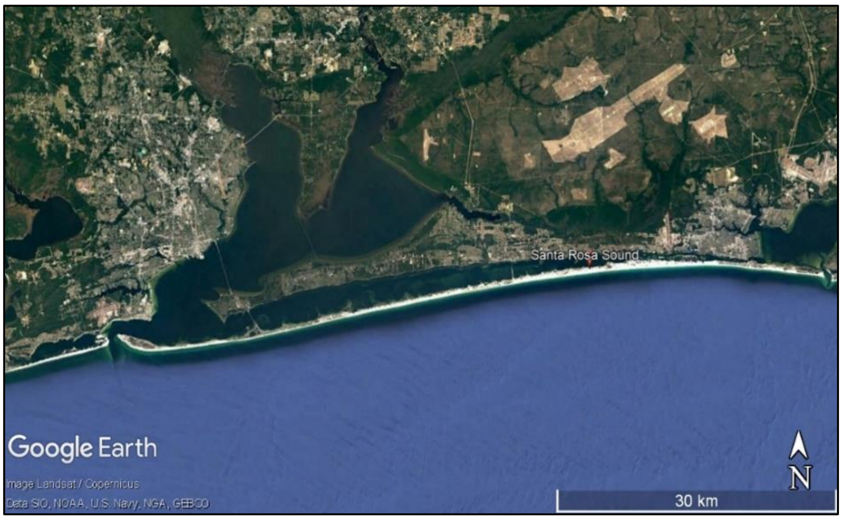

Figure 120 – the elongated bay/lagoon of Santa Rosa, Florida (US)

These unstable conditions found by Walton and Dean, and recently further analysed by Ashton and Murray (2006 a,b), can be detected also for the Italian seas, particularly for the Adriatic sea, which presents the same characteristics of the unstable case studies analysed in literature.

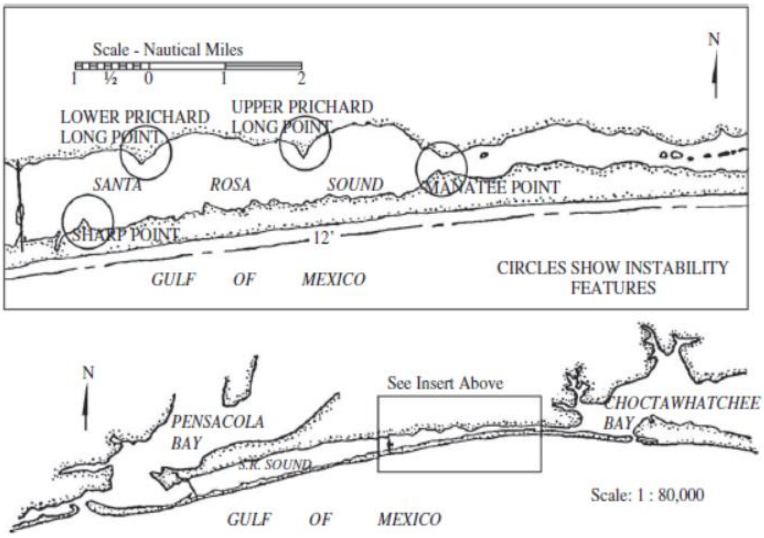

Figure 121 - Instability cuspate features in Santa Rosa Sound, Florida (upper panel encompasses the rectangle in the lower panel). (from Walton and Dean, 2010)

As shown in Figure 122, the Adriatic Sea resembles an elongated lagoon, in which longer fetches lies quite parallel to the shore, while shorter fetches are normal to the shore.

Figure 122 – the Adriatic Sea

According to the LDR approach, the birth of unstable conditions on a certain stretch of coast, and consequently the formation of unstable plane shapes, will be clear in the light of the null-type of the LDR graph. Therefore, for the case of the Adriatic Sea an unstable LDR is expected.

Anyhow, there could be the possibility that, even if longer fetches are more oblique to the shore, a stable LDR results, instead of the expected unstable one. As will be shown in the following, in this case, the unstable components are not predominant within the wave climate, they simply superimpose to the stable components (generated from the smaller fetches), which instead prevail in terms of frequency. This is due to drawback detected by Ashton and Murray (2006b) in examining the LDR potentials in the prediction of the High-wave angle instability.

However, although unstable wave components are not able to generate an unstable LDR, their presence determines a change in the LDR shape. Two different type of LDRs are presented in the following sections, and a comparison is made.

7.4.2.1. The LDR graph for the Tyrrhenian Sea

A stable LDR condition can be detected at the coastal site of Meta di Sorrento, which faces the Tyrrhenian Sea. As shown in Figure 123, for this case longer fetches lie quite normal to the shore; consequently, the predominant mode of wave climate results to be near orthogonal to the general shoreline orientation. As a consequence, the wave climate is of a monomodal type: in this case the more frequent direction originate from a single direction, which is responsible of the long-term sculpting of the coast (Figure 124).

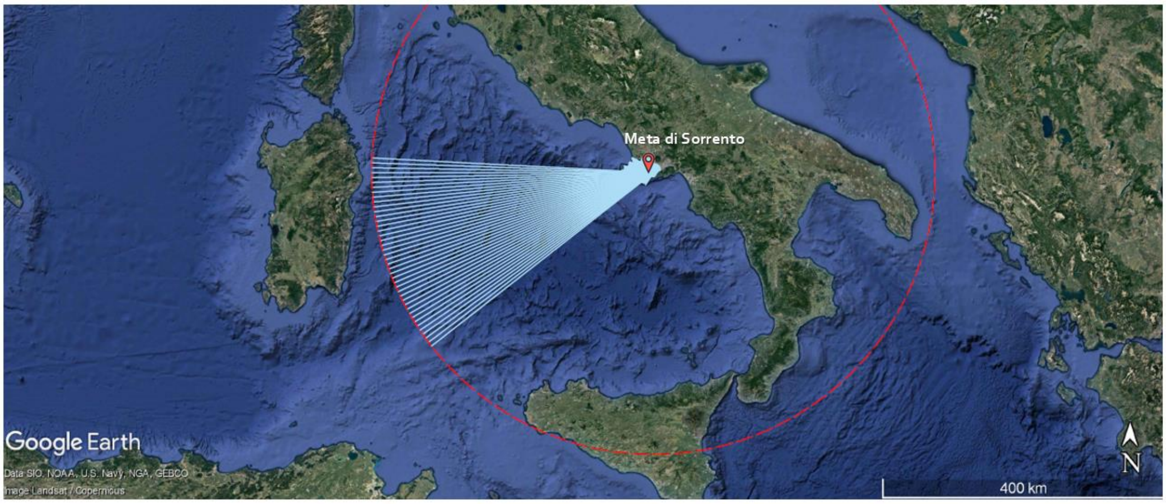

Figure 123 – Fetches of Meta di Sorrento which faces the Tyrrhenian Sea

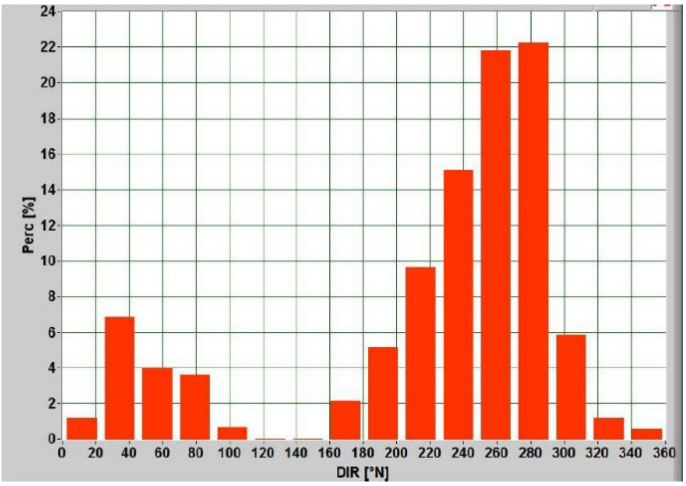

Figure 124 – wave climate directional frequencies for Meta di Sorrento

In Figure 125 is shown the resultant LDR graph: in this case, as expected the stable type is determined, and the graph shows nearly symmetrical lobes with the positive (net) littoral drift to the right to the negative (net) one. The equivalent wave component, calculated from the procedure suggested by Walton and Dean (2010), has a wave height of about 1m and an equivalent direction, corresponding to the null point of the total LDR, equal to 265°N. Most notably, Figure 125 shows that the equivalent component is able to accurately fit the total LDR, since the net drift rose average for the total wave climate has lobes that cause the magnitude to vary in a sinusoidal manner.

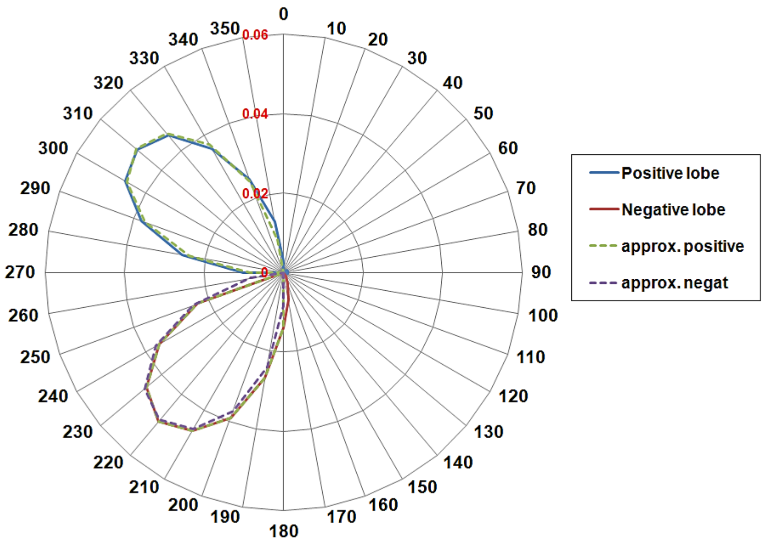

Figure 125 – Littoral Drift Rose of Meta di Sorrento. Solid lines represent the Total LDR (blue line positive drift, red line negative drift), while dashed lines represent the Equivalent rose, given by a sinusoidal component of parameters: $H_{0,eq}$=1m, $T_{p,eq}$= 5s, $\alpha_{0,eq}$=265°N

Particularly, from Figure 125 it is seen that the total LDR do not exhibits asymmetrical lobes: the net drifts varies over the shoreline normal in a sinusoidal manner and so the equivalent climate is able to accurately fit the transport due to the entire wave climate.

7.4.2.2. *The LDR graph for the Adriatic Sea*

Conversely, if we move to the Adriatic Sea, matters look quite different. Focusing on the Molise case of study, presented in the previous chapter, we can see long fetch lengths for wave growth more parallel to the shore, while short fetch lengths perpendicular to the shore (Figure 126). As a result, wave climate have been shown to be affected by an inherent bimodality, with two opposite modes, from 340°N and 80°N respectively (Figure 127).

Figure 126 - Fetches of Molise coast which faces the Adriatic Sea

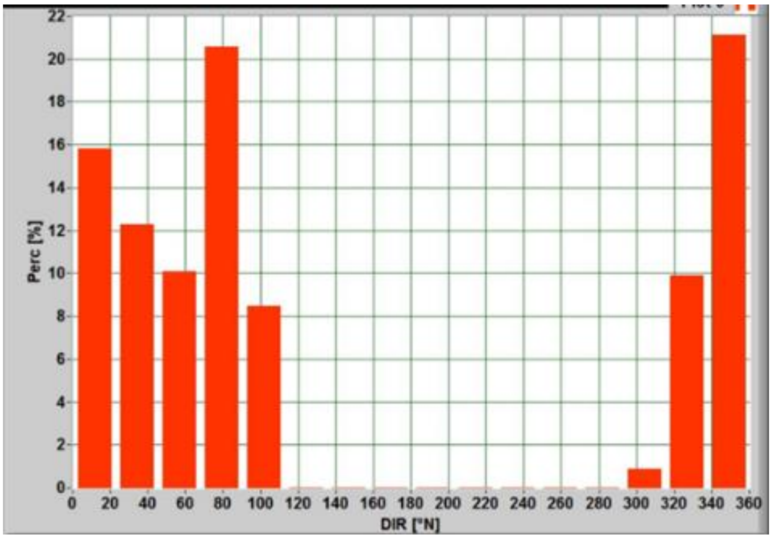

Figure 127 - wave climate directional frequencies for Molise

Surprisingly, the net littoral transport here results in a stable LDR (Figure 128). Anyhow, as shown, the LDR graph, differently from the Meta di Sorrento case of study, here exhibits nearly asymmetrical lobes. The shape of the LDR graph suggests that the magnitude of littoral transport does not vary in a sinusoidal manner.

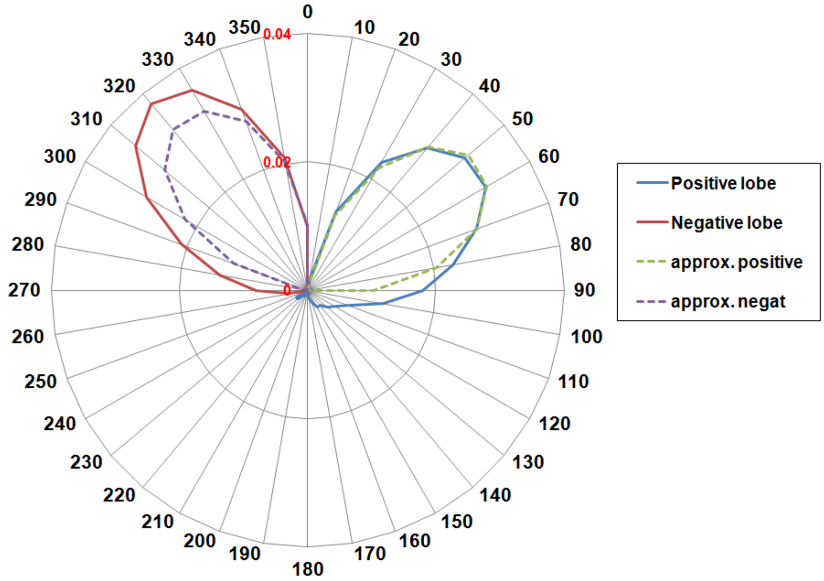

Figure 128 - Littoral Drift Rose of Molise coast. Solid lines represent the Total LDR (blue line positive drift, red line negative drift), while dashed lines represent the Equivalent rose, given by a sinusoidal component of parameters: $H_{0,eq}$=0.83m, $T_{p,eq}$= 5.08s, $\alpha_{0,eq}$=9°N.

As a matter of fact, the approximation given by the single equivalent sinusoidal wave component is not more satisfactorily. In this case, the equivalent wave height is equal to 0.88 m, while the equivalent wave direction is about 10°N, but since the magnitude does not follows a sinusoidal trend, a proper approximation is only for the positive lobe, while, an underestimation of the negative lobe is detected, as shown in Figure 128. This happens because longer fetches lies more oblique to the shore, which generates unstable wave components with a high angle with respect to shore, which could generate a possible unstable condition. This suggests that the unstable waves superimpose to the stable one, and their effect is appreciable depending on the shoreline orientation. In fact, with the scope of determine the unstable components which generate the skewed LDR, we considered a wave climate only made up of the more oblique direction, generated by fetches comprised between 320 and 339°N from the northern quadrant and between 93 and 104°N from the east quadrant.

Considering only the more oblique direction, the resulting LDR graph is determined by two opposite wave components, with different magnitude, from 330°N and 100°N respectively (Figure 129). These two components lead, within the shoreline orientation range of Molise coast (340°N-110°N), to an unstable LDR. The equivalent “unstable” wave component is oriented toward 50°N, (red line in Figure 129). The unstable component detected from the graph can cause, in turn, a negative diffusion zone within coastal stretches nearly orientated towards 50°N.

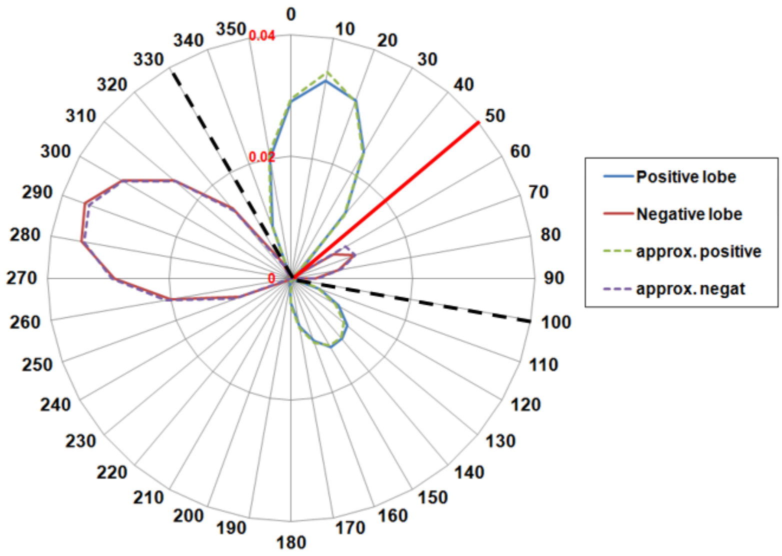

Figure 129 - Littoral Drift Rose of Molise coast computed from the more oblique directions (320-339°N and 93-104°N). Solid lines represent the Total LDR (blue line positive drift, red line negative drift), while dashed lines represent the Equivalent rose, given by two equivalent component of parameters: $H_{0,eq}$=0.91m, $T_{p,eq}$= 5.08s, $\alpha_{0,eq}$=330°N and $H_{0,eq}$=0.56m, $T_{p,eq}$= 5.08s, $\alpha_{0,eq}$=110°N (dashed lines indicates the equivalent directions). The red solid line represent the direction of the unstable component which generates within the shoreline orientation range of Molise coast (340-120°N)

The medium term shoreline analysis of the Molise coast, just presented in the previous paragraph, led us to gather that the unstable components, generated by the longer fetches, are responsible of peculiar aspects of the shoreline evolution. In fact, as shown in Chapter 5, recently (Buccino et al., 2020) analysed the average rate of shoreline change of the entire Molise coast within the reference time-interval 2004-2016, using the Linear Regression Rate (LRR) as indicator. Figure 130 shows the 2004–2016 LRR function, just presented in Chapter 6, but here reported for sake of clearness.

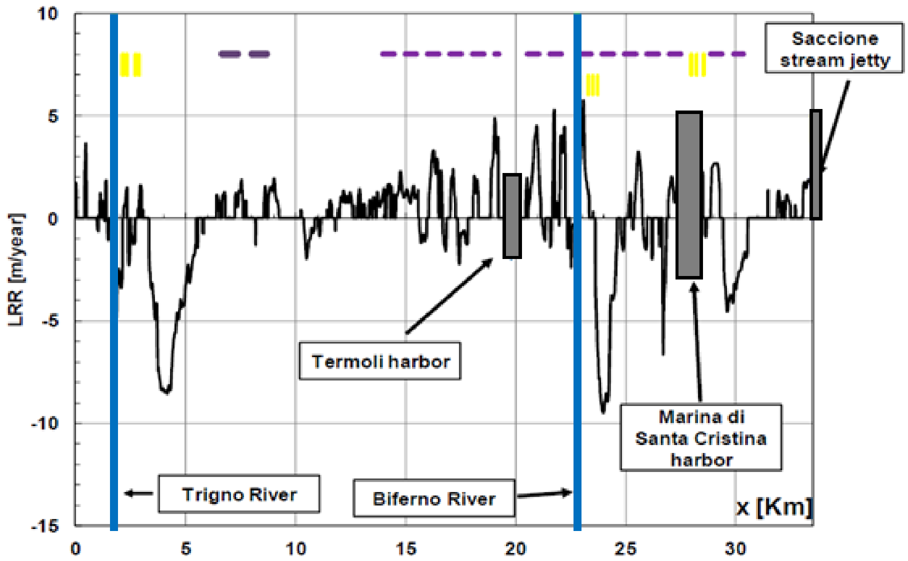

Figure 130 – LRR of Molise coast

As shown in Chapter 6, the stable component is sufficient to explain the bulk of the Molise coastline evolution and the detailed analysis presented for the Trigno river mouth area verified it. Nevertheless, a more accurate analysis revealed that, more recently, the erosion processes widely accelerated, suddenly widespreading to the neighbouring areas of the foremost erosion zones. These latest dynamics are depicted in Figure 131, where the LRR function has been determined by splitting the analysis time window into two parts, from 2004 to 2011 and from 2014 to 2016, respectively.

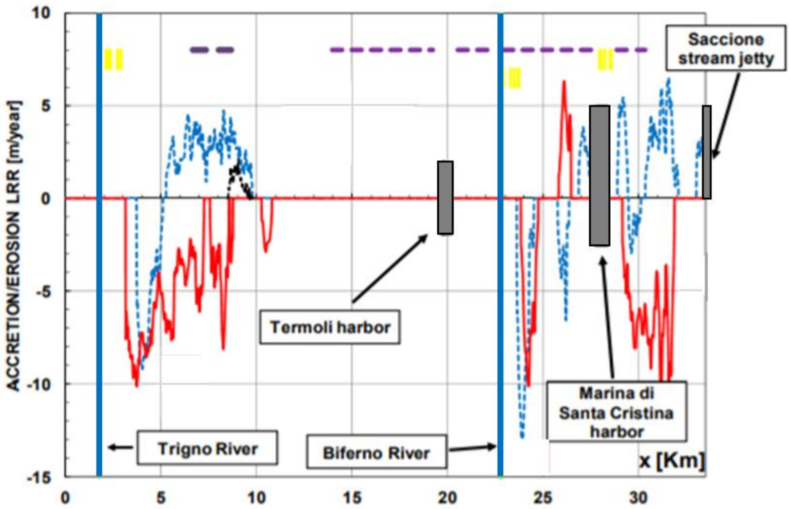

Figure 131 – LRR of Molise coast. Red line 2014-2016; blue dashed line 2004-2011

Figure 131 highlights that accretionary bulges preceded erosional depressions, in the area just south the river mouths (Trigno and Biferno respectively) and also for the area just south the Marina of Santa Cristina harbour. Particularly, as shown in Figure 132, the aforementioned areas affected by these instabilities features have shoreline orientations about 30-40°N, really close to the unstable orientation of 50°N detected from the LDR of Figure 129.

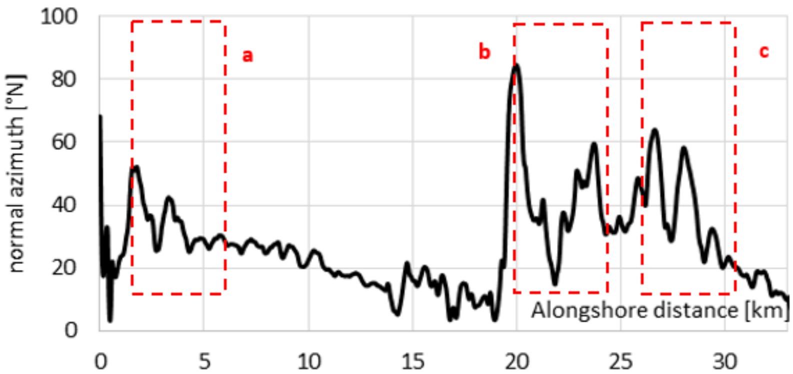

Figure 132 – Normal azimuth along the Molise coast. Area a. Trigno river mouth area, area b. Biferno river mouth area, area c. Santa Cristina Harbour area

This peculiar evolution of the Molise coast can be ascribed to the presence of accretion/erosion sand waves, which follow one another along the shore in the direction of the net littoral drift. These local irregularities of the beach form, appreciable by comparison of beach profiles with time and distance along the beach, can be associated to the negative diffusivity generated by unstable wave components, with a high angle with respect to the shoreline normal. Particularly, according to the analysis of Ashton and Murray (2006a), sand waves occur for climates with a slight predomination of high-angle waves and a moderate amount of directional asymmetry which is just the case of the directional distribution of the Molise wave climate.

7.5. Negative diffusion and breakwaters

Coastal erosion can be limited by two different kinds of actions: soft intervention (beach nourishment) and hard intervention (use of breakwater structures). Breakwaters are structures placed parallel to the coast, dissipating wave energy and slowing offshore sediment transport. In this way, sediment can accumulate behind the structures and allow the shoreline to advance.

This last section of Chapter 7 concerns the interpretation of the morphological response of the shore line behind an isolated breakwater based precisely on the concept of negative diffusivity. According to this approach, a single detached breakwater would behave as a positive to negative diffusivity modifier. In fact, if we have an incident wave climate roughly orthogonal to the shoreline, without any barrier, the shoreline diffusivity would be positive.

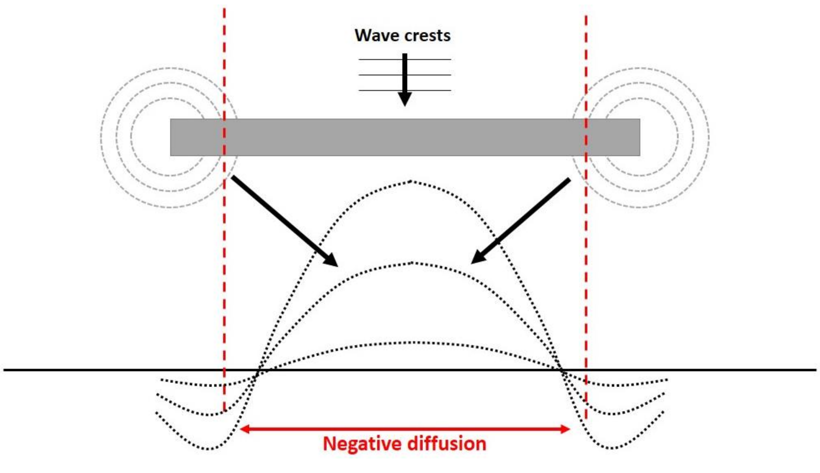

Figure 133 – Definition sketch for the single detached breakwater forming a negative diffusion area

By contrast, positioning a breakwater in front of the shoreline, the rotation of wave direction induced by the diffraction, would produce a negative diffusivity area behind the barrier, due to the large angle of the diffracted waves (Figure 133). Therefore, we could state that the formation of a tombolo or salient behind a breakwater can be interpreted as the enhancement of an initial perturbation of the coast, induced by the negative diffusivity behind the breakwater.

7.5.1. Key role parameters in shoreline evolution behind a breakwater

Basically, three different types of shorelines can develop behind a breakwater or a system of breakwaters.

If the breakwater is close to shore, long with respect to the length of the incident waves, and/or sufficiently intransmissible to the average waves, sand will continue to accumulate behind the breakwater until a tombolo forms; that is, the shoreline continues to build seaward until it connects with the breakwater. If a tombolo forms, long-shore transport is stopped until the entire updrift beach fills seaward to the breakwater and sand can move around its seaward side. The breakwater-tombolo combination functions much like a T-groin. If the breakwater is far from shore, short with respect to the length of the incident waves, and/or relatively transmissible, the shoreline will build seaward, but is prevented by wave action and long-shore currents from connecting with the breakwater. The shoreline bulge that forms is termed a "salient." If a salient forms, long-shore sand transport rates are reduced; however, transport is not completely stopped. The third beach type is termed limited shoreline response in which little beach plane form sinuosity is experienced, possibly due to a lack of adequate sediment supply. The final shoreline configuration and its location depend on the geometry of the breakwater system, the wave environment, the long-shore transport environment, and the amount of available sand. The variability of wave height, period, and direction coupled with the geometry of the breakwater system are all important in determining the final equilibrium plane form of the beach.

Wave heights behind a nearshore breakwater can be significantly reduced. Waves in the lee of a breakwater get there by transmission through the structure if it is permeable, regeneration in the lee of the structure by overtopping waves, and diffraction around the ends of the breakwater. If the structure is a low crested type, the amount of wave energy transmitted over the top of the breakwater increases as the crest decreases. High crest elevations preclude overtopping by all but the highest waves whereas low crest elevations allow frequent overtopping. Generally, low crests allow more wave energy to penetrate into the lee of the breakwater: the higher transmission the lower the shoreline response.

Transmissivity is usually quantified through the transmission coefficient, K_t, which represents the ratio between the wave height just shoreward of the structure (transmitted wave height, Ht) and wave height just seaward of it (incident wave height, Hi). For random waves, the definition of transmission coefficient is usually based on the significant wave height, which, depending on whether it is spectrally or statistically calculated, gives K_t a different physical meaning (Thompson and Vincent 1985). In general, transmissivity is a function of both the structure's characteristics (crest height and width, front slope angle, breakwater's roughness and permeability) and wave parameters (incident wave height, incident wave period, angle of wave attack), and its estimation can be assessed by using number of criteria and procedures based just on these parameters (eg., d'Angremond et al. 1996; Buccino and Calabrese, 2007).

7.5.2. Classical theories for shoreline response behind a detached breakwater

The functional design and prediction of beach response to single and segmented detached breakwaters systems have been the subject of numerous papers and reports (e.g. SPM 1984). A number of these references have been reviewed in Rosati (1990). Most references present morphological information on when tombolos will form and when minimal beach response to breakwater construction can be expected. These conditions are usually specified in terms of the dimensionless breakwater length, where y is the distance from the average shoreline; or the breakwater length-to-wavelength ratio, where g is the acceleration of gravity and T is the wave period. Anyhow, the evolution of the shoreline behind coastal structures is complicated by many factors. It may depend on the geometry of the breakwater, but also on wave conditions, e.g., tidal variation, wave height, and direction and steepness of the incident wave. Grain size and beach slope can also influence shoreline evolution.

The morphological response of shoreline behind a breakwater can be estimated by using simple geometrical empirical criteria, or, more accurately, by using analytical or numerical models which are able to consider the presence of coastal structures in the evaluation of shoreline evolution. In the following a literature review is presented.

7.5.2.1. A review of morphological response by empirical criteria

The examples of simple geometrical empirical criteria for the lay-out and shoreline response of the detached, exposed (emerged) breakwaters are given below (i.e., Harris & Herbich, 1986, Dally & Pope, 1986, etc.):

- for tombolo formation:

$$\frac{Ls}{X} > (1.0\ to\ 1.5) \quad (7.6)$$

- for salient formation:

$$\frac{Ls}{X} = (0.5\ to\ 1.0) \quad (7.7)$$

- for salients where there are multiple breakwaters:

$$\frac{\mathrm{G\,X}}{2Ls} > 0.5 \quad (7.8)$$

Where Ls is the length of a breakwater and X is the distance to the shore, G is the gap width, and the transmission coefficient K_t is defined for annual wave conditions.

These geometrical criteria do not include the transmission; however, the transmission coefficients K_t for exposed breakwaters are usually in the range 0.1 to 0.3. To include the effect of submergence (transmission) Pilarczyk proposes, at least as a first approximation, adding the factor ($1-K_t$) to the existing rules. Then the rules for low-crested breakwaters can be modified to (for example):

$$\text{Tombolo: } \frac{Ls}{X} > \frac{1.0\ to\ 1.5}{1-Kt}\ or\ \frac{X}{Ls} < \left(\frac{2}{3}\ to\ 1\right)(1-Kt), or\ \frac{X}{1-Kt} < \left(\frac{2}{3}\ to\ 1\right)Ls \quad (7.9)$$

$$\text{Salient: } \frac{Ls}{X} < \frac{1}{1-Kt}\ or\ \frac{X}{Ls} > (1-Kt), or\ \frac{X}{1-Kt} > Ls \quad (7.10)$$

$$\text{For salients where there are multiple breakwaters: } \frac{\mathrm{G\,X}}{2Ls} > 0.5\,(1-Kt) \quad (7.11)$$

The gap width is usually $L \le G \le 0.8\,Ls$, where L is the wavelength at the structure defined as: L = T (g h)0.5; T = wave period, h = local depth at the breakwater.

One of the first properly documented attempts to obtain criteria for detached breakwaters including transmissivity was made by Hanson and Kraus (1989). Based on numerical simulations (Genesis model) and some limited verification from existing prototype data, they developed the following criteria for a single detached breakwater:

$$\text{for a salient: } Ls/L \le 48\,(1 - Kt)\,Ho/h \quad (7.12)$$

$$\text{for a tombolo: } \frac{Ls}{L} \le 11\frac{(1 - Kt)Ho}{h} \quad (7.13)$$

Where L_s = length of the structure segment (breakwater), X = n h = distance from the original shoreline (n= bottom gradient), h = depth at the breakwater, H_o = deepwater wave height, L = wave length at the breakwater. These criteria can be used as preliminary design criteria for distinguishing shoreline response to a single, transmissive detached breakwater. However, the range of verification data is too small to permit the validity of this approach to be assessed for submerged breakwaters. In general, it can be stated that numerical models already be treated as useful design tools for the simulation of morphological shore response to the presence of offshore structures. A more complete review of these criteria can be found in Coastal Engineering Manual (CEM, 2003).

7.5.3. Interpreting shoreline response behind a breakwater with the negative diffusivity concept

We stated previously that the formation of a tombolo or salient behind a breakwater can be interpreted as the enhancement of an initial perturbation of the coast, induced by the negative diffusivity behind the breakwater.

> *However, what is the wave condition for which a negative diffusion area will be created behind a single breakwater?*

As deeply discussed previously, the diffusivity attains to negative values for wave angles greater than 45°, consequently, assuming straight and parallel contours, and considering relative depths at breaking of the order of 0.1, the triggering of the negative diffusivity occurs at about 20° at breaking. In other words, with waves approaching at breaking with an angle of 20 °, negative diffusivity phenomena could be induced.

Therefore, with this in mind, the condition for which behind a breakwater the diffracted components have an inclination of about 20° with respect to the shore is obtained when the ratio between the length of the structure and the distance from the shoreline is about 1 (Figure 134). Surprisingly, this result is congruent with most of the indications proposed in the literature for the formation of a tombolo behind a barrier, such as those seen in the previous section.

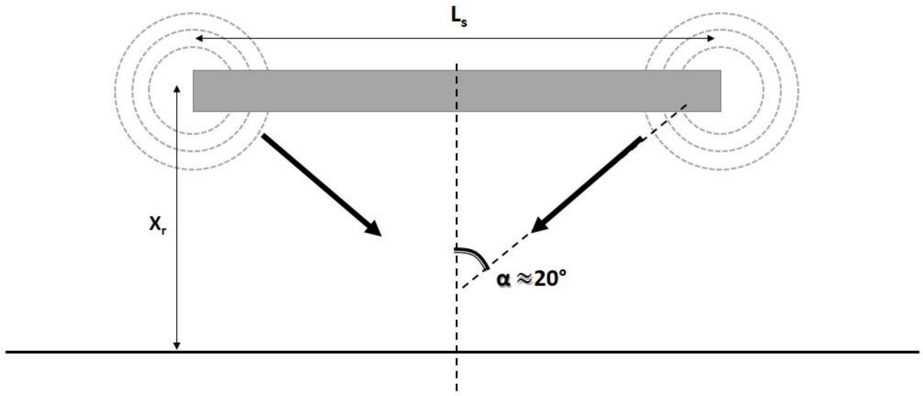

Figure 134 – Definition sketch

Let's consider a straight coastline of 1 km length, initially perturbed by a small bump of 20 cm (Figure 5 of section 7.4). The coastline has fixed limits at x=0 and x=1000m. Moreover, the bump is protected by a single detached breakwater with L_s=80m, and X_r=200m, with a transmission coefficient K_t of 0.4. We have modelled this situation with the software GENESIS, and compared shoreline over time with the corresponding analytical solution with the Dirichlet boundary condition given by a negative diffusion.

Figure 135 shows results and comparisons. Surprisingly it is seen that the shoreline response given by GENESIS follows properly the analytical solution with negative diffusivity.

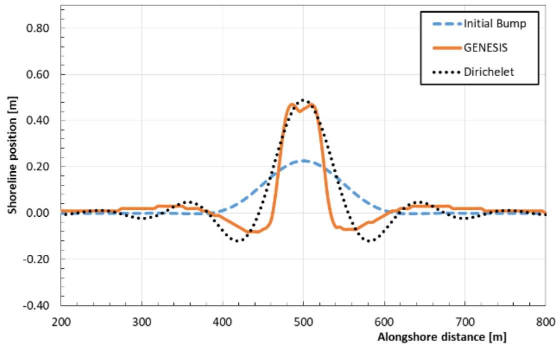

(a)

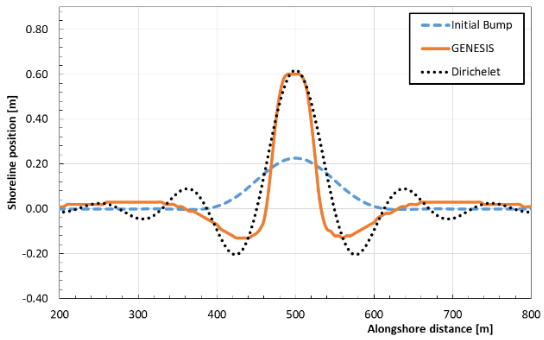

(b)

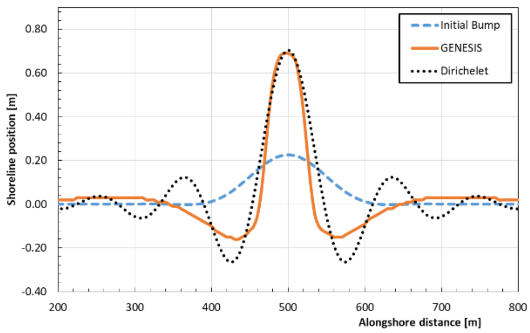

(c)

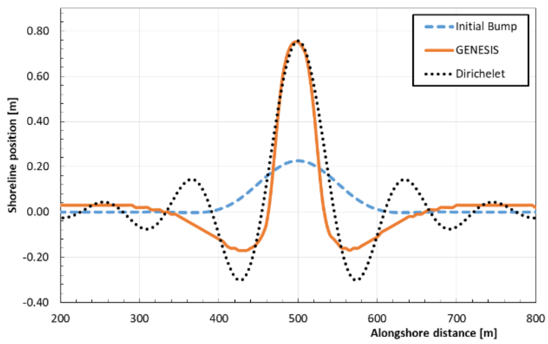

(d)

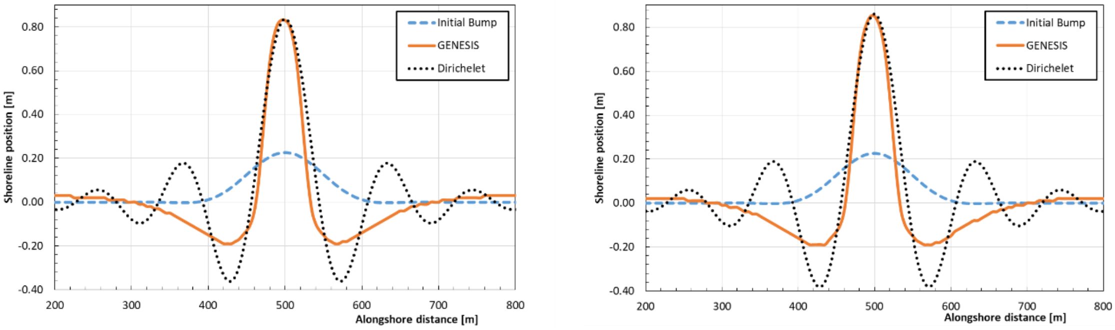

(e) (f)

Figure 135 – Comparison between GENESIS shoreline response behind a single breakwater (Ls=80m, and Xr=200m, Kt=0.4) with an initial bump of 20cm, and analytical solution given by a Dirichlet problem with a negative diffusion coefficient. (a) after 1 year (b) after 2 years (c) after 3 years (d) after 4 years (e) after 8 years (f) after 10 years.

Moreover, what stated seems to affirm that an equilibrium condition does not exists behind the barrier, as opposite stated by Pylartzcick in 2003. Actually, Figure 136, shows that an equilibrium condition is attained at the breakwater. As far the equilibrium condition (the stationary state) is concerned, it will be deepened in the Chapter 8, following the static Equilibrium of bays concept.

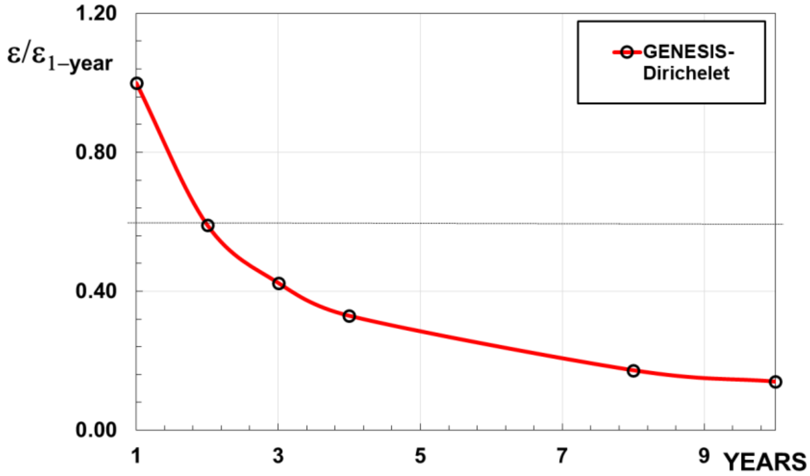

Figure 136 – Time reduction of diffusion

In conclusion that the concept of negative diffusivity represents an intriguing concept of the evolutionary theory of beaches, as on the one hand, it helps us to understand peculiar aspects of medium-term evolution, which with classic theories we would not be able to grasp. On the other hand, we can then interpret the formation of a salient behind a barrier as the exaltation of a perturbation induced by the negative diffusivity of the barrier.

Regarding this last point, then, what would happen if we protected a localized retreat of shoreline with a single detached breakwater? Paradoxically, the negative diffusivity would tend to enhance the setback, and erosion would occur.

This is surprising, but actually this is what happened in many cases, in an inexplicable way. An example is that of the P.E.P. documented by Dean et al., in 1996. In an attempt to reduce beach erosion and wave impact on a protective seawall, an experimental proprietary submerged breakwater (Reef) of 1,260 m length was installed in a water depth of approximately 3 m off the Town of Palm Beach, Florida. To provide a basis for evaluating the effects of this installation, a comprehensive field monitoring program was carried out and included: wave measurements, beach and offshore profiles, settlement of the units, local scour data and information related to the background coastal processes. The profile data documented erosion in the entire monitored area with the greatest erosion landward of the Reef. Particularly, for this reef great transmission coefficients have been measured, ranging between 0.8-0.9.

The erosional trend behind the barrier have been interpreted by the authors as due to water conveyed over the submerged breakwater as mass transport, a partial ponding of this water due to its return flow being impeded by the presence of the breakwater, resulting in a portion being redirected as long-shore currents.

Actually, it should be the negative diffusion created by the long reef to be responsible of the erosion.

Chapter 8: The “stationary state” behind a breakwater, analysis with the equilibrium bay-shape concept

8.1. Introduction

In previous Chapters, we have analysed the case of a single detached breakwater, and the role of its parameters in influencing the shoreline plane shape behind it. We noted that a single detached breakwater acts like a “diffusivity modificator”. Moreover, even if this approach seems to affirm that a stationary state (equilibrium condition), behind the structure is not reached, we noted that an equilibrium is almost attained, and the cancel of littoral transport is obtained.

The stationary state is commonly associated to a null gradient of littoral transport, or at least, to a cancel of the littoral transport itself, for which a static equilibrium condition is obtained. Particularly, the nullifying of littoral transport is obtained when the shoreline follows the wave front: in this condition, the shoreline reaches its stationary state. For example, between two groins, a stationary state is attained when the shoreline evolves becoming parallel to the wave fronts, nullifying the long-shore transport. The same must occur for the shoreline behind a detached breakwater: here the shoreline tends to align to the diffracted wave front, nullifying the littoral transport, and assuming the classical shape of an equilibrium crenulated bay.

The leading purpose of present Chapter is establish to which extent current expressions of static equilibrium crenulated-bay shape effectively correspond to the position of the diffracted downdrift wave front.

In fact, for crenulate-shaped bays, the coastal outline assumes a specific shape related to the predominant waves in the area. When a sandy coastline is comprised among natural capes, promontories or man-made hard structures (namely breakwaters), the shoreline plane shape is governed by the diffraction of waves: it generally consists of a tangential zone downcoast and a curved portion upcoast.

Many coastal engineers have attempted to derive an expression of the headland bay shapes that emerge when a full equilibrium is reached (stable or dynamic). It is commonly believed that shoreline profiles tend to follow wave fronts, but this has been never fully verified. In fact, even though models for static equilibrium bays exist, they are merely of an empirical kind, lacking further insight on relationships between incident wave characteristics and beach shape.

In this Chapter, we investigate a possible correlation between static equilibrium profiles and wave front shapes. Numerical experiments have been performed using the MIKE 21 Boussinesq Wave module, and the generated wave fronts have been compared to one of the most famous equilibrium bay shape theory: the hyperbolic-tangent equilibrium profile. A thoughtful analysis of results revealed that a single-headland equilibrium profile do not match perfectly the diffracted wave front, rather it lies between two subsequent wave fronts. Particularly, it is noted that the equilibrium shape is merely the wave front translated perpendicularly to the wave direction at the headland tip, without any influence of wave period or in wave direction. A new function called the "*wave-front-bay-shape equation*" has been obtained, and the validation of this formula has been assessed with the case-study bay of the Bagnoli coast (south-west of Italy). Finally, a theoretical interpretation of the phenomena is given, and the shoreline static-equilibrium position behind a breakwater is given.

8.2. Headland-bay beaches

Crenulate-shaped or headland bays are quite common on exposed sedimentary coasts containing headlands, and represent about 50% of the world's coastline. The term headland-bay beach has been used to define a shoreline bounded by rocky outcrops or headlands, either natural or man-made, which lead to diffraction of incoming waves.

Particularly, the predominant waves are diffracted in such a way as to break simultaneously around the periphery of the bay once an equilibrium plane shape has been established (static equilibrium condition, Hsu et al., 2010). The fame of the headland bay beaches, in fact, lies in their equilibrium condition, static or dynamic, which ensures that they are considered a way to achieve coastline stabilization (Silvester, 1960). Static equilibrium is a condition characterized by the absence of littoral drift, without the need for sediment supply to preserve its long-term stability; on the other hand, a dynamic equilibrium condition requires sediment supply, from updrift and/or from another kind of source, to maintain its stability and not retreat towards the limit defined by static equilibrium position (Hsu et al., 2010).

Typically, the plane shape of a single-headland bay is characterized by an upcoast curved zone (diffraction zone), a gentle transition zone and a relatively straight tangential segment on the downdrift end of the bay (illuminated zone), which is largely orthogonal to the dominant wave direction; this equilibrium plane form is that assumed by the bay at a relatively long-term scale (e.g., annual to decadal) as a response to the predominant wave direction. Short-term fluctuations arising from beach-storm interactions, which could cause severe beach berm retreat, can be neglected due to their reversibility.

8.2.1. Static and dynamic equilibrium of a bay beach

Headland-bay beaches exist at downdrift of protruding headlands, natural or man-made, appearing in different configurations and in various sizes and shapes.

Headland-bay beach is in static equilibrium when a supply of sediment is not needed to maintain its long-term stability and no further littoral drift takes place. This occurs when waves diffract in the lee of a headland and after diffraction, the waves then proceed across the bay, suffering some refraction before arriving at the beach. Any wave takes the same time to reach any point on the shoreline starting from the diffraction point to, this causes that breaking of the predominant wave occurs concomitantly around the whole bay periphery.

On contrary, the dynamic equilibrium consists in a requirement of external sediment supply or a source within the embayment to maintain its stability. If supply diminishes, the bay in dynamic equilibrium could recede toward the limit defined by the static equilibrium under the same wave condition. In other words, a bay may be in dynamic equilibrium when sediment is still passing through it and its periphery is not so indented compared with that in static equilibrium.

Natural reshaping is a state of unstable condition normally associated with wave sheltering due to addition or extension of structures on beach where a curved plane form could result with accretion in the lee accompanying by erosion downdrift. This scenario is normally arising from the construction of a new breakwater or extending an existing breakwater for a harbour (Hsu and Silvester, 1996), which is often called “groin effect” for causing downdrift beach erosion, or with a natural headland, as a rocky outcrop, promontory, cape, offshore island.

8.2.2. Stable bay theory and equations

Since the beginning of nineteenth century, many coastal geologists, geographers and engineers have been trying to predict the shoreline plane shape of headland-bay beaches. Despite the complexity involved in coastal processes, simple empirical expressions have been derived since the 1940s in order to fit part or whole of the bay periphery. Among these approaches, the logarithmic spiral model (Krumbein, 1944), hyperbolic tangent model (Moreno and Kraus, 1999; Kemp et al. 2018) and parabolic model Hsu and Hevans, 1989; Hsu et al., 1989) have turned out to be the most acceptable expressions for practical applications to headland bay beaches in static equilibrium. However, none of these models are derived directly from the acting physical processes that developed the shape; rather, they are based on the observation of the shoreline plane shape, and so are lacking in a correlation between shoreline response and wave forcings (refraction and diffraction). The chronological development of the theory and key equations over the years has been rewieved in Kemp, 2018.

8.2.2.1. Logarithmic spiral equation

The logarithmic spiral equation was the first empirical expression proposed to fit bay’s shape. It was proposed by Krumbein (1944), an American geologist, who fitted an early 1940 imagery of Half-Moon Bay in California, USA.

He observed that a headland-bay beach adopts an equilibrium shape that is similar to a log spiral. The pole of the spiral is identified as the diffraction point, and the characteristic angle of the spiral is a function of the incident wave angle with respect to a reference line. For headlands of irregular shape and for those with submerged sections, the diffraction point cannot be specified unambiguously, a problem entering specification of all equilibrium shapes. In fitting the log-spiral to data, the location for of the pole can be considered as free parameter to be determined in a best-fit search. In design, some ambiguity exists as to where to locate the pole (Moreno and Kraus, 1999).

The equation proposed, expressed in polar coordinates, is:

$$R_1 = R_2 \exp(\theta cot\alpha) \tag{8.1}$$

where R_1 is the length of the radius vector for a point measured from the pole; θ is the angle from an arbitrary origin of angle measurement to the radius vector of the point; R_2 is a length of radius to arbitrary origin of angle measurement; and α is the characteristic constant angle between the tangent to the curve and radius at any point along the spiral.

Eq. (8.1) specifies a relationship between two consecutive radii, R_1 and R_2, measured from the centre of a logarithmic spiral with angle θ apart on the curve which has a constant outer tangent α. In fact, a property of the log-spiral curve is that the angle a between the tangent to the curve and the vector radius at any point along the curve is constant. This leads to the interesting result that the shape of the log spiral is controlled only by α, with the parameter R_2 determining the scale of the shape. The functioning of R_2 is equivalent to setting a different origin of measurement of the angle θ. In other words, graphically the log-spiral may be scaled up or down by turning the shape around its pole (Moreno and Kraus, 1999). Values of α for headland-bay beaches reported in the literature range from about 45º to 75º. In general, the smaller α, the wider the log spiral. In fact, the log-spiral shape is sensitivity to little changes in α, because the angle is contained in the argument of an exponential function. Additionally, the smaller the characteristic angle α, the larger the difference for the same percentage of angle variability. The practical consequence is that, because the purpose is fit this log-spiral shape to headland-bay beaches, especially in design of shore-protection a projects, has to be accurately defined. If the pole position is known, a solution procedure for the best-fit shape, that is, to find the best-fit value of α, follows. Eq. (8.1) can be rewritten as:

$$\ln R_1 = \ln R_2 + \theta cot\alpha \tag{8.2}$$

This linear relationship is convenient for fitting a log-spiral curve to data. The slope of the straight line is cotα, from which can the angle α be obtained.

Since 1944s, the log spiral model has been applied for many bays in various studies. In 1980 Silvester et al. applied this model to crenulate shaped bay between headlands and found a relationship between the indentation dimension a and the space between two headlands b for a given obliquity of incident wave to headland alignments β.

Nevertheless, the logarithmic spiral model, presents two important drawbacks: the centre of the spiral does not coincide with the wave diffraction point at the updrift headland.

8.2.2.2. Hyperbolic-tangent model

The hyperbolic-tangent shape model was proposed by Moreno and Kraus in 1999, to simplify the fitting procedure and reduce ambiguity in attaining an equilibrium shoreline shape. 46 bay beaches in Spain and North America have been fitted in a mathematical form of:

$$y = \pm a tanh^m(bx) \tag{8.3}$$

The x-axis is parallel to the general trend of the shoreline, the y-axis pointing shoreward, the origin of the coordinates is placed at the point where the local tangent to the beach is in perpendicular to the general trend of the shoreline. The terms of *a*, *b* and *m* are empirically-determined coefficients (*m* is dimensionless; the dimension of *a* is length; and the dimension of *b* is 1/length). First, the curve is symmetric with respect to the x-axis. Second, the values y =±*a* define two asymptotes; particular of interest here is the value y = a giving the position of the down-drift shoreline which is no longer under the influence of the headland (Figure 137). Third, the slope dy/dx at x = 0 is determined by the parameter *m*, and the slope is infinite if *m* < 1. This restriction on slope indicates m to be in the range of *m*<1.

Sensitivity testing of the hyperbolic tangent shape was performed to characterize its functional behaviour and assign physical significance to its three empirical coefficients.

The parameter a controls the magnitude of the asymptote (distance between the relative origin of coordinates and the location of the straight shoreline), *b* is a scaling factor controlling the approach to the asymptotic limit, m controls the curvature of the shape, which can vary between a square and an S curve. Larger values of *m* ($m > 1$) produce a more rectangular and somewhat unrealistic shape, whereas smaller values produce more rounded, natural shapes.

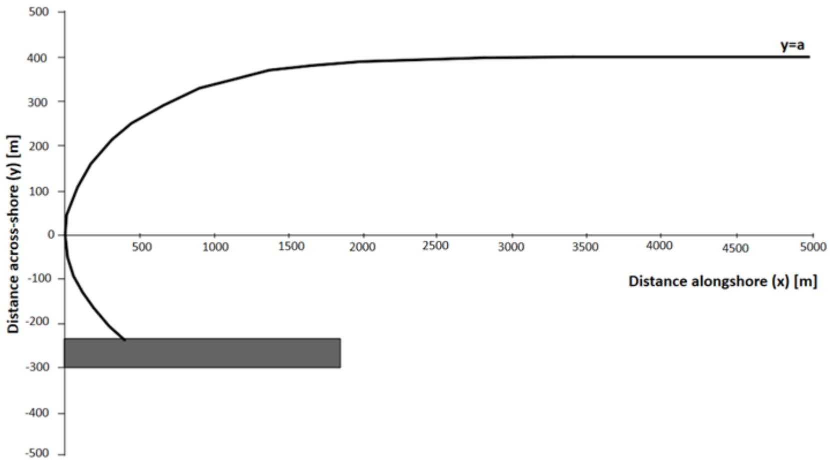

Figure 137 - Definition sketch for the hyperbolic-tangent shape equation (a = 400 m, b = 0.0009 m^{-1} and m = 0.5)

To found a location of the wave diffraction point, Martino et al. (2003) used a trial and error approach with a computer program, the point was located in the middle of the ocean. This seems unrealistic because the diffraction point is a fixed point, which is physically apparent and should not be obtained by trail-and-error.

Fitting the headland-bay equilibrium shape of 46 beaches Moreno and Kraus (1999) found the following relationships for reconnaissance-level guidance:

$$ab \cong 1.2 \tag{8.4}$$

$$m \cong 0.5 \tag{8.5}$$

The physical meaning of the first relationship is that the asymptotic location of the downdrift shoreline increases with the distance between the shoreline and the diffracting headland. This relation is the main result from the database, least-squares fitting for the linear function between $log_{10}a$ and $log_{10}b$ led to another relationship with a correlation coefficient R^2 of 0.8696:

$$a^{0.9124}b = 0.6060 \tag{8.6}$$

It is noted that the hyperbolic-tangent model is appropriate to fit part or whole of any bay beach, nevertheless the equation can be applied to fit the plane shape of any bay beach in static equilibrium or non-equilibrium and therefore cannot be used to assess the stability of a bay in static or non-equilibrium. Others shortcomings are the fact that the model fails to take into account the point of wave diffraction, even thou the updrift headland which controls the process of plane form evolution of a bay beach; and the fact that the origin of the curve is insensitively found by trial and error, until the errors are minimal.

In 2018, Kemp et al. presented a development of the hyperbolic tangent equation, which eliminated the requirement of placing the down coast control point and relied on defining a minimum beach width instead. They tried to overcome those shortcomings with a relationship linking the geometric origin of the hyperbolic tangent equation with a wave diffraction point needed to be determined, using a database of case studies comprising of 46 beaches in Spain, Southern France and North-Africa. The beaches of the database, extending from a small project scale (hundreds of metres) to larger scale (up to a few kilometres), are selected based on several requirements: they show a crenulated bay shape; have only one headland, so that a straight section of the beach can be seen; and were in equilibrium. Digitising the shorelines of all the case study beaches in ArcGIS, from high quality aerial images, and importing them on Matlab, the coefficients a, b and m are determined. Those three coefficients are obtained with a best-fit hyperbolic curve based on a minimal value for the sum of squares due to error with their 95% confidence limits. The value of m found is 0.496 circa, supporting the original findings of Moreno and Kraus (1999), and a narrower confidence interval was observed in this investigation. To estimate the correlation between a and b, least-squares fitting for a power function between them was carried out.

The relationship between a and b, with R^2=0.9372, is:

$$b = 1.794a^{-1.097} \tag{8.7}$$

By reason of the fact that the value of R^2 of this new relationship is better compared to the one for the data used by Moreno and Kraus, it is convenient use this one. The hyperbolic tangent shape equation becomes:

$$y = \pm atanh^{0.496}(1.794a^{-1.097}x) \tag{8.8}$$

Moreover, further analysis has been carried out to determine the location of the diffraction point relative to the origin of the hyperbolic tangent equation. The coordinates of the diffraction point, c and d, have been determined in a dimensionless form, in a such way any modification of the hyperbolic tangent equation is applicable for designing new beaches or assessing the influence of a headland on a beach. The non-dimensional expressions have been obtained dividing the coordinates by a scaling distance measured for each bay, the measurement is a, the distance between the x=0 line and the straight section of the beach. The relationships to determine the diffraction point's coordinates are:

$$\frac{c}{a} = 1.256 \ \text{ for the x coordinate} \tag{8.9}$$

$$\frac{d}{a} = 0.517 \ \text{ for the y coordinate} \tag{8.10}$$

The modified hyperbolic tangent shape equation also produces a curve which is symmetric with the x-axis and produces two asymptotes. These are found at y = ±0.86*c*. The line y = +0.86*c* indicates the location on the shoreline that is no longer under the influence of the headland. As the hyperbolic tangent shape equation produces a curve which is symmetric with the x-axis and produces two asymptotes it removes the difficulty in locating the position of the downcoast control point. Only the c position is required, which is directly related to the beach width. Therefore, the application of this modified equation requires only the wave diffraction point, the wave direction and the beach width.

8.2.2.3. Parabolic model

The parabolic model was proposed by Hsu et al. (1989a,b) and Hsu and Evans (1989), in two separates works, from fitting the plane form of 27 mixed cases of 14 prototype and 13 model bays believed to be in static equilibrium. The first relationship presented defines the shape of bays formed between two headlands, with complete cessation in the sediment supply (neither from upcoast or from a river debouching into it), which causes that shoreline erodes back to a limit beyond which no further erosion is possible; this is the static equilibrium value. The parabolic shape is expressed mathematically in polar coordinates by the two following empirical equation (the first for the curved section of the beach and the second for the straight downdrift section):

$$\frac{R_n}{R_\beta} = C_0 + C_1\left(\frac{\beta}{\theta_n}\right) + C_2\left(\frac{\beta}{\theta_n}\right)^2 \qquad \theta \geq \beta \qquad (8.11)$$

$$\frac{R_n}{R_\beta} = \frac{sen\beta}{sen\theta} \qquad \theta \leq \beta \qquad (8.12)$$

The two basic parameters are the reference wave obliquity β and control line length R_β (Figure 2). The variable β is a reference angle of wave obliquity, or the angle between the incident wave crest (assumed linear) and the control line, joining the upcoast diffraction point to a point on the near straight beach, namely the downcoast control point. The radius R to any point on the bay periphery in static equilibrium is angled θ from the same wave crest line radiating from the point of wave diffraction upcoast. The three C constants, generated by regression analysis to fit the peripheries of the 27 prototype and model bays, differ with reference angle β. Their analytical expressions have been provided by (Hsu and Sylvester, 1993):

$$C_0 = 0.0000000479\beta^4 - 0.00000879\beta^3 + 0.000352\beta^2 - 0.00479\beta + 0.0715 \qquad (8.13)$$

$$C_1 = -0.000000128\beta^4 + 0.0000182\beta^3 - 0.000487\beta^2 + 0.00771\beta + 0.955 \quad (8.14)$$

$$C_2 = 0.0000000944\beta^4 - 0.000012\beta^3 + 0.000316\beta^2 - 0.00828\beta + 0.0265 \quad (8.15)$$

Moreno e Kraus (1999) studied the effect on the parabolic shape of the shoreline if the length of the control line R_n or the reference wave obliquity β change. They found that the shape of the parabola is controlled by β, its size is controlled by R_n.

In contrast to the log-spiral, the parabolic equation origin coincides with the diffraction point and therefore the equation is directly related to wave direction. However, it is affected by a drawback: the uncertainty of locating the downdrift control point. Despite that there are several interpretations of the downcoast control point of the parabolic bay shape equation (Kemp et al., 2018) it is a considerable limitation which inhibits the application of the parabolic model in designing new beaches.

Among the three aforementioned models, the parabolic model prevailed over the others since it was the only one that used the wave diffraction point as the origin of the co-ordinate system, ensuring that the effect of relocating the diffraction point can be assessed (Kemp et al., 2018). Despite that, in comparing the origin of the three coordinates system in studying a headland bay (using a computer program based on a trial and error approach), Martino et al. 2003) found that the parabolic equation's origin was located in the middle of the ocean. This outcome weakens the strong point of parabolic model, revealing an uncertainty about its alleged robustness.

It is noteworthy that further investigations have been carried out, over the last few decades, towards the comprehension of the correlation between crenulate-shaped bays and wave characteristics. Anyhow, despite it is commonly believed that equilibrium beach profiles follow the wave front trend, this has not been proved in literature so far, and no research has clarified in depth to what extent the "stationary state" of a crenulated bay should coincide to the diffracted wave fronts.

8.3. The possible relation between equilibrium bay-shape and wave fronts

In order to investigate the relationship between the headland-bay static equilibrium profile and wave propagation characteristics, numerical modelling of a single headland case study has been implemented. Moreover, the possible influence of wave direction and wave period has been verified on this researched correlation. Several experiments have been carried out using the wave driver BW of MIKE 21 (Danish Hydraulic Institute) (2017), which is based on the numerical solution of the time domain formulations of Boussinesq-type equations (Madsen et al. 1991; Madsen et al., 1992; Madsen et al., 1997, I,II; Sørensen et al 2004). The BW module is able to reproduce the combined effects of all important wave phenomena, among them diffraction and refraction, which play an important role in headland-bay equilibrium profile shaping.

8.3.1. A short description of BW model of MIKE 21 (DHI)

The Boussinesq model is capable of reproducing the combined effects of important wave phenomena, such as diffraction and refraction. Therefore, it has been used in numerical experimentation to obtain diffracted wave fronts generated by headland.

MIKE 21 BW includes two modules, the 2DH wave model and 1DH wave model, both based on the numerical solution of time domain formulations of Boussinesq-type equations, which are solved using a flux-formulation with improved linear dispersion characteristics. The enhanced Boussinesq equations were originally derived by (Madsen et al. 1991; Madsen et al., 1992), making the modules suitable for simulation of the propagation of directional wave trains travelling from deep to shallow water. Moreover, it contains wave breaking and moving shorelines, as described in Madsen et al., 1997, I,II and Sørensen et al 2004. The 2DH BW model has been used in this work.

The enhanced Boussinesq equations are expressed in terms of the free surface elevation, ξ, and the depth-integrated velocity-components, P and Q. The continuity and the momentum-conservation equations read:

$$n\frac{\partial \xi}{\partial t}+\frac{\partial P}{\partial x}+\frac{\partial Q}{\partial y}=0 \tag{8.16}$$

$$n\frac{\partial P}{\partial t}+\frac{\partial}{\partial x}\left(\frac{P^2}{h}\right)+\frac{\partial}{\partial y}\left(\frac{PQ}{h}\right)+\frac{\partial R_{xx}}{\partial x}+\frac{\partial R_{xy}}{\partial y}+n^2gh\frac{\partial \xi}{\partial x}+n^2P\left[\alpha+\beta\frac{\sqrt{P^2+Q^2}}{h}\right]$$
$$+\frac{gP\sqrt{P^2+Q^2}}{h^2C^2}+n\psi_1=0 \tag{8.17}$$

$$n\frac{\partial Q}{\partial t}+\frac{\partial}{\partial y}\left(\frac{Q^2}{h}\right)+\frac{\partial}{\partial x}\left(\frac{QP}{h}\right)+\frac{\partial R_{yy}}{\partial y}+\frac{\partial R_{yx}}{\partial x}+n^2gh\frac{\partial \xi}{\partial y}+n^2Q\left[\alpha+\beta\frac{\sqrt{P^2+Q^2}}{h}\right]$$
$$+\frac{gQ\sqrt{P^2+Q^2}}{h^2C^2}+n\psi_2=0 \tag{8.18}$$

with the dispersive Boussinesq terms ψ_1 and ψ_2, defined by:

$$\psi_1 = -\left(B+\frac{1}{3}\right)d^2\left(P_{xxt}+Q_{xyt}\right)-nBgd^3\left(\xi_{xxx}+\xi_{xyy}\right)$$

$$-dd_x\left(\frac{1}{3}P_{xt}+\frac{1}{6}Q_{xt}+ngBd\left(2\xi_{xx}+\xi_{yy}\right)\right)$$

$$-dd_x\left(\frac{1}{6}Q_{xt}+ngBd\xi_{xy}\right) \tag{8.19}$$

$$\psi_2 = -\left(B+\frac{1}{3}\right)d^2\left(P_{xyt}+Q_{yyt}\right)-nBgd^3\left(\xi_{xxy}+\xi_{yyy}\right)$$

$$-dd_x\left(\frac{1}{6}P_{xt}+\frac{1}{3}Q_{xt}+ngBd\left(2\xi_{yy}+\xi_{xx}\right)\right)$$

$$-dd_x\left(\frac{1}{6}P_{yt}+ngBd\xi_{xy}\right) \tag{8.20}$$

where d is the still water depth; g is the gravitational acceleration; n is the porosity; C is the Chezy resistance number; $\alpha$is the resistance coefficient for laminar flow in porous media; $\alpha$is the resistance coefficient for turbulent flow in porous media; B is the Boussinesq dispersion coefficient; the terms R_{xx}, R_{xy} and R_{yy} indicate the incorporation of the wave breaking by means of the surface roller model (Svendsen, 1984).

In MIKE 21 BW, the waves may either be specified along open boundaries or be generated internally within the model through the generation line; the latter must be placed in front of a sponge layer absorbing all outgoing waves. Moreover, porosity (e.g., to model partial transmission through porous structures) and sponge layers can be used on an ad hoc basis. At open boundaries, either a level boundary, namely wave energy given as time series of surface elevation, or flux boundary, where flux density is perpendicular to the boundary, can be set.

8.3.2. Methodology

The method followed involves comparing the diffracted wave fronts generated by the BW simulations with static equilibrium profiles sketched out by the hyperbolic-tangent model. The procedure obeys to the following steps:

1. generating the diffracted wave front through the BW module;
2. extrapolating the wave front from the model;
3. starting with the illuminated zone of the front, drawing out the hyperbolic-tangent profile.

The third step is directly related to one of the major findings in the field of static equilibrium bays, namely that equilibrium crenulated beaches tend to align transverse to the direction of dominant waves. The main assumptions in applying the methodology here proposed are that (1) the equilibrium headland-bay plane form follows the wave front; and (2) that the predominant wave direction is perpendicular to the straight area of the bay. In this way, in order to obtain the hyperbolic tangent plane form of every model configuration, we supposed that the asymptote of the hyperbolic tangent matches the illuminated zone of the wave front, out of the shadow zone where the influence of diffraction is negligible. Therefore, once the distance between asymptote and diffraction point is measured (distance *c* in Figure 138), the origin of the hyperbolic tangent is automatically obtained through Eq.s (8.9) and (8.10), and the x,y coordinates of hyperbolic tangent profile are achieved through Eq. (8.8) (Figure 138). It is worth pointing out that, in order to compare equilibrium static profile and wave front, the latter must be able to expand without any kind of physical interference (e.g., presence of additional obstacles).

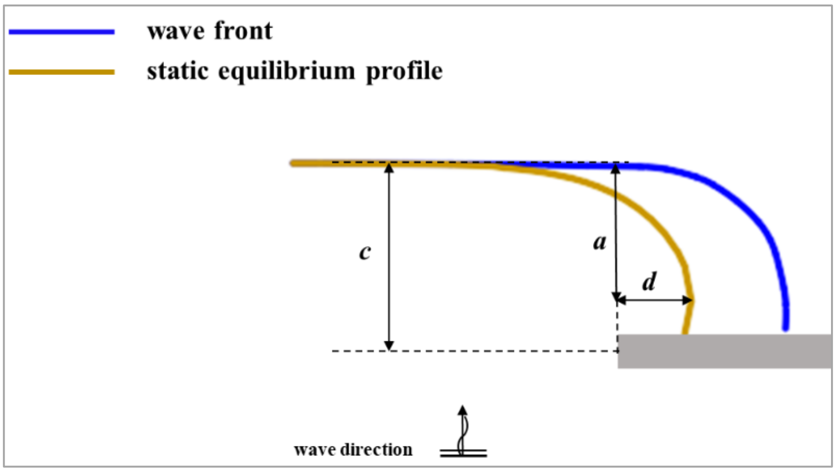

Figure 138 - Definition sketch to obtain the hyperbolic tangent profile starting from a wave front.

Additionally, in order to investigate the influence of wave characteristics on the relationship between wave fronts and equilibrium profiles, we performed different numerical simulation scenarios by varying wave direction, wave period and refraction conditions. For each scenario, more wave fronts were extrapolated from the BW module, each progressively further away from the headland tip, in order to examine the influence of dimensionless distance (c/L) on the researched correlation.

Finally, before describing the model set up, a clarification regarding the choice of the headland bay shape model is necessary. The two possible models to be implemented to sketch out the static equilibrium profile were the hyperbolic-tangent model and the parabolic model (the logarithmic spiral model has been rejected a priori given its difficulty in practical application). Thus, the same methodology has been implemented to both the hyperbolic model and parabolic model. The results proved that there was no difference: there is no change, regardless of the model adopted. Nevertheless, given the uncertainty due to the determination of the downdrift control point of the parabolic profile, the hyperbolic tangent model turned out to be the best static equilibrium model to be compared to the BW simulations wave fronts.

8.3.2.1. *Boussinesq Wave Module Set Up*

The primary aim of this research is to investigate the relationship between headland-bay static equilibrium profile and wave propagation characteristics (diffraction and refraction). Therefore, we created different numerical simulations scenarios, in order to generate different wave fronts, by varying wave direction, wave period and refraction conditions.

First, to evaluate refraction conditions, two bathymetry configurations were been investigated. The first one (called *''gentle slope''*) is characterised by a linearly varying cylindrical bathymetry, with a gentle bottom slope of 1/100 and a diffraction point, modelled through a breakwater, located at a water depth of 3 m. The water depth at the offshore boundary is 20 m (Figure 139a). A gentle slope has been adopted to allow an expansion of the wave fronts without the influence of bottom abrupt raising. The second configuration (called *''flat bottom''*) exhibits a bottom with a constant water depth equal to 10 m (Figure 139b).

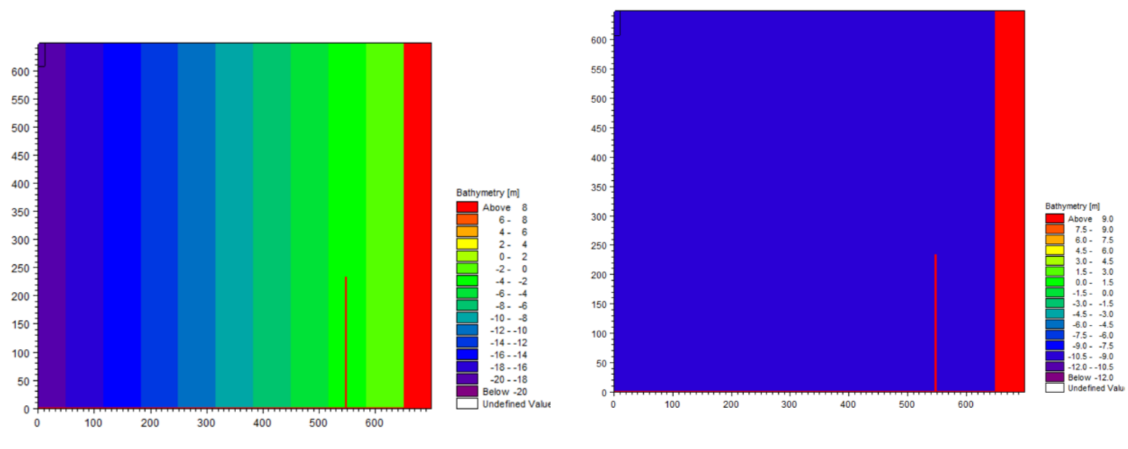

(a) (b)

Figure 139 - (a) Gentle slope configuration bathymetry; (b) flat bottom configuration bathymetry

Secondly, numerical experiments have been conducted considering the possible effect of wave period and wave direction; conversely, the influence of wave height was not explored. This is because the correlation function describing the relationship between static equilibrium profiles and wave characteristics, at this first stage of the research, is obtained through a ‘’linear approach’’ based on simple geometric consideration. Therefore, the only parameters that could geometrically affect the aforementioned correlation are period, wave direction and bottom inhomogeneity. Conversely, wave height does not represent a variable of the problem. Three different wave directions have been investigated; one is normal to the breakwater, while the other two are angled of 25° and −35° with respect to being perpendicular to the structure. For each direction, three wave periods have been tested: 5.9 s, a typical wave period of the Mediterranean wave climate; and 10 s and 15 s, which simulate swell conditions. The wave height used was 0.8 m for each numerical scenario. Since the predominant wave shapes the crenulated beach, for the numerical experimentation the value of wave height has been chosen equal to the LDR equivalent wave height value for the case study of Bagnoli bay (see following sections). Simulations have been implemented using regular waves. It is important to underline that the effect of breaking waves was not considered in the trials. For each bathymetry configuration (‘’gentle slope’’ and ‘’flat bottom’’), the scenarios analysed are summarized in Table 12.

Table 12 - Scenarios analyzed in the numerical experimentation

	Gentle Slope	Flat Bottom
Wave Direction	0°; 25°;−35°	0°; 25°;−35°
Wave Period	5.9 s; 10 s; 15 s	5.9 s

Models are made up of a fine grid (square cells with grid spacing 3 m), upon which orientation coincides with wave direction; the time step used is 0.1 s. The wave generation line has been used and wave absorbing sponge layers have been applied at the model boundaries. Near the land, one sponge layer has been applied in order to avoid the occurrence of wave reflection which could influence the expansion of the wave fronts. Geometric characteristics are summarized in Table 13, and are valid for both bottom configurations.

Table 13 - Grid geometric characteristics.

Grid Dimension [m^2]	Grid Spacing [m]	Grid Orientation [°]	Headland extension [m]
2100 × 1950	3	0	690
2700 × 1500	3	25	330
2700 × 1500	3	−35	630

8.4. Results

At first sight, comparisons suggest that wave front does not represent a static equilibrium profile: within the shadow zone, the wave front is located backward from the static plane form position, according to the wave propagation direction. In fact, as seen in Figure 140, the hyperbolic tangent profile (red line) crosses various fronts until it tends to the asymptote; the farther the asymptote from the breakwater tip, the more the profile is placed on additional wave fronts. On the other hand, wave fronts distant less than a wave length from the diffraction tip represent an exception, since they coincide with their corresponding hyperbolic tangent profile (Figure 141).

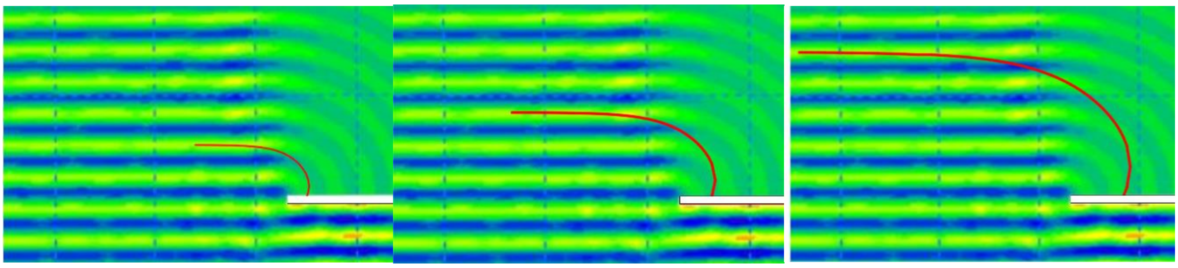

(a) (b) (c)

Figure 140 - Comparison between wave front (obtained with flat bottom configuration) and hyperbolic tangent profile (red line), images from (a) to (c) show profiles sketched out, starting with fronts gradually further from the headland.

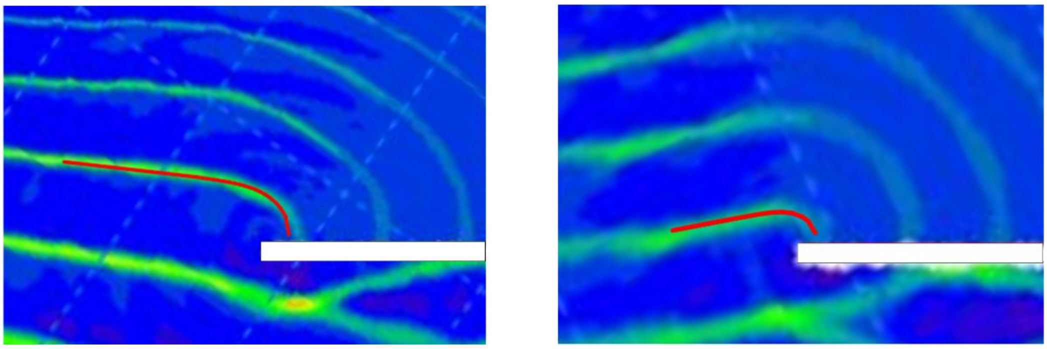

(a) (b)

Figure 141 - Hyperbolic tangent profile (red line) corresponds to relative wave front; both pictures have been obtained with the gentle slope configuration, (a) with wave direction −35° and wave period of 10 s and (b) with wave direction 25° and wave period of 10 s.

The behaviour outlined has been detected for each wave period and wave direction investigated, as shown in Figure 142. Moreover, this behaviour has been observed in both bottom configurations (gentle slope and flat bottom); consequently, it seems that the correlation between hyperbolic tangent profile and wave fronts is not influenced by the effect of refraction phenomenon. At the same time, although as a first approximation results indicate that wave front does not represent a static equilibrium profile, a more accurate inspection revealed that equilibrium beach profiles of single headland bays correspond to a simple translation of a wave front normal to the propagation line at the headland head: once shifted, it completely superimposes on the equilibrium profile (Figure 142). Specifically, this issue is elaborated and discussed in the next section.

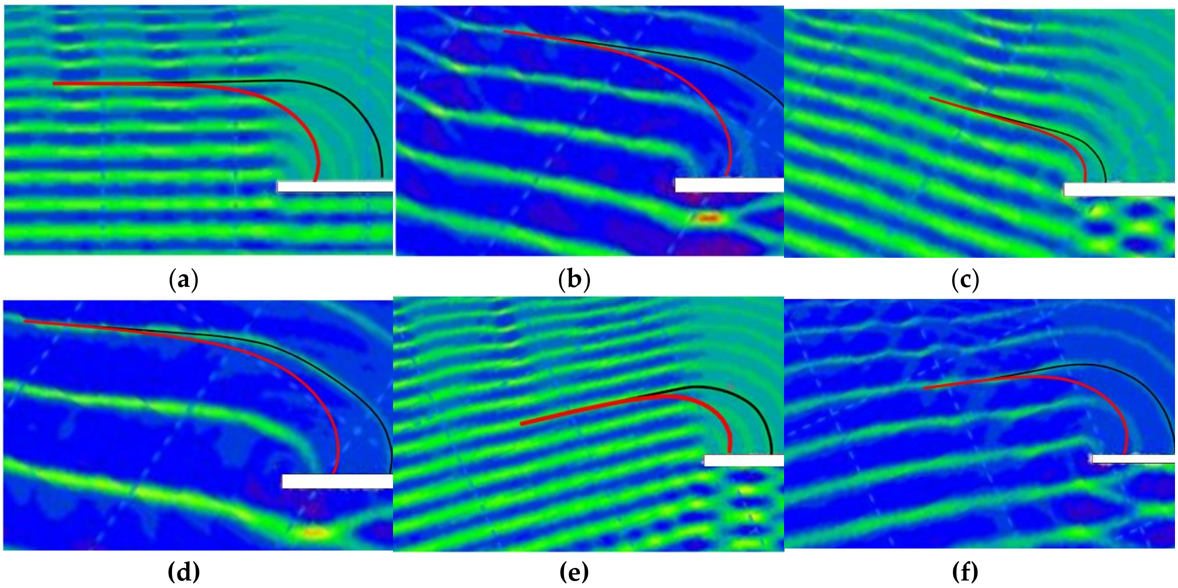

Figure 142 - Comparisons between wave fronts (black line) and hyperbolic tangent profiles (red line): (a) wave direction 0°, wave period 6 s, gentle slope configuration; (b) wave direction −35°, wave period 10s, gentle slope configuration; (c) wave direction −35°, wave period 6s, gentle slope configuration; (d) wave direction −35°, wave period 15 s, gentle slope configuration; (e) wave direction 25°, wave period 6 s, gentle slope configuration; (f) wave direction 25°, wave period 10 s, gentle slope configuration.

8.4.1. Relationship between Wave Fronts and Equilibrium Profiles

As described in the above paragraph, numerical experiments demonstrated that, in contrast to what is usually supposed, wave fronts do not represent a static equilibrium profile. However, it is possible to establish a correlation between them. Regarding the fact that an equilibrium profile actually is a wave front translated perpendicularly to the wave direction at the headland head, and recognizing that wave period, wave direction and wave refraction do not influence this behaviour, it is possible to calculate a direct relationship between wave fronts and equilibrium profiles, called the "*wave-front-bay-shape equation*".

Therefore, in order to derive this relationship, for each comparison between wave front and hyperbolic tangent profile, we measured the minimum distance between the diffraction point and the asymptote of the profile (distance *c* of Figure 143), and, also, the distance needed to overlap the front on the profile (distance *s* of Figure 143).

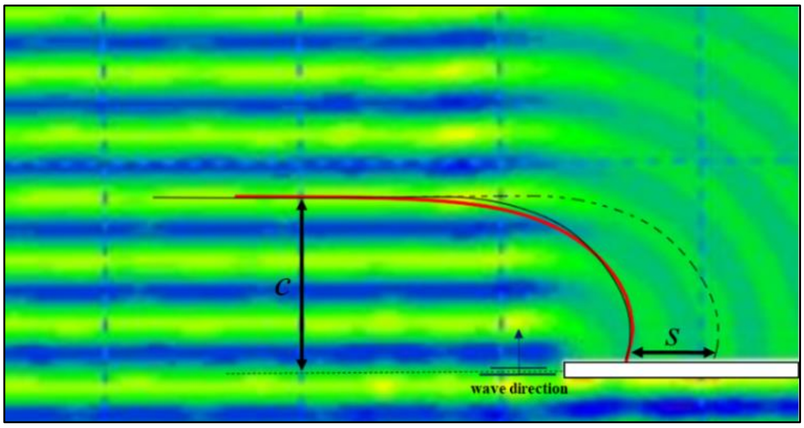

Figure 143 - Definition sketch for parameters c (distance between the diffraction point and the asymptote of the profile) and s (distance needed to overlap the front on the profile).

These two distances have been standardised to the local wave length, L (the wave length at the diffraction point water depth), so obtaining *c/L* and *s/L*. Moreover, it is necessary to take into account that wave fronts far from the diffraction point by less than one wave length coincide with the corresponding hyperbolic tangent profile. Therefore, it has been assumed that for a value of $c/L \leq 0.7$, it is not necessary to shift the wave front to overlap it on the profile; they are already superimposed (Figure 141).

Hence, for each configuration, results have been plotted on a graph where on the x-axis there is "*c/L – 0.7*" and on the y-axis there is "*s/L*". It can be noted that all results analysed tend to follow an increasing trend, which suggests that an equation to describe the correlation between diffractive wave fronts and static equilibrium profiles can be derived (Figure 144).

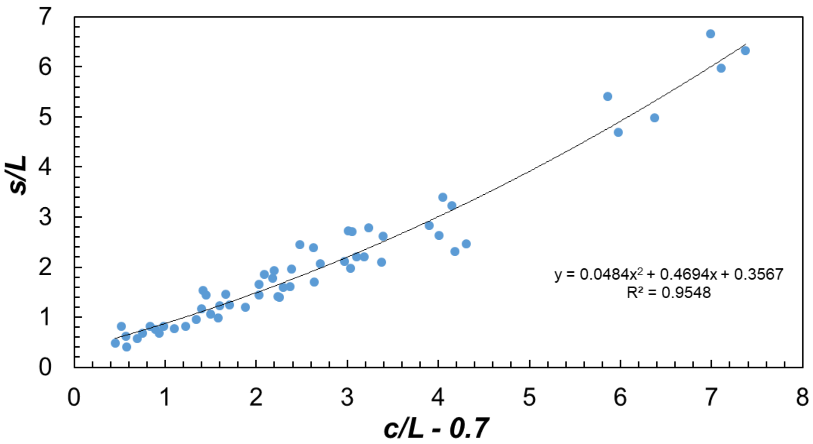

Figure 144 - Numerical simulations values of s/L in function of c/L, together with the best line

The relationship is:

$$\frac{s}{L} = 0.0484\left(\frac{c}{L} - 0.7\right)^2 + 0.4694\left(\frac{c}{L} - 0.7\right) + 0.3567 \tag{8.21}$$

with a correlation coefficient R^2 of 0.9548.

8.5. Bagnoli bay case study

To assess the results carried out with numerical experiments, a small beach has been taken into account. It is located on the Bagnoli coast, West of Naples, in southern Italy (Figure 145). The beach is delimitated on the right (looking offshore) by a revetment which protects the road behind, on the left by a little mound and behind by a seawall which marks out the road; it extends for about 190 m from North-West to South-East. This little bay appears to be fundamentally governed by a single headland located on the left side, next to the drain of Bagnoli (Figure 145). The orientation of the downcoast section of the bay is approximately 210 °N and its distance from the diffraction point is approximately 47 m (Figure 146).

As will be demonstrated in the next section, the case study can be considered a static equilibrium bay governed by a single headland. For this reason, the application to the Bagnoli bay is of particular interest, as it allows us to verify the behaviour observed with numerical experimentation and to check the validity of Eq. (8.21).

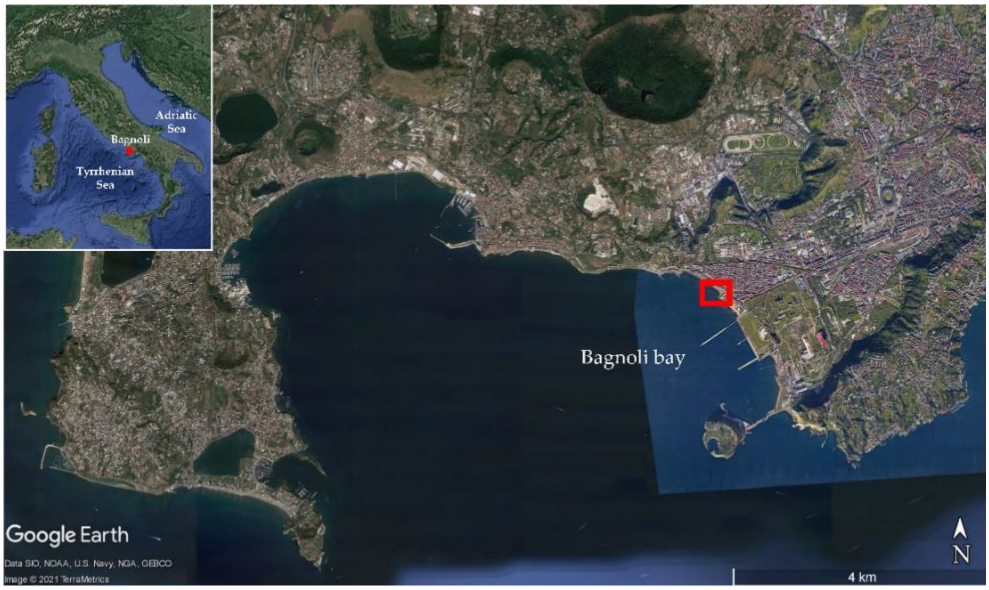

Figure 145 - Location of the Bagnoli bay case of study.

Figure 146 - Distance from diffraction point and shoreline orientation in downdrift section of the Bagnoli bay case study.

Wave Climate

The wave climate for the case study coast has been inferred from the MEDA-A buoy, an Acoustic Doppler Current Profile (ADCP), located approximately 800 m offshore from the bay (Figure 147a). The device is located at a depth of about 19 m below the low tide level, at a Latitude of 40°48.550’N and a Longitude of 14°09.300’E E. The histogram of wave direction for angular sectors of 22.5°N is shown in Figure 147b, where the offshore directed waves have been removed for sake of clearness. The graph exhibits how the bay is exposed to waves coming from a relatively narrow wave sector, included between 150 and 240°N, with a clear mode in the Southern quadrants (180°–210°N). It is important to highlight that, despite the short recorded time interval of the buoy (only three years), we employed its data, taking the advantage of being placed in the near-shore zone, bypassing all the procedures concerning the determination and propagation of the offshore wave climate (procedures which involve a certain degree of uncertainty, however).

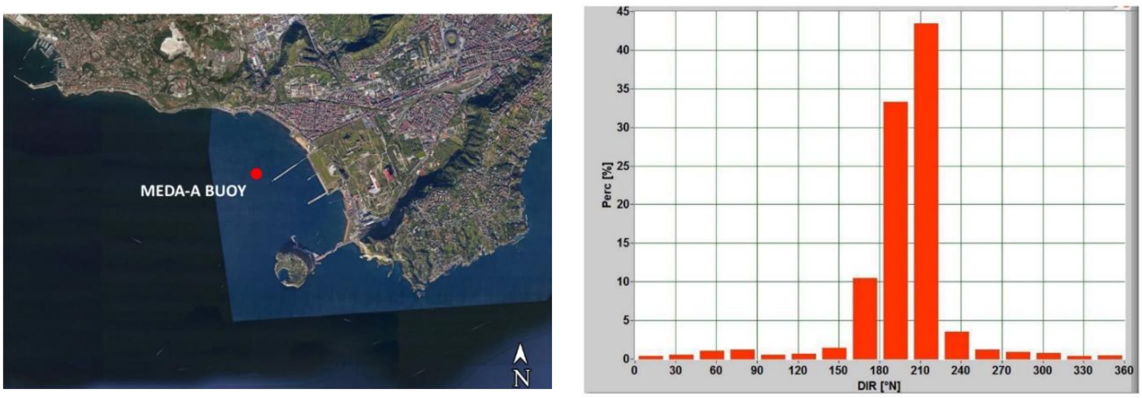

(a) **(b)**

Figure 147 - (a) Location of the MEDA-A buoy; (b) histogram of wave direction for angular sectors of 22.5°N.

The drift rose of Bagnoli bay has been derived using the LDR concept and the available wave data inferred through the MEDA-A Buoy. The range of shoreline orientations that exists at the site of interest has been also considered, and the net littoral drifts for each possible shoreline orientation have been calculated. LDR for the Bagnoli climate is shown in Figure 148: positive (transport to the right), and negative (transport to the left) lobes can be distinguished; moreover, the graph shows the null point; that is, the shoreline orientation at which no sediment transport is taking place.

From the LDR, the equivalent wave component parameters have been estimated. The equivalent direction corresponds to the null-point of the real LDR (205°N for the present case), while $H_{s,eq}$ and $T_{p,eq}$ are fitted to have the same littoral transport magnitude, obtaining $H_{s,eq}$ =0.8 m and $T_{p,eq}$ =5.89 s. It is surprising to observe that the equivalent wave direction (205°N) is extremely close to the orientation of the downcoast section of the bay (illuminated zone, Figure 146), confirming that the LDR equivalent wave is responsible of the sculpturing of the bay, in the long run, bringing it to its static equilibrium plane form.

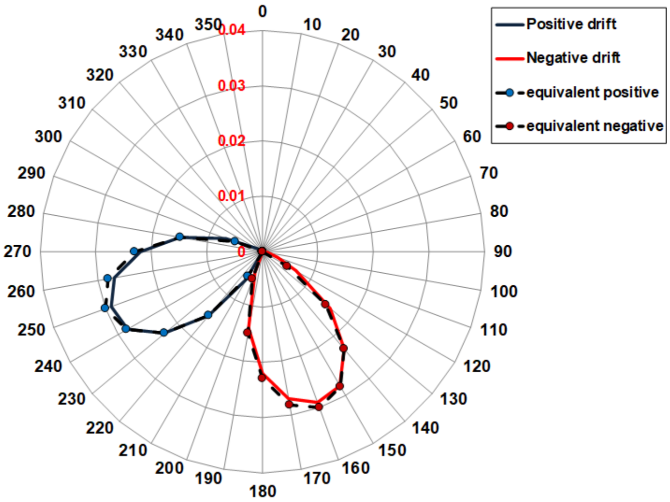

Figure 148 - Comparison between Climate-LDR and Equivalent-LDR of the Bagnoli bay; blue solid line represents drift to right when looking offshore, while red solid line represents drift to left when looking offshore; dashed lobes represent the equivalent drifts. Littoral drift in cubic meters/s.

Moreover, this is confirmed also by the wave climate mode shown in Figure 147b: waves with the largest percentage of occurrence are those comprised within the south west wave sector, in which the 205° equivalent direction can be detected. In fact, it can be said that the LDR equivalent wave approximately represents the average climate; in other words, it is the wave component that usually affects a given region from a certain direction. Therefore, when in narrow wave sector, as the present case of Bagnoli bay, we are used to observe mono-modal wave climate, so with a single high-frequency direction. In such conditions, the directional mode corresponds to the average one, which corresponds, in turn, to the LDR equivalent wave direction.

Static Equilibrium Condition

Before moving on the application of the methodology exposed in the previous paragraphs to the case study, it has been verified that the bay under study is in a static equilibrium condition. Therefore, we analysed the shoreline position over 10 years, specifically from 2008 to 2018. Data comes from the digitalization, in QGIS environment, of historical imageries of the area from Google Earth (Figure 149a).

The *Linear Regression Rate (LRR)* and the *End Point Rate (EPR)* have been used as indicators of the rate of shoreline change. LRR corresponds to the slope of a least-square straight-line, fitted through the shoreline positions at the various available times; EPR, takes into account exclusively shoreline positions at the first and the last years concerned and represents shoreline movement during that time.

From the analysis of both LRR and EPR (Figure 149b), an erosive trend has been observed in the curved zone, meanwhile the linear stretch has been accreted. Therefore, this suggests that a long-shore transport occurs, which moves sediments from the shadow zone to the downcoast sector (illuminated zone). Nevertheless, the maximum rate of erosion and accretion are negligible, as they are approximately 0.2 m/year and 0.4 m/year, respectively. Therefore, it can be asserted that the case study bay is in a static equilibrium condition.

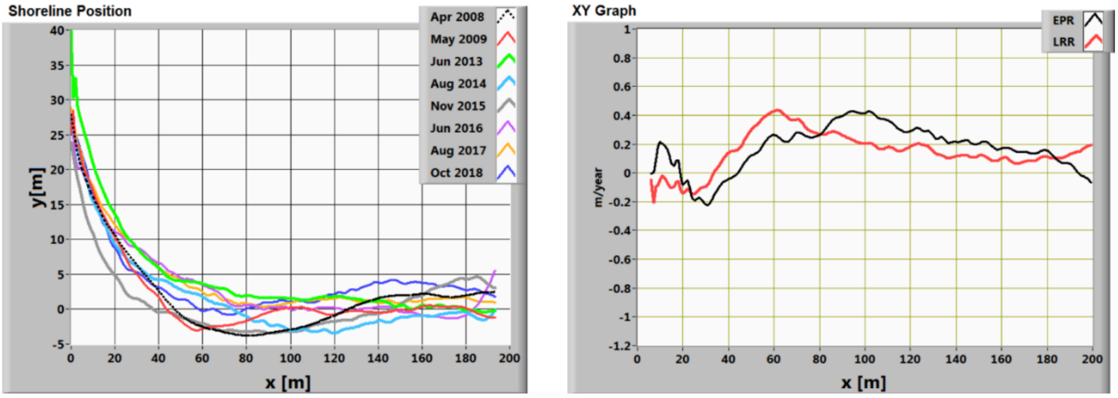

(a) (b)

Figure 149 - (a) y(x,t) coordinates of shorelines over time; (b) EPR (black line) and LRR (red line).

8.5.1. Numerical Modelling of the Bay and Results

Numerical modelling of the bay has been performed through the wave driver MIKE 21 BW (DHI), which allows for obtaining the growth of the wave fronts leeward of the headland. In order to follow the method used in the numerical trial, the bay has been modelled in such a way that wave fronts could extend leeward the headland without any interference: the real bathymetry of the area has been employed until the diffraction point location, where the water depth is about 3 m, then a gentle slope of 1:100 has been adopted; the coastline has been shifted and cut landward and a sponge layer has been used, in order to avoid reflection phenomenon (Figure 150).

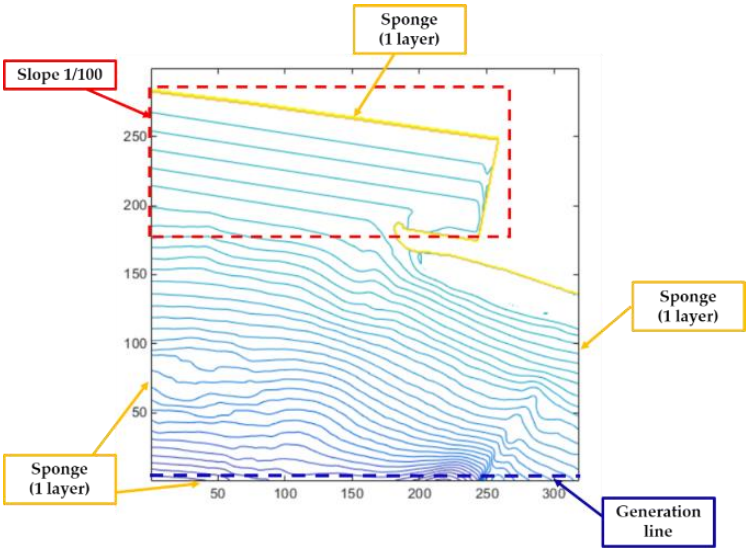

Figure 150 - Model setup of case study bay

Numerical simulations have been performed wave detecting the equivalent direction of 205°N, since it is representative of the effects of the entire wave climate on long-shore sediment transport. As concerns wave period, the average measured omni-directional peak period (5.9 s) has been investigated. Simulations have been carried out using regular waves, which wave height has been set at 0.8m; the breaking phenomenon has been neglected. Fine grid has been used (square cells with grid spacing 3 m), for which the orientation coincides with wave direction, with a time step of 0.1. A wave generation line has been used and wave absorbing sponge layers have been applied at the lateral boundaries. Grid geometric characteristics are summarized in Table 14.

Table 14 - Grid geometric characteristics.

Grid Dimension [m^2]	Grid Spacing [m]	Grid Orientation [°N]
900 × 960	3	205

Comparison between equilibrium profile and wave fronts carried out through BW model, shown in Figure 150, demonstrates that wave fronts' direction in the illuminated zone matches shoreline orientation, confirming the goodness of the LDR equivalent wave to represent the entire wave climate in the act of shape the beach plane form. Specifically, simulations results confirmed the behaviour observed in the previous section: the shoreline plane form of the headland bay is placed on more wave fronts, the downdrift section overlaps the wave front while the curved section is placed on the wave front closer to the headland (Figure 151a).

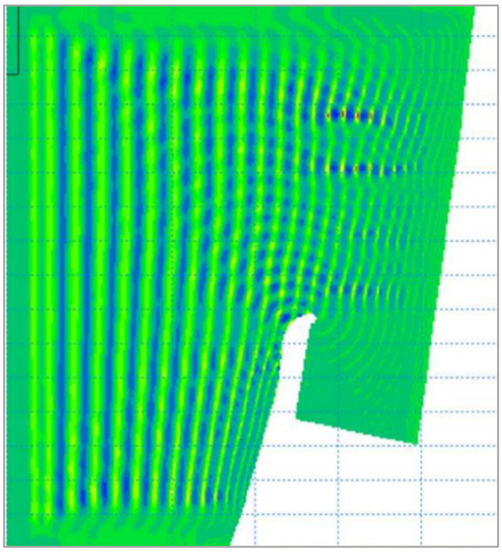

(a)

(b)

Figure 151 - (a) Wave fronts generated by means BW; (b) comparisons between wave fronts (green lines) and shoreline (red line).

In order to attain an effective validation of the *wave-front-bay-shape equation*, Eq. (8.21) has been applied. The minimum distance between the diffraction point and the asymptote has been measured (distance c in Figure 152a) and it has been standardised with respect to the local wave length, *c/L*. Applying Eq. (8.21), we obtained the value of the shift, *s*, which represents the distance needed to superimpose the whole wave front on the shoreline.

(a)

(b)

Figure 152 - (a) Wave front (green line) that overlaps the shoreline (red line) in the downdrift section and the latter's distance, c, from the diffraction point; (b) wave front shifted by s, which was derived from Equation (15).

After shifting the wave front, as shown in Figure 152b, it is perfectly superimposed on the bay shoreline, thus verifying the correlation found between wave fronts and shoreline profile, reached by Eq. (8.21).In conclusion, to sum up, to assess a possible correlation, numerical experiments have been carried out using the MIKE 21 Boussinesq Wave Module (BW), where wave fronts have been compared to the hyperbolic-tangent equilibrium profile, analysing the influence of wave direction, wave period and refraction phenomenon. Results proved that equilibrium profiles are located seaward compared to their relative wave fronts, and they lie over two or more wave fronts.

Additionally, a correspondence function, called the "*wave-front-bay-shape equation*" has been established, offering an easy application to engineering uses due to the simple geometric interpretation of its controlling parameters. The function seems to indicate that equilibrium beach profiles of a single headland bay correspond to a simple translation of wave front normal to the propagation line at the headland tip.

Moreover, the application of the "*wave-front-bay-shape equation*" to the case-study bay of the Bagnoli coast (south-west of Italy) has been performed. The numerical model has been set up, and the LDR equivalent wave concept has been used to embody the dominant wave attack that rules the long-term evolution of the little bay. Results confirm the behaviour observed from numerical experiments outcomes; the "*wave-front-bay-shape equation*" has been verified, thus confirming that a correlation between equilibrium plane form and wave fronts can be found.

Nevertheless, the research still stands at a primary stage, and requires improvement and accurate verification in future research works in order to develop an enhanced guidance which could help in engineering and morphological practice.

In the following section a theoretical interpretation of these results will be provided.

8.6. A theoretical interpretation of the results

As commonly thought by practical engineering, the "stationary state" or the equilibrium position plane shape of a bay is substantially the position of the wave front.

However, as shown in the results section, by comparing the equilibrium position of an headland bay, given by a *tanh* function, with the wave fronts, the stationary state does not properly match the front, but it is positioned between two wave fronts.

The static equilibrium position is reached when the littoral drift is zero, as known. If we intend the littoral drift as related only to the variation of the wave angle to the shoreline, we obtain that the shoreline equilibrium occurs when shoreline orientation equals the breaking wave angle, therefore it must follow the wave front. Actually, when in the presence of diffractive structures, along-shore wave height gradients has heavy effects on sediment transport, and so on the littoral drift.

Therefore, in this regard, the littoral drift must be modelled as proposed by Ozaka et al (1980), see Chapter 2, for which the long-shore sediment transport rate can be written as:

$$Q_l = Q_0 \left[G_1 \sin 2(\beta - \alpha_b) - G_2 \cos(\beta - \alpha_b) \frac{dH_b}{dx} \right] \tag{8.22}$$

In which Q_0 is the littoral drift amplitude function of shore properties and breaking wave characteristics, G_1 and G_2 are considered as empirical parameters, β is shoreline orientation, α_b is the breaking wave angle and H_b is the breaking wave height.

By reaching the equilibrium condition, the littoral drift must be zero, therefore the terms in square brackets must equal to zero. We obtain:

$$G_1 \sin 2(\beta - \alpha_b) = G_2 \cos(\beta - \alpha_b) \frac{dH_b}{dx} \tag{8.23}$$

By simplifications we obtain:

$$\sin(\beta - \alpha_b) = \frac{G_2}{2G_1} \frac{dH_b}{dx} \tag{8.24}$$

By assuming that β and α_b are quite close to each other at breaking, we can approximate $\sin(\beta - \alpha_b) \cong \beta - \alpha_b$. Therefore:

$$\beta = \alpha_b + \frac{G_2}{2G_1} \frac{dH_b}{dx} \tag{8.25}$$

Eq. (8.25) states that the shoreline normal deviates from the wave front, in fact, β is not strictly α_b at the equilibrium, but it is increased by an extra quantity related to the along-shore wave height gradients. Therefore, shoreline should fit exactly the wave front only if $\frac{dH_b}{dx}$ is zero, this condition occurs in undiffracted areas, namely far from the diffraction tip (illuminated area), where $K_d = const = 1$, and deeply within the sheltered zone, where wave height is null and $K_d = 0$.

As the shoreline orientation is modelled as $-\arctan \frac{\partial y}{\partial x}$, therefore:

$$\arctan \frac{\partial y}{\partial x} = -\alpha_b - \frac{G_2}{2G_1} \frac{dH_b}{dx} \tag{8.26}$$

And considering $H_b = H_{bi}K_d$:

$$\arctan\frac{\partial y}{\partial x} = -\alpha_b - \frac{G_2}{2G_1} H_{bi} \frac{dK_d}{dx} \tag{8.27}$$

According to Penney and Price (1952), for $\frac{y}{L} \cong 2$ we can assume that wave fronts are nearly circular within the sheltered area, and so (Figure 153):

$$\alpha_b = -\arctan\left(\frac{x}{y_R - y}\right) \tag{8.28}$$

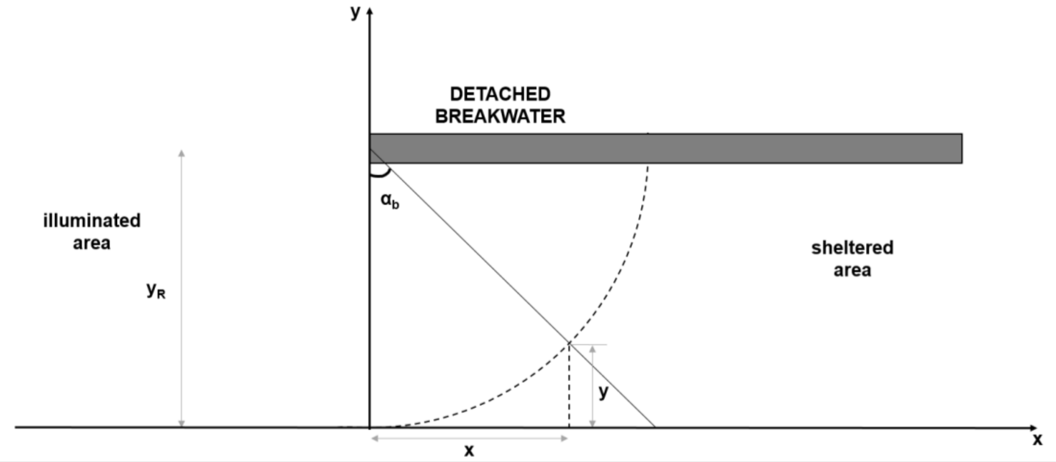

Figure 153 – Definition sketch

By substituting in Eq. (8.27):

$$\arctan\frac{\partial y}{\partial x} = \arctan\left(\frac{x}{y_R - y}\right) - \frac{G_2}{2G_1} H_{bi} \frac{dK_d}{dx} \tag{8.29}$$

Consider the study of Eq. (8.29) in the neighbourhood of the diffraction disturbance, where we expect small curvatures, and so small x. With this hypothesis, Eq. (829) becomes:

$$\frac{\partial y}{\partial x} = \frac{x}{y_R} - RH_{bi} \frac{dK_d}{dx} \tag{8.30}$$

Let's now consider a possible modelling of the diffraction coefficient K_d. According to Penney and Price, for $2 < \frac{y}{L} < 4$ the diffraction coefficient varies along x as:

$$K_d = 0.1 + 0.41 \exp\left(-0.74\ \frac{x}{L}\right) \quad for \qquad -1 < \frac{x}{L} < 5 \tag{8.31}$$

Therefore:

$$\frac{dK_d}{dx} = -\frac{0.287}{L} \exp\left(-0.74\ \frac{x}{L}\right) \tag{8.32}$$

And substituting in Eq. (8.29), and assuming slightly variation of the shore:

$$\frac{\partial y}{\partial x} = \frac{x}{y_R} + 0.287R\frac{H_{bi}}{L}\exp\left(-0.74\ \frac{x}{L}\right) \tag{8.33}$$

By integrating:

$$y = \frac{1}{y_R}\frac{x^2}{L} - 0.41\ RH_{bi}\exp\left(-0.74\ \frac{x}{L}\right) + c \tag{8.34}$$

Let's assume that y_R is related to the wave length by $y_R = mL$, and by dividing first and second term by L, we have:

$$\frac{y}{L} = \frac{1}{2m}\frac{x^2}{L} + 0.287\ \frac{RH_{bi}}{L}\left(\frac{x}{L}\right) + \left(c - 0.41\ \frac{RH_{bi}}{L}\right) \tag{8.35}$$

Eq. (8.35) is a parabolic shape equation.

For $\frac{x}{L} = -1$, far from the diffraction tip, in the illuminated zone, $\frac{\partial y}{\partial x} = 0$, and $y = 0$, so:

$$\frac{1}{2m} - 0.287\ \frac{RH_{bi}}{L} + \left(c - 0.41\ \frac{RH_{bi}}{L}\right) = \frac{1}{2m} - 0.697\ \frac{RH_{bi}}{L} + c = 0 \tag{8.36}$$

Imposing $\frac{\partial y}{\partial x} = 0$:

$$-\frac{1}{m} + 0.287\ \frac{RH_{bi}}{L} = 0 \tag{8.37}$$

From Eq. (8.37), we can determine the R coefficient considering that the m coefficient is about 1, while wave steepness is about 0.01 at breaking conditions:

$$R = \frac{1}{m}\frac{1}{0.287\ \frac{H_{bi}}{L}} \cong 10^2 \tag{8.38}$$

Therefore, from Eq. (8.36) we can calculate the value of the constant c:

$$c = \frac{1}{2m} - 0.697\ \frac{RH_{bi}}{L} \tag{8.39}$$

When going deep in the sheltered zone, x approaches higher values $\left(\frac{x}{L} = 5\right)$. In this case, the exponential function of Eq. (8.33) tends to zero, therefore the shoreline curvature becomes:

$$\frac{\partial y}{\partial x} = \frac{x}{y_R - y} \tag{8.40}$$

By separing variables:

$$(y_R - y)dy = xdx \tag{8.41}$$

$$-\frac{(y_R - y)^2}{2} = \frac{x^2}{2} + c_1 \tag{8.42}$$

This is the equation of a circular wave front, which centre is defined when c_1 is defined. Particularly, c_1 is the x value when the shoreline has reached the breakwater, in other words when $y = y_R$, this is obtained for a value of x greather than y_R, as sketched in Figure xx.

Therefore, c_1 must be equal to $\frac{{x_R}^2}{2}$, and

$$\frac{(y_R - y)^2}{2} + \frac{(x - x_R)^2}{2} = 0 \tag{8.43}$$

Eq. (43) describes a circumference, which centre is $(0; y_R)$ and ray equal to x_R.

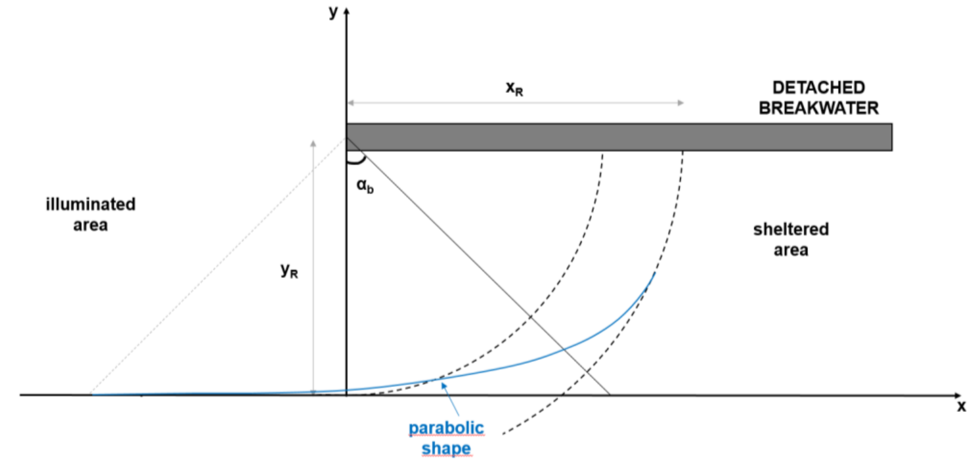

Figure 154 – definition sketch

Therefore, it is seen that the equilibrium condition varies from a parabolic profile to a circumference.

Chapter 9: Conclusions and future research

Importance of understanding the parameters that govern the long-term sediment transport processes is vital in order to establish the evolution trend of a coastal area, or overcome the problems occurring after the construction of structures. As emerged in the core of this work, diffusion theory, on which analytical and numerical models are based, finds a great echo in the field of practical coastal engineering. The common thread of present Ph.D. thesis is grasping if, and in what measure, the shoreline diffusion equation could be able to provide theoretical guidance, also useful under the practical point of view, regarding the long-term evolution of sandy coasts. Seeking and further deepening these aspects has been the *leit motiv* of this work. The innovative contributions of this work can be summarized in the following points.

- The evolution of a stretch of coast of finite length bounded by solid boundary, for which a complete analytical model has been developed. The proposed model provides a clearer view on the limits of the diffusion approach on this problem. The model performances have been studied by varying the offshore wave angle up to 40°, (exceeding the small angle hypothesis). Moreover, the role of the confining constraints on the long term response of an artificial nourishment of a given plane shape has been assessed.
- The effect of a time-varying diffusivity on long-term shoreline evolution has been accomplished. This aspect regards the theoretical foundations of the "equivalent wave" concept, frequently used in the practical coastal engineering. Adopting simple and mere considerations, the theoretical framework of this important hypothesis has been assessed. A new analytical solution for a time dependent diffusion has been given, which suggest that over a long period the evolution of a shoreline may be governed by a constant diffusion. The mid-term analysis of the Molise coast has been used to validate in such a way this result. In fact, the qualitative and quantitative

analysis of the Molise coast revealed that the explanatory power of the time-varying shore diffusivity $\frac{\partial \varepsilon}{\partial t}$, is surprisingly lower than the constant (equivalent wave) one. It is noted that the time-varying shore diffusivity seems to not affect the shoreline trend. Such results indicate a doubtful role of the time-varying diffusivity.

- The organic introduction to the effect of a negative diffusivity on long-term evolution of sandy coasts, and the existence of possible instabilities of the coast have been detected through the Littoral Drift Rose concept. An original interpretation of the effects of a detached breakwater on shoreline change has been studied. In fact, under an intriguing perspective, but not sufficiently deepened, at all, it is assumed that the positioning of a transmissive breakwater is nothing but the introduction of a negative diffusivity into a restricted area of the coast. The validation of this assumption has been assessed through an analytical approach.
- A more stringent relationship between wave crests and equilibrium shore profile, which demonstrates that the equilibrium position of shoreline does not corresponds to the wave fronts. The theoretical interpretation has been found through the diffusion approach.

Further studies are necessary to introduce new sets of analytical solutions, studying new shape of beach nourishments. Particular attention will be given to the negative diffusivity effect on long term shoreline evolution, on one hand by applying finding of this research to other case of study of the Italian peninsula, and, on the other hand, by deepening the interpretation of the effect of a detached breakwater on shoreline evolution. This aspect could be able to explain some sudden and unexpected retreating phenomenon that have been really observed behind coastal structures.

RINGRAZIAMENTI

Questa tesi, oltre a rappresentare il traguardo finale del mio corso di Dottorato, è l'espressione di un'esperienza scientifica e umana alimentata dall'incontro con tante persone, soprattutto "virtuali" dati i due anni trascorsi in totale chiusura dovuti al Covid-19. Tanti Maestri ho incontrato in questo percorso; ciascuno di loro mi ha dedicato tempo prezioso, speso a discutere e a trovare risposte ai miei interrogativi e alle mie convinzioni. Non posso esimermi dal ringraziare loro e tutte le persone che hanno condiviso con me questi anni e questo progetto di ricerca.

Tutta la mia riconoscenza va innanzitutto al Professore Mariano Buccino, il primo ad aver creduto in me. Lo ringrazio per le enormi conoscenze che ha messo a mia disposizione; egli ha costituito per me in questi anni una guida e, con la sua passione e la sua esperienza, ha per primo trasmesso in me un profondo interesse per le materie di Ingegneria Marittima e Costiera.

Un affettuoso ringraziamento va al Professore Mario Calabrese per la disponibilità accordatami e per il prezioso aiuto scientifico. Gli sarò per sempre grata per avermi concesso la possibilità di intraprendere questo importante percorso di studi.

Ringrazio tutti i professori del Dipartimento con i quali ho avuto occasione di interagire, e ringrazio il Professore Andrea Papola, coordinatore scientifico del Dottorato in Ingegneria dei Sistemi Civili che sostiene ormai da qualche anno la ricerca dei giovani ingegneri della scuola napoletana con valide iniziative didattiche e scientifiche.

Ed ancora, desidero ringraziare Gianluigi Di Paola, e tutto il gruppo dell'Università degli Studi del Molise per i consigli, la partecipazione e disponibilità al confronto e per avermi supportato nella raccolta di materiale scientifico per la stesura di questo lavoro nonché degli articoli scientifici pubblicati in questi anni di collaborazione.

Un ringraziamento a tutti i colleghi del 34° ciclo del Dottorato in Ingegneria dei Sistemi Civili della Federico II di Napoli, per il costante confronto, supporto e per i suggerimenti ricevuti. Desidero ringraziare specialmente l'ing. Maria Rella Riccardi per i suoi consigli come collega e per la sua pazienza come amica. Grazie all'ing. Sara Tuozzo, mia collega dottoranda in Ingegneria Costiera e ormai "convivente" in Dipartimento.

Ringrazio le mie amiche di una vita, che in questi anni di veri e propri "subbugli" mi sono state sempre accanto. Senza di loro non avrei mai potuto superare uno dei momenti più bui della mia vita, non solo di questo percorso di studi.

Ringrazio la mia anima gemella, fonte di sostegno e coraggio, di energia e di luce, di intelligenza e di amore.

Non avrei mai potuto concludere questo percorso se non avessi avuto il sostegno della mia famiglia, a cui dedico questo lavoro, che mi ha seguita con affetto e pazienza, incentivandomi anche nei momenti più duri. A loro va la mia gratitudine ed il mio affetto.

REFERENCES

Abramowitz, M., and Stegun, I. 1965. Handbook of Mathematical Functions with Formulas, Graphs and Mathematical Tables, Dover Publications, New York, NY.

Ashton, A.; Murray, A.B., and Arnault, O., 2001. Formation of coastline features by large-scale instabilities induced by high-angle waves, Nature, 414, 296–300.

Ashton, A.D., A.B. Murray, and B.G. Ruessink, 2003. Initial tests of a possible explanation for along-shore sandwaves on the Dutch coast, *3rd IAHR Symposium on River, Coastal and Estuarine Morphodynamics*. International Association of Hydraulic Researchers, Barcelona, Spain

Ashton, A.D. and Murray, A.B. 2006a. High-angle wave instability and emergent shoreline shapes: 1. Modeling of sand waves, flying spits, and capes. J. Geophys. Res., 111, F04011. doi: 10.1029/2005JF000422

Ashton, A.D.; Murray, A.B. 2006b High-angle wave instability and emergent shoreline shapes: 2. Wave climate analysis and comparisons to nature. J. Geophys. Res., 111, F04012.

Aucelli, P.P.C.; Izzo M.; Mazzarella A.; Rosskopf C.M.; and Russo M. 2004 L'evento meteorico estremo di gennaio 2003 sul Molise. *Quad. Geol. Appl.*, *11*, 101-119.

Aucelli, P.P.C.; De Pippo, T.; Iannantuono, E.; Rosskopf, C.M. 2007. Caratterizzazione morfologico-dinamica e meteomarina della costa molisana nel settore compreso tra la foce del torrente Sinarca e Campomarino Lido (Italia meridionale). Studi Costieri, 13, 75–92. (In Italian)

Aucelli, P.P.C.; Iannantuono, E.; Rosskopf, C.M. 2009. Evoluzione recente e rischio di erosione della costa molisana (Italia meridionale). Ital. J. Geosci., 128, 759–771. (In Italian)

Aucelli, P.P.C.; Fortini P.; Rosskopf C.M.; Scorpio V. and Viscosi V. 2011. Recent channel adjustments and riparian vegetation response: some examples from Molise (Italy)." *Geogr. Fis. Dinam. Quat., 34 (2),* 161-173. doi: 10.4461/GFDQ.2011.34.15.

Aucelli, P.P.C.; Di Paola, G.; Rizzo A.; Rosskopf C.M. 2018. Present day and future scenarios of coastal erosion and flooding processes along the Italian Adriatic coast: The case of Molise region. *Envrion. Earth Sci, 77 (10)*, 371. doi: 10.1007/s12665-018-7535-y

Bailard, J. A. 1984, A simplified model for long-shore sediment transport, Proc. Int. Coastal Eng. Conf., 19th, 1454– 1470.

Bakker, W.T., 1968. A mathematical theory about sand waves and its application on the Dutch Wadden Isle of Vlieland. Shore and Beach, 36(2), 4–14.

Bakker WT, 1969. The dynamics op a coast with a groin system. Proceedings of the 11th Coastal Engineering Conference, 492-517

Bakker, W.T., Klein Breteler, E.H.J., and Roos, A., 1970. "The Dynamics of a Coast with a Groin System", Proceedings of the 11th Conference on Coastal Engineering, ASCE, pp. 1001-1020.

Bakker, W.T., 1971. The influence of long-shore variation of the wave height on the littoral current. *Study Report WWK 71-19*, Ministry of Public Works (Rijkswaterstaat), The Hague, The Netherlands.

Bart L.J.C. 2017. Long-term modelling with XBeach: combining stationary and surfbeat mode in an integrated approach,. Tu Delft.

Bijker, E.W., 1967. Some considerations about scales for coastal models with movable bed. Delft Hydraulics Laboratory Publication No 50.

Bodge, K.R., 1989. A literature review of the distribution of long-shore sediment across the surf zone. 448 Journal of Coastal Research, 5(2), 307-328. 449

Bodge, K.R., and Kraus, N.C., 1991. Critical examination of long-shore transport rate magnitude. 450 Proceedings of the Coastal Sediments *'91*, ASCE, pp. 139-155.

Bruun, P. 1954. “Coast Erosion and the Development of Beach Profiles”, TM- 44, US Army Corps of Engineers, Beach Erosion Board

Buccino M. and Calarese M. 2007. Conceptual Approach for Prediction of Wave Transmission at Low-Crested Breakwaters. J. Waterway, Port, Coastal, Ocean Eng. 2007.133:213-224.

Buccino, M.; Di Paola, G.; Ciccaglione, M.C.; Rosskopf, C.M. 2020. A Medium-Term Study of Molise Coast Evolution Based on the One-Line Equation and “Equivalent Wave” Concept. Water, 12 (10), 2831. doi:10.3390/w12102831

CEM (Coastal Engineering Manual), 2003. U.S. Army Corps of Engineers, Coastal Engineering Research Center, U.S. Government Printing Office

Cooper, J.A.G., and Pilkey, O.H., 2004. “Alternatives to the Mathematical Modeling of Beaches”, Journal of Coastal Research, Volume 20, No. 3, pp. 641- 644.

Contini, P.; and De Girolamo, P. Impatto Morfologico di Opere a Mare: Casi di studio. In Proceedings of the VIII Conference Italian Association Offshore and Marina, La Spezia, Italy, 1998.

Crowell, M.; Leatherman, S.P.; Buckley, M.K. 1993. Shoreline Change Rate Analysis: Long Term versus Short Term Data. *Shore Beach*, *61*, 13–20.

Dabees, M.; Kamphuis, J.W. ONELINE, a numerical model for shoreline change. In Proceedings of the 26th Int. Conf. On Coastal Engineering, ASCE, Copenhagen, Denmark, 22–26 June 1998; pp. 2668–2681.

Dabees, M.A., 2000. “Efficient Modeling of Beach Evolution”, PhD Thesis, Queen’s University, Canada, 174 pp

Dally, W.R. and J. Pope, 1986. Detached breakwaters for shore protection, Technical report CERC- 86-1, U.S. Army Engineer WES, Vicksburg, MS.

d'Angremond K., J. van der Meer, and R. de Jong . 1996. Wave transmission at low-crested structures. Proc. 25th Int. Coastal Eng. Conf ASCE. 2,418–2,427.

Davidson-Arnott, R. G. D. and Heyningen, A. G. V. 2003. Migration and sedimentology of long-shore sandwaves, Long Point, Lake Erie, Canada. Sedimentology, 50(6): 1123–1137, ISSN 00370746. [11, 173]

Dean, R.G., 1977. “Equilibrium Beach Profiles: U.S. Atlantic and Gulf Coasts”, Department of Civil Engineering, Ocean Engineering Report No. 12, University of Delaware, Newark, Delaware.

Dean R.G. 1984. CRC Handbook of Coastal Processes and Erosion, Komar, P. D., editor, CRC Press Inc., Boca Raton, Fla.

Dean R.G., Chen R., Browder A.E., 1997. Full scale monitoring study of a submerged breakwater, Palm Beach, Florida, USA. Coastal Engineering 29 291-315

Dean RG, 2003. Beach nourishment – theory and practice. World Scientific, Singapore

Deigaard, R., J. Fredsoe, and I. B. Hedegaard (1988), Mathematical model for littoral drift, J. Waterw. Port Coastal Ocean Eng., 112, 351– 369.

Deltares. 2011. UNIBEST-CL+ Manual: Manual for Version 7.1 of the Shoreline Model UNIBEST-CL.; Deltares: Delft, The Netherlands.

Del Valle, R., Medina, R., and Losada, M. A. 1993. Dependence of Coefficient K on Grain Size, Technical Note No. 3062, *J. Waterway, Port, Coastal and Ocean Engineering*, 119 (5), 568-574

De Vincenzo, A.; Covelli, C.; Molino, A.J.; Pannone, M.; Ciccaglione, M.C.; Molino, B. 2019. Long-term Management Policies of Reservoirs: Possible Re-use of Dredged Sediments for Coastal Nourishment. *Water*,*11 (1)*, 15. doi: 10.3390/w11010015

De Vriend, H.J. and Bakker, W.T., 1993. Sedimentary processes and morphological

DHI. 2005. Litpack: Noncohesive Sediment Transport in Currents and Waves. User Guide; Danish Hydraulic Institute: Hørsholm, Denmark.

Di Paola, G.; Ciccaglione, M.C.; Buccino, M.; Rosskopf, C.M. 2020. Influence of hard defence structures on shoreline erosion along Molise coast (southern Italy): A preliminary investigation. *Rend. Online Soci. Geol. Ital*, 2–11, doi:10.3301/ROL.2020.10.

Falques, A., 2003. On the diffusivity in coastline dynamics. *Geophys. Res. Lett.*, Vol. 30.

Falque´s, A. and Calvete, D., 2005. Large scale dynamics of sandy coastlines: diffusivity and instability. Journal Geophysical Research, 110, C03007, doi:10.1029/2004JC002587.

Falque´s, A., 2006. Wave driven along-shore sediment transport and stability of the Dutch coastline. Coastal Engineering, 53, 243–254.

Goda, Y., Takayama, T., and Suzuki, Y. 1978. "Diffraction Diagrams for Directional Random Waves," Proceeding of 16th Coastal Engineering Conference, American Society of Civil Engineers, pp 628-650.

Grijm W. 1961. Theoretical forms of shoreline. Proceedings of the 7th Coastal Engineering Conference, New York, pp 197‑202

Hallermeier, R. J. 1983. "Sand Transport Limits in Coastal Structure Design," Proceedings of Coastal Structures '83, American Society of Civil Engineers, pp 703-716.

Hanson, H., and Larson, M., 1987. "Comparison of Analytic and Numerical Solutions of the One-Line Model of Shoreline Change", Proceedings of Coastal Sediments '87, ASCE, pp. 500-514.

Hanson, H.. 1987. "GENESIS: A Generalized Shoreline Change Numerical Model for Engineering Use", Ph.D. Thesis, University of Lund, Lund, Sweden.

Hanson, H., and N. C. Kraus. 1989. GENESIS: Generalized model for simulating shoreline change, report 1, Technical reference, U.S. Army Eng. Waterw. Exp. Stn., Coastal Eng. Res. Cent, Vicksburg,

Hanson, H., and Kraus, N.C., 1986. "Forecast of Shoreline Change Behind Multiple Coastal Structures", Journal of Coastal Research, Vol. 5, No. 1, pp. 1-27.

Hanson, H.; Kraus, N.C. 1990. Shoreline response to a single transmissive detached breakwater. Coast. Eng. Proc. 22, 2034–2046.

Hanson, H., Larson, M., Kraus, N.C., and Capobianco, M. 1997. Modeling of Seasonal Variations by Cross-Shore Transport Using One-Line Compatible Methods, *Proc. Coastal Dynamics '97*, ASCE, pp. 893-902.

Hanson, H., Larson, M., and Kraus, N.C. 2001. "A New Approach to Represent Tidal Currents and Bathymetric Features in the One-Line Model Concept," *Proc. Coastal Dynamics '01*, ASCE, 172-181.

Hapke, C.J.; Himmelstoss, E.A.; Kratzmann, M.; List, J.H.; Thieler, E.R. National Assessment 528 of Shoreline Change: Historical Shoreline Change along the New England and Mid-Atlantic 529 Coasts; open-file report 2010-1118; U.S. Geological Survey: Reston, VA, USA, 2010; p. 57.

Harris, M.M. and J.B. Herbich, 1986, Effects of breakwater spacing on sand entrapment, *Journal ofHydraulic Research*, 24 (5).

Hasselmann, K.; Dunckel, M.; Ewing, J.A. 1973. Directional wave spectra observed JONSWAP. *J. Phys. Oceanogr,10*, 1264–1280.

HoangVC, Tanaka H, and Viet NT, 2016. Theoretical study on erosion at Cua Dai river delta coast induced by the reduction of sediment supply. Proceedings of the 9th International Conference on Coastal and Port Engineering in Developing Countries ‑ IX PIANCCOPEDEC.

Hoang VC, Tanaka H,Mitobe Y, 2019. Long-shore propagation of beach erosion in the vicinity of tsunami-induced concave shoreline. J Hydro Environ Res 23:1‑9

Hoang VC, 2020. Analytical solutions of one-line model to shoreline change on a coast bounded by solid boundaries. Geo Marine Letters 41:42

Holthuijsen, L.H. 2007. *Waves in Oceanic and Coastal Waters*; University of Cambridge Press: Cambridge, UK.

Hsu, J.R.C.; Evans, C. 1989. Parabolic Bay Shapes and Applications. *Proc. Inst. Civ. Eng. Part 2*, *87*, 557–570, doi:10.1680/iicep.1989.3778.

Hsu, J.R.C.; Yu, M.J.; Lee, F.C.; Benedet, L. 2010. Static bay beach concept for scientists and engineers: A review. *Coast. Eng.57*, 76–91, doi:10.1016/j.coastaleng.2009.09.004.

Huisman B.J.A. Van Thiel de Vries J.S.M., Walstra D.J.R., Roelvink J.A., Ranasinghe R., Stive M.J.F., 2013. Advection and diffusion of shore-attached sand nourishments. Coastal Dynamics.

Hulsbergen, C.H., Bakker, W.T., and van Bochove, G., 1976. “Experimental Verification of Groin Theory”, Proceedings of the 15th Conference on Coastal Engineering, ASCE, pp. 1439-1458.

Istituto Superiore per la Protezione e la Ricerca Ambientale (ISPRA). Annuario dei dati ambientali, 2013. Biblioteca Nazionale Centrale, Roma.

Kamphuis, W., 1991. Along-shore Sediment Transport Rate. *Journal of Waterway, Port, Coastal,* 473 *Ocean Engineering,* Volume 117, pp. 624-640.

Kamphuis, J.W., 2000. “Introduction to Coastal Engineering and Management”, World Scientific, Singapore-New Jersey-London-Canada

Kærgaard, K. H. 2011.. *Numerical Modeling of Shoreline Undulations*. DTU Mechanical Engineering

Kemp, J.; Vandeputte, B.; Eccleshall, T.; Simons, R.; Troch, P. 2018. A modified hyperbolic tangent equation to determine equilibrium shape of headland bay beaches. In Proceedings of the 13th International Conference on Coastal Engineering, Baltimore, MD, USA. doi:10.9753/icce.v36.papers.106.

Komar, P.D., and Inman, D.L., 1970. Long-shore sand transport on beaches. *Journal of Geophysical Research,* 75, No 30.

Komar, P. D., 1971. “Nearshore Cell Circulation and the Formation of Giant Cusps,” Geol. Soc. Am. Bull., Vol. 81, pg. 2643-50.

Komar PD 1973. Computer models of delta growth due to sediment input from rivers and long-shore transport. Geol Soc Am Bull 84: 2217‑2226

Komar, P.D., 1976. *Beach Processes and Sedimentation,* p 211, Prentice-Hall, Inc.

Komar, P.D., 1998. Beach Processes and Sedimentation, 2nd edition. Upper Saddle River, New Jersey: Prentice Hall.

Kraus, N.C., and Harikai, S., 1983. “Numerical Model of the Shoreline Change at Oarai Beach”, Coastal Engineering, Vol. 7, No. 1, pp. 1-28.

Kraus, N.C., Hanson, H., and Harikai, S., 1985. “Shoreline Change at Oarai Beach – Past, Present and Future”, Proceedings of 19th Coastal Engineering Conference, ASCE, pp. 2107-2123.

Kraus, N.C., Hanson, H., Scheffner, N.W., Chou, L.W., Cialone, M.A., Smith, J.M., and Hardy, T.A., 1986. “Coastal Processes at Sea Bright to Ocean 93 Township, New Jersey”, Unpublished Draft Report, US Army Engineer, Waterways Experiment Station, Coastal Engineering Research Center

Kriebel, D.L., and Dean, R.G., 1985. “Numerical Simulation of Time- Dependent Beach and Dune Erosion”, Coastal Engineering, Vol. 9, pp. 221-245.

Krumbein, W.C. Shore processes and beach characteristics. In *Technical Memorandum, vol. 3. Beach Erosion Board*; U.S. Army Corps of Engineers: Washington, DC, USA, 1944; p. 47.

Larson, M., Hanson, H., and Kraus, N.C., 1987. “Analytical Solutions of the One-Line Model of Shoreline Change”, Technical Report CERC-87, U.S. Army of Engineer Waterways Experiment Station, Coastal Engineering Research Center.

Larson, M. and N.C. Kraus, 1991. Mathematical Modeling of the Fate of Beach Fill. *Coastal Eng.*, Vol. 16, Issue 1, 1991, pp. 83-114

Larson M, Hanson H, Kraus NC 1997. Analytical solutions of one-line model for shoreline change near coastal structures. J Waterw Port Coast Ocean Eng 123(4):180‑191

Larson M, Nunes A, Tanaka H 2020. Semi-analytic model of tidalinduced inlet flow and morphological evolution. Coast Eng 155: 103581

Le Mehaute, B. , and Brebner, A. 1961. "An Introduction to Coastal Morphology and Littoral Processes," Report No. 14, Civil Engineering Department, Queens University at Kingston, Ontario, Canada.

Le Mehaute, B., and Soldate, M. 1977. "Mathematical Modeling of Shoreline Evolution," CERC Miscellaneous Report No. 77-10, US Army Engineer Waterways Experiment Station, Vicksburg, Miss.

Longuet-Higgins, M.S., 1970, Long-shore currents generated by oblique incident sea waves, 1. *Journal of Geophysical Research,* 75, No 33.

Madsen, P.A.; Murray, R.; Sørensen, O.R. 1991. A new form of the Boussinesq equations with improved linear dispersion characteristics. *Coast. Eng. 15*, 371–388, doi:10.1016/0378-3839(91)90017-B.

Madsen, P.A.; Sørensen, O.R. 1992. A new form of the Boussinesq equations with improved linear dispersion characteristics. Part 2: A slowly-varying Bathymetry. *Coast. Eng.*, *18*, 183–204, doi:10.1016/0378-3839(92)90019-Q.

Madsen, P.A.; Sørensen, O.R.; Schäffer, H.A. 1997. Surf zone dynamics simulated by a Boussinesq type model. Part I: Model description and cross-shore motion of regular waves. *Coast. Eng.*, *32*, 255–287.

Madsen, P.A.; Sørensen, O.R.; Schäffer, H.A. 1997. Surf zone dynamics simulated by a Boussinesq type model. Part II: Surf beat and swash zone oscillations for wave groups and irregular waves. *Coast. Eng.*, *32*, 289–230.

Martino, E., Moreno, L., Kraus, N.C., 2003. Engineering guidance for the use of bayed beach formulations. Proc. Coastal Sediments'03. ASCE.

Mil-Homens, J., Ranasinghe, R., Stive, M., and de Vries, J.v.T., 2013. Re-evaluation and 486 improvement of three commonly used bulk long-shore sediment transport formulas. *Coastal* 487 *Engineering,* Volume 75, pp. 29-39.

Moore, B. 1982. "Beach Profile Evolution in Response to Changes in Water Level and Wave Height," M.S. Thesis, Department of Civil Engineering, University of Delaware, Newark, DE.

Moreno, L.J., Kraus,N.C., 1999. Equilibrium shape of headland-bay beaches for engineering design. Proc. Coastal Sediments '99, vol. 1. ASCE, pp. 860–875.

Ozasa, H., and Brampton, A. H. 1980. "Mathematical Modeling of Beaches Backed by Seawalls," Coastal Engineering, Vol 4, No. **1,** pp 47-64.

Pelnard-Considere´, R. 1956. Essai de theorie de l'evolution des formes de rivage en plages de sable et de galets, in 4th Journees de l'Hydraulique, Les Energies de la Mer, III, pp. 289– 298, La Houille Blanche, Grenoble, France.

Penney William George, Price A. T., Martin J. C., Moyce W. J., Penney William George, Price A. T. and Thornhill C. K. 1952. Part I. The diffraction theory of sea waves and the shelter afforded by breakwaters. 244, Philosophical Transactions of the Royal Society of London. Series A, Mathematical and Physical Science.

Perlin M, Dean RG 1983. A numerical model to simulate sediment transport in the vicinity of coastal structures. In: Report MR-83- 10, US. Coastal Engineering Research Center, Army Corps of Engineer

Pilarczyk KW, 2003. Design of low-crested (submerged) structures – an overview –, 6th International Conference on Coastal and Port Engineering in Developing Countries, Colombo, Sri Lanka.

Pranzini E, Rossi L. 2014. Protocollo per il monitoraggio dell'evoluzione costiera, 2014. In: Cipriani F (ed) Monitoraggio dell'erosione costiera - una rete di osservatori regionali, Progetto ResMar. Firenze.

Price, W.A., Tomlinson, D.W., and Willis, D.H., 1973. "Predicting Changes in the Plane Shape of Beaches", Proceedings of 13th Coastal Engineering Conference, ASCE, pp. 1321-1329.

Reeve DE, Valsamidis A 2014. On the stability of a class of shoreline plane e formmodels. Coast Eng 91:76‑83

Roelvink, J.A., and Broker, I., 1993. "Cross-shore Profile Models", Coastal Engineering, Volume 21, pp. 163-191

Rosskopf, C.M.; Di Paola, G.; Atkinson, D.E.; Rodriguez, G.; Walker, I.J. 2018. Recent shoreline evolution and beach erosion along the central Adriatic coast of Italy: The case of Molise region. *J. Coast. Conserv. 22*, 879–895.

Samaras, A.G., and Koutitas, C.G., 2014. Comparison of three long-shore sediment transport rate 497 formulae in shoreline evolution modeling near stream mouths. *Ocean Engineering*, Volume 92, 498 pp. 255-266.

Saville, T. 1952. The E_ect of Fetch Width on Wave Generation; TM-70; US Army Corps of Engineers, Beach Erosion Board: Washington, DC, USA.

Scorpio, V.; Aucelli, P.P.C.; Giano, S.I.; Pisano, L.; Robustelli, G.; Rosskopf, C.M.; Schiattarella, M. 2015. River channel adjustments in Southern Italy over the past 150 years and implications for channel recovery. *Geomorphology*, *251*, 77–90.

Silvester, R. 1960. Stabilization of sedimentary coastlines. *Nature*, *188*, 467–469, doi:10.1038/188467a0.

Silvester, R. 1984. Fluctuation in littoral drift. In Proceedings of the International Conference on Coastal Engineering, Houston, TX, USA, 3–7 September 1984; ASCE: Reston, VA, USA.

Shore Protection Manual (SPM), 1984. U.S. Government Printing Office, Washington D.C.

Sørensen, O.R.; Schäffer, H.A.; Sørensen, L.S. 2004. Boussinesq type modelling using unstructured finite element technique. *Coast. Eng*, *50*, 181–198, doi:10.1016/j.coastaleng.2003.10.005.

Svendsen, I.A. 1984. Mass flux and undertow in a surf zone. *Coast. Eng.*, *8*, 347–365, doi:10.1016/0378-3839(84)90030-9.

Swart, D.H., 1974. Offshore sediment transport and equilibrium beach profiles. *Delft Hydraulics Laboratory PubUcation No 131.*

Thieler, E.R., Pilkey, O.H., Young, R.S., Bush, D.M., and Chai, F., 2000. "The Use of Mathematical Models to Predict Beach Behavior for U.S. Coastal Engineering: A Critical Review", Journal of Coastal Research, Volume 16, No.1, pp. 48-70.

Tomasicchio, G.R.; D'Alessandro, F.; Barbaro, G.; Malara, G. 2013. General long-shore transport model. Coast. Eng., 71, 28–36.

Tomasicchio, G.R.; D'Alessandro, F.; Frega, F.; Francone, A.; Ligorio, F. 2018. Recent improvements for estimation of long-shore transport. Ital. J. Eng. Geol. Environ., 1, 179–187.

Tomasicchio, G.R.; Francone, A.; Simmonds, D.J.; D'Alessandro, F.; Frega, F. 2020. Prediction of Shoreline Evolution. Reliability of a General Model for the Mixed Beach Case. *J. Mar. Sci. Eng.*, *8*, 361. https://doi.org/10.3390/jmse8050361

Valsamidis A, Reeve DE, 2017. Modelling shoreline evolution in the vicinity of a groin and a river. Cont Shelf Res 132:49‑57

Valsamidis A, Reeve DE, 2020. A new approach to analytical modelling of groin fields. Cont Shelf Res 211:104288

Valsamidis A, Reeve DE, Cai Y, Dodd N. 2017. On the morphodynamic evolution of mega-nourishment. Proceedings of the Coastal Dynamics 2017:830‑840

Van der Meer, J.W. 1988. Rock Slopes and Gravel Beaches under Wave Attack. Ph.D. Thesis, Delft Hydraulics Laboratory, Delft, The Netherlands.

Van Rijn, L.C., 2002. "Long-shore Sediment Transport", Report Z3054.20 Delft Hydraulics, Delft, the Netherlands.

Van Rijn, L.C., 2014. A simple general expression for long-shore transport of sand, gravel and shingle. 513 *Coastal Engineering*, Volume 90, pp. 23-39.

Verhagen, H. 1989. Sand waves along the Dutch Coast. Coastal Engineering, 13(2): 129–147, July 1989. ISSN 0378-3839. [10, 14, 64, 169, 170]

Walton, T.L.; Dean, R.G. 1973. Application of littoral drift roses to coastal engineering problems. In Proceedings of the Conference on Engineering Dynamics in the Surf Zone, Sydney, Australia; Institution of Engineers: Sydney, VIC, Australia; pp. 221–227.

Walton, T.L.; Dean, R.G. 2010. Long-shore sediment transport via littoral drift rose. *Ocean Eng.*, *37*, 228–235, doi:10.1016/j.oceaneng.2009.11.002.

Walton TL, Chiu TY 1979. A review of analytical techniques to solve the sand transport equation and some simplified solutions. Proceedings of Coastal Structures 79:809‑837

Walton TL 1994. Shoreline solution for tapered beach fill. JWaterw Port Coast Ocean Eng 120(6):651‑655

Walton TL, Dean RG 2011. Shoreline change at an infinite jetty for wave time series. Cont Shelf Res 31(14):1474‑1480

Wang, J.D. and Le Mehaute, B., 1980. Criterion for stability of shoreline plane form. In: 17th International Conference on Coastal Engineering (Sydney, Australia, ASCE), pp. 1295–1305.

Willis, D.H., 1977. “Evaluation of Along-shore Transport Models”, Proceedings of Coastal Sediments '77, ASCE, pp. 350-365.

Yasso, W.E., 1965. Plane geometry of headland bay beaches. J. Geol. 73, 702–714.

Zacharioudaki A, Reeve DE 2008. Semianalytical solutions of shoreline response to time-varying wave conditions. J Waterw Port Coast Ocean Eng 134(5):265‑274

Zenkovich, V.P., 1959. On the genesis of cuspate spits along lagoon shores. Journal of Geology, 67, 269–277.